Interaction between Electrical Discharges and Materials for Wind Turbine Blades - particularly related to lightning protection

Madsen, Søren Find; Holbøll, Joachim; Henriksen, Mogens; Sørensen (fratrådt), Troels

Publication date:
2007

Document Version
Publisher's PDF, also known as Version of record

Søren Find Madsen

Interaction between electrical discharges and materials for wind turbine blades – particularly related to lightning protection

PhD thesis, 2006

Ørsted•DTU, Electric Power Engineering
The Technical University of Denmark

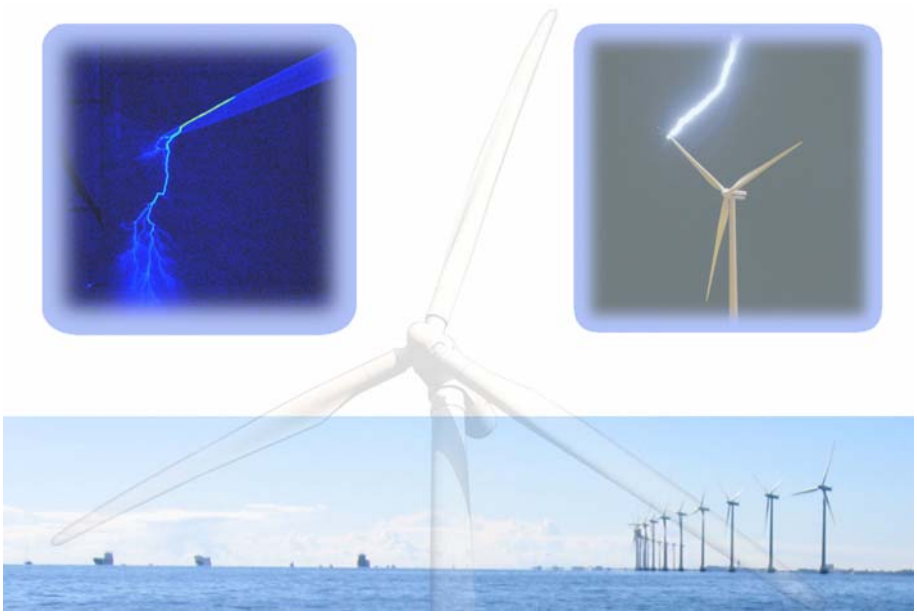

Preface

The present Ph.D. thesis is submitted as part of the requirements for achieving the Danish Ph.D. degree at the department Ørsted•DTU, Electric Power Engineering at the Technical University of Denmark. The research has been conducted from the 1st of March 2003 to the 14th of March 2006. The project is financed by means of the Danish PSO-F&U funding with project number 4517 and *Energinet.dk* as responsible administrator.

I would first of all like to thank my supervisors at Ørsted•DTU, Associate Professors Dr. Joachim Holbøll and Dr. Mogens Henriksen, for their guidance and encouragement. The steering committee, constituted of Troels Sørensen, *Energi-E2*, Niels Bjært, *Fiberline Composites* and Hans Jørgen Jørgensen, *DEFU,* has also contributed with numerous ideas and fruitful discussions. The work and support of Mr. J. Anderson Plumer, *Lightning Technologies Inc*. is greatly appreciated. Besides his highly respected skills within lightning protection I am also grateful for the kind and warm welcome my wife and I received during the 4 months stay at LTI in fall 2004. The kindness of the rest of the staff at LTI was likewise overwhelming.

During the project, four meetings for all interested were held. The participants came from the wind turbine manufacturers and related industries, electric power utility companies, consultant engineers, etc. I am truly impressed of the many participants and their level of involvement, their ideas and discussions as well as the supply of the large amount of test specimens and material data. Special thanks are given to Kim Bertelsen, *Vestas Wind Systems*, Lars Bo Hansen, *LM Glasfiber*, Flemming Møller Larsen, *SSP Technology* and Niels Bjært, *Fiberline Composites,* without whom this project would have been limited to only theoretical considerations.

Finally, the work load and commitment of further employees at Ørsted•DTU is appreciated. Especially the construction of various test setups and test specimens by Jørgen Larsen, Jørn Berril, Freddie Fahnøe, Erik Andersen and Kjeld Martinsen is acknowledged. The aging of composites conducted as part of the investigations of breakdown strengths was performed with employees at The Department of Mechanical Engineering at DTU. A special thanks to Associate Professor Peder Klit for designing the test rig, and Erik Petersen for help with conducting the tests.

Kgs. Lyngby, December 2006

Søren Find Madsen

Abstract

Lightning protection of composite wind turbine blades has become an issue of great importance considering the location and size of modern wind turbines. This thesis focuses on which parameters in the manufacturing process of the composite materials can be optimised to ensure an overall more efficient lightning protection of the blades.

Initially, the wind turbine blade is described from an electrical point of view, where common methods of lightning protection are mentioned, Chapter 2. Basic lightning theory is presented, and particularly the interaction of the composite structure with the electrical environment surrounding the blade during a thunderstorm is treated, Chapter 3. This macroscopic view leads to formulations regarding the materials used for blade manufacturing, mainly Glass Fibre Reinforced Polymers (GFRP), but also the use of Carbon Fibre Composites (CFC) is commented. The material characterisation is based on experience from the high voltage industry and covers both surface properties and conditions defining the bulk material, as described in Chapter 4.

Numerical modelling is widely used within the high voltage industry to predict which areas of a certain construction are stressed excessively. By doing so, the structure can be optimised by means of changing the geometry or selecting different materials. Such calculation methods are also a valuable tool when designing wind turbine blades. Examples of the calculation of possible attachment points and anisotropic material behaviour are shown in Chapter 3 and Chapter 4.

Besides these theoretical considerations, the parameters characterising composite materials are investigated by means of laboratory testing. Surface properties are identified by tracking tests according to IEC Publ. 587 [1] and a test method constituting surface flashovers for various surface contaminants. The bulk material is investigated by two different test setups measuring the electrical breakdown strength of these inhomogeneous composite materials. Such breakdown tests are performed on different blade materials and on specimens aged mechanically. A correlation between the tracking results and breakdown field strength can also be found in Chapter 5.

When the knowledge concerning lightning physics and the selection of materials based on testing is integrated in the design of a new wind turbine blade, the entire solution comprising blade design and applied lightning protection must be verified. Experience with such full scale testing aiming at identifying lightning attachment points, and possible high current tests to visualise the damage associated with lightning discharges, are described in Chapter 6.

The experience gained within the present work considering general design of lightning protection on wind turbine blades, material properties and related test methods, full scale testing and numerical modelling is summed up in Chapter 7, and finally described as a list of practical recommendations in Chapter 8.

Resume

Lynbeskyttelse af vindmøllevinger lavet af kompositmateriale er blevet et vigtigt emne, placeringen og størrelsen af møllerne taget i betragtning. Denne afhandling fokuserer på hvilke parametre i produktionen af kompositmaterialerne der kan optimeres, for at opnå en mere effektiv lynbeskyttelse af vingerne.

Indledningsvist bliver vindmøllevinger beskrevet ud fra et elektrisk synspunkt, hvor typiske beskyttelsesmetoder introduceres, Kapitel 2. Generel teori for lynudladninger præsenteres, og specielt vekselvirkningen mellem vingekonstruktionen og det elektriske miljø der eksisterer ved tordenvejr behandles, Kapitel 3. Denne makroskopiske analyse leder til retningslinier for valg af kompositmaterialer til vinger, primært indenfor glasfiber forstærket polymerer (GFRP), men også brugen af kulfibre (CFC) kommenteres. Karakteriseringen af de forskellige materialer er baseret på erfaring fra højspændingsteknikken, og omhandler både overfladefænomener og forhold der beskriver selve materialevolumenet, Kapitel 4.

Numeriske simuleringer benyttes ofte i højspændingsteknikken til at beregne det elektriske felt i forskellige dele af en given konstruktion. Ved at udføre en sådan analyse, kan konstruktionen designes optimalt ved små ændringer i geometrien eller ved valg af materialer med andre egenskaber. Disse værktøjer er også meget anvendelige ved design af vindmøllevinger. Eksempler på beregning af lynets indslagssteder og anskueliggørelse af kulfiberkompositters anisotropi er vist i Kapitel 3 og Kapitel 4.

Udover disse teoretiske anskuelser, er de bestemmende parametre for kompositmaterialer undersøgt i laboratoriet. Overfladeegenskaber er bestemt ved 'Tracking Tests' i.h.t. IEC Publ. 587 [1] og en testmetode bygget op omkring overflade udladninger ved forskellige forureningsgrader. Selve materialevolumenet er undersøgt vha. to forskellige metoder til bestemmelse af den elektriske gennemslagsfeltstyrke for de stærkt inhomogene kompositmaterialer. Gennemslagstestene er udført for forskellige vingematerialer, og på testemner udsat for mekanisk ældning. En korrelation mellem 'Tracking Index' og gennemslagsfeltstyrke er blevet fundet i Kapitel 5.

Når modeller for vekselvirkningen mellem det elektriske miljø og vingekonstruktionen kombineres med et materialevalg baseret på forsøg i laboratoriet, opnås et teoretisk optimalt design der efterfølgende bør testes eksperimentelt. Erfaringer fra sådanne fuldskalaforsøg, med henblik på at definere indslagssteder og simulere skaden som følge af lynstrømmen er beskrevet i Kapitel 6.

Resultaterne opnået gennem dette projekt, angående general design af lynbeskyttelsessystemer på vindmøllevinger, materialeegenskaber og relaterede testmetoder, fuldskalaforsøg og numerisk analyse er summeret op i Kapitel 7, og beskrevet ved en række konkrete anbefalinger til industrien i Kapitel 8.

Table of contents

INTRODUCTION **1**

1.1 LARGE TURBINES PLACED AT OFFSHORE LOCATIONS 2
1.2 EXPERIENCES FROM OTHER INDUSTRIES 3
1.3 MATERIAL OPTIMISATION VERSUS LIGHTNING PROTECTION 4
1.4 THE PRESENT THESIS 4

WIND TURBINES **7**

2.1 WIND TURBINES IN GENERAL 7
2.1.1 Rotor *7*
2.1.2 Nacelle *8*
2.1.3 Tower *8*
2.2 WIND TURBINE BLADES 8
2.3 LIGHTNING PROTECTION, SUCCESS CRITERIA 9
2.4 LIGHTNING PROTECTION OF COMPOSITE MATERIALS 9
2.4.1 Air termination and down conductor *10*
2.4.2 Temperature rise associated with conductive materials or surfaces *12*
2.4.3 Conductive materials *13*
2.4.4 Conductive surfaces *14*
2.5 CURRENT STATUS ON LIGHTNING PROTECTION 15

ELECTRICAL ENVIRONMENT AND LIGHTNING DISCHARGES **17**

3.1 LIGHTNING THEORY 17
3.1.1 Charge accumulation *17*
3.1.2 Static field and leader initiation *18*
3.1.3 Final jump *22*
3.1.4 Parameters of a lightning strike *24*
3.2 ELECTRICAL DISCHARGES RELATED TO A WIND TURBINE BLADE 27
3.2.1 Attachment to air terminations *29*
3.2.2 Attachment on insulating surfaces *30*
3.2.3 Time span for attachment process *31*
3.2.4 Swept stroke phenomena *32*
3.2.5 Further attachment processes *35*
3.3 NUMERICAL METHODS 36
3.3.1 Attachment point on wind turbine *38*
3.3.2 Exposed turbines in a wind farm *40*
3.4 ELECTRICAL ENVIRONMENT AND LIGHTNING DISCHARGES 43

MATERIAL ASPECTS AND PROPERTIES **45**

4.1 COMPOSITE MATERIALS 45
4.1.1 Manufacture *46*
4.1.2 Mechanical properties *47*
4.1.3 Application *47*
4.2 ELECTRICAL PARAMETERS AND DEFINITIONS 48
4.2.1 Electric field *48*
4.2.2 Conductivity *49*

4.2.3 Permittivity ... *50*
4.2.4 Electrical breakdown ... *51*
4.2.5 Surface flashover ... *51*
4.3 ELECTRICAL PROPERTIES OF THE BULK MATERIAL ... 51
4.3.1 Voids and cavities ... *52*
4.3.2 Fibre orientation ... *54*
4.3.3 Breakdown strength ... *54*
4.4 SURFACE CHARACTERISTICS ... 56
4.4.1 Tracking resistance ... *56*
4.4.2 Hydrophobicity ... *57*
4.5 MULTIFACTOR EXPOSURE ... 58
4.6 RELEVANT TESTS ... 58
4.6.1 Tracking tests ... *59*
4.6.2 Breakdown tests ... *60*
4.6.3 Arc resistance ... *60*
4.6.4 Hydrophobicity ... *60*
4.7 CARBON FIBRE COMPOSITES ... 61

LABORATORY WORK ... 65

5.1 TRACKING TESTS ... 65
5.1.1 Purpose ... *65*
5.1.2 Test method ... *65*
5.1.3 Evaluation of test method ... *67*
5.1.4 Results ... *67*
5.2 BREAKDOWN FIELD STRENGTH ... 73
5.2.1 Purpose ... *73*
5.2.2 Initial approach, rectangular specimens ... *73*
5.2.3 Second approach, quadratic specimens ... *90*
5.2.4 Mechanical aging ... *100*
5.2.5 Importance of sizing and air content ... *106*
5.3 CORRELATION BETWEEN TRACKING AND BREAKDOWN TESTS ... 109
5.3.1 Purpose ... *109*
5.3.2 Test specimens and test procedure ... *110*
5.3.3 Results ... *110*
5.3.4 Discussion ... *114*
5.4 SURFACE FLASHOVER TESTS ... 114
5.4.1 Purpose ... *115*
5.4.2 Test specimens and test procedure ... *115*
5.4.3 Results ... *119*
5.4.4 Discussion ... *127*
5.5 LABORATORY WORK ... 129

FULL SCALE TESTING ... 131

6.1 HIGH VOLTAGE TEST ... 131
6.1.1 Purpose ... *131*
6.1.2 SAE ARP 5416 ... *132*
6.1.3 Test method adjusted to a wind turbine blade tip ... *134*
6.1.4 Recent tests of six blade tips ... *136*

6.1.5 Streamer propagation tests ... 141
6.1.6 Evaluation of test method ... 143
6.2 HIGH CURRENT TEST ... 143

DISCUSSION ... 147

7.1 BREAKDOWN TEST METHOD FOR COMPOSITE MATERIALS ... 147
7.2 TRACKING TESTS VS. BREAKDOWN TESTS ... 148
7.3 FULL SCALE ATTACHMENT TEST METHOD ... 149
7.4 NUMERICAL MODELLING ... 149
7.5 IEC PRE-STANDARDISATION ... 150
7.6 FUTURE WORK ... 150

RECOMMENDATIONS ... 153

8.1 GENERAL PRINCIPLE ... 153
8.2 COMPOSITE MATERIAL PROPERTIES ... 153
8.2.1 Surface properties ... 153
8.2.2 Volume properties ... 154
8.3 BLADE DESIGN ... 155
8.3.1 Down conductor ... 155
8.3.2 Attachment point ... 155
8.4 NUMERICAL MODELLING ... 156
8.5 TEST METHODS ... 156

CONCLUSION ... 157

REFERENCES ... 159

APPENDIX A – NUMERICAL MODELLING ... 165
APPENDIX B – ISSUES OF SCALING ... 170
APPENDIX C – PHOTOGRAPHIC DOCUMENTATION ... 172
APPENDIX D – TEST RESULTS FROM SECTION 5.4 ... 178
APPENDIX E – SCALE MODEL EXPERIMENTS ... 183
APPENDIX F – LIST OF PAPERS ... 184

Chapter 1

Introduction

The design of wind turbines has experienced many drastic steps from the small farm mills pumping water towards the larger plants capable of producing several MW of electric power. During this journey, the design engineers are facing larger and more complex challenges every day.

The mother of all modern wind turbines producing alternating current is believed to be the 200 kW 'Gedser Møllen' built in 1957 in the southern part of Zealand, Denmark [2]. On top of a 25m concrete tower, the nacelle was mounted, carrying the generator, gear and three blades with a rotor diameter of 27m. The turbine was a marvellous structure and was in operation for ten years up to 1967. At that time, prices of fossil fuels was rather low, so it was not until 1977, along with the oil crisis, that the wind turbine was restored with financial support from American researchers. In parallel, in 1978, a Danish carpenter 'Christian Riisager' had built a small wind turbine based on three aero dynamical blades and an asynchronous generator. Modern wind turbines today are still based on these two early designs [2].

Engineers and energy researchers were divided in two camps; those who believed in this new energy resource, and those who thought it was a waste of time because they already had invented the safe and reliable nuclear power plants. Although engineers still disagree as to whether or not to believe in wind turbines, nobody can argue against the fact that the wind turbine industry has grown into a large commercial business.

Thirty years ago, the manufacturing of wind turbines in general was something done by local smithies. However, due to the increased focus on renewable energy sources and the perspective of lots of jobs, the Danish government decided to give extensive subsidies to owners of wind turbines. This catalyst caused the Danish wind turbine industry to grow rapidly during the last couple of decades, such that more than 50% of all wind turbines worldwide were produced by Danish companies in 2002. Lately, the ownership of some major companies has changed hands and this has changed the situation somewhat.

Nowadays, the size of wind turbines has increased dramatically. The largest turbine at present time is the Repower 5M [3], a 5MW wind turbine with a hub height of 100m – 120m and a rotor diameter of 126m. Several other manufacturers offer 4MW and 4.5MW wind turbines, also with blades in the range of 45m - 60m, and at least the blade manufacturers believe that the limit has not yet been reached. During the development through the 80's and 90's, many critical issues have been solved, so that we now have reliable highly automated wind turbines that even can act together in large wind farms and participate in active power regulation as known from conventional centralised power plants.

The development in the last 10 years has been explosive. Many manufacturers competed to be the first with a certain turbine size, and as a result in some cases, the progress

was highly initiated by the market. Solutions that, due to stressed time schedules, have been forced and rushed through by marketing and sales personnel might not be the optimal solutions from a technical point of view. This is the case on major parts as gears, generators, dry type transformers and even the lightning protection of wind turbine blades. In general, the problem is that technical solutions which, over time, have proven to be reliable on small land based wind turbines, cannot just be scaled up and placed at offshore locations in a harsher environment.

Especially wind turbine blades have experienced a large development. Up til the late 80's, wind turbine blades were regarded as just a mechanical component. The only purpose was to convert the kinetic energy in the wind to rotational energy on the main shaft. This demand was satisfied by constructing blades of wood or glass fibre reinforced polymers, which gave good aero dynamical properties and a construction that could withstand the wear during the lifetime of the wind turbine. In the early 90's where blades exceeded lengths of 20m-30m, direct lightning strikes to the blades became an increasing issue. It was difficult to accept since the materials used for construction were electrically insulating, but as a result Danish engineers in particular, within the wind turbine industry began developing a suitable lightning protection system. The work was summed up in 1999 in *DEFU Rekomendation 25* which deals with all aspects of lightning protection of blades, control systems, bearings etc. [4].

The problems seemed to be solved at that time, and the results and guidelines were published internationally in 2002 in a technical report in the IEC, *IEC TR 61400-24 Wind turbine generator systems – Part 24: Lightning Protection* [5]. This technical report gives guidelines on how to integrate the different parts of a lightning protection system on a wind turbine in order to obtain the highest reliability. Since the work leading to this report took several years (it was published nearly ten years after the problems arose) the technical committee has given some comments on recommended future work. It is emphasised that future standards must cover structures exceeding 100m-150m in height and placed at offshore locations. Furthermore, issues regarding lightning protection of blades must be investigated, particularly how lightning interacts with the installed air terminations, the receptor efficiency.

Based on these considerations, a large PSO funded project was established in 2002 involving Danish power utilities and research institutes. The aim was to investigate how wind turbine blades are affected by the electrical environment during a thunderstorm or a lightning strike, how to avoid damages initiated by lightning discharges and finally, how to verify or test that the blade design or the lightning protection system installed by the manufacturer can handle the effects resulting from a direct lightning strike. The project was initiated in September 2002 with a MSc thesis entitled *Lynbeskyttelse af Vindmøller* (Lighting protection of Wind turbines) [6], and followed by the present PhD thesis from March 2003 until March 2006. As well as the PhD thesis several MSc and BSc projects were initiated, all with the above stated issues in mind.

1.1 Large turbines placed at offshore locations

As discussed previously, the size of modern wind turbines is increasing worldwide. This has made it difficult to find land based locations, why manufacturers in the early 90's began creating the first off shore wind turbine farms, starting with Vindeby in Denmark [7]. In 2002 Elsam Engineering, and Vestas Wind Systems lifted offshore wind farms to a

new level by creating the world's largest wind farm of 160MW [8]. The wind farm (Horns Rev) consists of eighty V80-2MW wind turbines placed 20km off shore and connected to the electrical power grid in a single point. It was the first of its kind, and due to the highly complex design, it is capable of participating in regulation of active power as the case with conventional centralised power plants. Offshore wind farms have also been a focus area in the rest of Northern Europe lately. Until now, 587MW on 16 different sites have been installed and more than 30GW are planned in the near future [7].

Taking Horns Rev as an example, the 80 turbines are placed on an area of app. 20km^2 [8]. Before installation of the wind farm, the average ground flash density was approximately 0.3 strikes per km^2 per year. By calculating the equivalent collection area, an estimation of 6 strikes to the wind farm per year was expected [6]. Experience has shown quite a different situation, where more than fifty strikes per year has occurred. It is also obvious that placing grounded structures of 110m height on open sea will increase the risk of having direct lightning strikes to the structures.

In IEC TR 61400-24 the cost and probability of failures due to lightning is discussed. Based on experience from German, Swedish and Danish databases from the years 1990-1998 it is clear that the most frequent damages happens to the blades, which are also the most expensive single components, and the components where repair or replacement results in the longest outage time [5]. Since many of the largest offshore wind farms have been built after the technical report was published, it is expected that this trend of blades causing the largest problems has increased ever since.

1.2 Experiences from other industries

Lightning has always been a great issue for the avionics industry, and today it is a rule of thumb that commercial aircrafts are struck averagely once a year [9]. Lightning strikes to aircrafts usually happen during takeoff or landing, and constitutes of both cloud to cloud and cloud to ground flashes. One of the reasons that this average number is not higher is that aircrafts can avoid thunderstorms simply by selecting a different route.

Large commercial aircrafts are mostly made with a conductive skin (aluminium alloy) so that a lightning strike basically enters and exits through this surface. The current flows in the surface layer which acts as a faraday cage surrounding the interior wiring. The only insulating surfaces that interrupt this perfect outer boundary are the windshield, the passenger windows, the radar dome, other antenna coverings etc. These have to be protected by means of sufficient thicknesses or lightning diverter strips in the case of a radome.

The outer skins of smaller aircrafts are typically made of glass or carbon fibre reinforced polymers. Materials like these can be sufficiently protected against a single direct strike by means of applying a conductive skin on the surface. The conductive skin might act as an attachment point for the lighting current, resulting in extensive resistive heating. Due to the thickness of the layer, the skin surrounding the attachment point evaporates, and draws the arc root out to a larger area. The heating of the underlying structure is thereby minimised so that the mechanical structure will be unaffected. When the aircraft lands, the damages can easily be inspected and repaired if necessary. On modern wind turbine blades, on the other hand, the lighting protection system is expected to work without maintenance during the entire lifetime of the turbine, 20 years or more.

In this thesis, it is discussed to which extent the protective measures used in the avionics industry can be incorporated in the wind turbine blade manufacturing.

1.3 Material optimisation versus lightning protection

When trying to minimise the frequency of lightning related damages to wind turbine blades, it is necessary to analyze both internal and external conditions. Internal conditions cover the construction of the blade and the material compositions used, whereas external condition would be the different weather conditions experienced by the blade.

By selecting appropriate materials and combining them in a suitable manner, the manufacturer can optimise the ability of the construction to withstand these electrical discharges. This can be done by improving the dielectric breakdown strength of insulating materials, by considering how the electric field will act upon conductive elements in the blade and try to foresee from where streamers and leaders will be initiated prior to a lightning discharge. All these relations can to a certain extent be considered and incorporated during design and construction of the blade.

In addition to this, it is possible to apply different lightning protective measures. These systems are either installed during manufacturing of the blade or applied as a retrofit and are supposed to protect the blades from damages related to direct lightning strikes. Most often the systems can be divided into two parts, a lightning attachment point and a lightning down conductor.

The attachment point is where the lightning channel is supposed to attach to the structure. On wind turbine blades it is often desired that this attachment point stays the same during conduction of the lightning current. The lightning engineer can, in this case, design the attachment point or receptor to handle the current and charge transfer during a strike.

Once the lighting attachment point has been defined, the current must be conducted safely towards ground. This is done along the down conductor, which can be installed in several different ways. The majority of all blades are equipped with an internal down conductor made of a metal wire with a sufficient cross sectional area, while other solutions are based on a conductive mesh attached to the outer surface of the blade. Recently many new solutions have been presented, especially since carbon fibres have been introduced. Some solutions even combine the two parts, such that the down conductor can act as an attachment point as well.

The external parameters cover the weather conditions met by the wind turbine blade during fine weather as well as the electrical field experienced during severe thunder storms. Many books and articles have been published on the matter regarding lightning protection of avionics and land based structures, so the aim of this thesis is to apply the knowledge on wind turbines, and especially wind turbine blades.

1.4 The present thesis

As described above, wind turbine blades are complex structures designed primarily with the mechanical properties in mind. They must have superior aero dynamical properties, be lightweight, and strong enough to withstand the short duration load at a gust of wind and the wear during the lifetime of the turbine. To optimise the construction, the variety of materials and constructions suitable is very narrow, and leaves only very few

parameters left for optimising the overall lightning protection. Based on these considerations, one of the two main questions treated in this thesis is:

Which parameters can be optimised in the production procedure of blades based on common technology, in order to improve resistance towards electrical discharges?

For a conventional wind turbine blade installed with a common lightning protection system, the optimisation of certain design and material parameters will improve the overall lightning protection efficiency. Despite this qualitatively statement, it is still important to verify and compare different solutions of the lightning protection system considered. This calls for considerations regarding test methods and principles, covered by the second main question:

How are blades to be tested in order to verify the blade design and the installed lightning protection system?

In close cooperation with Danish wind turbine blade manufacturers, the principles and different designs are investigated. By knowing the materials and the considerations upon which they are selected, a dialogue with the manufacturer is established. This dialogue will reveal certain focus areas in the manufacturing process, where minor adjustments can be introduced.

Besides these theoretical considerations, it is important to verify the suggestions by means of testing in the high voltage laboratory. These tests cover both materials testing in the optimisation process, and experiences with full scale tests on blade tips etc.

Chapter 2

Wind turbines

To place lightning protection of wind turbine blades in a larger context, this section has been written to give a very short overview of the very complex machine, the modern wind turbine. Secondly different principles for lightning protection of composite materials are introduced, and discussed to which extent they can be applied to wind turbine blades.

2.1 Wind turbines in general

The main purpose of a wind turbine is to transform the kinetic energy in the moving air to a desired energy favour. This energy favour has changed during the past 150 years, from the need of milling grains to flour or pumping water for farming to the needs today where a wind turbine must produce electricity at the lowest possible cost with the highest possible reliability. Since 1991 when the first offshore wind farm was built at Vindeby in Denmark [7], there has been an increased focus on making numerous turbines act together as an entire power plant. The result so far is that large offshore wind farms such as Horns Rev [8] can participate in voltage and frequency regulation just as a conventional centralised power plant. Furthermore, this regulation can be performed at a much faster pace, such that the production at Horns Rev can be regulated from zero to full load within less than ten seconds [10].

Several designs of wind turbines have been introduced by different manufacturers. These range from gearless models with variable rotor speed ([11] and [12]) through Vestas' newest model where the rotor is mounted directly on the gearbox [13] to the majority of all modern wind turbines having the rotor mounted on a main shaft connected to the gearbox. The specific design of gearbox and generator also varies among the different manufacturers, subjects not covered by this thesis.

The following gives a very brief description of the three major parts of a typical modern wind turbine.

2.1.1 Rotor

The assembly of the three blades called the rotor is mounted on the main shaft [14], the gearbox [13] or directly on the generator [12] depending on the specific model. On modern wind turbines the rotor and the blades are not just passive components. The blades can be pitched at different angles depending on the wind speed and production demand, they contain measurement systems capable of monitoring mechanical strain and stress, and they are sometimes equipped with lightning sensors identifying peak currents and specific energies. All these features are powered and handled by hydraulics, electricity and digital communication, which is fed through advanced couplings from the stationary nacelle to the rotating hub.

2.1.2 Nacelle

The nacelle contains the power conversion from the rotational energy at the main shaft to the electrical energy where the power cables exits. The main shaft is typically fixed by main bearings and is connected either directly or through a clutch to the gearbox. To stop the turbine ordinarily, the blades are pitched 90 degrees with respect to the wind direction. As an emergency, all turbines are also equipped with a mechanical brake, usually at the high speed side of the transmission. Electrical power is generated by the generator, until now, mostly at voltages not exceeding 1000V. The current at this potential is either conducted through low voltage cables to a transformer at the bottom of the tower, or transformed to medium voltage by a transformer in the nacelle. Besides these main components, the nacelle might contain switchgear and a lot of control and monitoring facilities to act upon wind speed and direction, temperatures, humidity, voltage quality etc. The nacelle is mounted on the tower via the yaw bearing.

2.1.3 Tower

The tower is usually made of steel and mounted on a basement depending on the specific erection site (concrete, tripod, monopile, etc.). Due to the size, the tower is usually constructed by several sections bolted together along interior flanges. The power cables from the nacelle (as well as several communication links) are guided freely across the yaw bearing through the top section of the tower allowing the nacelle to turn relative to the tower. Switchgear and excessive control systems are typically placed on a platform at the bottom of the tower as well as a transformer in case of low voltage power cables from the nacelle.

Further detailed information can be found on the different manufacturers' homepages [11-18] or by contacting the Danish Wind Industry Association [19].

2.2 Wind turbine blades

The design of wind turbine blades has changed a lot since the early wind rotors used on farms for pumping water or grinding flour. When the three bladed rotors were introduced fifty years ago, the blades were initially massive and made of wood. The size of turbines and the length of blades have increased ever since, such that the design had to focus more on weight issues. This resulted in the construction of hollow blades with a wooden structure covered by a skin of wood laminate, and finally, by the introduction of composite materials as glass fibre reinforced polymers (GFRP). Recently carbon fibre composites (CFC) have been used on large blades, due to the light weight and the stiffness compared to GFRP. Not only the use of materials has been improved, also the principle from stall regulated to pitch regulated blades has changed.

Modern blade design must reflect considerations and be optimised with respect to the aerodynamics, the weight, the stiffness, the flexibility and the cost efficiency. By combining these features and stretching the individual materials to their limits, modern blades now contain glass and carbon reinforced plastics, light weight balsa wood, polymer foam, dynamic damping weights, different monitoring sensors, etc.

A good example of excessive mechanical engineering is the LM 61.5 P blade, more than 60m long, weighing in excess of 17 tons, pre-bent to optimise the swept area and built to withstand the wear and tear over a lifetime of 20 years [15].

2.3 Lightning protection, success criteria

The evolution of these wind turbines has happened very rapidly. During the development, many issues have caused problems and been solved along the way. Regarding lightning protection it is suggested to treat the exterior of the nacelle and the tower as a single faraday cage. Within this boundary the different components are divided into Lightning Protective Zones (LPZ) depending on the internal connections and the threat from lightning [5]. Each time a possible path for the lightning transient or surge passes across an interface between two LPZ, the amplitude and frequency of these surges must be limited to an acceptable level.

The blades are the most exposed structures on the wind turbine and are therefore assigned to be in the zone having the harshest environment, the LPZ0. This means they must tolerate the attachment of a direct lightning strike, and be capable of conducting the full lightning current safely towards ground. When manufacturing wind turbine blades, the lightning engineer must account for the different lightning parameters (current, current gradient, charge, specific energy, etc.) and aim at a solution that handles all the influences without damages during the lifetime of the turbine.

2.4 Lightning protection of composite materials

The reason for using composite materials in these applications is mostly due to the mechanical properties. Depending on the composition of the resin and fibre reinforcement, it is possible to construct a material with many desirable properties, which in general is very light in weight compared to metal structures with the same strength.

When wind turbine blades exceeded a certain size, it was a natural choice to use GFRP due to the above mentioned mechanical properties. The choice was primarily based on static and dynamic mechanical calculations, while the electrical properties were of minor concern. As a matter of fact the good insulating properties were regarded as an advantage, since lightning, according to common understanding, is attracted to metallic structures such that GFRP would be invisible to the lightning discharge. This assumption led to the manufacturing of wind turbine blades without any conducting parts. However, these blades were also hit occasionally and followed by fatal damages. Now experience and research have shown that despite the insulating characteristics of composite materials on new blades, the situation might change during the lifetime of the blade often depending on external environmental conditions.

GFRP materials on wind turbine blades, as well as radar domes on aircrafts, are subjected to a certain probability of direct lightning strikes. Depending on the protection applied, a sudden amount of these incidents results in punctures of the ‘skin’. In severe cases the puncture is followed by a large area with delamination, which decreases the mechanical strength of the structure [9].

Both constructions are hollow structures, containing conductive components in the presence of a radar antenna or a down conductor and polluted moist. Very early in the development of lightning protection of composite materials, it was realised that the physical damages are minimised when the current path is kept on the exterior surface or in the uppermost layer of the composite. In this way internal arcing is avoided, a situation responsible for the rapid pressure rise and crucial delamination, section 3.2.2.

Considering carbon fibre composites, several experiments on different laboratories indicates that the large current density at the arc root, combined with the high resistivity of the materials, results in dissipation of a great amount of energy. The release of this energy causes the material to delaminate and, in some cases, even evaporation of resin and fibres are evident. Both of these situations might be crucial to the mechanical strength of the structure.

Especially within the Avionics industry, there have been several attempts to protect composite materials from the effect of lightning currents. These attempts are both macroscopic, where the electrical conductivity of the final GFRP structure is increased by introducing a conducting layer on the whole structure, and microscopic, where the material itself is improved by adjusting the properties of the different parts of the composite.

The principle of protection can be divided into two categories:

1. Minimising the heat generation in vicinity of the arc root.
2. Conducting the current safely towards ground, possibly through metallic structures capable of carrying the current.

In the following sections, the different protection measures are described. Many of the principles have been developed and used by the avionics industry [9], why the application with respect to wind turbine blades is discussed in each case.

2.4.1 Air termination and down conductor

This principle is originally used in lightning protection of buildings and comprises a distinction between an air termination where the lightning should attach, and a down conductor responsible for conducting the current from the air termination towards ground potential.

The air termination or ‘receptor’ in the case of a wind turbine blade has to penetrate the insulating skin of the blade. Since the blade is optimised with respect to the mechanical properties, there is a limit of how many mechanically degrading penetrations that can be accepted. In the recommendations from 1999 it is advised to apply receptors from radius 20m to the blade tip, evenly spaced with a distance of 5m between each [4]. Although receptors are designed to handle the current and charge transfer, minor wear and pit marks are typically visible after a few years of service.

2.4.1.1 External/internal down conductor

Once the lightning has attached to the receptor, the current and charge must be conducted towards ground. This is usually done by connecting the receptors to one or more down conductors, either located internally in the hollow structure or attached to the external surface of the blades. One of the dimensioning criteria for this conductor is to keep the temperature rise due to ohmic losses within reasonable limits [5].

Large turbine blades are very flexible, which introduces the second issue with this solution. The fastening must be rigid enough to handle both the mechanical forces during normal blade operation and the magnetic forces during lightning strikes. An obvious solution to this matter is to use a stranded conductor fastened to the centre line of the blade beam.

A minimum cross sectional area acceptable for conducting the current is in standards given as 16mm² for copper and 25mm² for aluminium down conductors [5]. This is due to the mechanical requirements increased to 50mm² for stranded conductors of either cobber or aluminium.

When selecting a specific conductor to this application the inductance per metre length must be considered, since inductive voltage drops may cause side flashes along the current path. This requires additional equipotential bonding along parallel current paths (down conductor, CFC structural components, control wires, etc.). The combination of an inner down conductor and surface mounted receptors is described in section 3.2, where a case considering lightning discharges to a modern wind turbine blade is described.

Since receptors, as well as internal down conductors, emit streamers prior to lightning attachment, some manufacturers have decided to place the down conductor on the external surface of the blade. This way they tend to avoid streamer formation from interior parts of the blade, which sometimes lead to puncture and fatal lightning damage, section 3.2. Introduction of external down conductors may, however, change the aero dynamical behaviour in a way that results in decreased efficiency and an increased noise level.

2.4.1.2 Diverter strips

A well known method for lightning protection of radomes on aircrafts is application of solid or segmented diverter strips [9]. Solid diverter strips act as an extension of the metal airframe to cover the exposed parts of the radome. The basic idea is that the solid diverter shields the conductive radar antenna underneath the radome and emits the streamers and leaders towards the lightning leader approaching the structure. Once attachment on the solid diverter strip has been decided, the solid bar conducts the current towards the airframe. Although the solutions seem pretty suitable from an electrical point of view, the fastening of conductive bars on smooth surfaces disturb the aerodynamic properties.

Segmented diverter strips are realised as tapes applied on the surface of the radome in which several metal buttons (app. diameter 1.5mm-5mm) are fastened with mutual distances of app. 0.13mm-0.26mm. The high electric field in the initial phase of a lightning strike ionises the gaps between neighbouring buttons, producing conductive plasma just above the diverter strip. Thereby a conductive channel between the lightning attachment point and the metallic airframe has been established, allowing the current to flow above the surface intentionally without significant damage [9].

Segmented diverter strips also affect the aerodynamical properties in a negative manner. They must be attached directly onto the surface, and will, as was evident for the solid diverter, decrease the overall efficiency. A patent has recently been filed to solve this issue, where the performance of segmented diverter strips covered with an insulating layer was tested. The research indicates that the interception efficiency can be maintained even if the segmented diverter strip is covered by a very thin layer of insulation. This allows the diverter strip to be incorporated in the design of the final surface, and even covered with the finishing coating or paint, ensuring smooth surfaces.

One criterion which must be fulfilled to make the diverter strips function is that the individual buttons must be electrically insulated. An exemption is that some types are shorted with a highly resistive compound to remove static charges due to precipitation, which fortunately does not affect the behaviour during transient fields. The cleaning of

aircraft surfaces is a scheduled maintenance, ensuring that the insulation level between neighbouring buttons is maintained. Considering wind turbines, it is questioned whether dirt and impurities deposited over time will change the behaviour of such diverter strips.

The only application of this technology in the wind turbine blade industry known to the author is the lightning protection of the LM 61.5 P blade from LM Glasfiber [15]. Here the specially developed segmented diverter strips act as an extension of the discrete lightning receptors, covering the otherwise exposed carbon fibre sections within the blade. LM Glasfiber reports only good experiences with the blades which have been in service on a REpower 5M wind turbine since February 2005.

2.4.2 Temperature rise associated with conductive materials or surfaces

One way of minimising the heat generated in vicinity of the arc root is, as mentioned earlier, to use a solid conductor as attachment point. The attachment point is susceptible to both heating and melting due to the specific energy of the current and to melting or pitting on the surface due to the charge transfer. By using a suitable material and selecting an appropriate design of the lightning receptor, these two issues can be minimised. In case of severe lightning strikes, most receptors are even replaceable on site.

Occasionally lightning tends to attach to insulating surfaces elsewhere than the intended air terminations. This was first realised by the avionics industry [9], and has certainly been an issue to the wind turbine blades as well, section 3.2.2. Since receptors apparently do not secure the entire surface, an obvious approach was to alter the materials for blade skins towards a more conductive nature, or alternatively, to apply a conductive surface on top of the insulating structure.

The lightning attachment process is straight forward with this solution, since streamers and leaders are easily emitted from all areas of the protected structure. Following the lightning attachment comes the conduction of the lightning current which is a situation where several kA's enter a thin conductive surface at an area of a few cm².

To illustrate the matter of temperature rise in vicinity of the arc root, a simple calculation is performed. Figure 2.1 shows how a 0.01mm thin copper foil measuring 1m x 1m is affected by a lightning current injected in the centre of the specimen containing a specific energy of 2MJ/Ω. The copper foil is regarded isotropic with temperature dependant resistivity, and the process adiabatic.

The very simple calculation shows that the temperature of the copper foil exceeds the melting temperature at a radius of 7.8cm from the arc root. If the enthalpy of fusion is incorporated analytically, the radius of evaporation increases to 11.6cm [20].

Increasing the surface conductivity of composite materials is widely used in lightning protection of small aircrafts. Here the evaporation of the protective meshes in vicinity of the attachment point is part of the design, thereby affecting the underlying structure on a wider area. Deterioration of the surface is evident, but since the aircraft easily is taken out of service for inspection and maintenance, the damage is acceptable. The applicability of this principle towards wind turbine blades is however doubtful. It is not possible within reasonable economics to take down a blade for inspection, and if necessary, repair the damages. Therefore the lightning protection must be of a kind that doesn't degrade over time and possess a great reliability.

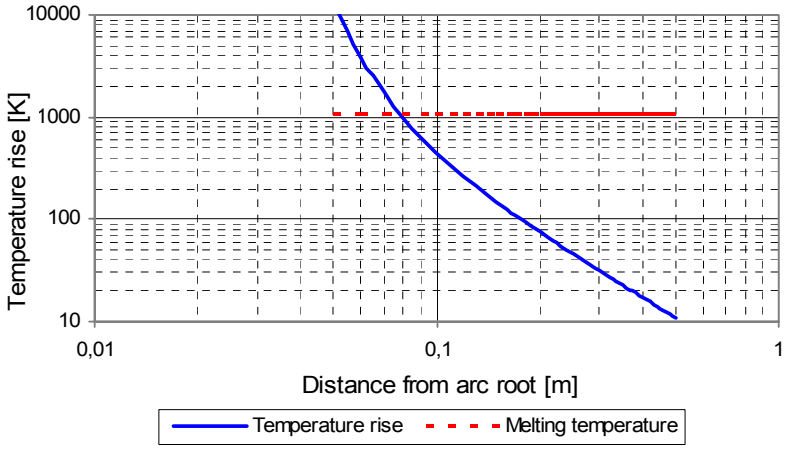

Figure 2.1 Temperature rise in a 0.01mm thin copper foil as a result of arc injection of a lightning current with a specific energy of 2MJ/Ω. The copper foil is regarded isotropic with temperature dependant resistivity, and the process adiabatic.

2.4.3 Conductive materials

'Conductive materials' covers the situation where otherwise insulating composite materials are made partially conducting by using special fibres, or weaving in metal wires etc.

2.4.3.1 Interwoven wires

Interwoven wires as a mean of lightning protection were initially developed for protection of carbon fibre composites. Due to the partly conductive nature of CFC, a lightning discharge usually attaches to a confined area of a few cm². The resulting high current density tends to vaporise the resin and cause delamination on a wide area of the surface. Furthermore, the depth of damage could be several plies depending on the severity of the impact. By weaving in thin metal wires in a manner such that the wires appears periodically at the surface, all the protrusions will emit streamers at the electric field present prior to a lightning strike. In case of subsequent attachment, the arc root is dispersed across a larger area, minimising the current density and hence the damage of the carbon fibre plies [9].

The interwoven wire solution is integrated in the manufacturing of the upper most ply in the composite material making it very flexible regarding complex geometries. If weight issues are of great concern, this solution is also suitable since typically the constructions only add weight in the order of 10-60 g/m² using aluminium wires [9] and [21]. However, laboratory research, as well as in flight experience, have shown that the protection only serves as a single shot protection, such that a surface subjected to a direct lightning attachment must be repaired afterwards. This disqualifies the solution regarding the wind turbine blade industry.

2.4.3.2 Internal coated fibres

Instead of weaving in additional conductive wires in the insulating composite, the individual glass fibres in the upper most ply can be coated with a conductive aluminium alloy [8]. This kind of protection is commercially available and changes the highly insulating nature of GFRP towards a more conductive material. The attachment point of the lightning discharge may suffer from extensive heating and rise of pressure from the vaporised aluminium. If coating or paint is applied above the ply of aluminised fibres, the damage tends to spread inwards to GFRP layers below the protection ply. Experiments have shown that the damage tends to be more pronounced for GFRP covered with a ply of coated fibres, compared to the solution described below with the GFRP protected by expanded foil or similar.

Again the need of frequent repairing disqualifies this solution for a wind turbine blade.

2.4.4 Conductive surfaces

Since many composite materials (GFRP and CFC) are too insulating to handle lightning currents, a way of avoiding puncture and excessive delamination is to keep the current at the surface by making the surface conductive.

2.4.4.1 Coated surfaces and conductive paints

Protection of both GFRP and CFC can be obtained by spraying a molten metal surface on the structure [9]. This results in a very continuous and conductive surface which enables attachment and conduction of full threat lightning currents. The only drawbacks are the cost of the spraying process and the weight issues, since thicknesses of 0.1-0.2 mm are usually required.

Adding metal particles to the coating or paint is another approach, although the surface conductivity is far less compared to a molten metal surface. The conductivity is only achieved due to random contact between neighbouring particles, such that the coating merely acts to guide a flashover towards a more conducting path. If conductive components are present below the conductive paint, voltage drops along the surface flashover might be sufficient to cause a puncture of the insulating laminate [9].

Considering the size of modern wind turbine blades, the molten metal surface is regarded as being too expensive and the conductive paint too inefficient.

2.4.4.2 Solid metal foil

Solid metal foils applied on top of insulating surfaces give some protection from direct lightning strikes. Depending on the thickness of the foil and the specific energy of the lightning current, more or less of the foil tends to vaporise in vicinity of the arc root. As being part of the design, the spreading of the arc root minimises the thermal effects on the underlying GFRP structure. Some of the drawbacks include difficulties in making a solid foil drape around complex geometries, so that cutting and overlapping often is required. Moreover, the smooth characteristic of a metal surface makes it difficult to be properly attached to the insulating surface considered. As discussed previously, wind turbine blades are very flexible, making interaction with a solid metal foil difficult.

2.4.4.3 Woven meshes and expanded foil

By weaving a fine mesh of metal wires, a conductive layer that can easily be interacted in the manufacturing process is obtained [9]. The mesh gives a good protection from all lightning environments (depending on the coarseness and dimensions of the wires), but has, as the solid metal foil solution difficulties, in complying with complex geometries. Regarding the application towards large structures as wind turbine blades, it is believed that bonding a woven mesh on the surface of a GFRP laminate would be much easier than the solid foil solution.

Expanded foil is a product of a process in which numerous slits are cut in a solid foil whereafter the sheath is stretched, forming an electrically continuous structure [9]. The materials and coarseness of the expanded foil are custom selected, so that conductivity and cross sectional area in either direction are selected to the specific task. Expanded foils are widely used within the avionics industry in protection of composite materials, and generally exhibit better performances than woven meshes and solid foils.

Vaporisation in vicinity of the arc root is still an issue, but compared to the solid foil, arc dispersion is more pronounced considering expanded foil. Depending on the thickness of insulating coating or paint applied on top of the expanded foil, the damage to be expected at the arc root varies. In general, all solutions considering conductive surfaces should be left fully exposed to minimise the damage associated with direct lightning attachment.

Considering the edges on conductive foils, the electric field experienced by the mesh would be greatly enhanced due to the sharp geometry. For this reason it is expected that lightning discharges to the mesh often will be initiated from streamers originating at the edges. When lightning attaches to these places, initially only half the amount of material is available for current and heat conduction until the current has been distributed across the entire cross section. This might lead to unforeseen damage.

Although the solutions have been used with success in avionics applications, the wind turbine industry still aims at a protection method for blades not requiring frequent maintenance. Many research projects have shown that damage to the underlying CFC is a fact, almost regardless the effective cross sectional area of the mesh. This is partly due to the arc movement of continuing currents and attachment to CFC where the mesh above has been vaporised [22] and [23].

2.4.4.4 Conductive tape

A variety of the expanded foil is a tape especially used for retrofitting a lightning protection system on unprotected blades [24]. By manufacturing a strip of expanded foil (app. 150mm wide in infinite lengths) with a strong adhesive, the result is a conductive tape glued directly onto the blade surface. With respect to initially unprotected blades, the solution might offer some protection from minor lightning discharges, whereas it is expected that more energetic discharges would require replacement of the tape [5].

2.5 Current status on lightning protection

In the early days of lightning protection of wind turbine blades, it was simply done by placing a discrete air termination (the lighting receptor) in the tip area, and connecting this

attachment point to an inner down conductor, grounded safely on the flange of the root end of the blade. The idea was inspired by common protection methods of buildings and other land based structures and assumed that the lightning discharge would attach to the receptor and be conducted safely along the down conductor towards the grounded flange.

Several designs of down conductors and receptors were tried, and the experience showed that the principle worked for shorter blades with lengths up to 20m-30m. For larger blades it was suggested placing further receptors along the length of the blade, in compliance with the rolling sphere theory. In all cases, the lightning protection was treated as an add-on to the mechanical structure [5].

Recently the lightning protection has become an integrated part of the blade. This has happened due to an increased focus from both industry and custumers. The fatal lightning damages evident for blades larger than 30m was explained by changes in lightning attachment physics. These lightning attachment processes have been described in literature for static land based structures, with total heights not exceeding 60m. The protection measures have been adopted by international standard committees, so that several IEC standards describe how to assess the risk and install the protection. For offshore installations with heights exceeding 60m, there have not yet been published any official documents describing the lightning physics and the protection measures, so that designers, manufacturers, owners and insurance companies must define their own practices regarding large offshore wind turbines.

In addition to this, it has been realised that the blades can not be regarded solemnly as homogeneous insulating structures, due to the presence of moisture, dirt and partly conductive materials like CFC. The effects of these components are described more thoroughly in Chapter 3 and Chapter 4.

Chapter 3

Electrical environment and lightning discharges

In this chapter is given an overview of lightning physics and relevant parameters of discharges occasionally affecting wind turbines. Secondly lightning attachment to a modern wind turbine blade is treated on a macroscopic basis giving examples of lightning attachment processes and consequences. Finally some recent published numerical methods for predicting possible attachment points are presented.

3.1 Lightning theory

To predict the risk of having direct lightning strikes to a wind turbine, the electrical environment surrounding the structure must be analysed. Theories regarding atmospheric electrical discharges have been of interest since the first lighting strikes were observed. Up till the eighteenth century [25] it was more or less believed that thunder and lightning was associated with revenge or anger from respectable Gods. Nowadays scientists have found that it has to do with movement and precipitation of electrical charged particles and establishment of concentrated charge regions in clouds which finally leads to the large electric fields and lightning discharges associated with thunderstorms.

The following sections regarding lightning physics are intended to give a short overview of the mechanisms prior to a lightning strike, which might have an impact on how to construct the wind turbine blade. Several books and articles cover the subject on general lightning physics in details, (Golde, Malan, Uman, Bazelyan, Rakov, etc.) so further information should be sought here.

3.1.1 Charge accumulation

Before any electrical discharge can take place, two separate charges of opposite polarity must be present. This is necessary in laboratory experiments having sparks of a few mm as well as with lightning discharges of several km. In the atmosphere the vertical charge separation happens on behalf of several mechanisms, the constant electrical current from the atmosphere to the earth and local phenomena associated with the formation of thunderclouds.

Around the world there is a constant drift of positive charges from the atmosphere towards the earth. The current density from this phenomenon as well as from vertical currents associated with thunderclouds has been estimated to $2 \cdot 10^{-12}$ A/m² giving an overall charge transfer of 1000 C/s [25].

Despite this global charge transfer, there exist local mechanisms capable of separating charges in a much faster pace. This happens during the creation of cumulonimbus clouds, which is very well described in the literature [25]. Conditions for cumulonimbus clouds are in coastal areas fulfilled when warm and moist air arrives from the see and ascends due to extensive heating of the ground ashore. Due to decrease in temperatures while the air ascends, the moist tend to condensate and form water droplets, still light weight enough to continue their upward motion. At a certain altitude the temperature drops below the freezing point of water, changing the water droplets to ice crystals. The ice crystals are initially still light weight and continue to rise, but once formed they begin to grow and ad weight. Suddenly the ice crystals have reached a size where they are too heavy to continue their up draft, and begin to fall as hail [25].

The precipitation between upward moving water droplets, ice crystals and particles and downward moving hail is believed to result in charge separation. The upward moving particles gain charges of positive polarity which are deposited in the upper part of the cloud whereas the downward moving hail gain charges of negative polarity deposited in the lower part of the cloud. Usually the process and formation of the cumulonimbus cloud takes place during less than an hour, resulting in a charge distribution as seen in Figure 3.1.

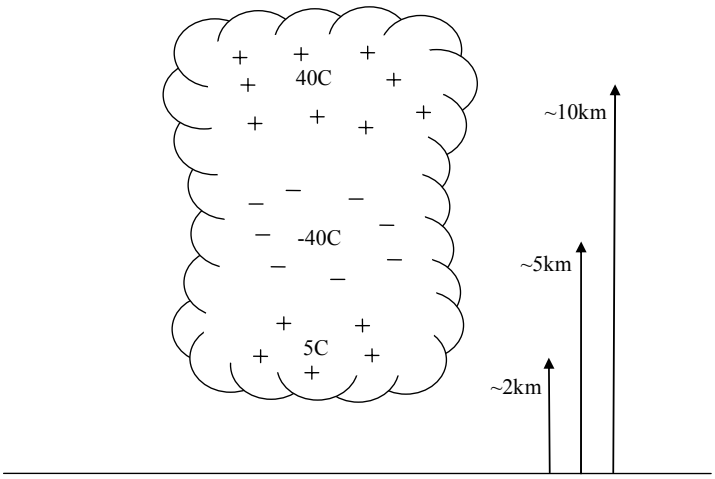

Figure 3.1 Typical charge distribution in cumulonimbus cloud adopted from Uman [25].

3.1.2 Static field and leader initiation

The charge distribution in Figure 3.1 is build up until the electric field surrounding the charges increase to a level where ionisation and partial discharges affect the stability. Once these partial discharges have formed into streamers and, the static electric field driving the leaders is usually high enough to accomplish the short circuit of the two charge centres, the lightning discharge.

The constant vertical downward oriented current distributed somewhat evenly around the world is outbalanced with the cloud to ground discharges. In this way the electric circuit of the atmosphere is complete, and the fine weather electric field of 100V/m is maintained in a longer time perspective [25].

In literature on this subject, the different lighting discharges are divided into categories based on their characteristics (cloud to cloud lightning, cloud to ground lightning, etc.), their polarity with respect to the cloud, the initial leader direction, etc. The mechanisms in the different types are basically the same and discussed below. In this thesis only discharges between cloud and ground are interesting, giving rise to the following four categories:

1. *Downward initiated cloud to ground discharge of negative polarity.*
   When initial leaders are formed from the lower part of the cumulonimbus cloud towards the ground, the discharge is said to have negative polarity (it removes charge from the negatively charged regions in the cloud) and to be downward initiated.
2. *Downward initiated cloud to ground discharge of positive polarity.*
   These discharges begin by leader formation from the upper positively charged regions of the clouds towards the ground.
3. *Upward initiated ground to cloud discharge of negative polarity.*
   Some discharges are upward initiated typically when high structures are present. The electric field surrounding a steel mast on a mountain ridge might be higher than the electric field in the cloud above. This gives rise to an earlier ionisation and thereby leader formation from the grounded structure towards the cloud. The charge neutralised in the cloud still determines weather the discharges is said to be of positive of negative polarity.
4. *Upward initiated ground to cloud discharge of positive polarity.*
   This situation happens when a negatively charged leader from the grounded structure interacts with a positively charged region in the cloud.

Whether an initial leader is upward or downward initiated usually depends on the height of the structure concerned. On flat areas most discharges are downward initiated due to the field smoothening along the ground surface, whereas tall structures results in field enhancements and thereby possible upward initiated leaders. These tall structures would be mountains, towers, high buildings, communication masts, and certainly modern wind turbines.

To visualise how much the electric field is enhanced by tall structures, a simple 3D model of a cumulonimbus cloud is treated. The model is adapted from Uman [25] and consists of a charge concentration of 40C positioned at a height of 10km, -40C positioned at 5km and 5C at a height of 2km. The charges of 40C and -40C are distributed evenly within spheres of a radius of 2km, while the minor positive charge of 5C at the bottom is distributed within a sphere of radius 800m. The plane surface of the ground is assigned a potential of 0V.

By implementing the model in a Finite Element Program and solving Poisson's equation for the entire volume, a 3D plot of the absolute electric field and a 2D slice plot through the vertical axis connecting the three spheres are made, Figure 3.2. Red colours correspond to high field regions and blue colours shows the low electric field regions.

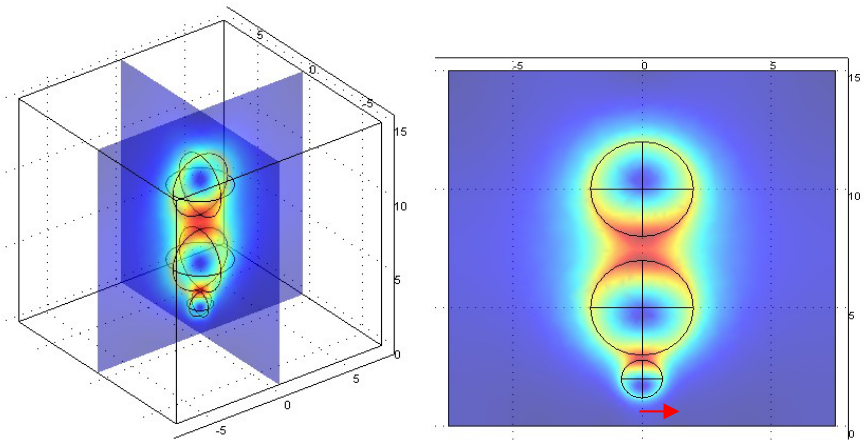

Figure 3.2 Left: A 3D FEM model showing the electric field distribution around a simple model of a cumulonimbus cloud adapted from Uman [25], Right: A plot of the absolute electric field across a plane intersecting the centres of the three spheres, all axis are in km. Red colours show regions with high electric fields whereas blue colours corresponds to low field regions. The red arrow shows the line and direction along which the vertical electric field is calculated.

To compare the two situations with and without a tall structure present, the vertical electric field along a horizontal line 190 m above ground level from a point directly below the charge centres to a point 300 m away is calculated, shown as a red arrow on the right image of Figure 3.2. The electric field is shown as the blue curve on Figure 3.3, where the negative values correspond to the downward oriented field.

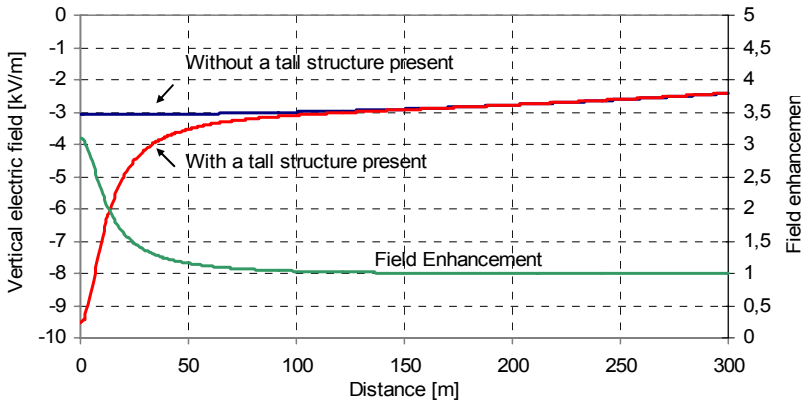

Figure 3.3 Vertical electric field along a horizontal line 190 m above ground level, from a point directly below the charge centres to a point 300 m away on the right image of Figure 3.2.

A second calculation is performed where a wind turbine is placed directly below the charge centres, modelled as a grounded vertical rod with a height of 180m and a diameter of 2m. The end pointing towards the charge centres is rounded with a 1m radius of curva-

ture. By calculating the vertical electric field along the line described previously, the field enhancement as a result of introducing the grounded structure can be found. The vertical electric field with a grounded structure present is shown as the red curve in Figure 3.3, while the field enhancement is shown as the green curve.

As seen on the calculations on Figure 3.3 the tall grounded structure tends to enhance the electric field compared to a situation with a flat ground. Details about the FEM program used are given in Appendix A.

The distribution of positive and negative polarity discharges is different from place to place, and also changes with the season. Some sources have found a correlation between the distribution and the height of structures, such that higher structures are more susceptible to lightning strikes of positive polarity than the average distribution for flat ground dictates [26].

In Denmark nearly 90% of all cloud to ground lightning strikes are negative whereas only the remaining 10% are positive [4]. The positive lightning strikes however are responsible for the largest threat because the energy, current amplitude, charge transfer etc. as discussed later is larger.

Below the different processes regarding streamer and leader initiations are described. The mechanism of atmospheric streamer and leader initiation prior to lightning is somewhat similar to general gas discharge physics except one thing. The formation of short sparks in the laboratory often relies on what is known as secondary electrons. For cathode initiated streamers these electrons are generated by feedback mechanisms, where either positive ions or photons hit the cathode with sufficient energy to cause electron emission. The streamers and leaders associated with long sparks can often origin somewhere inbetween the electrodes, a so called mid gab streamer. A more thoroughly description of matters concerning gas discharges is found in literature [27-30].

When the electric field gets above a certain threshold value the air molecules starts to ionise. This value is app. 3kV/mm for homogeneous electric fields in a controlled standard laboratory environment [27], whereas practical experience from measurements in thunderstorms shows values of somewhere around 0.5kV/mm [9]. Ionisation under these conditions means that electrons are drawn from neutral molecules leaving positively charged ions behind. Both the ions and the electrons are accelerated in the electric field, although the ions seem to rest compared to the acceleration of electrons. The mass of electrons are more than 2000 times smaller than the mass of nucleus, meaning that during the short period of time where these initial steps take place the electrons will gain much higher velocities.

According to general gas discharge physics, the free electrons will gain energy during their acceleration proportional to the mass, the mean free path and the electric field. If the electrons gain sufficient energy in the electric field, they will participate in generation of further electrons. This can happen either through ionisation or excitation of gas molecules, and will eventually create a concentration of electrons moving towards the positive charge centre followed by a tail of conductive plasma of ions and electrons. The conductive channel of plasma extending towards the charge centres will enhance the electric field in the tip even further.

The conception of the leader phenomena concerning lightning discharges has changed during the ongoing research. It is believed that the conduction of current takes place in the leader core with a diameter of a few cm, surrounded by a corona sheath of several meters. The leader head usually contains the majority of the leader charge, such that the corona extends further than just the length of the leader, making the leader head appearing of a larger diameter than the rest of the leader channel [31]. The formation of this preliminary discharge happens in discrete steps, giving rise to the name stepped leader.

One way of explaining this step phenomenon is by regarding the leader as a glow discharge extending downwards with a constant velocity, Figure 3.4. The current in the leader increases continuously with the length of the leader due to the radial current, and once this current exceeds ~1A the glow discharge transform into an arc discharge. This results in an increased conductivity such that the charge in the leader is conducted rapidly to the leader head, giving rise to heat and emission of light.

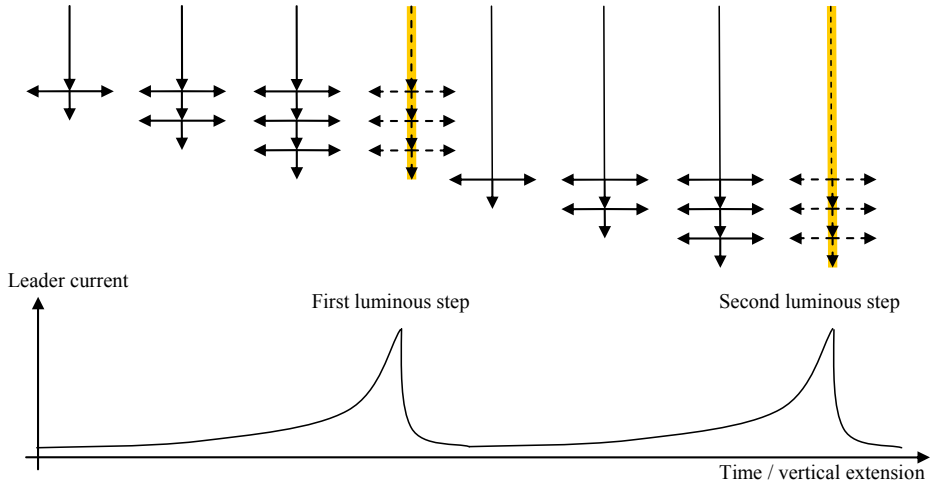

Figure 3.4 The stepped leader phenomenon, where the glow discharge of a constant velocity changes into a more illuminating arc discharge in discrete steps [25].

As the leader approaches the ground, the direction is more and more directed towards grounded structures. The final step where the ground and the charge region in the cloud are shorted is denoted the final jump.

3.1.3 Final jump

The final jump describes the situation when the leader tip has reached a certain distance of a grounded structure such that the attachment point is determined. When this happens the structure emits an answering leader which must traverse this striking distance in order to accomplish the final short circuiting of cloud and structure. This means that the attachment point for the lighting strike is determined before any particular current is conducted, explaining that not only metallic conductors can emit answering leaders. This fact

is commented more thoroughly when looking at the interaction between discharges and with turbine blades.

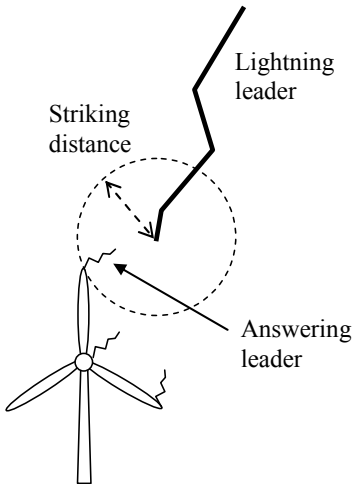

Figure 3.5 Striking distance to a wind turbine.

Measurements and video recordings of 89 negative lightning strikes to different objects, has revealed a correlation between the charge transferred in what is known as the first return stroke, the peak amplitude of the current pulse, and the striking distance [25].

$$\begin{aligned} I &= 10.6 \cdot Q^{0.7} \\ d_s &= 10 \cdot I^{0.65} \end{aligned} \tag{3.1}$$

Where 'I' is the peak current measured in kA, 'Q' is the charge transferred within the first return stroke measured in C and 'd_s' is the striking distance measured in m.

These formulas predict how close a leader needs to get to the grounded object, before the attachment point is decided. The information is used in designing lightning protection principles, for instance the rolling sphere method, protective mesh, protective angle, etc.

Taking the rolling sphere method as an example, a protection level II is reached if a sphere of radius 30m can be rolled around the structure, and only touch air terminations capable of handling a direct lightning strike. Protection level II promises a lightning protection efficiency of 95%, meaning that 95% of all lightning strikes will attach to the designed air terminations. This corresponds to the 95%-fraction of the cumulative distribution of the current amplitude of lightning strikes, where 95% of all positive lighting strikes have current amplitudes in excess of 4.6kA [32]. Using the formulas described by Uman [25], makes it possible to calculate the corresponding striking distances to app. 25m. For lightning strikes having lower current amplitude, the striking distance is shorter. The protection level II can in other words not guarantee protection against impacts from these lightning strikes.

Protection of insulating structures placed at offshore and polluted locations makes knowledge about the final jump situation very important. It is crucial to know that insu-

lated surfaces polluted with partly conductive contaminants, are able to participate in the generation of answering leaders as well.

3.1.4 Parameters of a lightning strike

During the last 60 years, a lot of lightning data has been collected. Since lightning strikes to flat surfaces happen pretty randomly, much of the data are from measurements on high towers, communication masts or by rocket triggered lightning [25]. There are some questions on how these structures affect the measurements and the phenomena, some of which are solved by correlating with data obtained from lightning location systems. These systems are installed many places world wide and are capable of measuring amplitude and polarity of lightning strikes to all possible areas.

A lightning strike is composed of several different components. Once ‘the answering leader’ has connected to ‘the lightning leader’, the first return stroke occurs. The first return stroke contains the highest specific energy, and results in the sudden temperature rise of the lightning channel, the flash and the audible thunder. The charge present in the leader head and the rest of the lightning leader is neutralised by this return stroke.

The first return stroke of a negative lightning strike is usually followed by subsequent strokes, which occurs some tens of milliseconds later. The subsequent strokes are of lower amplitude and specific energy than the first return stroke, but usually have higher current gradients, meaning higher inductive voltage drops along metallic conductors subjected to the lightning current. Subsequent strokes occur when new charge regions in the cloud are connected and neutralised by the lightning channel, something happening 1-20 times each lightning strike.

During the flash, the sequence is sometimes accompanied by a continuing current. This current with amplitude of a couple of hundreds of amperes can last up to a second, and is responsible for the primary charge transfer. The primary threat from this component concerns melting of the lightning attachment point.

A structure that is hit by lightning will suffer differently from the different components. The first return stroke is responsible for the major part of the specific energy, the energy that causes resistive heating of the current path (lightning down conductors etc.). Magnetic forces surrounding parallel conductors are also dependant on the current amplitude and time duration, making mechanical rupture susceptible to the first return stroke. The subsequent strokes usually have very steep current gradients such that inductive voltage drops along conductors can lead to side flashes. The continuing current can discharge several hundreds of coulombs making the attachment point very critical. Materials with high melting temperatures and specific heat capacities are most suitable for air terminations.

The available data of lightning current parameters has been collected during many years from all over the world. The rather large amount of data has been treated statistically by different standardisation comities, in the quest of defining some standardised lightning parameters. This has led to several different sets of standards, where the ones defined internationally by the IEC (International Electro technical Commission) for protection of buildings and land based structures and the ones concerning avionics in the SAE (Society of Automotive Engineers) and EUROCAE (The European Organisation for Civil Aviation Equipment) are commented here.

3.1.4.1 IEC

Lightning parameters has recently been covered by IEC 1024 [33], but since a new set of standards IEC 62305 [32] have been released in January 2006, the parameters described here is commented.

The lightning protection measures can be designed to comply with one of four different lightning protection levels, LPL I-IV, in terms of the efficiency of the protection system to intercept the lightning leader and to conduct the lightning current. Protection according to the highest level LPL I ensures that the structure will be unaffected of 98% of all naturally occurring lightning strikes. The resulting 2% have lightning current parameters that either exceeds the maximum amplitude, specific energy etc. meaning that the protective measures are not capable of handling the current, or have a peak current below a certain value, such that the striking distance is shorter than the design criteria for the air terminations.

Due to the high probability and the large consequences associated with a direct lightning strike to a wind turbine blade, protection according to LPL I is usually required. The maximum lightning parameters which must be met by the design of air termination, down conductors, grounding etc. as given for the different LPL in IEC 62305-1 are:

Table 3.1 Maximum lightning parameters according to IEC 62305-1 for the different lightning protection levels (LPL). The difference of LPL III and IV appears in terms of the minimum values of lightning parameters and rolling sphere radii, found in table 6 of IEC 62305-1 [32].

First short stroke			**LPL**			
Current parameters	**Symbol**	**Unit**	**I**	**II**	**III**	**IV**
Peak current	I	kA	200	150	100	
Short stroke charge	Q_{short}	C	100	75	50	
Specific energy	W/R	MJ/Ω	10	5,6	2,5	
Time parameters	T_1/T_2	$\mu s/\mu s$	10 / 350			
Subsequent short stroke			**LPL**			
Current parameters	**Symbol**	**Unit**	**I**	**II**	**III**	**IV**
Peak current	I	kA	50	37,5	25	
Average steepness	di/dt	kA/µs	200	150	100	
Time parameters	T_1/T_2	µs/µs	0,25 / 100			
Long stroke			**LPL**			
Current parameters	**Symbol**	**Unit**	**I**	**II**	**III**	**IV**
Long stroke charge	Q_{long}	C	200	150	100	
Time parameter	T_{long}	s	0,5			
Flash			**LPL**			
Current parameters	**Symbol**	**Unit**	**I**	**II**	**III**	**IV**
Flash charge	Q_{flash}	C	300	225	150	

In establishing a test method for verification of the lightning protection capability, it is also advised to use these parameters depending on the selected LPL, Chapter 6.

3.1.4.2 SAE and EUROCAE

Recently a set of standards describing lightning protection measures for aircrafts has been published. They consists of four parts where the first (SAE ARP 5412, Eurocae Ed 84) describes the lightning environment and related test waveforms, the second (SAE ARP 5413) considers certification processes, the third (SAE ARP 5414) shows how to define lightning zones on aircrafts, whereas the fourth (SAE ARP 5416, Eurocae Ed 105) describes indirect and direct aircraft lightning test methods. Since both lightning attachment processes as well as the structures ability to conduct the lightning current is important for avionics, the standard covering lighting environment considers both voltage and current waveforms [34]. In the standards it is emphasised that the waveforms do not represents a specific lightning event, but together they enable analysis and laboratory testing with an effect similar to what is seen on aircrafts subjected to natural lightning strikes.

Voltage waveforms are used for determining possible attachment points of lightning strikes as well as the breakdown strength of insulating materials subjected to high electric fields. Since natural lightning covers a very wide variety of electric field conditions, four specific waveforms for different purposes are selected.

Voltage waveform A simulates the electric field conditions associated with a re-attachment of a lightning discharge to an aircraft. It has a fast rate of rise of 1000kV/us, and is chopped by puncture or flashover before it reaches its peak.

Voltage waveform B is a standard lightning impulse waveform used by the electrical power industry to test dielectric breakdown strength. It has a rise time of 1.2us and a decay time of 50us, and is in this context specified to be completed without interruption of a puncture or a flashover. Because no chopping is allowed, the waveform is used to test for streamer development on various structures.

Voltage waveform C is used for fast front model tests, and is supposed to be chopped by flashover or puncture after 2us. No details of rise time, decay time or amplitude are specified.

Voltage waveform D is a long duration stroke simulating the electric field prior to the first attachment. Laboratory experience has shown that a structure subjected to these slow front waveforms tends to produce more streamers from lower field regions than the case for fast rising fronts. The waveform has a rise time in the order of 50us-250us, and a decay time app. 2000us. Breakdown or flashover is supposed to occur on the tail of the wave shape.

Current waveforms are divided in two groups, the ones for direct effect testing (the damage caused by the passage of current and charge etc.) and the indirect effect testing (induced voltages and magnetic couplings). Here are only the current components commented which are relevant for direct effects.

Current component A is supposed to simulate the threat from a negative or positive first return stroke. For indirect tests a unipolar double exponential waveform must be used, whereas direct effects can be simulated by either a double exponential or an oscillat-

ing waveform. The peak amplitude is 200kA and the specific energy is app. $2 \cdot 10^6 A^2 \cdot s$. The duration of the pulse must not exceed 500us.

Current component B simulates the intermediate current following some of the negative lightning strikes. For direct effect testing this component should be unipolar of either double exponential, rectangular or linearly decaying nature. The average amplitude over the time duration of 5ms must be 2000A, equivalent to 10C of charge transfer.

Current component C represents the environment with a continuing current typically following a positive cloud to ground return stroke or a negative cloud to ground re-stroke. The purpose is a charge transfer of 200C within a time duration of 0.25s - 1s. This is utilised by either a double exponential, rectangular or linearly decaying current component.

Sometimes a modified version of current component C is used (C^*), to simulate melt through of metal skins subjected to dwell times in excess of 5ms (current component B). In these cases the expected dwell time for the swept stroke phenomenon defines the duration of the pulse. The dwell time of a lightning strike sweeping across a conducting surface is usually in the order of 5ms, whereas if a thin insulating layer is present (coating etc.) the dwell time would be 20ms - 50ms. The average current should not be less than 400A.

Current component D simulates a subsequent return stroke of a negative cloud to ground lightning strike. For direct effect testing either a unipolar or a double exponential waveform can be used, with a peak amplitude of 100kA, and a duration not exceeding 500us. The specific energy is $0.25 \cdot 10^6 A^2 \cdot s$.

The different sections in SAE ARP 5416 covering indirect and direct effect test methods refer to a single waveform or a combination of these individual waveforms.

3.2 Electrical discharges related to a wind turbine blade

A wind turbine blade is a very complex structure when trying to determine its resistance towards lightning discharges. Some of the materials used are neither conductive, nor insulating, and some of the electrical characteristics tend to change during the lifetime. To understand the mechanisms that govern the interaction between lightning discharges and composite blades a scenario with a 40m common blade design hit by lightning is treated.

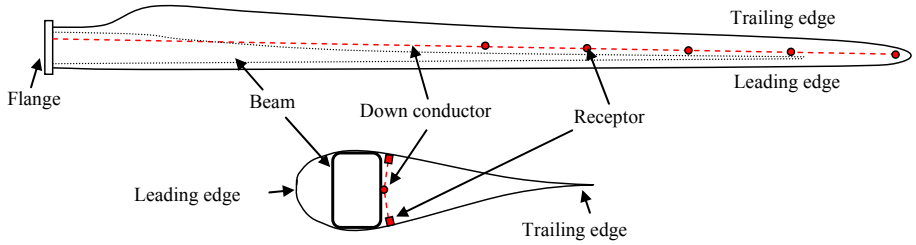

Figure 3.6 Common blade design, discrete receptors connected to an internal down conductor.

Two rather thin shells of insulating GFRP are built separately and wrapped around the mechanically load carrying beam, covering each side of the entire blade surface. Together they are responsible of the aero dynamical design and are optimised to make the blade achieve as much of the kinetic energy from the wind as possible. To protect the blade from lightning discharges, discrete air terminations have been installed according to IEC TR 61400-24 [5]. These receptors are installed on both sides of the blade from radius 20m to the tip region with a spacing of 5m giving five receptors on each side. The receptors are connected to an inner down conductor, a 50mm² copper conductor fixed to the beam with mechanical joints. In the root end of the blade, the down conductor is connected to the flange, which acts as the electrical interface to the rest of the turbine.

Initially this blade consists of only insulating components, except for the installed lightning protection system. The answering leader is supposed to be emitted from one or more of the receptors, such that the lightning discharge and thereby the current can be conducted safely towards ground along the down conductor. This design has been recommended by several authorities [4] and [5] and adapted by many manufacturers. However, experience has shown that blades equipped with this kind of protection are subjected to damages as well.

When such a blade is subjected to a sufficiently high electric field, streamers will be emitted from all conductive components. This situation occurs either prior to an upward initiated discharge were streamers and leaders are initiated from the structure towards the cloud, or as a result of an approaching lightning leader. When the lightning leader gets within a certain distance of the grounded structure, depending on the charge accumulation in the leader head, the grounded structures emits answering leaders.

For a new and clean blade, the discharges will mainly be initiated from metallic objects connected to the down conductor. This situation is illustrated on Figure 3.7.

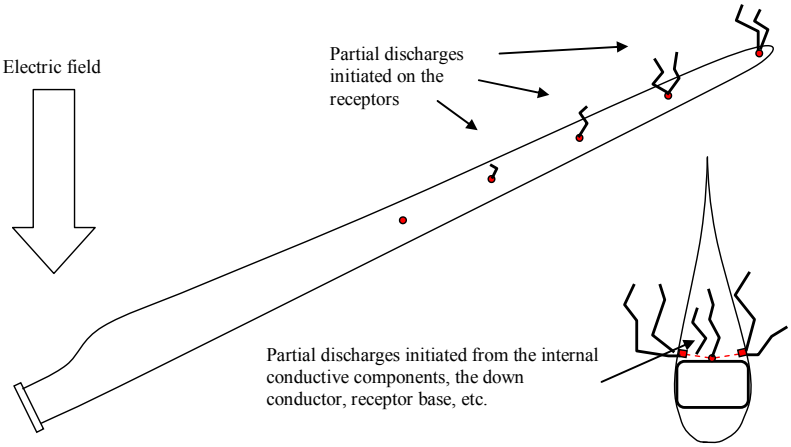

Figure 3.7 Discharges on new and clean blade, mainly from metallic components.

Exposed metal surfaces as the receptors will naturally emit streamers very early, but since the internal down conductor is exposed to the same electric field, partial discharges will also occur inside the blade. The internal electrical discharges deposit charges on the interior surface, with a sign similar to the apparent polarity of the down conductor where-

by the streamer activity is suppressed, Figure 3.8. This suppression of the internal discharges allows more time for the external discharges from receptors to develop further towards the charge concentration in the cloud or in the head of the lightning leader. Usually the answering leaders from the receptors reach the lightning leader first, such that the attachment point is established at a place suitable for the following steps; conducting the current, transferring the charge, etc.

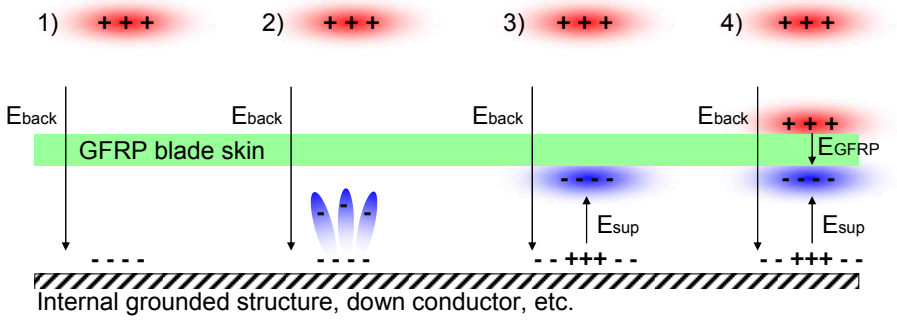

Figure 3.8 Internal discharges in wind turbine blades due to the electric field from a positive charge concentration. 1: The electric field 'E_{back}' induces negative charges on the grounded structure. 2: The electric field causes ionisation and initiation of streamers from the grounded structure. 3: The internal streamers deposit negative charge on the interior of the GFRP laminate, charge that furthermore induces positive charge on the grounded structure. The field 'E_{sup}' from the new charge distribution suppresses the internal discharges. 4: The electric field outside the blade may reach a level where external ionisation takes place, leaving the external surface positively charged, which stress the GFRP even further than the background electric field.

The effect of internal discharges might be minimised by avoiding exposed metal surfaces inside the blade [35]. This could in practice be obtained by covering all metallic joints and structures by insulating materials, and using unshielded high voltage cables as down conductors etc.

The situation is very similar to the common understanding of partial electrical discharges in solid high voltage insulation. When designing high voltage equipment using solid polymer insulation, breakdown strengths of 10-30kV/mm are usually required. This can easily be obtained by using very pure materials and avoiding air filled cavities. In such cavities, partial discharges (PD) might occur, also initiated to minimise the internal electric field within the cavity. In the polymer surrounding the cavity the field will increase just as in the case with the GFRP laminate in the skin of a wind turbine blade.

Depending on where the lightning discharge attaches to the structure, the damage of the different components may vary.

3.2.1 Attachment to air terminations

Once the attachment point has been defined to a suitable air termination, the design of the down conductor system gets important. As discussed previously, the different components of the lighting strike has different characteristics.

The first return stroke contains most of the specific energy, such that the impedance of the down conductor system must be designed to withstand this resistive heating. Following the first return stroke is the subsequent strokes with a higher current gradient. If the inductance of the down conductor system is too high, inductive voltage drops could lead to side flashes within the blade. These side flashes might occur along paths with lower impedances than the down conductor, possibly along moist and polluted internal blade surfaces. Depending on the actual path and extension of the side flashes, blade sensors and computers might be damaged. Design of the air termination point is important when regarding the major charge transfer in the continuing current. Depending on the specific heat, the enthalpy of fusion and the mass available, the surface of the air termination might erode or melt away.

In case of a minor lightning strike, and a well designed lightning protection system, the effect of such a strike will be a pit mark on the receptor, and perhaps a little increase in temperature of the down conductor.

3.2.2 Attachment on insulating surfaces

Attachment on insulating surfaces may occur if charge carriers are present, in form of induced charges from internal partial discharges, or charge conducted from external receptors due to a finite surface conductivity. The following description is based on theoretical considerations, and has not been verified by means of laboratory experiments, Figure 3.9.

As discussed previously, charges of same polarity as the lightning leader may be induced on the exterior surface of the blade due to extensive internal discharges. Since the polarity is of opposite sign compared to the down conductor system, exterior surface discharges from the receptor towards the induced charges occur, trying to neutralise the induced charge region. This thesis implies that the outer surface of a blade would be covered by streamers of opposite polarity relative to the lightning leader, streamers that during their search for the induced charges, also could emit streamers leaving the surface aiming at the charge centre in the lightning leader.

If such a streamer originating from the receptor but following a path along the surface gets in contact with the lightning leader, all the charge from the leader head will be conducted close to the surface of the specimen. This could result in further internal discharges stressing the laminate severely. In this situation one of two things might occur.

1. The charge is transferred along the ionised path on the exterior of the blade, such that the following return stroke, continuing current etc. happens to the receptor, but along the surface. This can either be a peaceful ‘flashover’ or result in thermal damage of the exterior surface below the arc, maybe even tracking erosion in severe cases, ‘8’ on Figure 3.9.
2. The increased electrical stress to the laminate causes a breakdown channel to form. If breakdown of the laminate occurs, this new path might be of lower impedance than the path along the surface, such that the following arcing happens through the laminate towards the down conductor system. Internal arcing is most often crucial, since the sudden rise of pressure causes delamination and weakening of the entire mechanical construction. When blades are replaced after a lighting strike, internal arcing is most often the cause, ‘9’ on Figure 3.9.

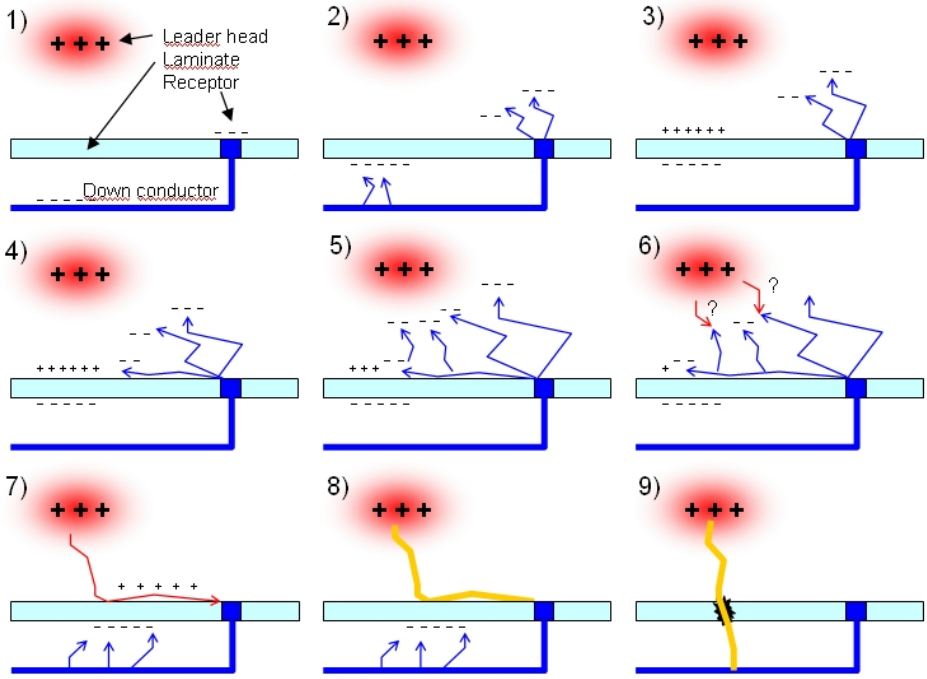

Figure 3.9 Streamer formation on the exterior of the blade, responsible for attachment points on insulating surfaces. 1: A positive charged leader head induces negative charge on the surface of grounded structures. 2: If the electric field gets beyond a certain threshold value, ionisation occurs depositing negative charge on the interior surface of the blade. 3: The internal discharges are suppressed, while positive charges on the exterior are induced by the internal negative charges. 4: Streamer formation on the exterior surface from the receptor towards the positive charges occurs, trying to neutralise the positive charges. 5: Along the path extensive negative streamers are emitted towards the positive charge centre of the leader head. 6: If a streamer with a path along the surface attaches to the lightning leader, an attachment point on the insulating surface has been established. 7: The positive charge from the leader head passes close to the surface, initiating further internal discharges. 8: Surface flashover might damage the surface thermally. 9: A breakdown often results in severe damage due to internal arcing and delamination.

3.2.3 Time span for attachment process

The theory for surface discharges established in Figure 3.9 shows charge build up and streamer formation during static conditions. These discharges usually occur during thunderstorms, such that the rotor blades are rotating at maximum speed. However the tip velocity of app. 50-70m/s does not affect the preliminary discharges much, because the time span from the final step of the initial leader gets into vicinity of the structure to the final jump is very short.

Leader velocities has been measured by means of photography, giving values within $1\text{-}20 \cdot 10^5$m/s [25] and [31]. With a 200kA lightning strike, the striking distance can be calculated to 313m using (3.1). This distance is traversed by the answering leader in 3ms using a conservative speed of $1 \cdot 10^5$m/s, whereas the blade tip only moves 0.21m at a speed of 70m/s. Using optimistic values for leader velocity, tip speed etc. and concerning a 10kA

lightning strike, the displacement of the blade tip is only around 1mm during the attachment process.

When the wind turbine experiences a high static electric field, the generated corona and partial streamer discharges will deposit space charge in the air around the receptors and other exposed areas. However, since strong winds are often associated with thunderstorms, the generated charges are believed to be blown away and only participate in the attachment process to a very limited extent.

In other words, the attachment process and selection of the attachment point is not affected by the rotating geometry.

3.2.4 Swept stroke phenomena

Within the avionics industry, a phenomenon called *swept stroke* is very common [9]. Once the attachment point on an aircraft or another structure has been defined, the following strokes and continuing current may last for as long as a second. In this time period the arc channel is maintained at the same position, relative to the surrounding air. Commercial aircrafts fly with a velocity of app. 800km/h, corresponding to more than 220m/s. This means that if a commercial aircraft is struck by lightning having an initial entry point at the radome, and an initial exit point at the trailing edge of the elevator, the attachment points will not remain the same during the entire strike.

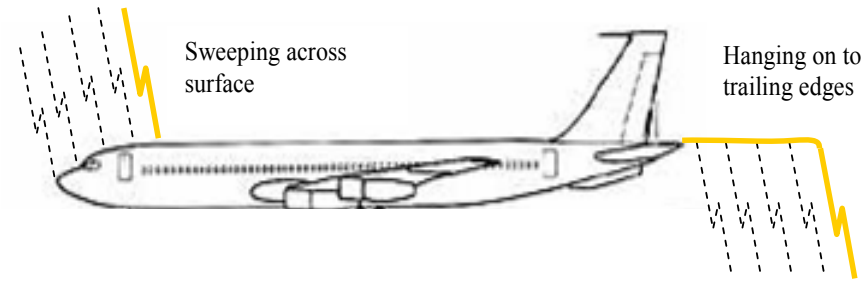

Figure 3.10 Swept stroke phenomenon. The entry point for the lightning discharge sweeps across the fuselage from the radome and backwards, whereas the exit point stays attached to the trailing edge of the elevator.

As seen on Figure 3.10 the initial entry point tends to sweep along the fuselage, as the aircraft moves, while the exit point will remain fixed at trailing edges. Exactly how the arc root sweeps across the surface depends on the conductivity of the surface, and whether the surface is covered with an insulating layer or not. Taking commercial aircrafts as an example, the fuselage is usually made of an aluminium alloy, and though conducting. If the path of a sweeping arc intersects with an insulating structure as the windshield, the arc will stay attached at the last point on the conducting structure, until the arc root has reached the opposite side of the insulating structure, Figure 3.11.

The entire structure will be affected in several different ways by the arcing along the insulating surface. Due to the dwelling arc, the point where the arc leaves the conducting structure will suffer from extensive heating and material deterioration, compared to the

situation where the arc sweeps continuously. Furthermore, the insulating structure must cope with the heat radiation from the arc channel and the pressure rise due to the thermal expansion of the air. Since the arc channel represents a very high potential relative to conductive structures located below the insulating structure, streamers might be emitted from these 'neutral structures' resulting in high electrical stresses to the insulating layer. As discussed previously, a puncture will occur if the electric field exceeds the breakdown field strength of the insulating structure.

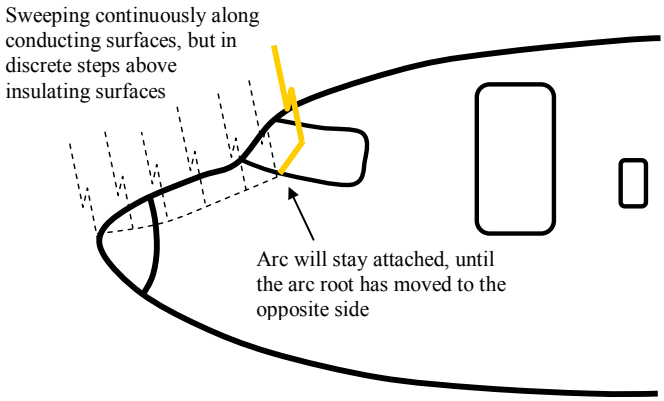

Figure 3.11 Swept stroke affecting insulating structures.

Depending on the breakdown field strength of the insulating layer, numerous breakdowns might occur. This would be the case if the insulating structure were a thin layer of coating or paint on the aluminium surface, were several pit marks or dwell points for the arc root will be visible after a strike.

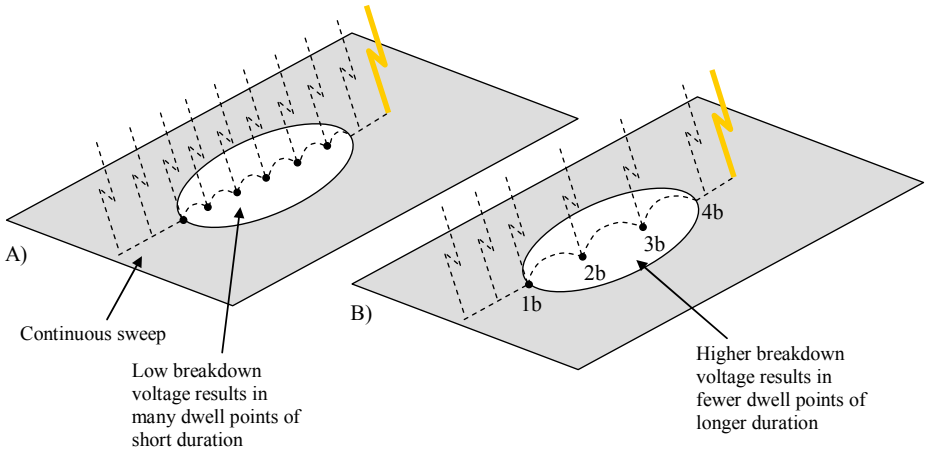

Figure 3.12 Swept stroke across insulating coating applied on a conducting surface. A) A thin layer of insulation results in numerous dwell points with shorter duration, B) A higher breakdown strength of the insulating layer gives fewer dwell points, but with longer duration.

As seen on Figure 3.12, the number of pit marks, and the duration of the dwelling is much dependant on the breakdown voltage of the insulation layer. Once the arc channel sweeps by the point marked 1b on Figure 3.12, a voltage drop across the insulating layer will build up due to the voltage drop along the arc channel. This voltage drop is proportional to the length of the arc channel, or in this case the distance from point 1b. When the voltage of the arc root (where the arc touches the surface of the insulating structure) relative to the conductive surface below exceeds the breakdown strength of the insulating layer, a puncture will occur. Now the attachment point between the arc and the conducting surface has moved to the point marked 2b, and the process with voltage build up and sweeping above the surface continues until a puncture at 3b occurs. Finally when the opposite side of the insulating layer is reached at 4b, the sweeping proceed continuously.

A similar situation is seen when applying this phenomenon to the wind turbine blade. Initially a lightning strike might attach to the designed air termination, the lightning receptor. This attachment process has been discussed previously, and is dependant on the ability of the receptor to emit answering leaders relative to the ability of the surrounding surface. If the blade is new and exhibits a clean and insulating surface, the arc root might stay attached to the receptor, such that the arc channel is kept in the air above the insulating blade. Contrary, if the blade is polluted with partially conductive particles (moist, salt, dirt, etc.) the surface becomes conductive such that continuous sweeping becomes evident. The sweeping continues until it reaches the trailing edge of the blade, where the arc channel will stay attached for as long as the entire strike lasts.

During the time period from the arc channel has reached the trailing edge, to the lighting strike vanishes, extensive heating of the attachment point will occur. The associated pressure rise also implies a risk of mechanical rupture of the very thin blade skin in the tip region. As discussed previously, the typical hollow structure design of the tip increases the probability of internal discharges opposing a great threat to fatal electrical breakdown of the insulating skin.

If lightning attaches to receptors further down the blade the same situation might occur, although the thickness of the laminates here is less susceptible to the mechanical influence.

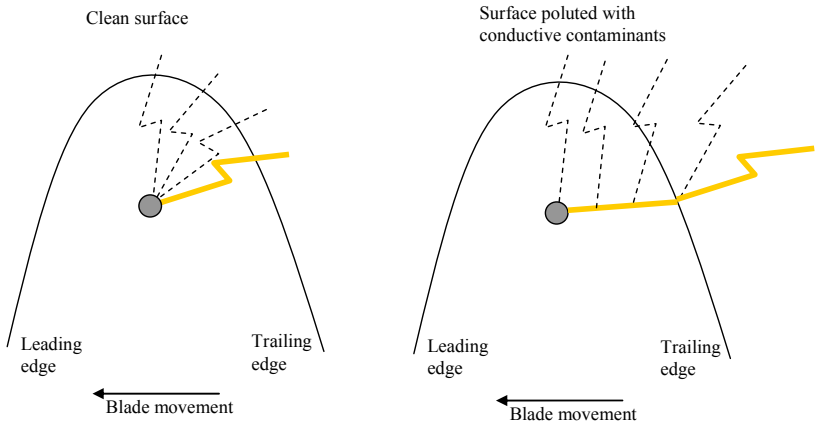

Figure 3.13 Swept stroke occurring at the tip of a wind turbine blade.

3.2.5 Further attachment processes

Several other situations might occur during the attachment process. Based on the swept stroke phenomena and the duration of the entire lightning strike, the following two cases are suggested possible.

Modern wind turbines rotate with app. 15 revolutions per minute [13]. This corresponds to 90 degrees of rotation within the time span of a long duration lightning strike. As a consequence, a lightning strike attaching to one blade might be shifted to another blade during rotation.

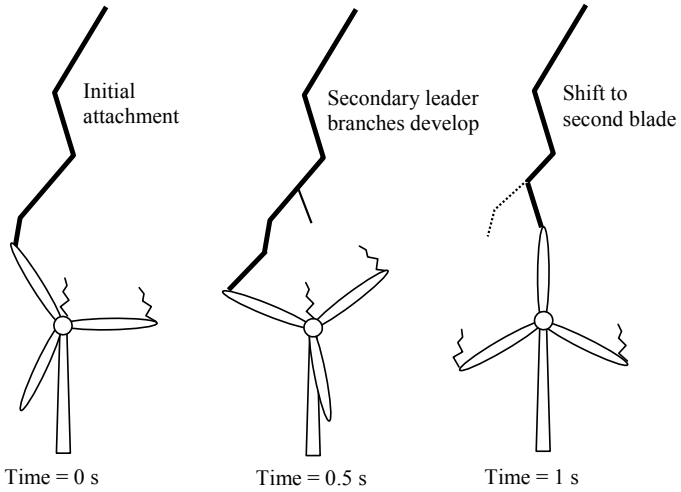

Figure 3.14 Shift of attachment point from one blade to another.

A majority of the specific energy is released during the first return stroke, such that the blade to which the lightning attaches initially is most affected. The phenomenon described here is thereby merely of academic interest, and serves primarily to explain pit marks on receptors on blades not hit initially. The length of the blades is constantly increasing and because a maximum tip speed usually is the dimensioning criteria for the rotational speed, the revolutions per second tends to decrease. Due to this tendency, the phenomenon is getting rarer and will eventually vanish.

A combination of the standard swept stroke phenomenon on Figure 3.13 and the problem with the rotating blades showed on Figure 3.14 happens when the lightning attaches to a blade receptor in a position similar to the one entitled *Time = 0 s* on Figure 3.15.

In this case, the lighting channel sweeps along the surface from the receptor towards the root end, opposing the same risk of electric breakdown as discussed previously. The continuous sweeping is a consequence of partially conducting surfaces, a problem that might be minimised by improving the hydrophobicity of the surface. This surface aspect as well as the reasons for improving the electrical breakdown strength of the laminate is discussed more thoroughly in Chapter 4.

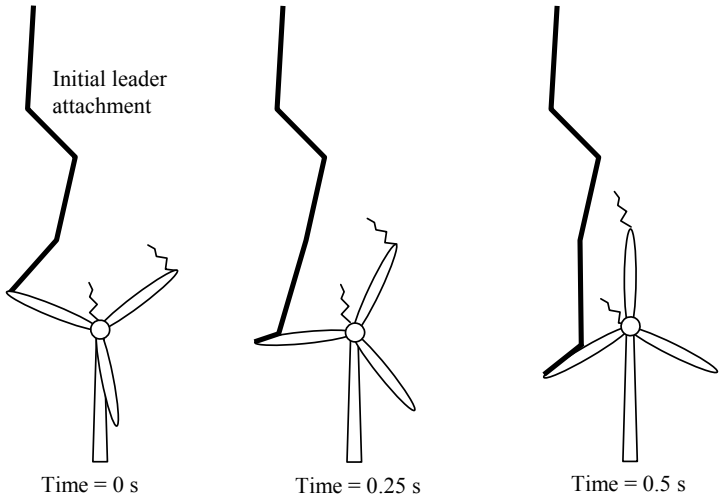

Figure 3.15 Swept stroke towards root end of blade.

3.3 Numerical methods

In the design phase of any physical structure subjected to a lightning environment it is important to predict where possible lightning discharges will attach. When attachment points are identified, the lightning engineer can place suitable protection measures as conductive surfaces, Franklin rods and down conductors. Such methods of predicting the vulnerable locations on structures are given in the lightning protection standards, where the 'rolling sphere method', 'protective mesh', 'protective angle' and 'collection volume' are presented [32] and [33]. All the methods rely on simplified geometrical models, which enable lightning engineers to apply them on actual structures. Lately the new lightning protection standards IEC-62305 comments on several of the above mentioned methods, which has led to some critical comments from experts within the lightning community [36]. In general the standard recommends the use of the rolling sphere method, due to its simplicity and ease of understanding.

Since the rolling sphere method is strictly geometrical, it is possible to implement it into CAD based software describing the geometry of the structure considered. By automating the rolling sphere analysis by means of computing, it is possible to consider more complex geometries, and even get a continuous surface distribution of the amplitude of possible lightning currents. Such a program was developed by *Salo Technologies*, which enabled the calculation of the probability distribution describing where structures are most likely to be hit. The program was applied on wind turbines at the International Conference on Lightning and Static Electricity 2003, aiming at defining possible attachment points along the length of the blades [37].

The rolling sphere method is partly selected based on its simplicity. Since modern FEM programs also import CAD data and enables advanced electric field and potential calculation, more physical oriented methods have recently been suggested [38] and [39]. The methods were presented at the International Conference on Lightning and Static Electricity 2005, and enabled a comparative (relative) analysis of the leader inception from

different points of a structure. Since the method uses a 3D potential distribution as input, it can even consider a cluster of buildings or different complex geometries shielding one another.

The first paper [38] describes the theory for inception of upward oriented leaders from grounded structures when a downward propagating stepped lightning leader is approaching. This physical model is derived with respect to a wide range of already published and well known models, and involves a simple iterative analysis based on the background potential distribution. Without going into details the model determines if conditions for launching a stable upward oriented answering leader from a grounded structure is fulfilled. The streamer initiation, the streamer to leader transition and the stable leader propagation are considered. Finally results from these simulations are compared with results from five different models, with very good agreement.

The second paper [39] considers the application of the model presented in the first paper, visualised in simulations on three actual building complexes which have all been struck by natural lightning. A comparison of the location of points which have been struck with the results from the simulations shows a good agreement. Since input to the algorithm is the vertical potential distribution above the points to be considered, a FEM program (Comsol Multiphysics) is suited for the potential calculation, whereas Matlab is used to incorporate the detailed algorithms. Further information on numerical modelling is given in Appendix A. The steps in the analysis are as follows:

1. Construct a 3D model of the structure to be considered within an analysis volume several times larger than the largest dimension of the structure.
2. Apply a background electric field and compute the potential distribution within the analysis volume.
3. For the point to be considered, compute the vertical potential distribution from the point and 20m upwards.
4. Perform the algorithms described by Becerra and Cooray [38] deciding whether the background field at step 2 was sufficient to fulfil the conditions for stable leader inception, at the specific point. In the process, the potential in the tip of the leader and the resultant corona charge in front of the leader tip is evaluated to determine whether the advancement of the leader will continue. If the leader extends beyond a 2m limit, the discharge will be self sustaining and hence the stable leader inception has occurred.
5. By iteration; find the least background electric field, the stabilisation field, sufficient for fulfilling the conditions for stable leader inception.
6. For each point of interest, repeat step 3-5.

Once the stabilisation field for each point is computed, they can be normalised to the lowest stabilisation field in the entire simulation. By sorting the normalised stabilisation fields the relative probability of being struck within the points considered can be estimated. The method is not suitable to compare absolute stabilisation fields from different simulations, but enables a comparison of the probability of being struck for different locations within the same simulation. So far the model at this premature stage assumes that streamers are generated before the leader inception, why it is only applicable to corners or sharp edges of structures. However since it is an area of large interest the development of such tools will certainly continue [40].

The method presented is based on more physical phenomena than the simple rolling sphere method, and should thus give more reliable results. Despite the relatively complex physics, it is simplified to a practical level suitable for applications on arbitrary structures. In the following sections the method is applied on a single wind turbine as well as an entire wind farm.

3.3.1 Attachment point on wind turbine

The formulas in the algorithm described above were derived for static structures as buildings and enabled a comparison of the strike probability to different corners of the building. In the following simulation an attempt to apply the formulas on a simple 3D model of a modern wind turbine has been made. Since the attachment process takes place during a very short period of time, the turbine can easily be regarded as a static structure, section 3.2.3. The turbine consists of a conical tower with a height of 100m, equipped with a box shaped nacelle measuring 12m x 4m x 4m, and three blades each 50m long. The surrounding volume considered for the electrostatic calculations measure 1km by 1km and is 500m high, Figure 3.16.

The normalised stabilisation fields are calculated for each of the blade tips, and each corner of the rear of the nacelle.

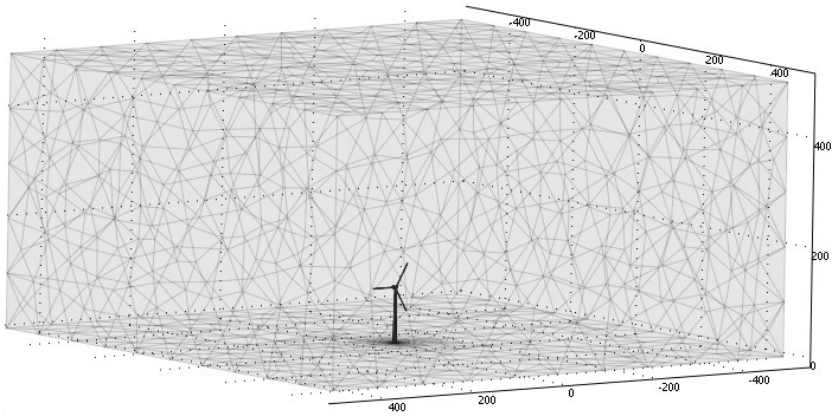

Figure 3.16 FEM model of a single wind turbine to determine the normalised stabilisation field at different locations.

The wind turbine and the surrounding ground area are assigned a reference potential of 0V, the sides of the analysis volume is assigned a boundary condition where the normal of the electric field is zero and the upper boundary is set to a certain potential. The sub domain within the boundaries is air defined by its relative permittivity of 1. By solving Laplace's equation for the subdomain, the potential distribution in the entire volume is computed and exported into Matlab.

The algorithms as presented in [38] and [39] are established in Matlab, such that the stabilisation field can be computed for each point considered. After computing the absolute values which as discussed above depends highly on the electrostatic computations,

the values are normalised to the lowest stabilisation field. The normalised stabilisation field for the different points on the turbine is shown on Figure 3.17.

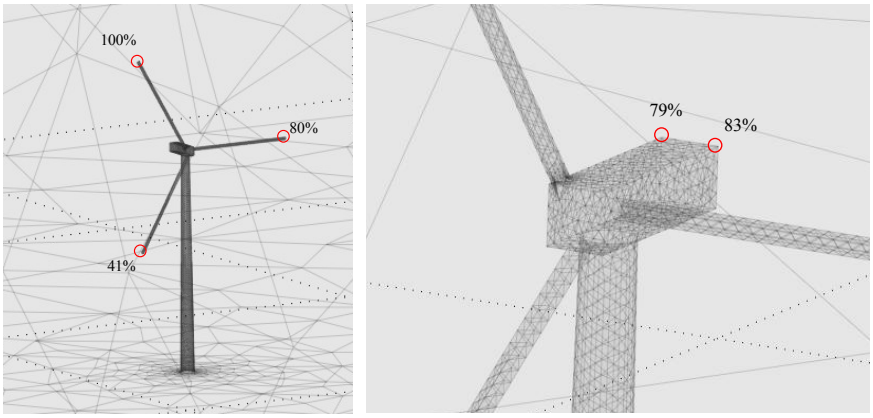

Figure 3.17 Normalised stabilisation fields for a wind turbine with one blade in horizontal position.

As expected for the specific orientation of the rotor in Figure 3.17, the blade pointing upwards has the highest normalised stabilisation field (100%) and hence the highest risk of being struck. The risk of having the horizontally oriented blade struck at its tip is comparable to the risk of getting a lightning strike to one of the rear corners of the nacelle. The left corner of the nacelle is partially shielded by the blade pointing upwards, such that the normalised stabilisation field for this corner (79%) is a little less than for the right corner (83%). In this case the right rear corner of the nacelle is most likely to be struck. Not surprisingly the lowest normalised stabilisation field occurred at the blade tip pointing downwards (41%).

A second simulation with one blade in an upwards vertical position revealed the following normalised stabilisation fields.

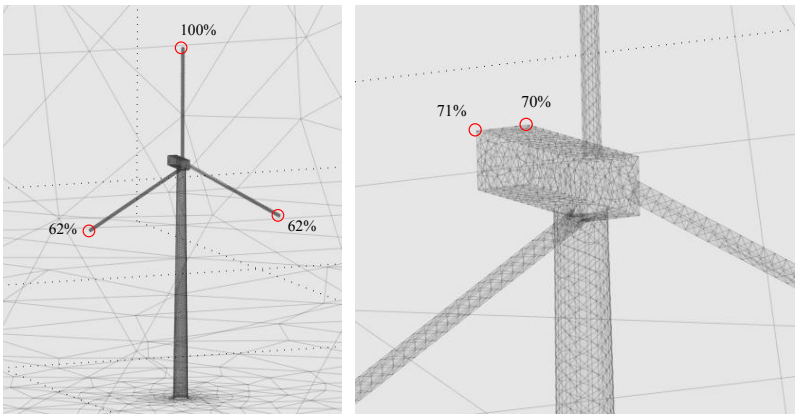

Figure 3.18 Normalised stabilisation fields for a wind turbine with one blade in vertical position.

At this blade orientation the geometry as well as the stabilisation fields are symmetric. The highest risk of getting struck is at the tip pointing upwards (100%) whereafter the rear of the nacelle is most exposed (70%). The blade tips pointing downwards are not likely to be struck considering these five points (62%).

One of the issues of modern lightning protection of wind turbine blades is how to justify the presence of side receptors distributed evenly along the length of the blade. According to different technical reports [4] and [5], it is recommended to place air terminations on the blades from radius 20m to the blade tip, found by applying the rolling sphere method on the blades. The experience however is that blades are only struck rarely at these side receptors (section 6.1), but to form a good argument against side receptors, such field experience must be supported by reasonable theoretical explanations. Once the method of estimating the stabilisation electric field is extended to cover more than just corners and sharp edges, it might be applied on wind turbine blades and show why the tips are that more exposed than the rest of the blades.

3.3.2 Exposed turbines in a wind farm

Considering wind farms where many turbines are erected in the same area, it has sometimes been discussed if the turbines in the periphery achieve most of the lightning discharges compared to turbines within the centre of the wind farm. If this was the case it could be possible to differentiate the lightning protection, such that turbines along the periphery intentionally were designed to handle the increased impact.

In the very initial stage of the planning of the Horns Rev wind farm the possibility of placing very high Franklin rods along the periphery was even considered. The idea was that these Franklin rods should achieve the major part of the lightning strikes, and thereby "discharge" the thunderstorm before it reached the wind farm.

The numerical method presented above is suitable to evaluate how pronounced this shielding effect among individual wind turbines in a wind farm is. To illustrate the phenomenon, a FEM model of a wind farm consisting of 25 wind turbines with an overall height of 150m is treated. The turbines are modeled by a cylinder of diameter 1m and a height of 150m, and are placed in a quadratic five by five array with 500m between each rows and columns. The volume for the electrostatic computations measure 5km by 5km and is 1km high, Figure 3.19.

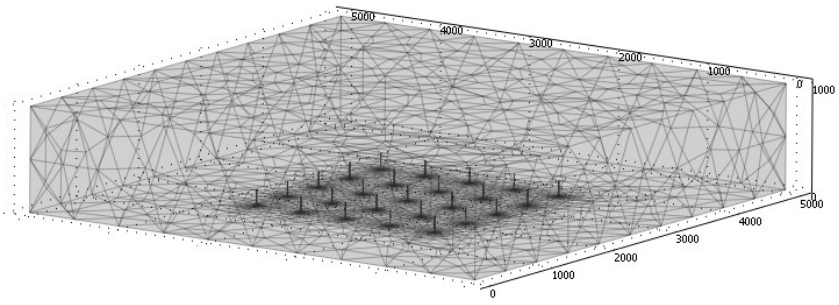

Figure 3.19 FEM model of wind farm consisting of 25 turbines placed in a quadratic array with

500m between each row and column.

As the case with the single turbine, the wind turbines and the lower boundary are assigned a potential of 0V, the four vertical sides has a boundary condition where the normal electric field is zero, and the upper boundary is set to a certain potential. Again the sub domain consists of air and is defined by its relative permittivity of 1. The Poisson's equation is solved in the FEM program, whereas the rest of the computations are performed in Matlab.

The normalised stabilisation field for each turbine in the wind farm is plotted in Figure 3.20.

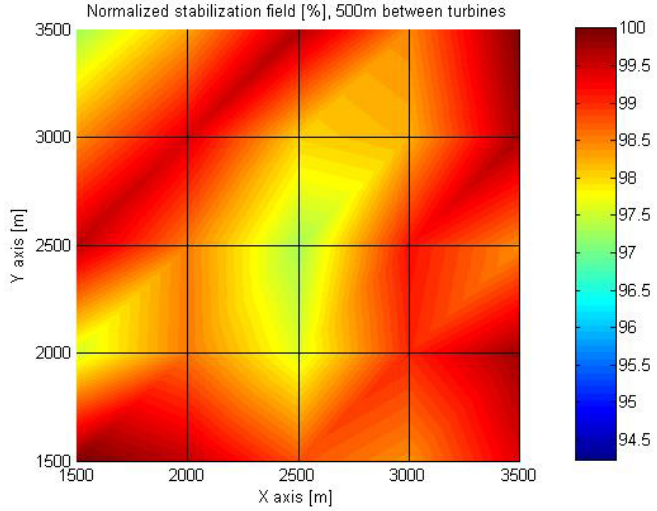

Figure 3.20 Normalised stabilisation field [%], 500m between turbines.

On the figure above, the turbines are located at the crossings of the black lines with coordinates (1500, 2000,…, 3500) along both X and Y axis. Due to the selected level of detail in the grid used for triangulation and further uncertainties in the numerical computations, the values shown on Figure 3.20 is not exactly symmetric as expected. However, it is seen that with a distance of 500m between the wind turbines the relative stabilisation field only varies between 100% and 97%, which in practice means that there is no difference in the probability of being struck.

To investigate the influence of how close the wind turbines are located, a second simulation is performed. The geometry is changed such that the turbines are placed only 200m apart, and the analysis volume is likewise decreased and measures 3km by 3km and 1km high, Figure 3.21.

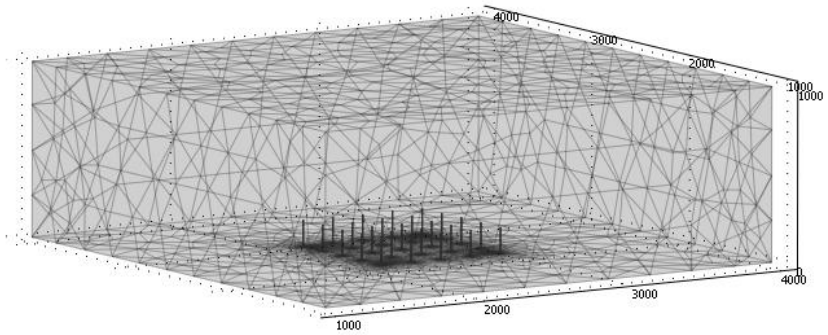

Figure 3.21 FEM model of wind farm consisting of 25 turbines placed in a quadratic array with 200m between each row and column.

The simulations are performed similar to the case with 500m between the turbines and the results are shown in Figure 3.22.

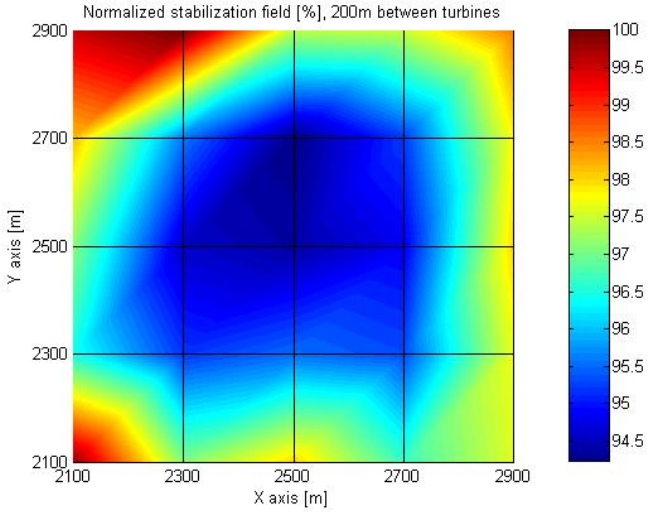

Figure 3.22 Normalised stabilisation field [%], 200m between turbines.

The turbines are now located only 200m apart at coordinates (2100, 2300,…, 2900) along both axis. At a distance between the individual wind turbines of 200m, the shielding of the inner turbines becomes more evident. The normalised stabilisation field in this case varies between 100% and 94% with the lowest value in the centre of the wind farm. In practical lightning protection this difference is too low to account for, but it illustrates the validity of the numerical code.

A distance of 200m between wind turbines of 150m height is in reality far too small since the effect of wakes will decrease the power output of the whole wind farm. Hence

the calculations shown above indicate that there is no significant difference in the risk of being struck among individual wind turbines for the practical distances used for other reasons. However, in some cases where the wind has a prevailing direction it has been found that the turbines that meet the thunderstorm initially would take a large amount of the lightning strikes. Such meteorological phenomena are not accounted for in this model, meaning that actual lightning protection can not be designed solemnly based on simulations, but must bee seen in a larger perspective.

Numerical models used in all aspects of engineering are constantly evolving. Considering the prediction of possible lightning attachment points on single structures as well as large clusters of structures the development of the leader inception model is considered an important step in the right direction. By means of a standard desktop computer it is now possible to compare the probability of successful leader inception of various points on the structure and thereby design the location of air terminations based on more than a simple geometric model. Only future can tell to which level of detail these models will get.

3.4 Electrical environment and lightning discharges

As seen from the above considerations, a modern wind turbine is a very large construction which is extremely exposed to the electrical environment. Because the blade consists of both conducting parts, insulating parts and confined air volumes, designing the lightning protection becomes a rather complex task.

The lightning engineer must focus on many parameters in designing the blade protection. These could be:

- Streamer or answering leader emission.
- The attachment process.
- Conduction of the current and charge.
- Absorption of the specific energy.
- Resistance against mechanical forces.
- Considerations regarding the swept stroke phenomenon.
- And finally a solution that could last the lifetime of the turbine with only a minimum of maintenance.

Another parallel approach for optimising the overall properties of the wind turbine blade, and its resistance towards electrical discharges would be to investigate how to improve different parameters within the materials used. Chapter 4 and Chapter 5 describe relevant features of the composite materials used in manufacturing wind turbine blades, and how to test the different fundamental material properties.

Chapter 4

Material aspects and properties

Materials used for manufacturing wind turbine blades must comply with very strict requirements concerning the mechanical properties. For this reason composite materials have been used widely due to a combination of high mechanical strength and low weight. Lately carbon fibre composites have been introduced in the structural components of wind turbine blades [13] and [15], but since they exhibit fundamentally different characteristics and often play a different role than the common GFRP skins, the electrical properties of CFC are treated separately in section 4.7.

4.1 Composite materials

Different structural materials have different desirable properties. In order to make optimum use of the different properties, they might be combined as composite materials exhibiting the best characteristics of each material. This is the case with reinforced concrete, where the iron exhibit great tensile strength towards an expanding force and concrete has a good resistance towards a compressive force. Together they form a material excellent for construction exhibiting high tensile strength with respect to both expanding and compressive forces, and the ability to handle a limited degree of deflection.

Composite materials using polymers and glass or carbon fibers are somewhat similar to reinforced concrete. Here the single fibers exhibit great tensile strength, but are very fragile concerning compression and bending. By tying bundles of fibers together and surrounding them by a matrix of polymer, the result is a low weight material with excellent mechanical properties. In specific applications there might be several design criteria within the structure. This can be dealt with by positioning the fibers in certain areas and with certain orientation with respect to the stress.

When dealing with composite materials, several terms applies [41]. *Fibres* are the thin threads made of glass, carbon, boron, aramid etc., and are used as the reinforcement of the composite. Often the fibres are collected in *Fibre bundles* to ease the handling during manufacturing. The *Resin* or *Matrix* is the name of the polymer surrounding and tying the fibres together. This resin can be composed in infinitely many ways very much depending on the actual application (mechanical strength, electrical insulation, etc.). In this context the resin is defined by being based on either *Polyester* or *Epoxy*. Since fibres generally are very smooth, it is difficult to obtain sufficient attachment between fibres and resin. For this reason each fibre is treated with a certain *Sizing* which is a chemical surface treatment ensuring optimised attachment.

The mechanical properties depend on the amount of fibres and air relative to the entire volume. For this reason terms describing the ratio between the volume of glass or air relative to the entire volume entitled the *Fill factor* and the *Air content* are used. Another issue that affects the mechanical properties is the weaving technique. Since the strength of

fibres is largest in the length direction, the fibres are often laid in the direction where the largest stress occurs. If stresses only occur in one direction, the composite is made *Unidirectional* with all fibres in one direction. This is could be the case of a core of a composite high voltage insulator only dealing with tensile stress.

Fibres can also be woven together to form organised mats, or laid up randomly to form a felt like structure, again depending on the application. If torsion in a composite pipe is to be avoided, the fibres are usually wound around the pipe with an angle of 45 degrees relative to the length direction. Similarly, resistance towards surface discharges and tracking might be improved if the uppermost layer at the surface is woven with randomly oriented fibres, se section 5.1.

4.1.1 Manufacture

In general composite materials constitutes of two components, the fibres and the resin, mixed and cured in a desirable manner. Depending on the specific application, composite materials are manufactured in several different ways [41].

Construction components as rods, pipes, I- and H-profiles all with constant cross section throughout the length are often made in a process called pultrusion. The fibre bundles are pulled through a tool with the desired cross section, in which the resin is added continuously. After passing this tool, the structure is heated such that the curing takes place. In this way the manufacturing is a continuous process and the length of the specimens is only limited by the length of fibres on the yawns and practical handling issues [42].

A different process is used when cylindrical containers and tanks are made. Here the dry fibres are passed through a bath of resin whereafter they are wound around a mandrel in different angles controlled by the fibre feeding and the rotation of the mandrel.

Considering wind turbine blade manufacturing, the size and geometry of the structure dictates how to fabricate it. Most manufacturers use two large moulds, one for each side of the blade, in which the fibre cloth is laid manually by hand. When all materials for the blade shell has been laid up, including 50-100 layers of ply, wood or foam for the sandwich construction etc., the plies are covered with an air tight plastic foil. This allows the resin to be injected into the dry cloth while applying a vacuum beneath the foil. The vacuum allows the resin to flow more easily into all corners and details, and helps air voids and bubbles to be released. During the resin injection and the subsequent curing the mould and blade shell are heated to a certain degree to achieve optimum curing properties. After both blade shells have been cured, they are glued together along the edges and possibly attached to a load carrying spar or beam in the centre of the blade.

Some manufacturers have decided to use prepreg fibre cloth in which the resin has been added to the ply prior to laying. This process avoids the complicated resin injection, although it is somewhat more expensive. To avoid gluing the edges after curing the individual shells and thereby minimising the risk of getting weaknesses, Siemens Wind Power [16] has developed a method where the entire blade is constructed in one process. The process is entitled *Integralblade technology*, and uses a closed outer mould and an expandable inner mould. After the cloths have been laid up between the two moulds, the resin is injected and cured while in the closed moulds. When curing has finished, the inner mould is contracted and the outer mould released.

4.1.2 Mechanical properties

The reason for using composite materials is usually the combination of high strength and stiffness, and low density compared to other materials for structural applications as iron and steel. Furthermore the structures made of composites can be designed with special requirements concerning mechanical properties in different locations of the structure. This could for instance be obtained by varying the fill factor of fibres along the cross section of pultruded specimens.

Although composite materials have desirable strength to weight ratios, the cost of raw materials and processing is also a factor that affects the choice [43]. The following example compares the tensile strength, density and cost of different construction materials, in order to optimise the choice of material for a certain application.

Table 4.1 Comparison of structural materials, prices are from May 1994 [43].

Material	Tensile strength, σ_{TS} [MN/m²]	Density, ρ [Tonne/m³]	Price, p [USD/Tonne]	ρ/σ_{TS} [10^3]	$(p \cdot \rho)/\sigma_{TS}$ [10^6]
CFC	650	1.5	80,000	2.3	184.6
GFRP	200	1.8	3,200	9.0	28.8
Aluminium alloy	500	2.8	1,600	5.6	9.0
Iron	200	7.9	400	39.5	15.8
Stainless steel	650	7.6	3,100	11.7	36.2

As seen from Table 4.1, the desirable weight to strength ratio of CFC is evident in the fifth column. Compared to Iron, CFC is more than seventeen times as good considering only weight and tensile strength. However, by incorporating the price of the materials, CFC becomes by far the most expensive, showing that the optimum material with these simple considerations wood be aluminium (sixth column). This very basic calculation shows that different materials exhibit very different properties, such that many parameters must be considered during the initial design. Further studies for the wind turbine blade application considering stiffness, yield strength, toughness, wear and aging etc., will eventually qualify or disqualify certain materials, which is the reason for using both CFC, GFRP, foam and wood on different regions of the blade.

4.1.3 Application

Composite materials are used widely within all industries where high strength, low weight, complex geometries or good electrical insulation properties are required.

Besides the desirable mechanical properties composite materials can be processed in many shapes and geometries which is also a great advantage. Furthermore, the surface of composite materials enables easy coating and painting allowing composites to be used for a large diversity of applications including window frames, panels for trains and buses, springs, ladders, construction elements for bridges, etc. [42].

The term composite insulators as used in the high voltage industry covers a post or string insulator consisting of a core of GFRP covered with an outer structure of silicone

rubber. The core is responsible for the mechanical strength of the insulator, whereas the silicone housing allows a sufficient creeping distance. Several issues regarding the core besides the mechanical strength are of great concern. The electrical insulation level of the core must be high enough two withstand the applied voltage, the resistivity of the material must be low enough to avoid excessive heating by leakage currents (even if moist is present), and the interface between the core and the housing must be designed to avoid flashover. All these demands can be met by GFRP manufactured carefully [44].

Composite materials as GFRP and CFC have been used widely in minor aircrafts. Most recently the amount of composites in commercial aircrafts has increased drastically, such that 25% of the structural components of the Airbus A380 are made of composites [45]. Considering the Boeing aircrafts, the amount of composites by weight has increased as well as seen in Table 4.2.

Table 4.2 Amount of composite materials used in commercial airlines from Boeing [46]

Product name	In service	Amount of Composite materials per weight
747	1970	1%
757	1983	3%
767/777	1982	11%
787	2010 (expected)	50% (*)

(*) The amount of composite materials used in Boeing 787, is remarkably high due to the entire fuselage being made of CFC.

4.2 Electrical parameters and definitions

When describing composite materials in relation to their electrical properties as done in section 4.3 and section 4.4, some fundamental parameters must be defined. This section describes fundamental terms in electrical engineering and how individual material properties for the two components glass and polymeric resin might affect each other once they are formed into a single composite. Only terms used directly in this thesis are defined, such that further information must be sought in relevant literature [47].

4.2.1 Electric field

An electric field ‘E’ is a quantity that exists in connection with electrical charges, and which opposes a force on all charged objects within the field. The electric field applies a force on charged objects equal to the charge itself multiplied with the electric field. This is somewhat comparable to a gravitational field which applies a force on masses equal to the mass itself multiplied by the acceleration due to gravity. The unit of electric field is Newton per Coulomb (N/C) or as used in practice, Volts per Meter (V/m). The direction of an electric field is determined by the direction of the force on a positive charge, se Figure 4.1.

When an electric field acts on neutral molecules the field strength might be strong enough to draw electrons off the molecules leaving positively charged ions behind. The acceleration of electrons in the electric field due to the force described above increases the energy of the electrons and might create an avalanche of ionisation. This is the first stage

of a discharge in air which in case several criteria are fulfilled might develop into streamers, leaders or a distinct spark. For further information, literature on high voltage engineering and discharge physics is recommended [27].

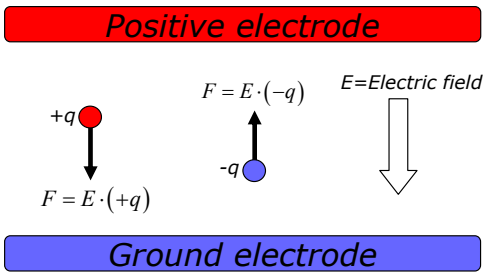

Figure 4.1 Electric field between two electrodes, the direction of the force on a positive charge determines the direction of the electrical field.

4.2.2 Conductivity

Conductivity 'σ' is a material parameter that explains the ability or willingness of charges within the material to move when a static electric field is applied. The conductivity links the electric field with the current density according to Ohms law where 'E' is the electric field measured in V/m and 'J' is the current density measured in A/m^2.

$$J = \sigma \cdot E \tag{4.1}$$

The unit of conductivity is hence A/V·m, 1/Ω·m or S/m. The reciprocal of conductivity is the resistivity 'ρ' which consequently is measured in Ω·m. Conduction of charges can take place through a bulk material like a metallic conductor or along an insulating surface in case of conductive contaminants on surfaces of insulating materials etc. The two corresponding conductivities are hence entitled volume conductivity and surface conductivity. Due to the missing dimension in surface conductivity, the unit for this parameter is only 1/Ω.

Considering glass and polymeric resin they are all good insulators having very high resistivities. In literature and from manufacturers data sheets volume resistivities of various types of glass for fibre manufacture is ranging from 10^{11}Ω·m to 10^{13}Ω·m [48]. Thermosetting polymers as epoxy and polyester have similar high resistivities in the range of 10^{10}Ω·m to 10^{15}Ω·m [49].

In this application where a composite material consisting of two very highly resistive components are subjected to an electric field, the conductivity does not play any role. In case a current actually flows through the laminate, it will not be governed by Ohms law but be an incidence of an electrical breakdown. In static field conditions over a long period of time the field distribution in composite materials is depending on the conductivities of the materials considered. Since most of the lightning phenomena are of a transient nature, it is instead the dielectric permittivity that defines the field distribution.

A special case of conductivity is treated in section 4.7. Here the current distribution in a material with isotropic conductivity is compared with the current distribution in CFC exhibiting a strong anisotropic conductivity.

4.2.3 Permittivity

Permittivity 'ε' of a material describes how an electric field is affected by the presence of the material, or how the electric field within the material is affected by the ambient electric field. The unit of permittivity is Farad per Meter (F/m). For isotropic nonconducting materials the value is a real scalar and links the electric field 'E' (V/m) with the electric flux density 'D' (C/m^2) according to the following equation.

$$D = \varepsilon \cdot E \tag{4.2}$$

Equation (4.2) states that the electric flux density or the concentration of electric field lines for an ambient electric field 'E' depends on the permittivity of the considered material subjected to the electric field. Usually an isotropic material is classified according to its relative permittivity or dielectric constant 'ε_r' which is a dimensionless factor linking the permittivity of the material in question 'ε' with the vacuum permittivity 'ε_0'.

$$\varepsilon = \varepsilon_r \cdot \varepsilon_0 \qquad \varepsilon_0 = 8.85 \cdot 10^{-12}\, F/m \tag{4.3}$$

When an electric field 'E' is applied across two dielectrics in parallel with two different relative permittivities, the electric field will be intensified in the media with the lowest relative permittivity. This is illustrated on Figure 4.2

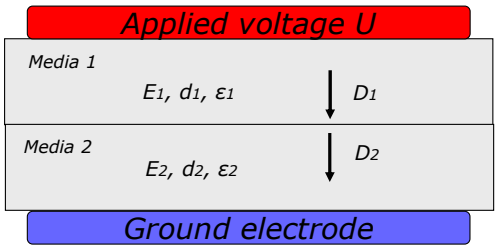

Figure 4.2 Electric fields are intensified in the media with the lowest permittivity

Across a boundary between two dielectrics, the electric flux density can only change if there is a surface charge present at the interface which is described by the following equation (4.4):

$$\left(\overrightarrow{D_2} - \overrightarrow{D_1}\right) \cdot \vec{n} = \varsigma \tag{4.4}$$

where 'D_1' and 'D_2' are the electric flux densities in each media, n is a normal vector to the interface and ς is the surface charge density at the interface [50]. If no charge is present at the interface, and the electric flux density is substituted with the electric field and the permittivity according to (4.2), the following equation applies:

$$\begin{aligned} E_2 \cdot \varepsilon_2 - E_1 \cdot \varepsilon_1 &= 0 \\ \frac{E_2}{E_1} &= \frac{\varepsilon_1}{\varepsilon_2} \end{aligned} \tag{4.5}$$

which shows that the relationship between the electric fields within two parallel layers of dielectrics are inversely proportional to the relationship between the permittivities of the dielectrics.

The relative permittivity of polymers is typically in the range of 3-6 while the relative permittivity of glass is app 4-8 [51]. When performing numerical simulations on GFRP materials a relative permittivity of 4-5 is typically used, indicating that the electric field within the composite will be lowered by a factor of 4-5 compared to the surrounding air. One place where this phenomenon is important is when air filled voids and cavities within the laminate are present, treated thoroughly in section 4.3.1.

4.2.4 Electrical breakdown

The electrical breakdown voltage is defined as the voltage at which the insulation between two energised electrodes is destructed, such that the voltage collapses due to a shortening of the electrode gap. The electrical breakdown field strength 'E_b' is the breakdown voltage divided by the distance between the electrodes, or specified further according to the actual geometry. The electrical breakdown field strength is measured in V/m, where laboratory experiments for long air gaps usually gives values of 500kV/m - 650kV/m depending on gap length, polarity of the discharge and wave shape of the voltage applied [52]. For comparison the breakdown field strength of solid polymeric insulation in high voltage applications is in the range of 10kV/mm - 30kV/mm, and do in general increase by decreasing the thickness of the specimen, the volume effect [51]. Considering solid insulation of glass or ceramics, the values might be a bit higher in the range of 30kV/mm - 50kV/mm, but here the main advantage is the ceramic materials resistance towards partial discharges, a phenomenon quit common in the electric power applications [51].

The breakdown strength of both glass and resin for this application is considerably higher than that of the surrounding air. When forming composites, the risk of getting undefined interfaces and air filled cavities might lower the breakdown strength as discussed in section 4.3.3.

4.2.5 Surface flashover

If an electrode gap is bridged by the surface of an insulator, a collapse of the voltage will often occur along the surface. The exact path of the discharge depends on surface properties and polarity of the discharge, issues that are treated experimentally in section 5.4. In theory the probability of having a surface flashover also depends on the permittivity of the bulk material, since a higher permittivity of the composite (ε_r=4 - 5) tends to push the electric field out in the region of air with the lower permittivity (ε_r=1). However, in practical application the presence of moist and dirt on the surface plays a larger role.

4.3 Electrical properties of the bulk material

As discussed in section 3.2.2 an attachment point on the blade surface some distance away from the lightning receptors might result in puncture of the blade skin and be followed by crucial internal arcing. Since distributed attachment points can not be avoided to a 100% certainty, the only way of minimising the probability of getting a puncture is by improving the breakdown strength of the GFRP laminate. This section tends to highlight

different issues governing breakdown mechanisms of composite materials in a theoretical and qualitatively manner.

4.3.1 Voids and cavities

From a mechanical point of view voids and air filled cavities represent a weakness in constructions using composite materials. To avoid these cavities in the wind turbine blade manufacturing, special precautions have been incorporated in the injection process, such that the resin flows easily around the fibres and allows most of the air to be evacuated. The injection process has to occur within app. 30 minutes, because otherwise the resin begins curing. By using prepreg cloth, the issue of resin injection is of course avoided, whereas the elimination of air voids still has to take place. After curing, the composite materials can be investigated to reveal the density of cavities, which usually lies within 2-10%.

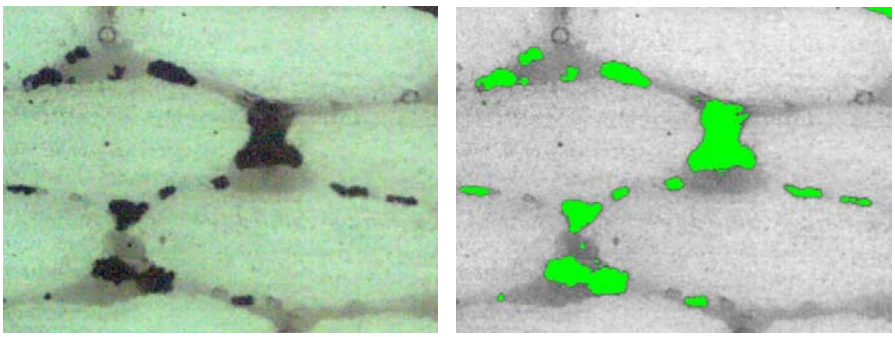

Figure 4.3 Air content of GFRP, Left: Cross section of GFRP captured by a digital microscope (air cavities coloured black), Right: Area analysis of the same image, reveals an air content of 5.9%.

The left image on Figure 4.3 shows a polished cross section of a GFRP structure captured with a standard digital microscope. The light areas are massive fibre bundles, whereas the darker areas are air cavities present in the laminate. The cross section intersects with several of these cavities. With respect to the fibre bundles, the contrast of the cavities has been increased by applying and wiping off a thin layer of black paint. By decreasing the colour depth to monochrome grey scale, an area analysis can be performed where certain distinct pixels are highlighted and counted. The number of highlighted pixels relative to the entire number of pixels in the image gives information about the relative air content by volume, in this case 5.9%.

Another method has also been used in measuring the air content and fill factor. This method relies on a measurement of the volume and weight of a certain specimen, whereafter the resin is removed by a burnout process at 600ºc. By weighing the remaining fibres, and knowing the densities of the resin and the fibres, an estimation of the air volume can be calculated. As the case with the method using digital microscopy, the analyzed volume is only a small fraction of the entire volume of a blade skin. This makes the methods somewhat sensitive to localised effects etc.

Considering the blade material with respect to its electrical properties, there is no doubt that the air content is very important. In traditional high voltage insulation techniques, air voids are one of the main causes for initiation of electrical breakdowns of solid insulation material. The reason for this should be sought in the difference in dielectric permittivity and breakdown strength of air compared to composites, se Figure 4.4.

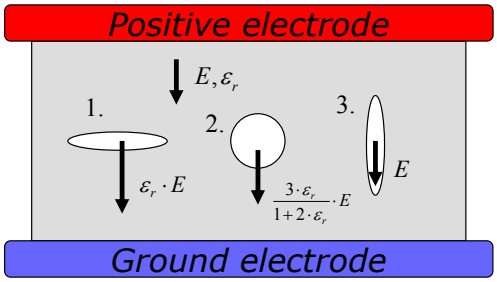

Figure 4.4 Air filled cavities in homogeneous insulation layer.

An electric field 'E' is applied across an insulation layer containing air filled cavities with different geometries. The insulation layer is characterised by its dielectric permittivity ε_r. Considering a cavity shaped as a disc extending perpendicular to the field direction, the field strength in the air filled cavity will be enhanced by a factor ε_r relative to the ambient field. A sphere shaped cavity experience a field enhancement of a little less as seen on Figure 4.4, whereas a cavity extending parallel to the field direction experience an electric field similar to what is seen in the bulk material.

When electric fields are present in air gaps, electrical charge carriers are accelerated and gain kinetic energy proportional to the charge itself, the electric field and the mean free path between subsequent ionising collisions. This means that although the electric field in cavity no. 1 is enhanced the most, the path for the accelerated charges (mostly electrons) is too short to gain sufficient energy for deterioration of the bulk material at the boundaries of the cavities. On the other hand, the electric field in cavity no. 3 is similar to the electric field in the bulk material, but since the breakdown field strength of air is an order of magnitude lower than for most insulation materials, discharges leading to breakdown will most often be initiated here before breakdown of the solid insulation layer itself.

Similar to other in homogeneities, the consequence of having air filled voids in an insulation material can be described by the volume effect. Considering samples cut for breakdown tests, the volume effect states that for thin samples the probability of finding a cavity of critical size located between the electrodes is smaller, than for thicker samples. As discussed above the energy gained by electrons necessary for further ionisation depends on the mean free path, and thereby depends on the physical size of cavities. In other words, by critical size means a size sufficiently large so that electrons gain enough energy to cause a breakdown of the insulation layer at the applied field.

Voids and air filled cavities have shown to be present in GFRP materials used in wind turbine blades, and since they play an important role with respect to both mechanical and

electrical considerations, manufacturing processes aiming at minimising the air content must be incorporated.

4.3.2 Fibre orientation

The fibre orientation is usually determined by the direction of the mechanical stress in the application. Considering wind turbine blades, the deflection near the root end is controlled by orienting most fibres parallel to the length of the blade, thereby stiffening the construction, whereas torsion in the tip end is avoided by using fibres with an angle of 45 degrees to the length at these positions.

With respect to the electrical properties of a composite material, it is expected that interfaces between fibres and resin might give rise to possible defects and voids with an extension parallel to the fibre direction. Having the former section in mind such cavities would in general reduce the electric breakdown strength of the material parallel to the fibre direction. Although the effect in theory would be most pronounced parallel to the fibre direction, the size of possible air filled cavities in GFRP is orders of magnitude larger than the size where ionisation occurs prior to breakdown [53].

At the surface of the composite material, the resistance towards electrical discharges is governed by the homogeneity and the material composition. Similarly it can be argued that fibres present at the surface impose a risk of interface issues, where minor deviations from the pure surface might alter the overall characteristics. This is discussed experimentally in section 5.1.

4.3.3 Breakdown strength

Glass, ceramics and polymers used in high voltage applications generally exhibit high breakdown field strengths. This is achieved by using pure and clean materials, and by avoiding air filled cavities as far as possible. The breakdown strength of such materials is usually determined using very thin samples and stressing them with well defined homogeneous electric fields, resulting in values far better than the ones used in engineering applications. Moreover, the breakdown or withstand field strength also depends on the electrode geometry and the test method applied, where impulse voltage tests usually gives higher values than AC and DC tests [49].

When such materials are combined in composite structures using glass fibres and polymers, the possibility of interfaces and impurities in the boundary layer between fibres and resin occurs. The manufacturers tend to optimize the adhesion between fibres and resin due to structural advantages and hence indirectly minimise the possibility of getting interface issues. Nevertheless the breakdown field strength is reduced for practical applications due to these impurities as discussed in section 4.3.1.

Some constructions using composite materials, wind turbine blades in particular, exhibit a great deflection during normal operation. This deflection is expressed as compressive and tensile strain along the edges furthest away from the centre line, and thereby also on a large part of the blade shell in the tip region. The breakdown strength is dependent on elongation which has been commented in literature [53], having a peak value at slight compression, and a decreasing characteristic at tensile strain.

The experiments considering a thin sample of glass fibre reinforced epoxy resin, revealed that composites exposed to a slight compression tends to experience an increase in breakdown field strength up to a certain level whereafter the breakdown strength decreases. At slight compression, the density of the composite is increased as evidence of closing up air cavities and voids, naturally leading to higher breakdown strengths as discussed in section 4.3.1. By increasing the compressive stress further, breakage of tie bonds, crack initiation and brittle fracture would eventually decrease the breakdown strength.

Figure 4.5 shows a qualitative interpretation of the effects concerning mechanical strain. 'A' shows a situation with an unstressed composite, where the breakdown strength is determined by the presence of cracks (infinitely thin voids) in either directions and spherical voids. By applying a compressive force at 'B', the voids otherwise oriented perpendicular to the plane will be closed, spherical voids slightly deformed, and cracks parallel to the plane turned into uncritical disc shaped voids. Contrary, an elongating force at 'C' will tend to open critical cracks oriented perpendicular to the plane, and thereby lowering the electric breakdown strength. The measurements have only been performed up to elongations of 3%, since fracture of the specimen above these stresses would be the case.

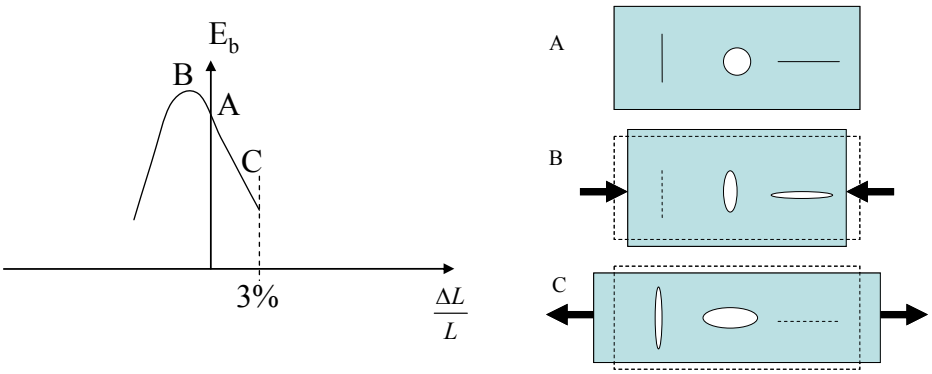

Figure 4.5 Left: The breakdown field strength depends on tensile strain for GFRP materials [53]. Right: Deformation of cavities in GFRP as a result of compression and elongation.

If the sample shown on Figure 4.5 was a section of a wind turbine blade skin at the tip area, the breakdown strength of the laminate would be reduced under load compared to a typical test situation where breakdown strengths are determined on unloaded specimens.

The composite materials in wind turbine blades are exposed to both static and dynamic mechanical loads. As with many other structural components, a certain mechanical aging takes place where the materials are weakened mechanically, looses stiffness and sometimes becomes ductile. By inspecting blades that have been in service for many years, it is seen that the otherwise fairly transparent composite becomes hazier due to the constant wear. The haziness is explained by a slip in the fibre/resin interface resulting in minor air filled pockets. When light passes through the composite, the refraction in the boundary between air/resin and air/fibres causes the material to appear brighter or hazier.

Mechanical aging is a very important topic for research within the wind turbine industry since the blade must be designed to cope with the wear and load over an entire lifetime of 20 years or more. For this reason all manufacturers perform accelerated aging tests, where fatigue and other failures due to static and dynamic loads are revealed.

Since the haziness of the mechanically aged composite is considered an evidence of partial delamination between the resin and the single fibres, it is expected that the breakdown strength would decrease with the aging as well. This phenomenon is treated experimentally in section 5.2.4.

4.4 Surface characteristics

Besides electrical properties of the bulk material, the surface characteristic is also expected to have great importance. In section 3.2 it is commented that attachment points besides the discrete receptors implies a risk of either electrical breakdown of the laminate or a surface flashover to the receptor. Furthermore, the arc following a successful attachment on a receptor might sweep along the surface and stay attached on the trailing edge for the duration of the entire strike. For this reason the ability of the surface to withstand electrical discharges and associated heating must be considered when designing the blade.

4.4.1 Tracking resistance

Outdoor high voltage insulators stressed with AC experience a phenomenon called tracking, where surface currents due to moist and impurities tend to erode the surface thermally. The mechanism governs the formation of dry bands, where the evenly distributed moist is evaporated locally due to ohmic heat generation. Once the dry band has formed, the electric field across the band might be sufficient to initiate a local surface flashover, which tears on the surface material itself. Tracking experienced on high voltage insulators is a long term aging mechanism, where the discharge scintillation after a while changes the otherwise insulating surface towards a partially conductive nature. Especially when moist is considered, the eroded surfaces containing carbonised byproducts might appear somewhat conductive and imply an increased risk of a total flashover.

By examining wind turbine blades hit by lightning during service, eroded tracks in the surface coating from the receptor towards the trailing edge have been found. This thermal damage has probably occurred during the sweeping of the arc root along the surface and is somewhat similar to what is experienced on high voltage insulators.

Partly conductive tracks extending from the receptor and outwards on the blade surface tends to draw the ground potential out to a larger area. This affects the receptor efficiency in a negatively manner, since both shielding of the receptor and numerous attachment points become the case.

In case of an undistorted and insulating surface, the receptor will have a higher tendency of emitting answering streamers and leaders compared to the surrounding surface, ‘A’ on Figure 4.6. If tracking paths on the surface extends from the receptor, the ground potential would be distributed to a larger area. This enables answering leaders to be emitted elsewhere than from the receptor, thereby exposing especially the trailing edge of having direct lightning strikes, ‘B’ on Figure 4.6.

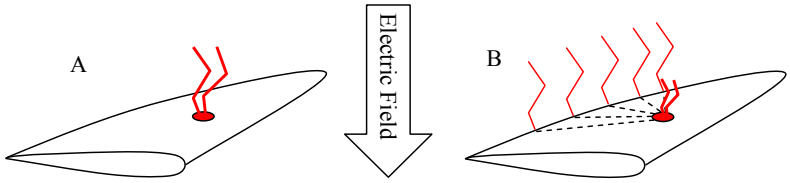

Figure 4.6 Ground potential extended from the receptor to a larger area as a consequence of tracking erosion, A: Clean and homogeneous surface, streamers are emitted from the receptor alone, B: Partly conductive tracks extends from the receptor and exposes the trailing edge to direct lightning strikes.

4.4.2 Hydrophobicity

On new blades coated and finished to perfection, surface discharges and tracking might not be an issue. This is due to the typical hydrophobic properties of the coating used, such that both moist and dirt are rejected. If moist and partly conductive contaminants on wind turbine blades are present, they might play a role as charge carriers for discharges in the high electric field regions. This affects the ionisation along the surface, such that discharges will form more easily along the surface compared to a path in free air.

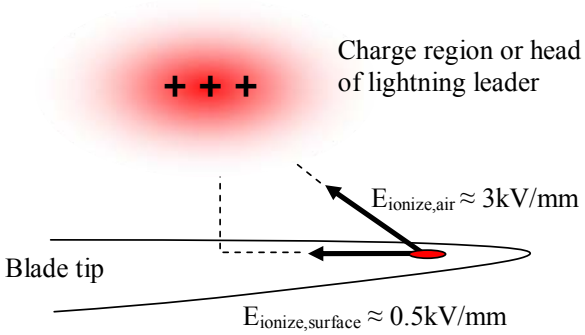

Figure 4.7 Ionisation occurs more easily along surfaces if moist and conductive contaminants are present. The values are typical for standard laboratory conditions.

A typical value of the electrical breakdown field strength for air in a controlled laboratory environment would be app. 3kV/mm. Compared to the value of app. 0.5kV/mm required for ionisation along a surface in case of conductive contaminants, surface discharges would clearly happen at lower electric fields than the competing discharges in air.

Since ionisation occurs more easily along insulating surfaces in case contaminants are present, a moist repelling surface would be desirable. In this way it is sought avoided that the surface participates in the discharge process, and consequently deteriorated by the following arc.

Surfaces which exhibit hydrophobic properties are usually based on silicones. This is the case with composite insulators where the mechanical load carrying core of GFRP is covered by a housing of silicone rubber. The silicone housing ensures sufficient creeping

distance, protects the core from the weather and exhibit hydrophobic behaviour repelling moist and dirt [44].

Lately a new group of materials have been invented entitled HCEP (Hydrophobic Cycloaliphatic Epoxy) aimed at serving medium-voltage outdoor applications. The GFRP material is based on the cycloaliphatic resin Araldite CY 184, doped with some additives. The special properties make the surface hydrophobic, and even enable hydrophilic pollutions on the surface to be converted to a hydrophobic state. Furthermore, the material has a recovery effect, meaning that the hydrophobic state will recover after a temporary loss due to electric surface discharges [54].

4.5 Multifactor exposure

During thunderstorms, many of the above mentioned issues degrading the performance of the composite material are present at the same time.

The mechanical stress in the tip area is at its maximum possibly causing the breakdown strength of the composite laminate to decrease according to the reasons mentioned in section 4.3.3. If turbines that have been in service for a while is considered, the surface might be polluted by salt and ionic compositions, acting as charge carriers for the streamer discharges from the receptor. Since rain often is associated with thunderstorms, the polluted surfaces are also wet, making the otherwise insulating surface even more exposed.

At protrusions on the blade surface besides the receptor (blade tip, trailing edge, impurities, water droplets, etc.) the background electric field prior to lightning would be enhanced to a degree were streamers and leaders are initiated. These streamers and leaders reaches out towards the charged regions in the cloud, and thereby exposes the points of streamer initiation to direct lightning attachment.

Consequently all the factors relevant for lightning attachment on insulating surfaces and the probability of having an electrical breakdown acts together in stressing the laminate in the most severe way.

4.6 Relevant tests

Chapter 4 has commented on various properties for GFRP materials which are regarded relevant towards improved lightning protection of wind turbine blades.

In the design phase of a wind turbine blade many theoretical considerations and simulations are performed. This ensures a blade that fulfils the requirements within mechanical and aerodynamical issues, and results in a highly complex construction using different composite materials. Since the group of GFRP materials are selected on behalf of their mechanical properties, the lightning engineer only have the possibility of optimising or varying a few parameters within the composite.

Such an optimisation could be a minor change in manufacturing practice aiming at lowering the air content, an adjustment which should not contradict the mechanical requirements. Once materials are specified and designed according to mechanical requirements and modified with respect to electrical considerations, another task is to test them and verify that they can deal with the threat from electrical discharges as discussed previously.

Various work groups and standardisation committees within the electric power and high voltage community have during time proposed a large variety of test methods for composite materials. The most recent document that sums up failure causes and relevant test methods has been written by a Working Group within CIGRE SC 15, WG D1.14.

This document, *Material properties for non-ceramic outdoor insulation – State of the Art* [55] comments on many issues in characterising and testing composite materials. Considering the application of composite materials in wind turbine blades from an electrical point of view, the sections dealing with *Resistance towards Tracking, Electrical breakdown strength, Arc resistance* and *Hydrophobicity* might contain relevant tests.

In general it is emphasised that the aim of testing is not to simulate a true lightning environment, but more to affect the materials in a way similar to what is seen on actual blades in service. The constant corona and streamer formation around tip receptors as consequence of the background electric field can not be represented directly by a small scale laboratory tracking test. However, both the resulting erosion as well as the mechanisms in which the material degrade might be similar such that a material that performs well in the standardised test will perform equally well in the true lightning environment.

Test methods aiming at simulating true environments on small scale models must consider the sometimes complicated issues of scaling very carefully. A simple example of scaling is given in Appendix B.

4.6.1 Tracking tests

Classification of a material according to its capability of withstanding tracking is covered by several standards as described in [55] and [56]:

IEC Publ. 587: The *Inclined Plane Procedure* as described in this standard stresses five specimens at a time, and generally gives very reproducible results. The specimens are stressed by a stepwise increasing AC voltage from 1000V – 6000V while a saline solution is flowing steadily across the surface. This ensures the formation of dry bands and discharge scintillation, such that failure typically occurs within 4-10 hours depending on initial conditions. The surface area subjected to the stress is 50mm long and app. 40mm wide [41].

IEC 61302: Four specimens formed as tubes are mounted in radial direction on a slowly rotating wheel, such that they alternately are whetted in a saline solution and subjected to a voltage stress. This supports the generating of dry zones, and accelerates the dry band arcing. However since the specimens are formed as tubes, they do not comply with the manufacturing practice of wind turbine blades [57].

IEC 60112: This test method determines the proof and comparative tracking index (PTI and CTI), by affecting a surface area with both drops of a saline solution and AC voltage below 1000V. The test method uses electrodes of 5mm width and a spacing of 4mm, such that the stressed surface is relatively smaller compared to IEC Publ. 587. Furthermore, the test procedure is quit complex involving many steps that requires manually operation [58].

All the mentioned standards aim at classifying the same aging or failure mechanism for materials used for high voltage outdoor insulation. Considering a wind turbine blade, the possible tracking erosion occurs during continuous corona and streamers from the

receptor initiated by the ambient electric field and from surface flashovers during a direct lightning strike. In this context a test method stressing a large area capable of handling both specimens produced for tests as well as specimens cut from blades in service is desirable. Based on these issues, and the recommendation from WG D1.14, the test method described in IEC Publ. 587 is used to investigate the tracking resistance of composite materials for wind turbine blade applications.

4.6.2 Breakdown tests

Breakdown tests are often used in determining suitable materials for insulation purposes. Depending on which type of materials to be tested (solid, liquid or gaseous) and which type of breakdown mechanism (intrinsic, electromechanical or thermal), there exists a large variety of test setups and procedures.

High voltage testing is generally described in IEC 60060-1, where tests considering AC, DC, impulse voltages and impulse currents are described [59]. Tests using artificial pollution and statistical treatment of recorded data are also commented. Breakdown strength of insulating materials in specific is treated by the IEC 60243 series comprising three documents covering tests at power frequencies [60], tests using direct voltages [61] and test using impulse voltages [62].

Solid materials used in components for high voltage insulation purposes, are usually in direct contact with electrodes at the two potentials they are to separate (cables, transformers, etc.). In principle this calls for a test method where surface discharges in air do not occur, meaning that most test setups uses electrodes encapsulated in the material to be tested, or setups where the specimen is lowered into mineral oil.

The GFRP skin of a wind turbine blade experience surface or streamer discharges on either side stressing the laminate with “electrodes” not geometrically defined by any standards. Furthermore, since GFRP by nature is rather inhomogeneous, the selected test method should stress a relatively larger volume, due to the volume effect, than stated in most standards for homogeneous insulation materials.

On behalf of the different issues considering the wind turbine blade application, the suggested test methods for evaluating the breakdown strength for composite materials must expose a rather large volume of the material to surface discharges. Both test setups and methods used in section 5.2 are based on principles described in the various standards.

4.6.3 Arc resistance

A test method covering arc resistance is described in IEC 61621, and becomes relevant in cases where insulating surfaces are exposed to a large number of flashovers [63]. Since the blade surface in the tip region only is exposed to surface flashover when a lightning strike has attached to the receptor the effect of a continuous corona and streamer formation acting on a long term basis is found more important. The results of these mechanisms are expected to be covered by the tracking test described in IEC Publ. 587.

4.6.4 Hydrophobicity

Measurement of hydrophobicity in terms of solid high voltage insulation is commented in a technical report by the IEC [64]. In this report the stability of the hydropho-

bicity is determined by salt-fog testing [65] and rotating wheel dip testing [57]. Other standards describe measurements of the wettability of insulator surfaces according to IEC 62073. As discussed in section 4.4.2 hydrophobicity may play a role considering discharges along the blade surface relative to having discharges jumping directly from the receptor in free air. However, since hydrophobicity is important not only from an electrical point of view, the manufacturers are already aiming at designing and testing the surfaces with maximum hydrophobic properties.

For this reason no standardised method for evaluation of hydrophobicity is considered in this thesis. A series of tests considering the willingness of an electrical discharge to follow an insulating surface has been completed. These tests and results which might be correlated with the hydrophobicity are described in section 5.4.

4.7 Carbon Fibre Composites

Carbon fibre composites have been used for several years in the avionics industry. Within the last couple of years the size of wind turbine blades have made it necessary to use the more expensive CFC for main structural components in the blades. Mechanically they exhibit excellent properties but from a lightning protection perspective they represent quit a challenge. CFC is a composite made of rather conductive carbon fibres surrounded by a matrix of insulating polymeric resin. As consequence of this composition, the conductivity of CFC is somewhere in between the conductivity of conductors and insulators. Depending on the amount of fibres and the actual construction, the conductivity of CFC is two to five orders of magnitude lower than for aluminium [66] and [67]. A rule of thumb used in simple engineering applications states that CFC has a conductivity a 1000 times less than the conductivity of aluminium, i.e. $3.77 \cdot 10^4$S/m [9].

Metals are electrically isotropic meaning that the conductivities measured in different directions are the same. Computation of temperature rise and current distribution is then straight forward since conductivity in this case is modelled as a scalar. Depending on the fibre orientation and weaving technique CFC is strongly anisotropic. This complicates simulations considering CFC, since a simple scalar suddenly is extended to a three by three conductivity tensor, containing different conductivities in the three main directions. Boeing has previously published a paper concerning FEM calculations of current distribution in riveted joints of CFC panels, where the values used were $4 \cdot 10^4$S/m, 10S/m and 2.5S/m for axial, transverse and inter-ply conductivities [66].

One of the effects of the anisotropic behaviour is the difficulties of current distribution. If a blade skin were made of unidirectional fibres oriented parallel with the length axis of the blade, the conductivity perpendicular would be much lower than the conductivity parallel with the fibres. Hence the current from a lightning striking the blade skin would flow more easily along the length of the section hit directly, in stead of being distributed evenly across the entire cross section [66]. This phenomenon is illustrated by computing the surface potential and current distribution using Finite Element Methods on both isotropic and anisotropic materials subjected to current injection in a single point, Figure 4.8.

The samples are 50mm thick and measures 1m by 0.3m. The left boundary is grounded, whereas the other five boundaries are insulating. 100A is injected into the sample at the circular area of radius 1cm shown on Figure 4.8, and conducted towards the

ground potential. By solving the equation of continuity (Ohms law) and Laplace's equation the potential and current distribution can be found for various conductivities [68].

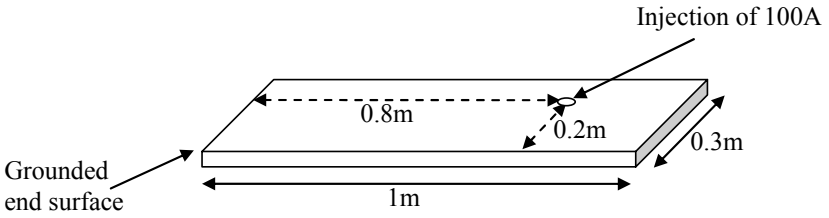

Figure 4.8 Sample used for computation of surface potential and current distribution for isotropic and anisotropic materials.

On Figure 4.9 the results are shown considering an isotropic material with a conductivity of $4 \cdot 10^4$ S/m. The left image shows the bulk potential distribution, with values ranging from 0.2V at the current injection point to 0V at the grounded boundary. The right image shows the current distribution, where the current gets evenly distributed across the entire cross section pretty fast. The absolute results in this context are irrelevant; hence no colour code is shown.

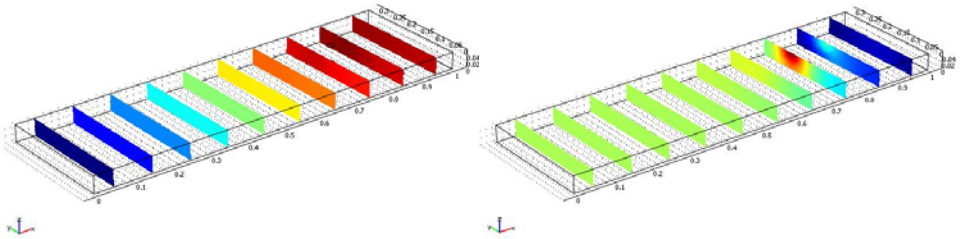

Figure 4.9 Left: Potential distribution for an isotropic material, Umax=0.2V, Right: Current distribution, isotropic material. Red colours correspond to high values and blue colours correspond to low values.

Figure 4.10 shows a similar calculation where the conductivity is made anisotropic. Comparable with unidirectional carbon fibres as experienced by Boeing [66] the conductivity in the length direction parallel with the carbon fibres (x-axis on Figure 4.10) is set to $4 \cdot 10^4$S/m, a value of 10S/m is used for the intra-ply conductivity (conductivity between separate fibres within the same ply, y-axis) and a value of 2.5S/m is used for the inter-ply conductivity, the conductivity between neighbouring plies, z-axis. Instead of treating the conductivity as scalar as for isotropic materials, a 3 by 3 conductivity tensor must be used in this case [67]:

$$\sigma_{CFC} = \begin{bmatrix} \sigma_{xx} & & \\ & \sigma_{yy} & \\ & & \sigma_{zz} \end{bmatrix} = \begin{bmatrix} 4 \cdot 10^4 & & \\ & 10 & \\ & & 2.5 \end{bmatrix} S/m \qquad (4.6)$$

Clearly the bulk potential distribution on the left image changes dramatically having a maximum of 10.3V at the current injection point, and primarily affecting the volume in a projection of the current injection point parallel with the fibres. The plot of the current distribution on the right image also shows that most of the current flows in the fibres directly in touch with the injection point, because the transversal conductivities of 10S/m and 2.5S/m does not allow an evenly distribution compared to the longitudinal conductivity of $4 \cdot 10^4$S/m.

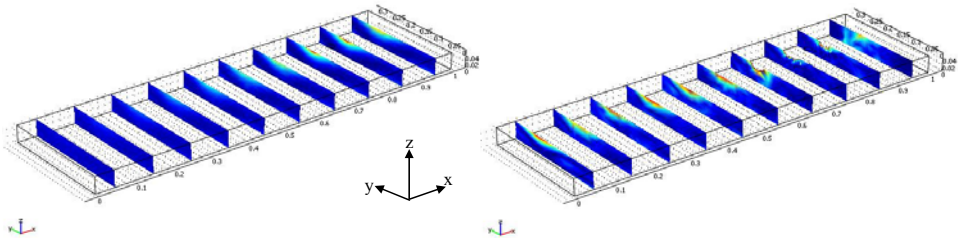

Figure 4.10 Left: Potential distribution for an anisotropic material, Umax=10.3V, Right: Current distribution, anisotropic material. Red colours correspond to high values and blue colours correspond to low values.

Such calculations for anisotropic materials are used more and more within the avionics industry. Lately it has been shown how 3D simulations for simple geometries of limited size are easily modelled on common desktop computers, with good correlations towards experimental results [67].

Besides the low conductivity compared to metals, the critical temperature where delamination and other structural damages occur is considerable lower for CFC (app. 300ºc) compared to aluminium (app. 660ºc). This is quit important considering ohmic losses and joule heating at conduction of lightning currents, and in particular at lightning attachment points where extremely high current densities will occur.

Although blades containing CFC typically are equipped with some sort of lightning protection, the CFC still represents a current path for the lightning current. Therefore it is crucial that lightning protection engineers are aware of the difficulties considering the interaction of the installed lightning protection and the CFC structural components.

Chapter 5

Laboratory work

In selection of appropriate materials for high voltage applications, material testing is of great importance. Many issues and parameters can be optimised theoretically, but when it comes to practical handling and manufacturing, several unidentified factors affecting the theoretical achieved properties might occur. This could be the introduction of impurities, voids, scratches and other defects lowering the breakdown strength or tracking resistance considerably, phenomena only identifiable by suitable testing.

Several test methods have been developed and used based on generic high voltage standards [1, 57-63, 65], and adjusted to the application on wind turbine blade materials. The test methods described in this section aim at classifying materials according to the behaviour of both the surface properties (tracking tests and surface flashover tests) and the bulk material (breakdown field strength).

5.1 Tracking tests

This section describes test procedures and evaluation of the tracking resistance of several GFRP specimens, tested according to IEC Publ. 587 [1].

5.1.1 Purpose

In Chapter 4 it is argued that tracking is an issue for composite material surfaces in the tip region of wind turbine blades. Furthermore, several test methods are commented, of which the method described in IEC Publ. 587 is selected as the most suitable. Twenty one series of five specimens each have been tested. Classification referring to the standard, as well as general comments on surface characteristics, fibre orientation, different types of resin etc. is performed. Finally some suggestions for material improvements are treated and held together with the manufacturing processes of wind turbine blades.

5.1.2 Test method

The IEC Publ. 587, ‘Test methods for evaluating resistance to tracking and erosion of electrical insulating materials used under severe ambient conditions’ describes a test procedure where five similar specimens are tested simultaneously, Figure 5.1. For the present investigations the five mounting devices were produced according to the standard, except for additional banana plugs on both the high voltage electrode and the earth electrode. This allowed faster replacement of test specimens, Figure 5.2.

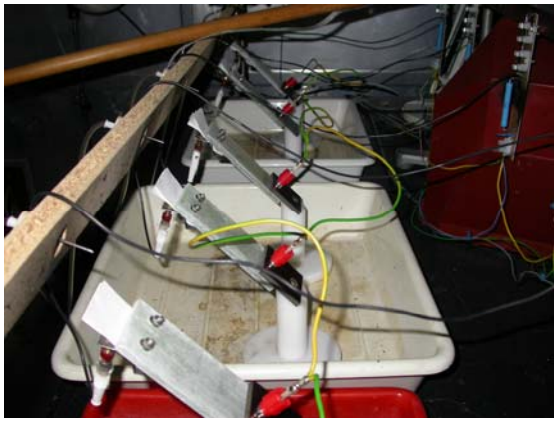

Figure 5.1 Five specimens tested simultaneously according to IEC Publ. 587 [1].

The tests were carried out by applying a high voltage AC on the top electrode, while the specimen was contaminated by a flow of a saline solution. The results sketched below were all obtained by testing according to 'Method 2: stepwise tracking voltage' and with the 'End criterion A: current not exceeding 60mA' [1]. This method implied that the applied voltage was raised 250V each hour, while the flow was increased according to a scheme in the standard. The single specimens failed as soon as the current exceeded 60mA, and the classification of the series of similar specimens was defined by the highest voltage which all five specimens survived. The initial voltage was selected such that all specimens experienced at least three voltage levels.

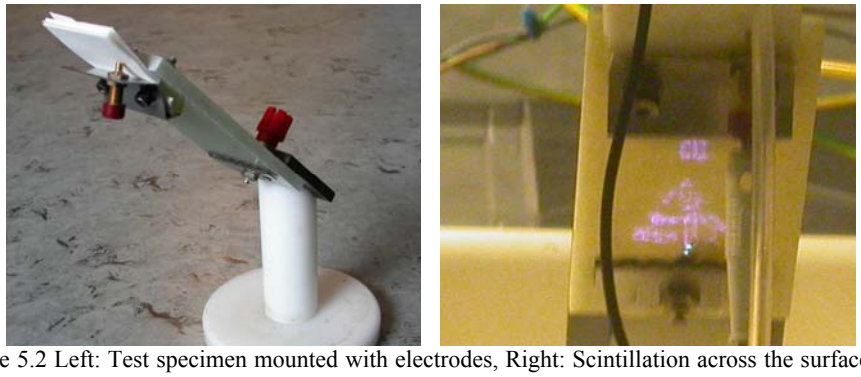

Figure 5.2 Left: Test specimen mounted with electrodes, Right: Scintillation across the surface of a specimen.

In order to control the applied voltage, the flow of saline solution and to measure the time of failure, a computer program was designed in NI LabView. The computer with the program installed was connected to an 'Agilent 34970A Data Acquisition/Switch Unit', which acted as the physical interface to the high voltage setup, Figure 5.3.

At first the flow was controlled with small valves which were difficult to adjust and introduced large inaccuracies. Later a medical pump 'Ismatic IPN-12' from 'VWR International' was introduced. With its RS-232 interface it was now possible to control the flow very accurately and reliably.

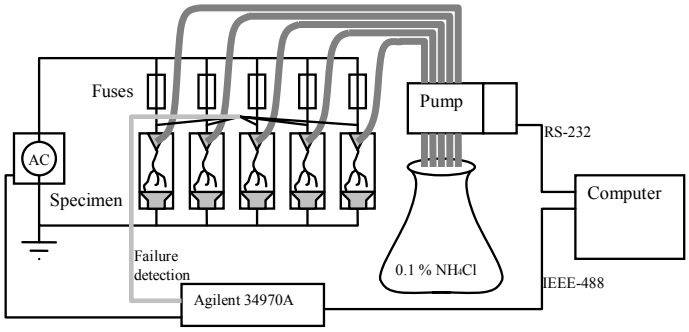

Figure 5.3 Test setup for tracking tests according to IEC Publ. 587 [1].

5.1.3 Evaluation of test method

With the medical pump installed, and by having a computer to control all settings and measurements, the experiments went very well. The results obtained within the same five set of test specimens were very unambiguous and reliable. The few deviations could be explained by surface impurities etc. After testing some different specimens and noting impurities and minor defects in the surface prior to testing, it was possible to predict deviating results within a set of five specimens before the tests were conducted.

5.1.4 Results

Twenty one different materials with different combinations of resin, fibres, weaving techniques, surface conditions etc. were tested. Out of these twenty one series (five specimens each series), only eight series were classified according to the standard. Nine of the remaining thirteen series were so poor that the first specimen failed at the first, second or third voltage level (although the tests were initiated at the lowest value of 1kV). The first voltage levels for the rest of the series (four series) were unfortunately selected too high, which led to a breakdown at the selected level for one or more of the individual specimens. Although thirteen of the tested specimens did not qualify for classification according to the standard, the conclusions from these tests still comply with the results from the classified specimens.

In order to compare the different mechanisms which led to failure, a certain code describing the results is adopted. Each characteristic sign or cause of failure is designated a certain letter, as described below:

A Properties of the resin, A1: Poor properties, A2: Good properties.
B Different types of fibres within the same specimen.
C Fibre orientation, C(F): Felt, with fibres in random direction, C(M): Mats, with fibres perpendicular and parallel to length direction, C(P): Parallel, with fibres only parallel to field direction.

D Defect introduced during production.
E Defect introduced during manufacture.
F Defect introduced during transport.
G Fasten points or pinholes on surface.
H Development of a narrow channel of erosion.
I Erosion on a wider area.

These letters form a code, Evaluation Results, which identifies the test evaluation. In the tables below the following nomenclature is used:

Id. Refers to an identification number unique for every series of specimens in this section. P… refers to a specimen based on a polyester resin, and E… refers to a specimen based on an epoxy resin.
Resin A code that identifies the specific resin.
U_0 The initial voltage.
U_1 The voltage where the first specimen failed.
U_2 The voltage where the last specimen failed.
Class Classification of the specimens according to IEC Publ. 587.
ER Evaluation Results.

Table 5.1 Specimens classified according to IEC Publ. 587.

Id.	Resin	U_0 [kV]	U_1 [kV]	U_2 [kV]	Class	ER
P1	P4600	1.00	1.75	2.25	2A 1.50	A1C(F)GI
P2	P2600	1.50	3.50	4.00	2A 3.00	A1C(F)GHI
P3	P2600	1.00	3.25	4.00	2A 3.00	A1C(F)GHI
P7	P4709	1.00	2.50	2.75	2A 2.25	A2C(F)GI
P11	P4506	1.00	2.75	3.00	2A 2.50	A2C(F)GI
E18	F944	1.25	2.75	3.00	2A 2.50	A2C(M)DHI
E20	F946	2.25	5.00	5.25	2A 4.75	A2C(F)I
E21	F951	1.25	2.75	2.75	2A 2.50	A2C(F)DI

Table 5.2 Specimens that failed within the three first voltage levels.

Id.	Resin	U_0 [kV]	U_1 [kV]	U_2 [kV]	ER
P4	P2600	1.00	1.50	5.00	A1C(F)FGHI
P6	P2607	1.00	1.25	2.75	A1C(F)GHI
P8	P6004	1.00	1.00	1.50	A2C(P)DH
P10	P3510	1.00	1.25	1.25	A2C(P)EH
P12	P6004	1.00	1.25	2.00	A2C(P)DH
P13	P2600	1.00	1.00	1.25	A1C(F)DH
P14	P2607	1.00	1.00	1.25	A1C(F)DFHI
P15	P4506	1.00	1.00	1.25	A1C(F)DHI
P17	P4601	1.00	1.00	1.00	A1C(F)DHI

Table 5.3 Specimens that failed due to too high initial voltage.

Id.	Resin	U_0 [kV]	U_1 [kV]	U_2 [kV]	ER
P5	P4506	1.25	1.25	5.00	A1C(F)HI
P9	P6004	1.50	1.50	2.50	A2BC(P)DH
P16	P2607	2.50	2.50	4.50	A1C(F)DGHI
E19	F945	2.25	2.25	2.75	A1C(F)HI

5.1.4.1 Comments on surface characteristics

In the following section a distinction between specimens with homogeneous and non homogeneous surfaces is made.

Homogeneous surface

Some of the specimens have a very homogeneous and smooth surface. The manufacturing process of these specimens must imply that the fibres are located a bit below the actual surface, such that the surface in principle only consists of resin, either polyester or epoxy. The moisturising of these specimens, according to the tracking tests, is thereby more uniform, and it is seen that the erosion is distributed evenly on the whole surface. The surface current density during this erosion is quite small due to the wide and uniform influence of the discharges, which means it requires longer time and a higher voltage to make the specimens fail. The influence of the discharges is seen as a wide erosion, where the upper most surface layer of the resin is removed as with a slight abrasion. Tiny furrows and holes are seen everywhere, and these are regarded as small starting points for the minor individual discharges. These tracks of scintillation are visible on Figure 5.4.

Figure 5.4 Specimen P7 with a uniform and widely distributed impact exhibiting tiny pinholes.

After this situation, one of two things usually happens:

1. The uniform erosion continues until the surface has been sufficiently roughened. The roughened surface attracts the moisture and fluid more easily and thereby acts as the charge carrier for the final jump. This requires that the surface initially is very smooth and without any scratches and defects.

2. If a minor inhomogeneity as a particle, a scratch or similar is present, the fluid will accumulate and the specimen experience a field enhancement and an increased current density at this place. A lot of the energy will thereby be dissipated at this particular spot implying an increase in temperature and a faster degradation. The degradation develops parallel to the field direction, while creating a narrow channel in the surface, Figure 5.5.

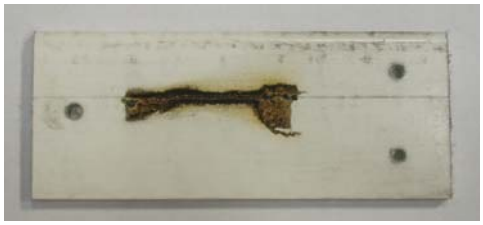

Figure 5.5 Specimen P13 failed at a relatively low voltage due to the presence of a scratch parallel to the field direction.

The channel, or furrow in the surface of the specimen, attains a higher conductivity than the rest of the surface. This is partly due to the conductive nature of the decomposition byproducts from the resin, and due to the fact that the conductive fluid accumulates in these defects. The voltage drop across the electrodes is thereby primarily located outside the channel, implying that the process intensifies itself due to the field enhancement in the tip of the channel. When this sort of channel has begun, the final jump usually occurs after a few minutes.

Inhomogeneous surface

Most of the specimens are pultruded, where the direction of manufacture equals the length axis and the field direction. In these specimens, the fibres in the surface are thereby located parallel to the length of the specimens, such that micro cracks, small voids of air and further in homogeneities lie in the longitudinal direction. If these defects are located in the surface, the fluid will accumulate and a similar situation with creation of a conducting channel is present. These specimens with in homogeneities present prior to testing will, in other words, skip the wide erosion and go directly to the creation of a conducting channel, Figure 5.6.

Figure 5.6 Specimen P12, where fibres located in the uppermost surface layer are the main cause of the fast deterioration.

Other defects which can result in sudden failure are single fibres or bundles of fibres with different characteristics (ex. colour, strength, size, etc.) woven into the surface laminate, Figure 5.7. With different materials brought together in one construction the possibility for failure in this interface usually increases. Scratches due to manufacture could also absorb the fluid and initiate the creation of the conducting channel.

Figure 5.7 Specimen P9, where the tracking erosion occurred along a fibre bundle with different characteristics in the surface.

5.1.4.2 Comments on types of resin

Four of the specimens are made with an epoxy resin as the matrix, while the rest of the twenty one specimens are made with a polyester matrix, Figure 5.8. The characteristic results obtained with the two different types of resin are summarised below.

Figure 5.8 Characteristic erosion of specimens with different resin systems. Left: Specimen P13 with a polyester based resin, Right: Specimen E20 with an epoxy based resin.

Epoxy

- The surface appears much more uniform prior to testing.
- None or very little erosion on the surface.
- The surface of the specimens appear faint or hazy.
- The matrix melts along with the fibres.

Polyester

- The matrix burns easier away than the fibres, maybe due to the lower temperature required.
- The fibres burn like the matrix at places where the current density is high, at narrow channels of degradation
- The degradation begins with wide erosion and ends up in a narrow channel, depending on impurities.
- The scintillation leaves some microscopic pinholes in the surface which is believed to form fastening points for the minor discharges.

5.1.4.3 Comments on fibre orientation and weaving techniques

When producing pultruded GFRP, it is possible to choose between different structures of the fibres. The specimens that have been tested are produced with either fibres parallel to the pultrusion direction, as regular perpendicular woven mats or as a felt structure where the fibres are oriented randomly in the uppermost surface layer, Figure 5.9.

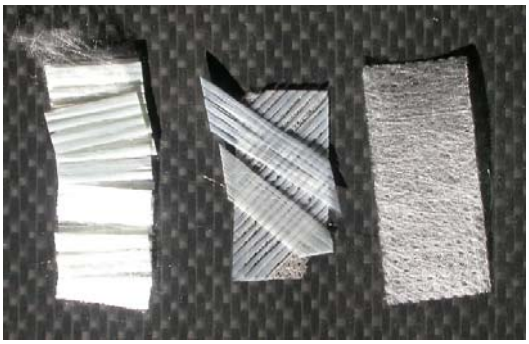

Figure 5.9 Different ways of organising glass fibres, as uniformly oriented fibre bundles, perpendicular woven mats with an angle between laying direction of 90 deg and as a felt structure ensuring randomly oriented fibres.

The overall conclusion is that optimisation of the tracking resistance of a structure is very much dependant on the fibre orientation in the uppermost surface layer. If it is selected to have fibres at the top layer, it is important to avoid fibres that are parallel to the electric field direction.

By choosing fibres perpendicular to the field direction or in a random structure at the surface, the probability of having oblong air pockets or voids with a fatal extent oriented parallel to the field direction, possibly leading to failure is minimised.

Concerning the manufacture of wind turbine blades, it is difficult to predict the field direction when a lightning hits the blade. With this in mind, a solution with randomly oriented fibres just beneath a surface layer of pure resin is suggested. This is believed to improve the overall tracking resistance.

5.1.4.4 Conclusion and suggestions of material improvements

Concerning the tests according to IEC Publ. 587 performed in this section, the following advices and general recommendations towards improved tracking resistance of wind turbine blades are suggested

1. Ensure that surfaces are as pure and homogeneous as possible, such that dirt and moisture do not stick to defects etc. If there are any impurities located at the surface, the discharge will quickly find this weakest spot and start the deterioration. The field enhancement due to the needle shaped discharges will increase the speed of tracking failure.
2. Do not introduce any inhomogeneities in the material surface, e.g. single interwoven fibres with different properties. Such discontinuities where different materials meet increase the risk of micro cracks etc., where moisture and dirt can attach more easily.
3. Make sure that no fibres in the outermost surface layer are oriented parallel to the expected direction of the electric field. If the direction of the electric field is unknown, construct the composite with randomly oriented fibres just beneath a skin of resin.
4. With respect to tracking resistance, it is advised to use an epoxy based resin instead of a resin based on polyester.

Coated specimens have not been treated in this thesis. However, it is believed that a homogenous coating layer will play an important role, and that a coating layer based on an epoxy resin will perform equally well as the homogeneous surfaces with epoxy matrices tested here.

The perfect material is both resistant towards tracking, and has very high breakdown strength. Only parameters regarding the first part have been investigated in this section 5.1, leaving the investigation of the breakdown strength to the following section 5.2.

5.2 Breakdown field strength

5.2.1 Purpose

As discussed in section 4.6.2, the following two test methods aim at determining the electrical breakdown strength of composite materials used for wind turbine blades. Due to the large degree of inhomogeneity and thereby a pronounced volume effect, the test methods must stress a larger volume than described by most standards covering this subject. In both cases the specimens are stressed by the presence of surface discharges resulting in an electrical breakdown of the bulk material.

5.2.2 Initial approach, rectangular specimens

To meet the requirements for testing the breakdown strength of insulating materials used in wind turbine blades, a test specimen capable of stressing well known volumes with surface discharges is relevant. The purpose of these particular tests was to determine the breakdown field strength of various materials and investigate the dependency of laminate thickness, coating thickness and the overall composite thickness. The test method

used is based on IEC-243-3 [62], and experience obtained previously with breakdown tests on composite pipe specimens [6] and [69].

5.2.2.1 Test specimen

When an electrical breakdown in the blade laminate is occurring, streamers on either side of the blade searches the surface for weakest spots to get connected. This would require rather large specimens, since the flashover field strenght along an insulating surface is much lower than the breakdown field strength through the bulk material. This is illustrated by a test with a 1.2/50us impulse voltage on a 1.2m by 1.2m GFRP plate, Figure 5.10. At this particular amplitude, the streamers emitted from the high voltage electrode on top of the plate move towards the edges, and get connected with streamers from the ground electrode below the plate. The creeping distance was in other words too short at this test.

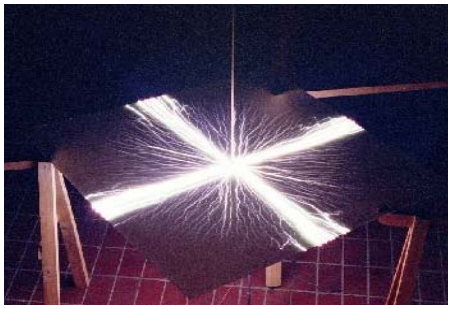

Figure 5.10 1.2/50us lightning impulse applied across a 1.2m x 1.2m GFRP plate. Streamers on either side searches the entire surface for weaknesses until shortening occurs along the edges, Upeak=242 kV [6].

Since all GFRP materials used on blades have rather high electrical breakdown field strength relative to the flashover field strength, this problem can not be avoided totally. However a test specimen where the surface flashover extends in only one direction combined with a test method allowing surface flashovers at low voltages minimises the materials used for manufacturing the test specimens, Figure 5.11.

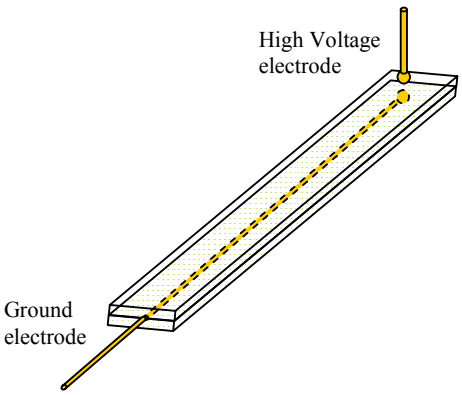

Figure 5.11 Rectangular test specimen for measuring the electrical breakdown field strength.

The specimens are 1m long and 15cm - 25cm wide, and consist of an upper side of GFRP laminate (which is the part that is stressed), a ground electrode mounted in the middle of the specimen, and finally, the lower side which is also made of GFRP thick enough to avoid breakdown from this side. After the specimens have cured, a primer and gelcoat is applied to the upper side depending on the manufacturer.

The ground electrode is a steel sphere with a diameter of 12.5mm, mounted on a brass rod with a diameter of 4mm. The brass rod is a bit longer than the specimen, as seen on Figure 5.11, which enables termination to facility ground.

As high voltage electrode, a similar steel sphere was used placed right above the steel sphere on the ground electrode. The distance between the surface of the test specimen and the high voltage electrode is kept at 50 mm, Figure 5.12.

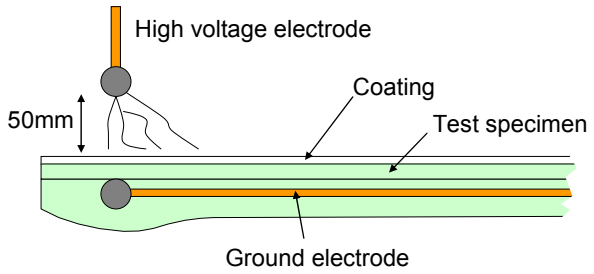

Figure 5.12 Rectangular test specimen for measuring the electrical breakdown field strength.

To investigate how the discharges from the high voltage electrode will form on the surface, a numerical model of the test setup in a FEM program was established. Details about the reason for using FEM models and other applicability towards wind turbines in general are given in Appendix A.

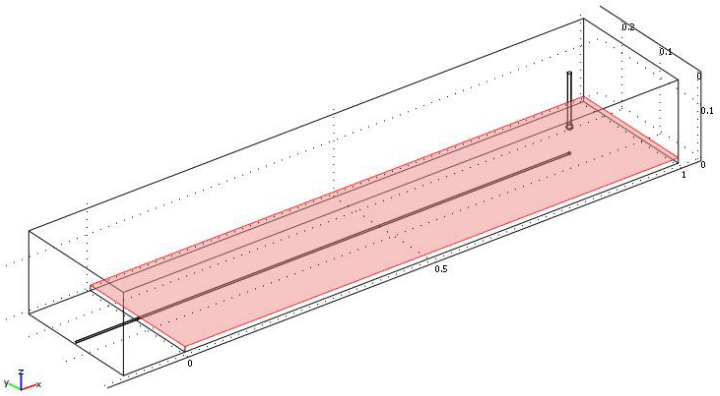

Figure 5.13 The electric field across the surface of the specimen in section 5.2.2 is calculated with a FEM 3D electrostatic model

By defining the materials according to their permittivities, and assigning a potential of 100kV on the high voltage electrode and 0V on the ground electrode, the electric field on the surface of the specimen is computed.

The upper image on Figure 5.14 shows the absolute tangential electric field on the surface of the specimen. At these static conditions without any discharges from the high voltage electrode, the electric field is higher above the ground electrode, and will thereby tend to guide the discharge along this path. At a certain potential, a discharge will form from the high voltage electrode towards the surface and propagate along the path of the ground electrode towards the ground termination. A simulation of this condition when the streamer discharge has traversed 20cm along the surface is shown on the bottom image of Figure 5.14. Here it is seen that the electric field in front of the streamer is still largest right above the ground electrode, indicating that the discharge will continue at the same path until the final flashover occurs. The results are only qualitative; hence no colour code for the actual computed fields is shown.

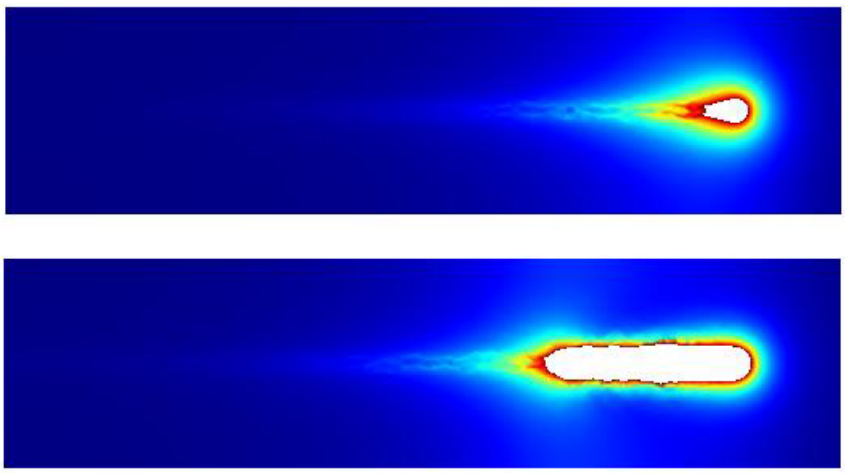

Figure 5.14 Absolute tangential electric field on surface of test specimen, where red indicates a high field region and blue corresponds to low field regions. Top: Electric field without streamer formation from high voltage electrode, Bottom: Electric field on surface when a streamer of full potential has propagated 20cm from the high voltage electrode towards the ground termination.

One of the results from these 3D simulations is that whenever a ground electrode is present below the surface, the discharge above the surface tends to be guided along the path of the ground electrode, as found elsewhere in literature [70]. This is in good agreement with the simulations conducted for the test setup in section 5.2.3, which was designed based on the exact same phenomenon.

The design of the test specimen minimises the material used for each specimen, while a large creeping distance, to avoid flashover, is still maintained. When a lightning impulse is applied on the high voltage electrode, an electrical discharge will form on the surface, searching for the weakest spot to develop a breakdown. Prior to testing, the surfaces of the

specimens were cleaned with ethanol to ensure that no dirt or moisture would affect the flashover probabilities.

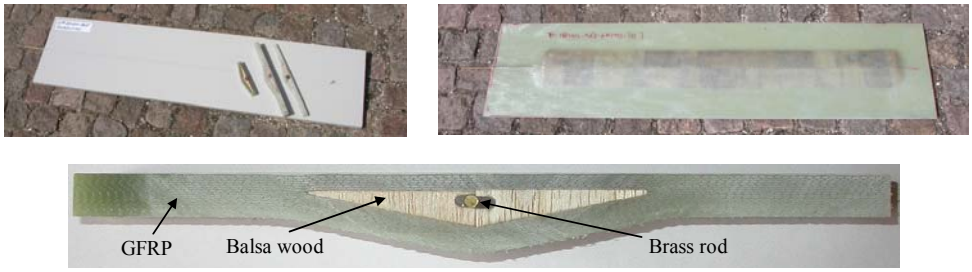

Figure 5.15 Rectangular test specimen for measuring the electrical breakdown field strength, Upper left: Front side of specimen and cross sections, Upper right: Back side of specimen, Bottom: Cross section perpendicular to the length of the specimen.

Fifty five specimens distributed on seventeen different types were made by three different Danish wind turbine blade manufacturers as seen on Figure 5.15. The large amount of specimens where specified such that three separate analysis could be performed, in which the entire thickness, the coating thickness or only the laminate thickness was varied.

5.2.2.2 Test method

As showed statistically in Chapter 6, wind turbine blades are usually hit in the outermost regions of the blade, where the thickness of the surface skin is around 2mm - 10mm. Previous experiments carried out at The Technical University of Denmark have shown GFRP material breakdown field strengths in the order of 15kV/mm-30kV/mm. With test specimen thicknesses of 1.2mm - 7.0mm, a certain amount of flashovers at lower voltages was expected before a breakdown could occur. Earlier research has shown that breakdown voltages recorded during test situations where both breakdown and flashover occurs, are very much comparable to breakdown voltages measured without a flashover [69].

The lightning test impulse was generated with a twelve stage Marx generator, with a maximum charging voltage on each stage of 100kV. Due to the geometry of the specimens, only four or six stages were necessary to create a breakdown. A standardised double exponential lightning impulse is defined by a rise time of 1.2us +/- 30%, and a decay time of 50us +/-20% [59] which is also approved as waveform B in the standards used by the avionics industry in dielectric testing of composite airframes [34]. A switching type pulse (usually 250/2500 us) would allow more time for streamers to develop, but here 1.2/50us pulses are used as the objective of this work is to study the breakdown properties of GFRP on relatively small specimens, and not the study of surface discharges [35].

A negative polarity on the high voltage electrode will result in the onset of streamers at a lower voltage than with positive polarity [27]. This streamer initiation is essential as the discharge is supposed to search the surface for defects finally leading to a breakdown. Recent work within the subject also indicated that negative polarity results in the lowest

breakdown strengths [69], and since the number of specimens was limited it was selected to use negative polarity for all these tests as well.

Based on previous experience and standardised methods [6, 59, 62], the test procedure followed the flow diagram in Figure 5.16.

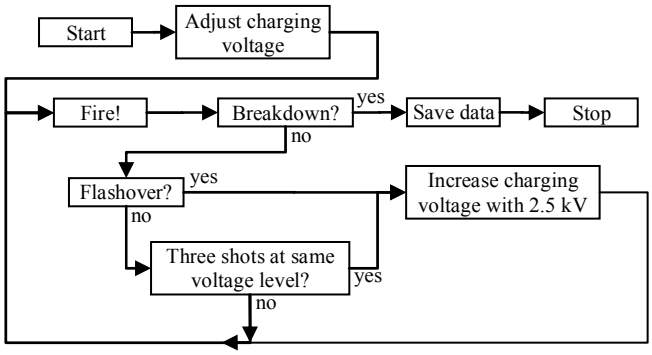

Figure 5.16 Flow diagram of test procedure for measuring the electrical breakdown field strength.

An initial peak value of the impulse voltage is selected so that the specimen will survive at least three voltage levels. The generator is charged and three discharges at the selected voltage level are initiated. If neither breakdown nor flashover occurs within these three shots, the charging voltage is increased by 2.5kV (10kV-12kV increase in peak value considering six stages in the Marx generator), and three more discharges are initiated at this new voltage level. If a flashover occurs during one of three shots at the same level, the voltage is raised immediately to the next level. This described procedure where the voltage is increased depending on whether a flashover occurred or not, is continued until breakdown, Figure 5.16. The breakdown voltage is defined as the highest voltage achieved at the pulse causing breakdown.

Charging voltage, peak value, rise and decay times are recorded for each discharge. For those discharges leading to flashover or breakdown, the time-voltage curve is saved as well.

Evaluation of test method

In general, the experiments went very well. All specimens ended up having a breakdown through the upper side, except one where the breakdown occurred in the interface between the front and the back side. Throughout the text, capital letters in brackets refer to the specific test specimens listed in Table 5.4 and Table 5.5.

Experience and pictures of discharges have shown that the streamer approaching from the high voltage electrode tends to follow the brass rod towards the ground termination. In cases where flashover occurred, it was very obvious that the brass rod attracted the discharge. Photographs of discharges leading to breakdown have also shown that before the breakdown channel developed through the stressed specimen, streamers approached the ground termination along the surface as expected from the numerical simulations, Figure 5.17.

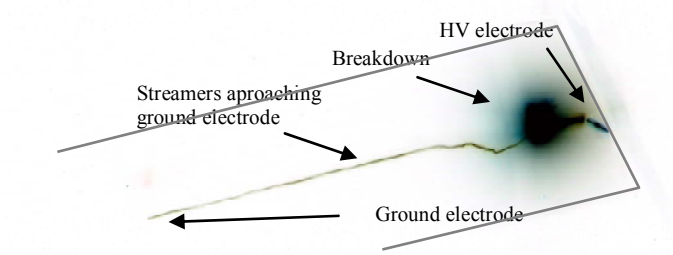

Figure 5.17 Negative image of the surface of specimen (I) during breakdown test. A breakdown beneath the high voltage electrode is visible to the right, whereas a streamer approaching the ground termination is seen to the left.

Occasionally the breakdown occurred right between the steel spheres, but most often the breakdown was located some distance away from the high voltage electrode, between the sphere on the ground electrode and the end of the brass rod. It was also very obvious from photos of the discharges, that the streamers searched the surface above the ground electrode, and when they found the weakest spot, they punctured the laminate, Figure 5.18.

Some of the specimens experienced two separate breakdowns within the same discharge, a phenomenon commented in the following section, Figure 5.18.

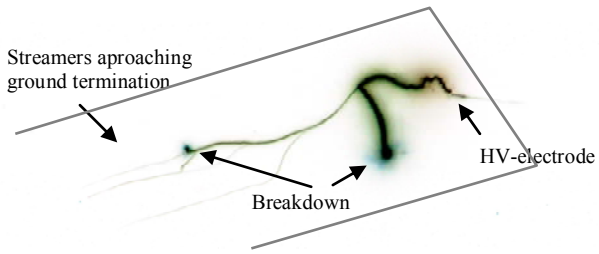

Figure 5.18 Negative image of two breakdowns at the same specimen and streamers approaching the ground termination searching the surface for weakest spots (E).

The particular specimen on Figure 5.18 was equipped with a copper mesh as ground electrode, explaining the search of streamers on a wider area.

5.2.2.3 Results

The results were obtained using materials produced by three Danish wind turbine blade manufacturers. Conclusions are based on tests of a total of fifty five specimens distributed on seventeen different types. For each type of specimen, the dimension and the electrical properties are listed in Table 5.4 and Table 5.5.

Table 5.4 Layer thicknesses of the seventeen different types of specimens for measuring the electrical breakdown strength. Not all specimens are constructed similar which explains the empty cells.

Id.	Coating [mm]	Primer [mm]	1. layer laminate [mm]	Foam [mm]	2. layer laminate [mm]	Overall thickness [mm]
A	0.16	0.50	2.10			2.76
B	0.16	0.50	6.30			6.96
C	0.60		5.05			5.65
D	0.60		0.61			1.21
E	0.60		2.83			3.43
F	0.40		0.80	5.00	0.80	7.00
G	0.40		1.60			2.00
H	0.60		2.83			3.43
I	0.60		5.05			5.65
J	0.60		2.83			3.43
K	0.48	0.50	2.10			3.08
L	0.16	0.50	4.20			4.86
M	0.60		2.83			3.43
N	1.20		0.80	5.00	0.80	7.80
O	1.20		1.60			2.80
P	0.32	0.50	2.10			2.92
Q	0.16	0.50	2.10			2.76

Table 5.5 Measured values of electrical breakdown voltage, withstand voltage and time to breakdown. Each value is found as an average value based on several tests on the same type of specimen.

Id.	Breakdown voltage [kV]	Withstand voltage [kV]	Time to breakdown [us]
A	-130.7	-132.5	5.3
B	-133.5	-149.7	0.8
C	-135.5	-184.9	1.3
D	-115.9	-119.3	4.1
E	-99.8	-107.3	2.3
F	-104.6	-136.9	2.3
G	-95.6	-95.5	3.1
H	-104.3	-102.6	2.6
I	-144.6	-169.6	2.9
J	-124.4	-127.2	2.7
K	-141.8	-130.2	2.2
L	-142.7	-134.1	1.1
M	-128.6	-121.2	3.9
N	-147.0	-152.2	4.9
O	-106.8	-105.7	4.9
P	-113.1	-147.2	0.9
Q	-128.2	-138.5	1.5

Three different analyses are performed.

1. A plot of the breakdown and highest withstand field strength versus the overall thickness of the specimens including both laminate, primer and coating, Figure 5.19.
2. Two plots of the breakdown and highest withstand field strength versus the thickness of the laminate for fixed coating thicknesses. Among the specimens are two separate series with two different but constant coating thicknesses, which is the reason for plotting two sets of data, Figure 5.21 and Figure 5.22.
3. A plot of the breakdown and highest withstand field strength versus the thickness of the coating for fixed laminate thickness, Figure 5.24.

All the different data points for each test specimen are plotted with blue '+' signs for the breakdown field strength and red 'o' for the highest withstand field strength. Furthermore, a straight line representing the best linear fit of the data, based on the least square method, is drawn. The best fit lines are marked with '___' for the highest breakdown field strength and '…' for the withstand field strength. The intention is not to compare different actual values between the manufacturers or to relate the measured values with tabulated ones, but merely to recognise certain tendencies.

E_B versus overall thickness

Thirty eight of the specimens were constructed in a similar manner with a layer of laminate covered by a layer of coating. For these specimens it is possible to plot the breakdown electric field and highest withstand electric field to compare results at different total thicknesses. This analysis does not distinguish between different relations of coating thickness and laminate thickness, which is done in section 'E_b versus laminate thickness' and 'E_b versus coating thickness'.

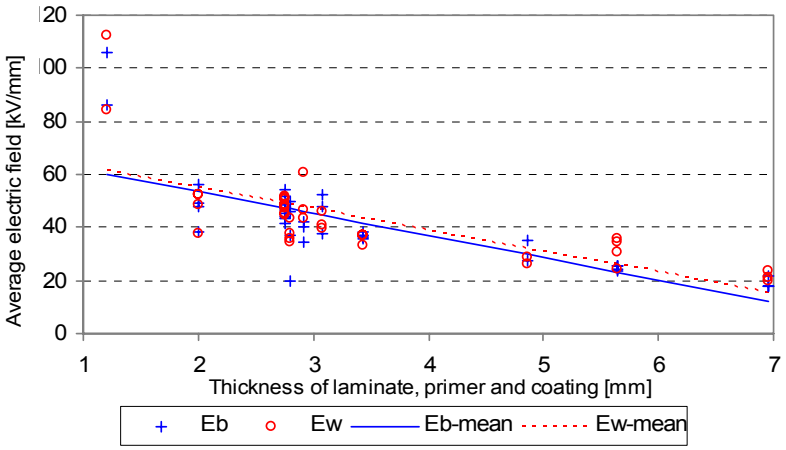

Figure 5.19 Average electric field at breakdown voltage and highest withstand voltage versus overall thickness of laminate, primer and coating.

Due to the comprehensive manufacturing processes, it is very difficult to maintain a high degree of homogeneity in large composite structures. Although an actual blade surface seems very smooth, and all precautions have been made to avoid differences in material thicknesses, the situation is somewhat different. By plotting field strengths versus overall thicknesses for different kinds of material compositions from different manufacturers, the natural inhomogeneities are to some extent equalised, Figure 5.19.

The results show a clear tendency of decreasing breakdown field strength with increasing overall thickness. Although the data are encumbered with a large dispersion, an indication of the volume effect is present, section 4.3.1.

Investigations of material defects

It was suspected that breakdown would be influenced by material defects, and in order to classify these defects, cross sections of the specimens were investigated with a microscope, Figure 5.20.

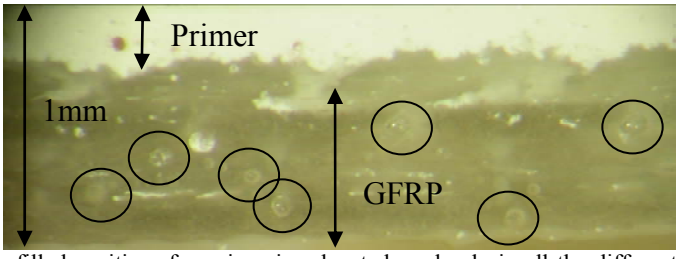

Figure 5.20 Air filled cavities of varying sizes located randomly in all the different types of laminate.

Close up pictures of cross sections revealed a rather large amount of air filled cavities present in all the different types of laminate. The interface between coating, primer and laminate also showed a risk of having impurities and other defects.

Subsequent to these microscopic investigations, volume and mass of randomly selected specimens were measured. This in connection with burnout tests for measuring the fill factor enabled an estimation of the air content relative to the total volume of the specimen, section 4.2.1.

The specific volume of air in twelve different specimens were estimated, with a span from 0% to 13% and an average value of 5.8%. When the volume of a stressed material with a certain content of air increases, the probability of finding a cavity large enough to initiate a breakdown at the applied voltage increases as well. Minor discharges in these small cavities will indeed affect the breakdown voltage, as discussed in section 4.3.1.

E_B versus laminate thickness

An estimation of the influence of the laminate thickness on the electrical properties is made in this section. Two separate series of test specimens (J, C, M, D, I, E, H) and (A, Q, L, B) were constructed with the same coating layer, but with different laminate thicknesses.

Again, figures of breakdown voltage and the highest withstand voltage, with respect to the thickness of the specimen are plotted, Figure 5.21 and Figure 5.22.

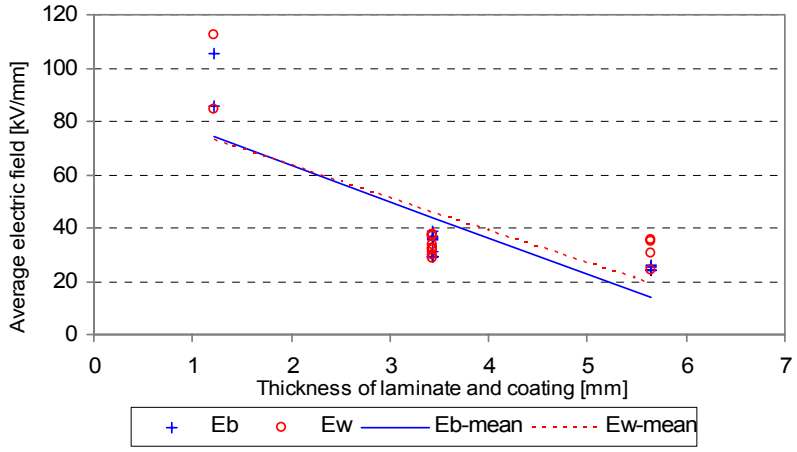

Figure 5.21 Average electric field at breakdown voltage and highest withstand voltage versus overall thickness for fixed coating thickness of 0.6 mm (J, C, M, D, I, E, H). The laminate thickness is varied between 0.6mm, 2.8mm and 5.1mm.

The breakdown field strength still tends to decrease with increasing laminate thickness, Figure 5.21. Despite the lack of measurements at thicknesses between 1mm and 3mm, it seems that a well fitted curve would be steeper for thinner specimens than for thicker specimens. This again indicates the presence of a volume effect, section 4.3.1.

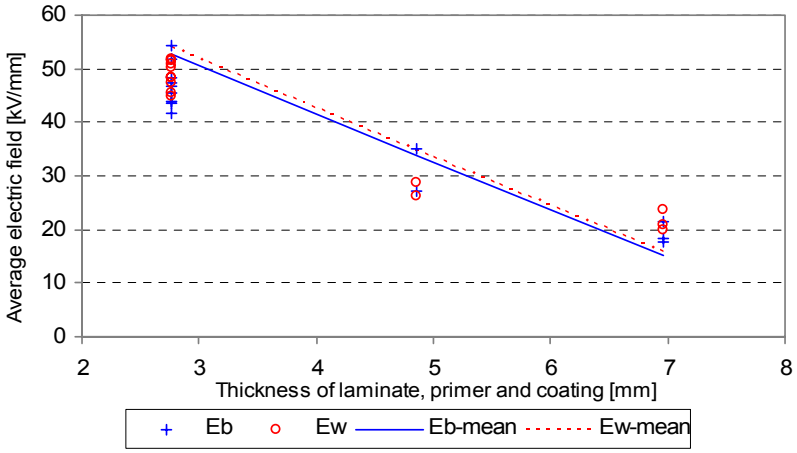

Figure 5.22 Average electric field at breakdown voltage and highest withstand voltage versus overall thickness for fixed coating thickness of 0.16mm, and fixed primer thickness of 0.50mm (A, Q, L, B). The laminate thickness is varied between 2.1mm, 4.2mm and 6.3mm.

Results from the second series with fixed thickness of coating and primer shows almost similar results, Figure 5.22. The field strength decreases with increasing laminate thickness, but not as rapidly as before.

The thinnest specimen in this second series is 2.8mm, with breakdown strengths between 42kV/mm and 54kV/mm. If these data were placed in the former diagram, they would almost fit a straight line with a larger gradient. Although the two types of specimens (coating and laminate) are of different origin and slightly different thickness, a plot with all data from specimens (A, Q, L, B) and (J, C, M, D, I, E, H) is made, Figure 5.23.

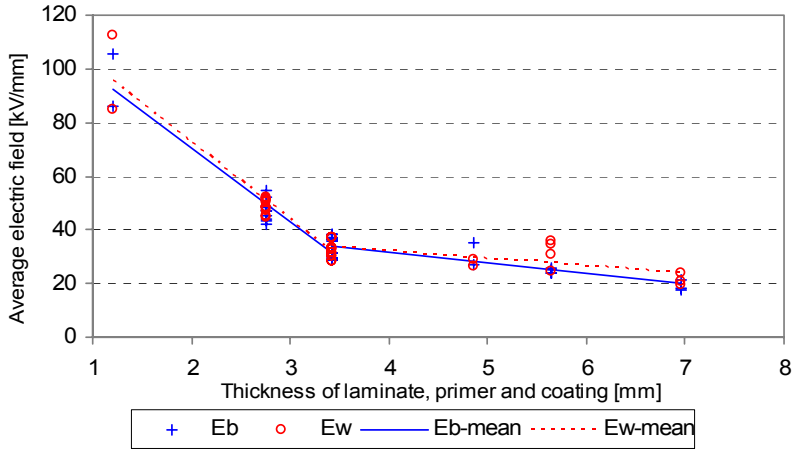

Figure 5.23 Average electric field at breakdown voltage and highest withstand voltage versus overall thickness for fixed coating and primer thickness of either 0.6mm coating or 0.16mm coating and 0.5mm primer (J, C, M, D, I, E, H) and specimens (A, Q, L, B).

The tendency lines are drawn in two steps. The first two lines with the highest gradients are based on the data sets at the three thinnest specimens, up to 2.8mm. The second two lines are based on the four thickest specimens with laminate thicknesses from 2.8mm to 7.0mm.

This picture indicates that two different mechanisms could be present. Initially the same explanation as mentioned earlier is valid, where the volume effect accounts for the rapid decrease in breakdown strength, Figure 5.23. When the thickness of the specimens get above a certain value, the volume is so filled with cavities of different sizes, that a further increase in volume does not increase the probability of finding larger cavities, hence the volume effect diminishes. This might be correlated with the manufacturing process where simultaneous injection by evacuation and curing of the resin might define an upper boundary for the size of cavities. These larger cavities (if they were present) would probably decrease the breakdown strength even further.

Exactly at which thickness this phenomenon takes place must depend on the different manufacturing processes.

E_B versus coating thickness

Another parameter to vary is the thickness of the coating. A series of specimens made with the same laminate thickness of 2.1mm, a primer thickness of 0.5mm, and coating thicknesses varying between 0.16mm, 0.32mm and 0.48mm, enables this comparison.

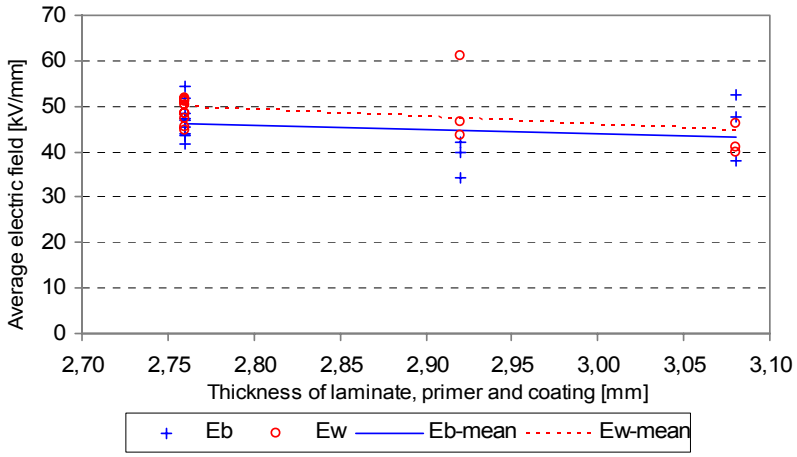

Figure 5.24 Average electric field at breakdown voltage and highest withstand voltage versus overall thickness for fixed laminate thickness of 2.1 mm, and fixed primer thicknesses of 0.50 mm (A, Q, P, K). The coating thickness is varied between 0.16mm, 0.32mm and 0.48mm.

Interestingly a change in coating thickness does not affect the breakdown or withstand voltages much. The very small gradient of the best fit curves could indicate a volume effect in the coating. Small defects and cavities are visible in the coating when looking at specimens in a microscope, but they are not as dominating in size and number compared to the amount of voids in the laminate. The minor decrease in breakdown and withstand field strengths on Figure 5.24 is probably just a coincidence.

Initial breakdowns

On all figures it is seen that the withstand field strength seems a bit higher than the breakdown field. This fact indicates that a breakdown is formed within several impulses. Some initially very high stresses may start minor discharges in the air filled cavities, discharges that suddenly led to formation of the final breakdown. This hypothesis is supported by some photos taken of pre-breakdowns and final breakdowns of specimens (L) and (B), Figure 5.25 and Figure 5.26.

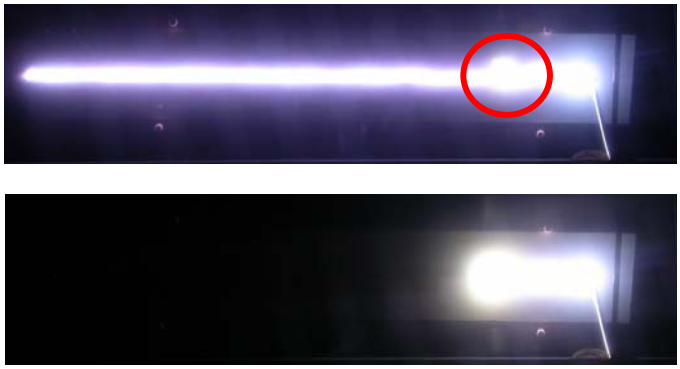

Figure 5.25 Image of breakdown in specimen (L). Note the strong light on the first picture indicating a pre-breakdown.

The first photo was taken of the discharge just before the final discharge leading to breakdown (the second photo). Only the final breakdown captured on the second photo was visible at the time-voltage curve. The exact same situation happened with specimen (M). An image of the discharge just before the one leading to final breakdown showed a pre-breakdown which was not visible on the time-voltage curve, Figure 5.26.

Figure 5.26 Image of breakdown in specimen (M). Note the strong light on the first picture indicating an initial breakdown.

Relating these observations with lightning attachments to wind turbine blades emphasizes something very important. Most often, lightning attaches to the discrete lightning receptors as discussed in section 3.2. However, situations occur where streamers develop along exterior surfaces where charges or streamers of different potential or even the opposite polarity are present on the interior side of the laminate. This could result in partial breakdown and weakening locally, and therefore the lifetime of the blade regarding lightning may be decreased after some of these surface flashovers.

Copper mesh or carbon fibres

For four of the test specimens the ground electrode (brass rod with steel sphere) was replaced with a copper mesh or a carbon fibre laminate. The breakdown of these specimens occurred on the edge of the mesh/laminate, which is rather obviously due to the field enhancement at sharp edges. If blade manufacturers intend to protect their blades with flat and sharp edged structures like a metal mesh or similar, the lightning will most certainly attach to the edges of these structures.

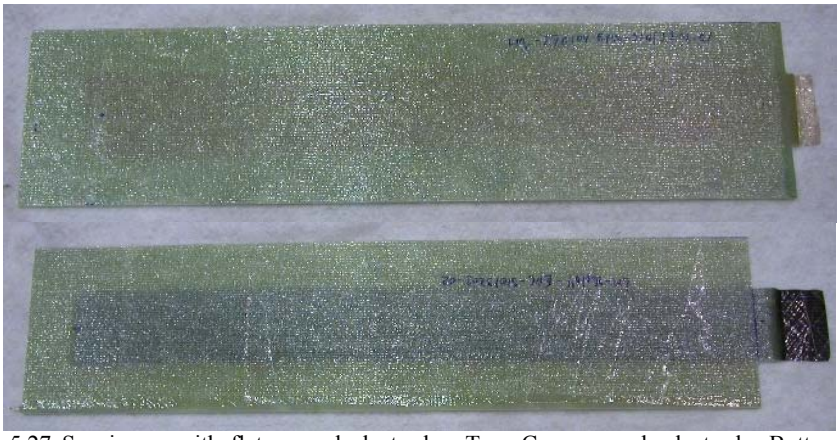

Figure 5.27 Specimens with flat ground electrodes. Top: Copper mesh electrode, Bottom: CFC electrode.

As discussed in section 2.4.4.3 this edge attachment might require additional attention.

Particularly for the specimens with copper mesh electrode, two separate breakdowns on each specimen were seen, Figure 5.18 and Figure 5.28.

An explanation of this phenomenon could be the impedance of the thin copper mesh. Assuming that the first breakdown occurs closest to the HV electrode, the high impedance will result in a voltage drop along the copper mesh during current conduction. The potential at the point where breakdown occurred initially will then not decay immediately after the first breakdown, giving time enough for further streamer propagation at nearly full potential towards the ground electrode. A voltage drop along the copper mesh combined with the development of surface streamers towards the ground termination applies a large stress on new areas of the specimens, Figure 5.28.

Nearly all the energy is released in the first breakdown, which does not leave much for the second one. This is also evident when looking at the image where the second breakdown is of a much smaller extent than the first one, Figure 5.28. The time-voltage curve of the breakdown in specimen (E) clearly indicates that a time of 0.7 us has elapsed from the first to the second breakdown, Figure 5.29.

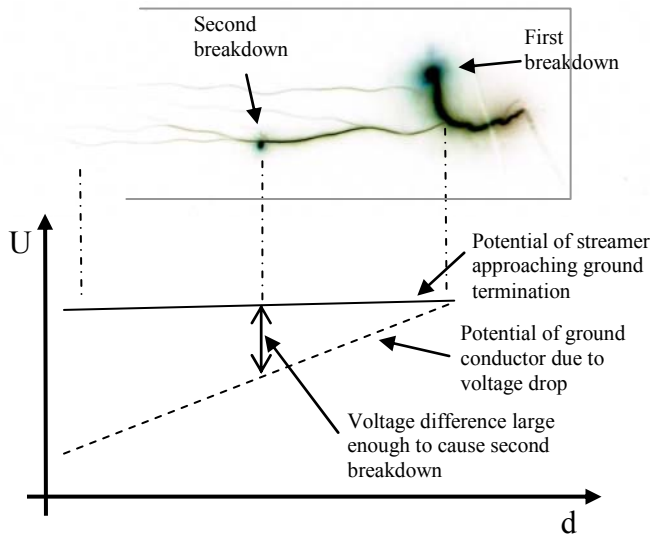

Figure 5.28 Negative image of two breakdowns at specimen 'E'. The potential after the first breakdown (right) decays so slowly that further streamer development is possible. The impedance of the copper mesh together with the streamers at high potential implies a large stress on new areas of the material. This results in a second breakdown (left).

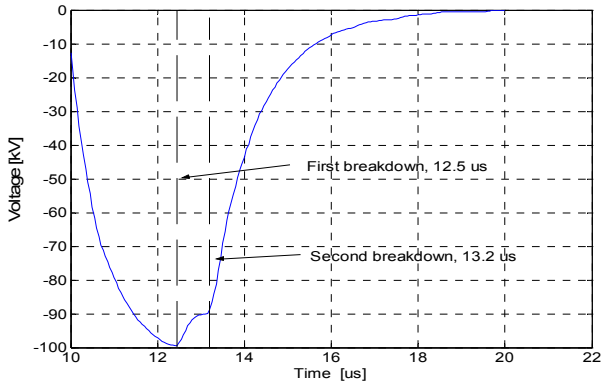

Figure 5.29 Time-voltage curve for breakdown in specimen 'E'.

When lightning has attached to a blade, the current must be conducted safely towards the ground connection in the root end. The conductor in this case must have an impedance low enough to ensure that no critical voltage drop along the conductor occurs. This could result in further streamer propagation on the blade surface, and finally a breakdown towards a streamer initiated from the inner down conductor.

5.2.2.4 Conclusion and suggestions for improvements

The above experiments indicate that the breakdown and withstand field strengths decrease with increasing thickness of composite materials used for blade manufacturing. This is both valid when dealing with the compound specimen consisting of laminate and coating, and when testing the laminate alone. Furthermore, it suggests that up to a certain thickness, the field strength decreases more rapidly than beyond this point. The phenomenon is explained by a volume effect partially caused by a relatively large content of air filled cavities.

Although air content is a very difficult parameter to adjust, manufacturers must try to minimise the amount of air filled cavities in the laminates. As wind turbine blades are continuously subjected to a higher risk of lightning attachment, the structure must be seen not only as a mechanical structure, but also as a high voltage component.

When eliminating the laminate thickness, and comparing different thicknesses of coating, the breakdown and withstand field strengths are not much affected. There have been observed small cavities and impurities in the coating layer, but to a much lower extent than in the laminate.

Photos of discharges have revealed the possibility of pre-breakdowns occurring during a flashover. These initial breakdowns are not visible on the time-voltage curve, but several series of pictures prove their existence. The pre-breakdowns are regarded rather problematic in relation to actual lightning attachment to wind turbine blades, since the arc of a successful receptor attachment tends to sweep along the insulating surface. As discussed in section 3.2, this sweeping phenomenon applies the full potential between the arc channel on the exterior and the internal streamers. As a consequence of this, both the breakdown strength and the ability to reject surface flashovers must be optimised.

Four specimens had the ground sphere and the brass rod replaced by either a copper mesh or a carbon fibre laminate. Breakdowns to these specimens always happened to the edges of the electrodes. Manufacturers that tend to develop lightning protection consisting of flat electrodes or flat down conductors must be aware of the field enhancement at possible sharp edges. This field enhancement might initiate streamers at lower ambient field strengths than expected for conductors with a more smooth geometry, as circular conductors etc.

When copper meshes were used as the ground electrode the rather large impedances implied a voltage drop along the conductor. In these two cases it led to the formation of two breakdowns in one single discharge. The impedance of down conductors must be kept as low as possible. If this is not the case, critical voltage drops will develop during the conduction of the lightning current, possibly leading to streamer initiation and side flashes along the blade surface and from the down conductor system, Figure 5.30.

Streamers propagating along the exterior surface of the blade are possibly attracted to charge deposited on the interior of the blade surface. The pair of streamers or charges at different potentials on each side of the blade skin applies electrical stress on a larger area. This stress may, in worst cases, lead to subsequent breakdowns.

During these initial breakdown tests, it was recognised that the test specimens and electrode configuration could be optimised to enable test of a larger variety of samples. The thin brass rod used as ground electrode also attracted the discharges and somehow

limited the stressed volume. Consequently, some ideas were proposed for an improved test method which is described in the following section.

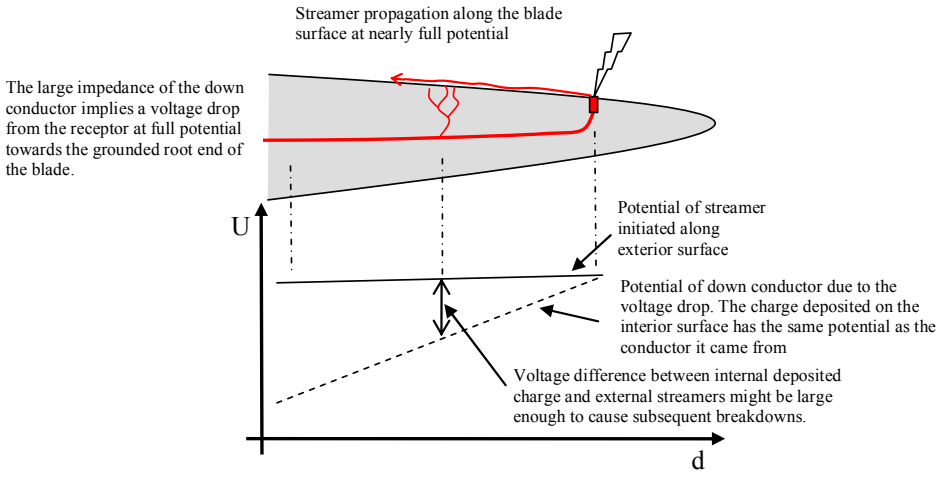

Figure 5.30 Voltage drop across blade skin due to high impedance down conductors.

5.2.3 Second approach, quadratic specimens

As a consequence of experiences with the initial breakdown tests performed in the previous section, a new method for evaluating the breakdown strength of composite materials with a plane geometry has been developed. Five main concerns have been incorporated in the final solution:

- The breakdown usually occurs in connection to defects, air filled cavities, in homogeneities or other impurities. This necessitates a setup where the stressed volume is well known.
- To compare measurements on new materials with samples taken from blades in service, the setup must be flexible enough to allow small differences in geometry.
- Testing specimens with high breakdown strengths usually implies a risk of surface flashover between the electrodes. The probability of surface flashover must be minimised, so that the size and thereby the cost of specimens can be limited.
- To simulate the effect of streamers occurring on the surface of turbine blades, the high voltage electrode must be elevated above the surface.
- In order to compare breakdown field strengths with tracking characteristics of the surface as described in section 5.3, only streamer formation on this side of the specimen is desired.

The present section 5.2.3, only aims at developing and performing design simulations on the test method. The outcome is a suitable test used in the following sections concerning mechanical aging (section 5.2.4), the importance of air and sizing in the composite (section 5.2.5) and a correlation between tracking and breakdown properties (section 5.3).

5.2.3.1 Test setup

The following test setup was suggested based on initial tests and experience.

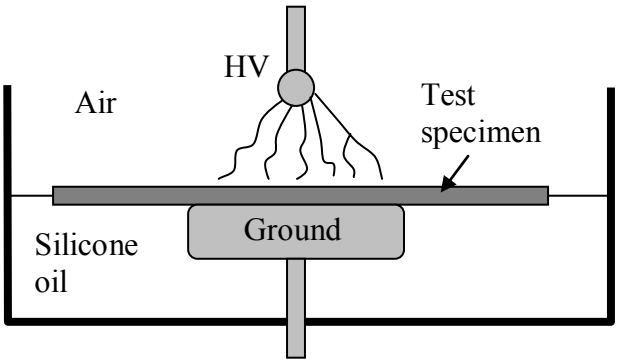

Figure 5.31 Test setup using quadratic specimens for determining the electrical breakdown field strength.

An impulse voltage is applied on the upper electrode marked HV which consists of a steel sphere with a diameter 12.5mm, welded onto a brass rod with a diameter of 4 mm. A cylindrical brass electrode of diameter 70mm with rounded edges is used as ground electrode. The connection from the electrode to facility ground is made with a similar brass rod, penetrating the bottom of an acrylic test vessel.

The test specimen rests on the surface of the ground electrode in the test vessel filled with silicone oil. The oil must cover the lower side of the specimen. This decreases the probability of discharges at the lower side of the specimen hereby preventing flashovers between the electrodes. The distance between the high voltage electrode and the surface of the specimen is 50mm, allowing streamers to form on the upper surface of the specimen.

The GFRP test specimens measure 150mm x 150mm with varying thicknesses. They are either samples produced under the same circumstances as real blades, or cut from blades that have been in service.

5.2.3.2 Dynamical modelling

Due to the volume effect considering composite materials, one of the purposes was to develop a test method which allowed tests of a well known volume. To make sure that this volume is in fact well known, some calculation and modelling of the test setup was performed.

When a discharge is initiated from the high voltage electrode, streamers will propagate towards the ground electrode at a velocity determined by the electric field, the geometry, etc. [28]. The test specimen blocks the path for the streamers, so depending on the applied field, the streamers will “search” the surface to find a way to the ground electrode. This path is affected by the electric field on the surface of the specimen which can be divided into two components, the tangential component along the surface, and the normal component perpendicular through the specimen.

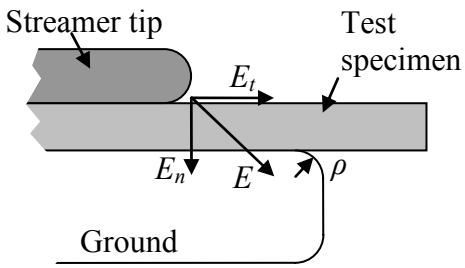

Figure 5.32 Electric field in tip of the streamer 'E' composed of two components, the tangential electric field 'E_t' and the normal electric field 'E_n'.

In Figure 5.32 these two components are entitled E_t (tangential electric field) and E_n (normal electric field). The streamer will continue to propagate towards the edge of the specimen as long as the tangential component of the electric field is larger than a certain threshold value. Electric fields between 200kV/m and 600kV/m for stable streamer propagation along a dielectric surface have been measured for different polymers [29] and [70]. Based on this, a value of 500kV/m is chosen for these simulations.

A two dimensional, axis symmetrical model has been built in a finite element program, Appendix A. This model is then exported to Matlab, where the dynamic features are incorporated. Due to the axis symmetrical model, the rectangular specimen is modelled as a circular disc of diameter 75mm while the electrodes are modelled correctly as a sphere and a cylindrical electrode with varying diameter and radius of curvature, 'ρ' on Figure 5.34.

Streamers developing along dielectric surfaces exhibit different images depending on polarity and voltage, Figure 5.33.

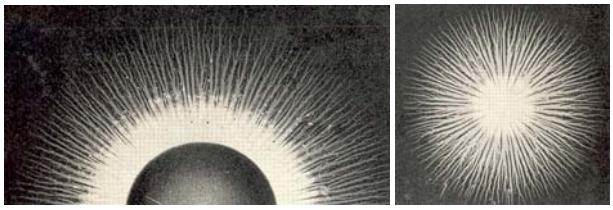

Figure 5.33 Lichtenberg figures on photographic plates [71].

Despite the discrete nature of surface streamers, the model regards streamers on the upper surface as a disc of thickness 1mm with a rounded edge, Figure 5.32, [64] and [70]. The streamer propagation is modelled by increasing the radius of the "streamer-disc" and calculating the tangential field component for each location. The disc is assigned a potential similar to the potential of the high voltage electrode.

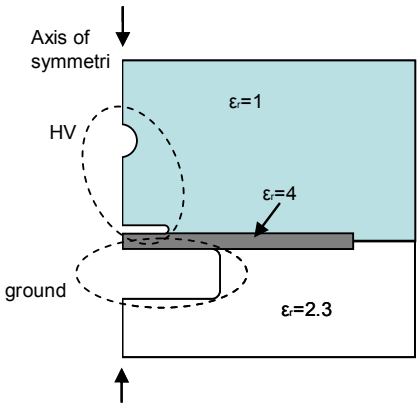

Figure 5.34 FEM model of test setup using quadratic specimens for measuring the electrical breakdown field strength.

In the two-dimensional model, the vertical axis between the two arrows in Figure 5.34 is the symmetrical axis. The boundary of the sphere, the streamer and the line between the sphere and the streamer are assigned full potential (indicated by HV), while the boundary surrounding the ground electrode is kept at zero potential (indicated by ground). All other external boundaries are regarded as electrical insulation, where the normal of the electric field is zero. The different materials are defined by their relative permittivity, which equals 1 for air, 4 for the GFRP specimen and 2.3 as the value for silicone oil.

The streamer propagation is calculated in steps of 1mm, starting from 1mm from the centre of the specimen to 70mm near the edge of the specimen. By solving Laplace's equation numerically the tangential field on the surface directly below the tip of the streamer is calculated in each step and saved for further evaluation.

Figure 5.35 shows how the tangential field in radial direction is calculated in each step, and saved in one large array consisting of the tangential electric field in the tip of the streamer versus the distance from the axis of symmetry.

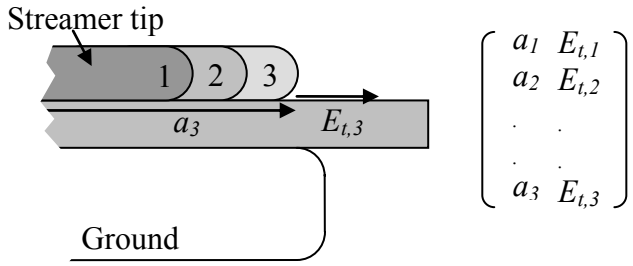

Figure 5.35 Tangential electric field calculated in discrete steps.

The electric field in the tip of the streamer for various geometries and thicknesses is plotted against the distance, and by knowing the limit for stable streamer propagation an estimation of the streamer extension and thereby the stressed volume is possible.

5.2.3.3 Results of dynamical modelling

Three different parameters have been investigated; the thickness of the test specimen, the radius of the ground electrode and the radius of curvature for the edge of the ground electrode.

Thickness of specimen

In this simulation the overall diameter of the ground electrode is kept at 80mm, the radius of curvature for the edge of the ground electrode is kept at 5mm and the thickness of the GFRP specimen is varied between 4mm, 6mm, 8mm and 10mm.

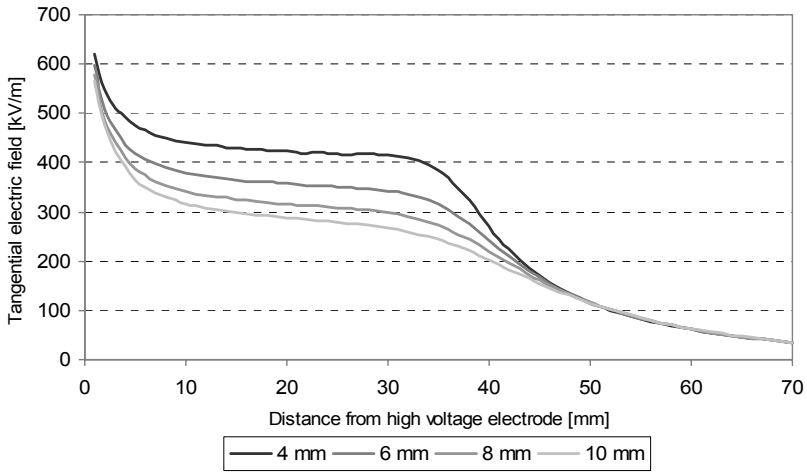

Figure 5.36 Tangential electric field vs. distance from high voltage electrode for various thicknesses, normalised to a voltage of 1kV. The diameter of the ground electrode is 80mm.

Figure 5.36 shows the tangential electric field in the tip of a streamer propagating from the centre of the specimen towards the edge. The electric field is calculated based on a voltage of 1kV on the streamer. Since the field is proportional to the voltage, and the ordinate is normalised to 1kV, the ordinate must be multiplied with the actual voltage in kV if other voltages are applied.

Example: If 2kV is applied, the streamer on the surface of a 4mm thick specimen would proceed out to a radius of 41mm, because the tangential field here decreases to the threshold value (500kV/m) of stable streamer propagation, see Figure 5.37. Note that the ordinate is multiplied with a factor 2 compared to Figure 5.36.

The results on Figure 5.36 indicate that the tangential electric field in radial direction increases when the thickness of the specimen decreases. Furthermore, the field tends to be highest directly below the high voltage electrode, decrease continuously to a stable level between the centre and the edge of the ground electrode, and finally decrease towards zero at the edge of the ground electrode.

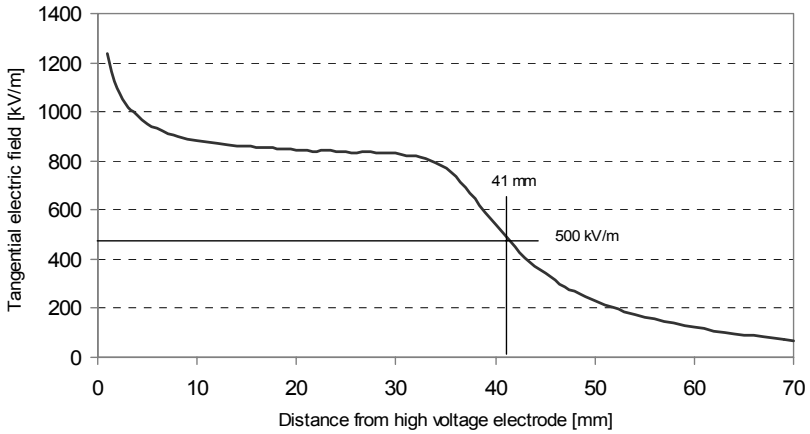

Figure 5.37 Tangential electric field vs. distance from high voltage electrode for a thickness of 4mm, and with 2kV applied.

The streamer propagation as calculated on Figure 5.37 assumes that a streamer with a potential of 2kV is present at the surface. However, at such a low voltage streamers are possibly not emitted from the high voltage electrode. Hence the main conclusion is governing the slope of the curves, showing that streamer discharges will either be concentrated just below the high voltage electrode, or proceed all the way to the edge of the ground electrode. This is especially evident for thin specimens (the 4mm curve on Figure 5.36).

Although streamers seem to cover a large area, the voltage is still far below the breakdown voltage. In the example above where 2kV is applied, the normal electric field will only be 0.5kV/mm.

Radius of curvature

For a fixed thickness of the specimen of 6mm, and a diameter of the ground electrode of 80mm, the radius of curvature for the edge of the ground electrode facing the specimen is varied between 2mm, 5mm and 8mm.

As seen on Figure 5.38, the electric field directly below the high voltage electrode is not affected by changes in the radius of curvature of the ground electrode. The main difference occurs close to the edge of the ground electrode, where the tangential field tends to drop earlier the larger the radius of curvature.

For a radius of curvature of 8mm, the ground electrode will lose contact with the specimen at a radius of 32mm, compared to a radius of 38mm for a 2mm radius of curvature. When this happens, a large part of the potential drop between the streamer and the ground electrode will be "pushed" down into the oil due to the lower permittivity of oil than that of GFRP. If the volume surrounding the ground electrode consisted of air, this effect would be even more pronounced, possibly leading to discharges from the ground electrode below the specimen.

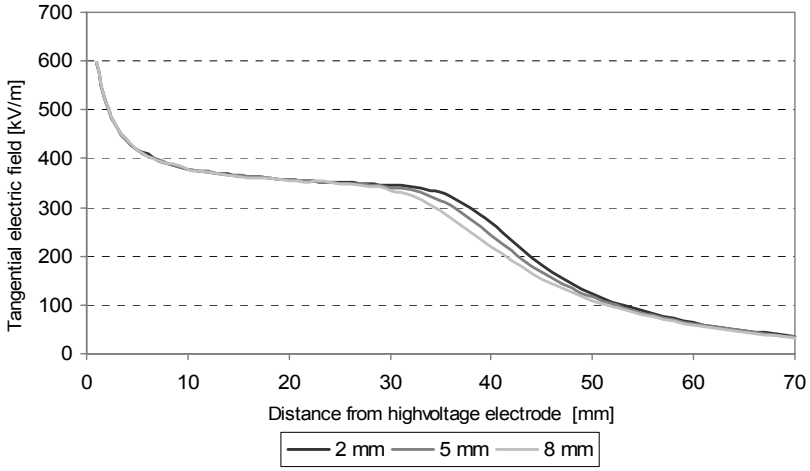

Figure 5.38 Tangential electric field vs. distance from high voltage electrode for various radii of curvature, normalised to a voltage of 1kV. The diameter of the ground electrode is 80mm.

The threshold value for stable streamer propagation will, in other words, be reached earlier for a larger radius of curvature of the ground electrode, when the overall diameter of the ground electrode is fixed.

Diameter of ground electrode

In the final simulation, the tangential electric field for varying diameters of the ground electrode (40mm, 80mm and 120mm) is calculated for a fixed specimen thickness of 6mm and a radius of curvature of 5mm.

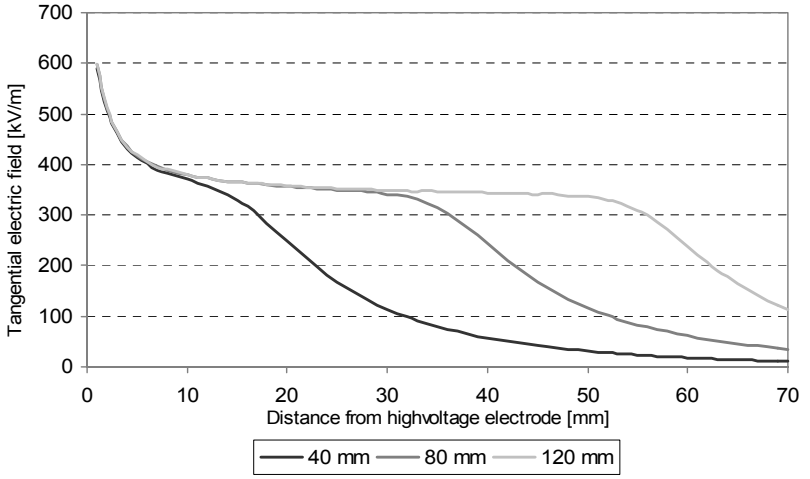

Figure 5.39 Tangential electric field vs. distance from high voltage electrode for various diameters of the ground electrode, normalised to a voltage of 1kV.

Not surprisingly, the calculations indicate that the tangential electric field drops off at a distance comparable to the radius of the ground electrode. The slopes of the three curves above the corresponding ground electrodes are almost identical which can be seen by performing a parallel displacement of two of the curves.

5.2.3.4 UV images

Based on the above simulations and design criteria, the test setup shown on Figure 5.40 was constructed.

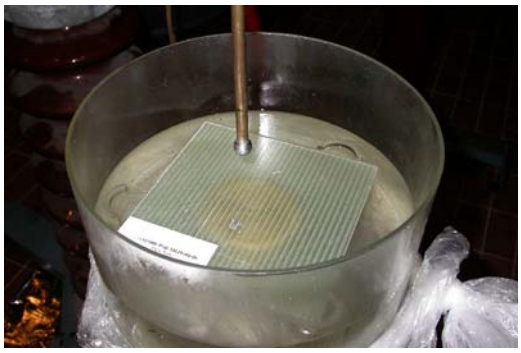

Figure 5.40 The final revised test setup used for measuring the electric breakdown field strength of smaller quadratic specimens.

If the applied voltage is high enough for the onset of corona and streamer discharges but too low to create a flashover or a breakdown through the specimen, only a tiny faint blue spark would be visible to the naked eye or a conventional camera. Since such partial discharges at 1atm emit most of its light in the Ultra Violet range, special cameras and optics are required. To investigate the test setup further and determine whether the boundary of the ground electrode actually defines the stressed area, UV images of the partial discharges was captured. This technique is mentioned more thoroughly in Appendix C.

The left image on Figure 5.41 shows a positive polarity discharge on a 6mm GFRP plate with a peak amplitude of 178kV. Corona is visible on the entire surface of the sphere, where only branches emitted towards the ground electrode are extended and becomes more intense streamers. At the next discharge the voltage was increased up to 199kV which resulted in discharge formation below the specimen from the ground electrode on the right image of Figure 5.41. Considering a flashover electric field strength of 500kV/m as discussed above, 40cm of creeping distance would in general be required to withstand 199kV. By using oil below the specimen, this distance is successfully reduced to 15cm. The subsequent shot with a slightly increased charging voltage resulted in a breakdown of the specimen at a peak voltage of app. 200kV.

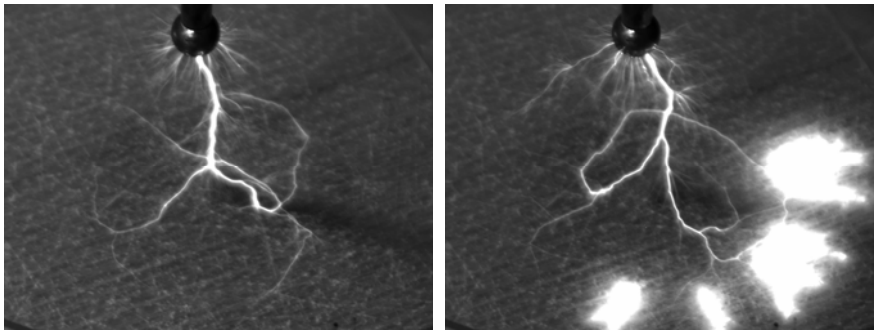

Figure 5.41 Left: UV picture of a positive polarity discharge on a 6mm GFRP plate at 178kV, Right: By increasing the voltage to 199kV discharges from the ground electrode in the oil below the specimen becomes evident.

Figure 5.42 shows a negative polarity discharge of 136kV on the same 6mm GFRP specimen. By subtracting a background image of the specimen without discharges, and finally adding an image of the test setup where the specimen has been removed, the right image appears. This clearly shows how the discharges are limited by the boundary of the ground electrode. At this specific picture it even seems as if the discharge follows a path at the radius where the rounding of the ground electrode begins, similarly to the findings in the simulations on Figure 5.38.

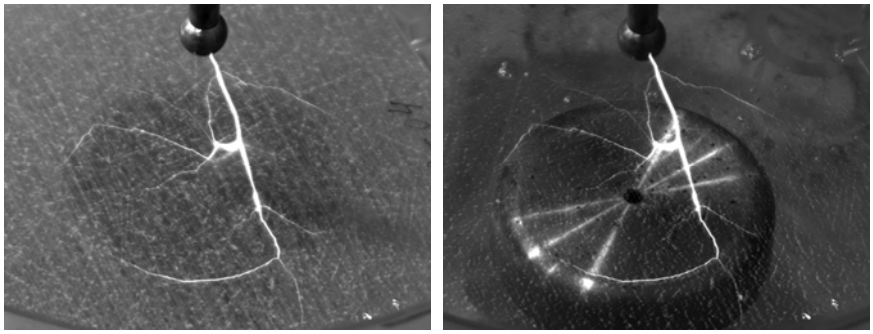

Figure 5.42 Left: UV picture of a negative polarity discharge at 136kV on a 6mm GFRP specimen, Right: A background image of the GFRP specimen without discharges has been subtracted from the left image, finally an image of the same test setup without the specimen is added. Clearly the discharge follows the boundary of the ground electrode.

Finally a comparison of positive and negative discharges is made. The images on Figure 5.43 are captured using a special setting on the camera that integrates the light intensity of the focus area continuously. This allows the capturing of several discharges within the same image. The idea of such pictures is to identify tendencies that are not covered by a single image. Both images show how the area above the ground electrode is evenly affected for either polarity, but still some fundamental differences between the two polarities are visible.

Positive polarity discharges appear as filamentary branches connected to the high voltage electrode extending and splitting up towards the surface of the specimen. By looking closer at the left image of Figure 5.44 the surface is met by streamers with very fine filaments, covering the entire area. This corresponds with the theoretical explanations given in [27] and [70]. The negative polarity discharges on the right image on Figure 5.44 appear as partial bushy discharges occurring randomly in the air above the specimen. Only a few of these discharges have led to a discrete streamer formation from the high voltage electrode as seen on Figure 5.43.

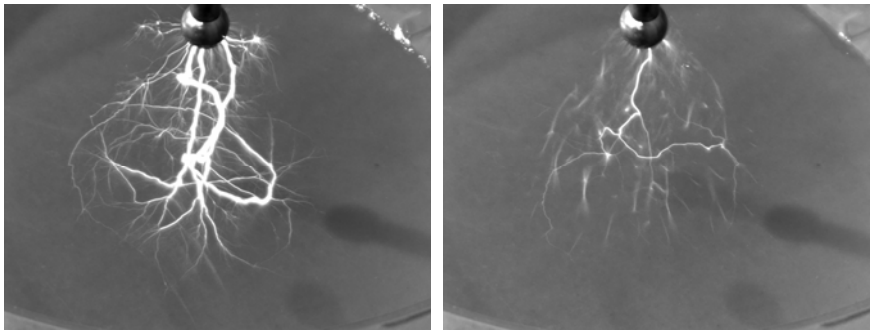

Figure 5.43 Left: UV pictures of Ten positive polarity discharges at app. 100kV on a 3mm plate of phenolic paper (Pertinax), Right: Three negative polarity discharges at app. 130kV on the same specimen.

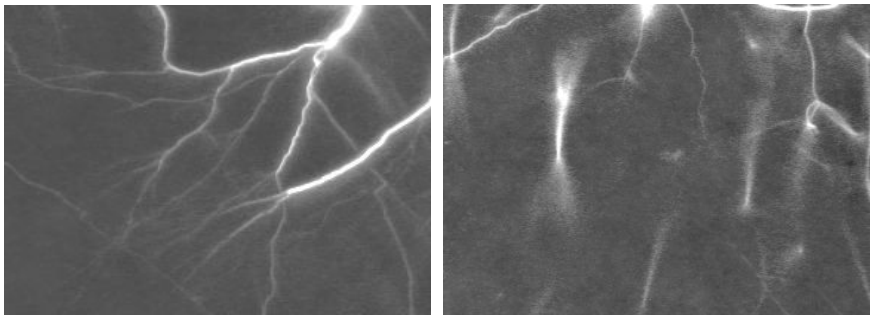

Figure 5.44 Left: Zoom on the positive polarity discharges of Figure 5.43, Right: Zoom on the negative polarity discharges of Figure 5.43.

As explained in the literature for mainly large point-plane gaps, the positive discharges do in fact develop as a positive leader extended by filamentary branched streamers [27] and [72]. The negative discharges are initiated similarly with a bushy negative corona from the high voltage electrode but develop further in several discrete steps. The initial negative corona is followed by a ‘pilot system’ somewhere in the electrode gap consisting of both a positive and a negative corona propagating in each direction. At a certain point in time the corona discharges in the pilot system changes into a ‘space leader’ appearing as a luminous channel between the electrodes and developing in both directions [72]. Bushy corona discharges of both polarities are visible in each end of the space leader,

which could be what is seen on the right image of Figure 5.44. If time and applied voltage allows for further developing of the negative discharge, the space leader is met by a negative leader originating from the high voltage electrode. A few such negative leaders are visible on the right image of Figure 5.43.

Based on these UV images it seems as if the surfaces above the electrodes are affected evenly for both polarities.

5.2.3.5 Discussion of test method

For the newly developed method for measuring breakdown strengths of composites, simulations of the tangential electric field in the tip of a streamer propagating along the surface has been described. By using these numerical calculations, the extension of streamers for certain geometries can be estimated. The influence of the thickness of the specimen, the radius of curvature for the ground electrode and the diameter of the ground electrode, on the extension has been calculated. The results are curves enabling a calculation of the streamer extension for a specific peak voltage.

Despite that the voltage necessary for onset of corona and streamers from the high voltage electrode is not considered, the calculations suggests that streamers do propagate towards the edge of the specimen at much lower field strengths than required to cause a breakdown. The main conclusion for this setup is then; that once streamers are initiated from the high voltage electrode and meet the surface, they would propagate to the edge of the ground electrode and stress a volume limited mainly by the radius of the ground electrode. Although the streamers might propagate beyond the edges of the ground electrode, the normal electric field responsible for possible breakdowns decreases rapidly outside the area defined by the ground electrode. Hence breakdowns will only occur within the area above the electrode, such that the tested volume is well defined.

The result from simulations is supported by several UV images, showing that the area above the ground electrode is stressed evenly. At one of the images of a negative polarity discharge the streamer followed the edge of the ground electrode very strictly, in good agreement with the simulations.

Several breakdown tests were performed on different composite materials. In all cases the breakdowns occurred randomly on the surface above the ground electrode and were apparently not affected by the possible field enhancements at the rounding of the ground electrode. Due to the good experience with the test method is was decided to use this setup for the rest of the breakdown tests.

5.2.4 Mechanical aging

The mechanical strength of composite materials depends to a high degree on the attachment between fibres and resin. As mentioned previously this adhesion is optimised by treating the fibres with a sizing agent, also aiming at minimising the risk of having air voids in the fibre/resin interface. Previously in section 4.3.3 it is discussed whether the mechanical aging due to the wear of a lifetime also affects the breakdown field strength of the composites, explained by an increased amount of air filled voids.

5.2.4.1 Purpose

Besides the reduction in mechanical properties, it would be interesting to determine whether the slip interfaces between resin and fibres as a consequence of mechanical aging reduces the breakdown strength of the material as well. For this reason, it is selected to perform breakdown tests on accelerated aged specimens.

5.2.4.2 Test specimens

All test specimens are supplied by a Danish wind turbine blade manufacturer, and represents the material and thicknesses used in the tip region of modern wind turbine blades. Two different types of laminate are tested. Type A is a 7 layer biaxially woven GFRP composite injected with polyester based resin, whereas type B is produced similarly but injected with a polyester resin with nano particles added. The nano particles are expected to improve the mechanical properties, and might as well increase the electrical breakdown strength. For competitive reasons the exact composition of resins and additives can not be disclosed. Both types of specimens are approximately 2mm thick and measure 150mm by 150mm when entering the breakdown voltage test, according to the specification in 5.2.3.

The procedure for accelerated aging is defined by the manufacturer, who has great experience within this field due to extensive mechanical tests on their products. To simulate the same aging as seen on blades after several years of service it was decided to apply a tensile stress on the specimen in the presence of a sinusoidal load between 1.8kN and 18kN at a frequency of 5Hz. The grip arrangement for fixing the specimen in the tensile testing machine and the machine itself is shown on Figure 5.45

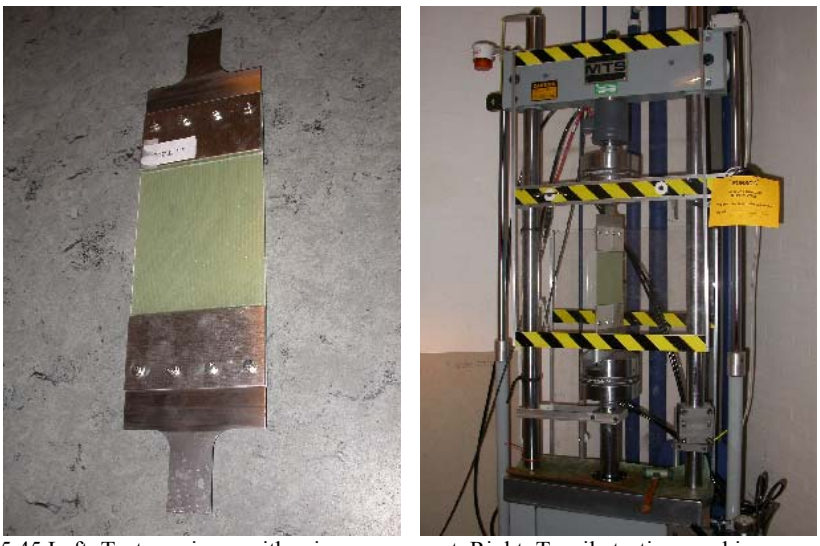

Figure 5.45 Left: Test specimen with grip arrangement, Right: Tensile testing machine.

After aging the specimens, they were cut loose from the grip leaving an evenly aged fairly quadratic specimen with a side length of 150mm suitable for the test method described in section 5.2.3.

5.2.4.3 Test method

The breakdown tests are performed according to the description in section 5.2.2 and section 5.2.3, by submerging the specimens partly into silicone oil and testing with a standardised 1.2/50us lightning impulse waveform.

For each type, 24 specimens were produced. Concerning type A specimens, eight of them were used as reference specimens tested without any mechanical aging, eight specimens were aged at a low level (1500 cycles) and eight specimens were aged at a high level (2400 cycles). For each aging level four specimens were tested with positive polarity and four were tested with negative polarity.

The type B specimens doped with nano particles were supposed to perform better mechanically than the standard type A specimens. Unfortunately this was not the case why the aging pattern was changed for this series. Four aging levels were used for each four specimens, 100, 200, 300 and 400 cycles respectively, besides the four reference specimens without aging. Only positive polarity was used to test type B specimens.

The maximum aging level for both types (2400 and 400 cycles) was selected such that the specimens visually appear more damaged than experienced on blades which have been in service for 20 years. In this way the most severe conditions on actual blades are covered by these tests.

5.2.4.4 Results

The results of the tests for both type A and B specimens are shown in Table 5.6.

Table 5.6 Withstand and breakdown electric field strengths for mechanically aged specimens.

Specimen	Aging, cycles (1.8kN-18kN, 5Hz)	Average withstand electric field strength [kV/mm]	Average breakdown electric field strength [kV/mm]
A1pos (3 spec.)	0	47.4	50.1
A1neg (4 spec.)	0	-51.9	-54.9
A2pos (3 spec.)	1500	42.4	44.7
A2neg (4 spec.)	1500	-50.5	-52.3
A3pos (4 spec.)	2400	49.9	52.5
A3neg (4 spec.)	2400	-50.3	-51.5
B1pos (4 spec.)	0	40.9	42.9
B2pos (4 spec.)	100	45.3	57.3
B3pos (4 spec.)	200	44.5	46.9
B4pos (4 spec.)	300	43.5	46.3
B5pos (3 spec.)	400	41.1	44.1

Type A

The breakdown and withstand field strengths dependency on mechanical aging for the standard specimen type A is visualised in Figure 5.46 and Figure 5.47. Test results for the individual three or four samples at each polarity and each aging level is marked by triangles, whereas the curves are drawn through the average values.

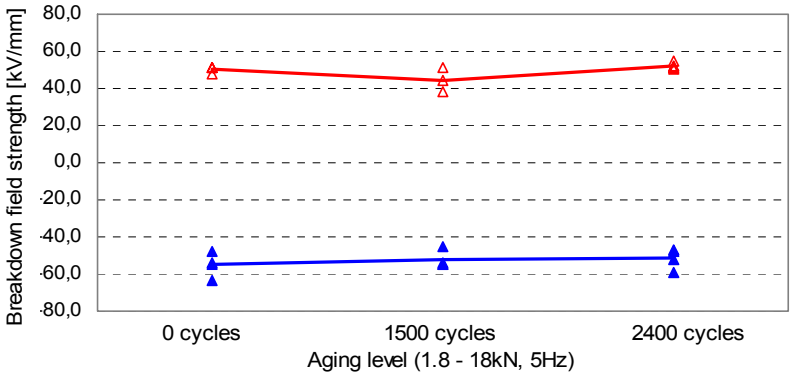

Figure 5.46 Breakdown field strength for type A specimens aged at three different levels.

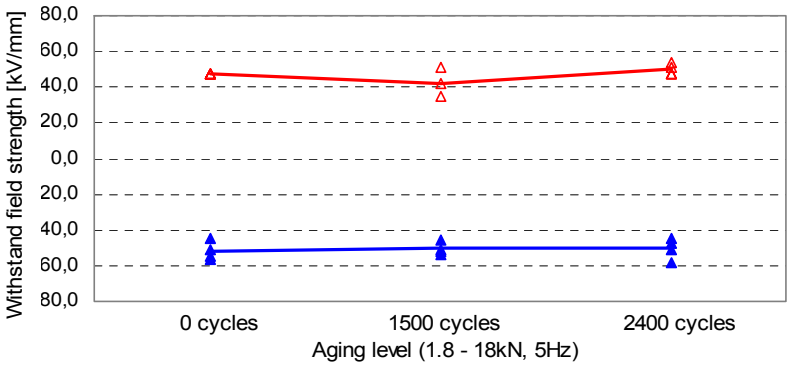

Figure 5.47 Withstand field strength for type A specimens aged at three different levels.

The results clearly indicates that both the withstand and the breakdown field strength for either polarity is unaffected by the mechanical aging. Although the tendency is based on only twenty two specimens (one of them was accidentally aged 7403 cycles, and another failed the requirements of withstanding three voltage levels, section 5.2.1.3) the dispersion among the individual results is small enough to draw these conclusions.

By examining the individual specimens after breakdown occurred, it seems as if the area of delamination increased with the aging level. Since the energy released in each breakdown at both negative and positive polarity is somewhat similar (comparable abso-

lute charging voltages at the Marx generator) the relative area of delamination as a function of aging can be found. This is done by capturing images of the twenty two breakdowns and performing digital area analysis as described in section 4.3.1. An example is shown in Figure 5.48.

The area measurements were performed on all type A specimens evaluating the delaminated area relative to the image size. For each aging level the average delaminated area was found, and normalised with respect to the average value at an aging level of 2400 cycles. The individual measurements were also normalised to the average value for the 2400 cycle series, and plotted in Figure 5.49.

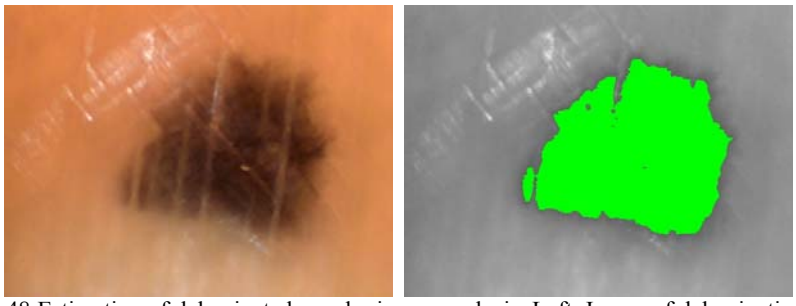

Figure 5.48 Estimation of delaminated area by image analysis, Left: Image of delamination on one of specimen A1pos, Right: The estimated area of delamination with respect to the image size is found to 21%.

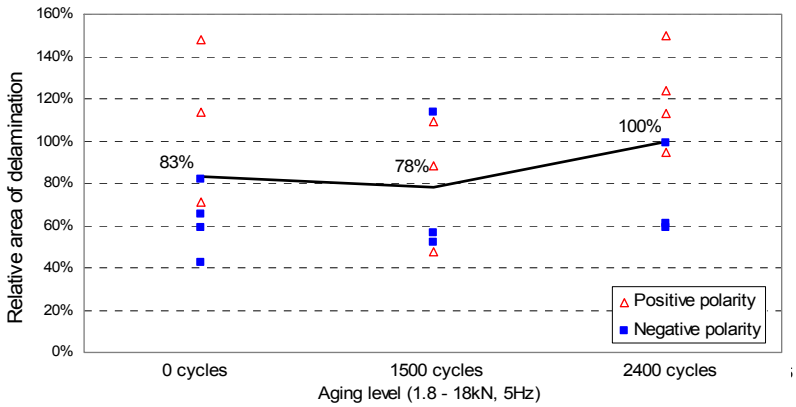

Figure 5.49 Relative area of delamination, normalised to the average area measured on specimens aged at 2400 cycles.

As seen on Figure 5.49, there were quit a dispersion among the area of delamination for the individual specimens (+/-60%). Although, there is a faint tendency that the area of delamination increases with the degree of aging, it is not possible to draw any conclusions based on these results. Since the delamination is dependant on the energy released in the

breakdown channel, impulse current tests of such specimens (containing higher energies and hence larger delamination) would probably give more reliable results.

Apparently the electrical breakdown strength of composite materials is not affected by mechanical aging. Initially it was suggested that the area of delamination increased with aging, but measurements of the delaminated areas on all twenty four specimens revealed too large a dispersion to prove this thesis.

Type B

Similar curves showing the average breakdown and withstand field strength as a function of the aging level are drawn for the type B specimens with nano particle additives.

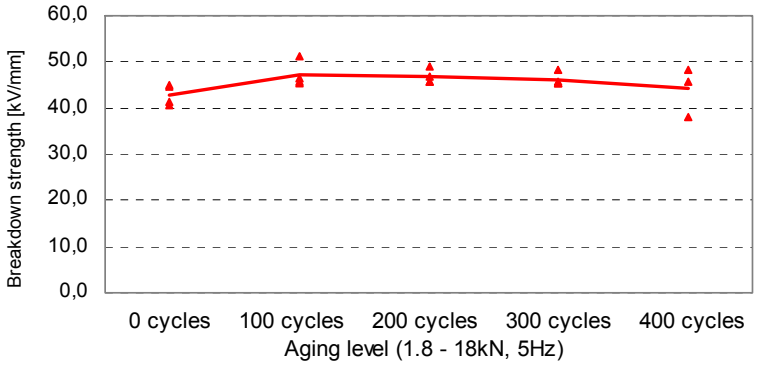

Figure 5.50 Breakdown field strength for type B specimens aged at five different levels.

Compared to the values obtained from type A specimens which have not been aged, both the withstand and breakdown strengths are app. 15% lower for type B reference specimens. The nano particles have in other words both decreased the mechanical properties and the electrical breakdown strength.

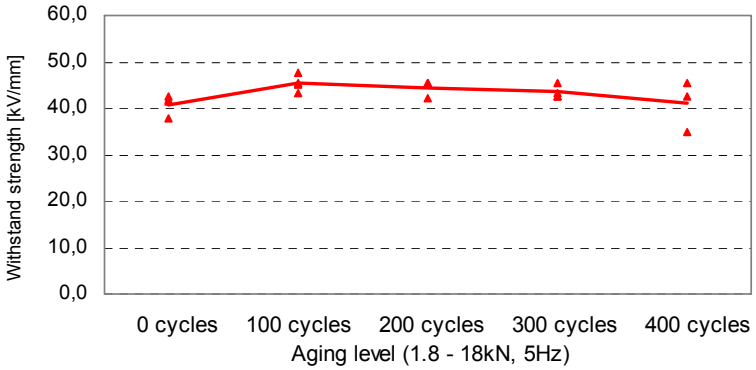

Figure 5.51 Withstand field strength for type B specimens aged at five different levels.

Besides the reference specimens who happened to have the lowest breakdown and withstand field strengths, a faint tendency of decreasing field strengths with aging is evident. However the last data set at an aging of 400 cycles experienced the largest dispersion. If the value of 35kV/mm for the withstand field strength and 38kV/mm for the breakdown field strength were expelled, the tendency vanishes.

The apparent increase in breakdown strength on Figure 5.50 during the first levels of aging from 0 cycles to 100 cycles contradicts common understanding of a decreasing breakdown strength with the degree of aging. Most structural materials exhibit a positive Poisson's ratio, such that the lateral strain is negative while subjected to tensile stress. In other words they become thinner if elongated. Some composite materials on the other hand appear to have a negative Poisson's ratio, at least in the beginning of the aging process. If the tendency on Figure 5.50 is not just incidental, the increase in breakdown strength could be a result of an increase in thickness of the specimen for this first aging level.

However, considering practical applications, the breakdown field strength and withstand field strength seems unaffected by the mechanical aging, as the case with type A specimens.

5.2.4.5 Conclusion

To investigate the influence of mechanical aging on the electrical properties, several GFRP specimens were subjected to an accelerated aging. The aging was performed in a tensile testing machine, by applying a sinusoidal force between 1.8kN and 18kN with a frequency of 5Hz to the specimens. Twenty two specimens of GFRP similar to the materials used in the blade tip region and aged in three different levels (0, 1500 and 2400 cycles) have been tested with both positive and negative polarity. Further twenty three specimens containing nano particles have been aged in five different levels (0, 100, 200, 300, 400 cycles) and tested with only positive polarity.

Based on tests of forty five specimens, the electrical withstand and breakdown field strength does not change significantly within the range of mechanical aging. However, the area of delamination seems to increase as the specimen is aged, such that the consequence of getting a puncture might increase despite that the breakdown strength remains the same.

Since the aging primarily affects the mechanical properties, it is suggested that high voltage testing of aged blade materials on a regularly basis would be unnecessary. The mechanisms of delamination associated with the current conduction through a blade skin, should on the other hand be investigated thoroughly to determine whether the damage on mechanically aged blade is more severe than initially expected.

5.2.5 Importance of sizing and air content

The conclusions based on the initial breakdown tests in section 5.2.2, states that the presence of air filled voids in the laminate is crucial with respect to the electrical properties. It is shown that the volume effect indeed is valid for these materials, and that breakdown channels often forms in series of such air filled cavities. As an offspring of these tests, it was suggested to manufacture some specimens where the air content and the effect of good or poor sizing could be varied and investigated further.

5.2.5.1 Purpose

The purpose of these tests is to compare breakdown and withstand field strengths for specimens having various combinations of air content and sizing quality.

5.2.5.2 Test specimens

All specimens are made by the same Danish manufacturer, ensuring similar production methods. By winding the fibres around a special mandrel and injecting the polyester based resin while the fibres are still on the mandrel, excessive components like additional weaving fibres etc. can be avoided. This ensures that only a single parameter is varied making the comparison more reliable.

The quadratic specimens are app. 2.3mm thick and measure 150mm by 150mm according to the description in section 5.2.3. Three different types of specimens are made for these tests:

A. Eight specimens made with the optimum combination of sizing and resin ensuring good adhesion between fibres and resin. The injection method is optimised resulting in the smallest air content possible.
B. Eight specimens made with poor sizing considering the polyester resin used, and a minimum of air content as type A.
C. Eight specimens made with good sizing as type A, and an injection method giving considerably larger air content than the other two types.

5.2.5.3 Test method

The test method as described in section 5.2.2 is used, where four of each of the eight different specimens are tested with positive polarity and the remaining four are tested with negative polarity. The highest withstand voltage as well as the breakdown voltage is noted in each case.

5.2.5.4 Results

The average values for the withstand and breakdown field strengths for all three types distributed on the two polarities are shown in Table 5.7.

Table 5.7 Withstand and breakdown field strengths for specimens with varying air content and sizing.

Specimen	Average withstand electric field strength [kV/mm]	Average breakdown electric field strength [kV/mm]
A pos (4 spec.)	49.5	50.9
A neg (4 spec.)	-50.9	-54.8
B pos (4 spec.)	52.6	56.3
B neg (4 spec.)	-51.9	-55.8
C pos (4 spec.)	43.6	44.8
C neg (4 spec.)	-49.8	-51.7

The results of the individual specimens as well as the average values are plotted in Figure 5.52 and Figure 5.53. It is emphasised that the classification of air content and sizing quality relays solemnly on the information from the manufacturer. None of these values have afterwards been proven or measured within this thesis.

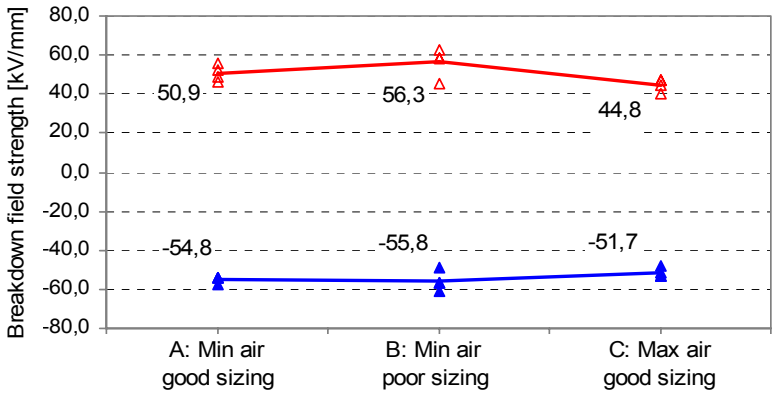

Figure 5.52 Breakdown field strengths of specimens with varying air content and sizing.

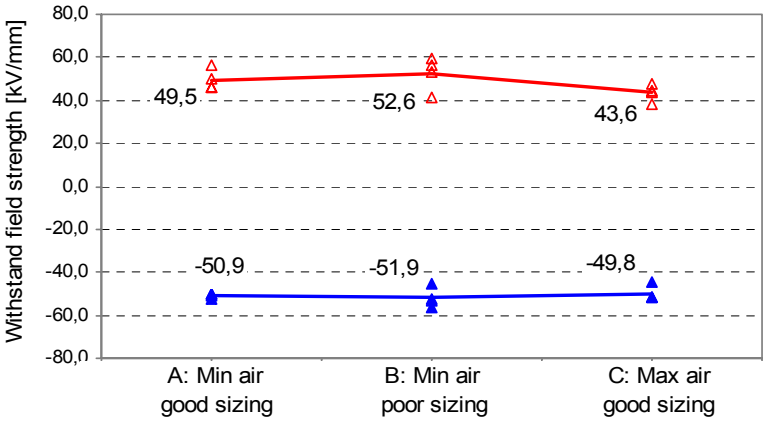

Figure 5.53 Withstand field strength of specimens with varying air content and sizing.

The sizing quality good or poor is defined by its influence on the mechanical properties, such that the good sizing treatment implies a greater adhesion between the fibres and resin. With a more porous composite resulting from a less suitable sizing, it was expected that the withstand and breakdown field strength would decrease. Considering specimens A and B in Figure 5.52 and Figure 5.53, the withstand and breakdown strength increased slightly for both polarities by changing the sizing towards a less mechanically suitable

one. Comparing with the data presented in Figure 5.50 for the specimens type B containing nano particles the aging at 100 cycles also increased the withstand and breakdown strengths. This supports the thesis that a certain slip between the fibres and resin occurs by using a less suitable sizing, similar to the slip experienced by aging composites mechanically at a low level.

Comparing results from specimens A and C reveals that the withstand and breakdown strength decreases by increasing the amount of air present in the laminate. This is in good agreement with the results obtained in section 5.2.2, where the volume effect is an evidence of non negligible air content. The thickness of specimens in section 5.2.2 varied from 1.2mm to 7.0mm and revealed a stronger evidence of the volume effect. Compared to these quadratic specimens with a thickness of app. 2.3mm it is probably easier to evacuate the resin during curing and thereby achieve a smaller difference in air content, giving a less pronounced volume effect as indicated by Figure 5.52 and Figure 5.53.

Again the recommendation towards manufacturers is to minimise the air content as far as possible.

5.2.5.5 Conclusion

From the plots in Figure 5.52 and Figure 5.53 it is evident that the dispersion within the different types of specimens for either polarity is sufficiently small to be capable of drawing conclusions.

Based on comparisons of specimens A and B there are only a slight increase in withstand and breakdown strengths when using a less mechanically suitable sizing. Since the sizing treatment is of great importance towards the mechanical application and the impact on the electrical breakdown properties shown by the present experiments is of minor concern, it is not suggested to change the mechanically most optimal sizing treatment.

An increase in air content has once more proven to decrease the withstand and breakdown strengths of composite materials. Based on these experiences the recommendation remains that the relative air content must be minimised in order to improve the electrical breakdown strength.

5.3 Correlation between tracking and breakdown tests

During the laboratory work and analysis of failure mechanisms governing the tracking and breakdown tests of composite materials, an idea of correlating the two results arose. The different steps in deriving the formula connecting the two test results are described in this section.

5.3.1 Purpose

It has been stated several times that determining and optimising the electrical breakdown strength and tracking resistance of composite materials is a method of selecting appropriate materials for blade manufacture. Since both results gives different relevant information about the ability of the material to withstand the environmental impacts, none of them should be left out.

Measuring the breakdown strength of composite materials requires a high voltage impulse generator capable of producing several hundreds of kilovolts as well as a monitoring

system made with considerable attention towards personal and apparatus safety. The test itself requires manual work and should only be performed by skilled personnel trained in a high voltage test facility. Tracking tests on the other hand use much lower voltages and can be highly automated as seen in section 5.1. Once the test specimens are mounted in the setup, the system controls both impact (applied voltage and water flow) and data acquisition.

Based on the above considerations, it was suggested to perform both tracking and breakdown tests of similar specimens to investigate the possibility of predicting the breakdown field strength of noncoated composite materials based on values for their tracking resistance and simple geometrical properties.

5.3.2 Test specimens and test procedure

Seventeen different types of specimens supplied by the Danish wind turbine blade manufacturers have been tested. All the specimens were made of uncoated GFRP under similar conditions and with the same materials and additives as used in the blade manufacture. Both polyester and epoxy based resins were represented among the samples.

Five specimens of each type were prepared for the tracking test which was carried out according to the description in section 5.1.

Considering the breakdown test, five quadratic specimens of each type were prepared according to section 5.2.3, giving a total of eighty five specimens. After placing the specimen on the ground electrode and adjusting the setup to comply with Figure 5.31, the test was initiated according to the description in section 5.2.2. Only four stages of the Marx generator was used corresponding to in increase of the peak voltage of 8kV-10kV at each step. Three of the five similar specimens were tested with negative polarity, while positive polarity was applied to the two remaining specimens.

5.3.3 Results

Three results are listed in Table 5.8 for each type of specimen; the average breakdown field strength at negative polarity, $E_{B,neg}$, the average breakdown field strength at positive polarity, $E_{B,pos}$, and the result from the tracking tests, tracking index (TI).

5.3.3.1 Establishing correlation

In order to develop an equation that links the results found by tracking tests with results from breakdown tests, some initial considerations must be discussed.

The initial breakdown tests as described in section 5.2 as well as the results sketched in Figure 5.23, show that the breakdown field strength tends to decrease with increasing thickness. This was explained by the large amount of in-homogeneities present in the laminate, giving rise to the volume effect.

The roughness of the surface is very important with respect to the tracking results. This has been found in section 5.1, where specimens exhibiting rough surfaces tend to fail at lower voltages than specimens with smooth surfaces. This is especially evident with coated surfaces, but was also seen on the bare laminate. Specimens manufactured with an epoxy based resin also performed better than specimens made with polyester based resin. If these conclusions can be extended to cover the breakdown characteristics, it is assumed

that specimens with a higher score in the tracking test will also have a higher breakdown voltage, for similar thicknesses.

Table 5.8 Breakdown strength and tracking index measured for various uncoated GFRP materials.

Specimen id.	Thickness [mm]	$E_{B,neg}$ [kV/mm]	$E_{B,pos}$ [kV/mm]	TI (2,A) [kV]
1	2.04	-47.5	53.5	4.50
2	2.04	-44.2	49.7	5.00
3	2.25	-39.5	33.6	2.00
4	3.06	-35.9	40.7	5.25
5	3.06	-33.7	37.8	4.50
6	4.08	-28.5	31.8	4.25
7	4.08	-25.5	34.4	5.25
8	2.04	-51.7	(*)	5.75
9	3.06	-32.2	43.3	6.00
10	3.06	-34.5	41.3	6.00
11	3.00	-28.7	22.8	2.00
12	4.00	-23.6	20.0	1.75
13	2.00	-43.0	39.1	2.50
14	6.00	-20.7	26.1	4.00
15	2.00	-54.4	47.1	6.00
16	4.50	-23.4	27.0	2.50
17	2.00	-46.1	53.9	6.00

(*) The breakdown field strength at positive polarity for specimen no. 8 has unfortunately not been measured.

With these considerations in mind, different formulas for correlating the tracking index 'TI' and the breakdown field strength '$E_{B,neg}$' or '$E_{B,pos}$' are established. Each formula tends to calculate E_B based on TI and the thickness of the specimen. To validate the accuracy, both the relative deviations between the actual and the calculated E_B as well as the squared deviations are calculated. To optimise the constants used in the formula, the sum of the squared deviations is minimised (least square method).

First approach

A formula where TI is multiplied with a constant 'c_1' and added to second constant 'c_2' divided by the thickness 'd' will satisfy the assumption that a higher TI increases E_b, and that a thicker specimen decreases E_b.

$$E_b = TI \cdot c_1 + {}^{c_2}\!/_{d} \tag{5.1}$$

By calculating $E_{B,neg}$ and $E_{B,pos}$ with (5.1) using the least square method, constants for negative and positive polarity are found to be; $c_{1,neg}$=-1.49, $c_{2,neg}$=-81.39 and $c_{1,pos}$=3.98, $c_{2,pos}$=58.47 respectively. The calculated results are shown in Table 5.9.

Table 5.9 Calculated results based on the tracking index and thickness of specimens according to (5.1). 'Dev. Squared' is the square of the deviation between the measured and the calculated results, whereas 'Dev. [%]' is the difference between the calculated and the measured results relative to the measured results.

Spec. id.	$E_{B,neg}$ [kV/mm]	Dev. squared	Dev. [%]	$E_{B,pos}$ [kV/mm]	Dev. squared	Dev. [%]
1	-46.58	0.80	-1.88	46.58	47.66	-12.91
2	-47.32	9.69	7.04	48.58	1.16	-2.17
3	-39,14	0.10	-0.81	33.95	0.13	1.07
4	-34.39	2.32	-4.24	40.02	0.48	-1.70
5	-33.28	0.17	-1.21	37.03	0.58	-2.01
6	-26.26	4.84	-7.73	31.26	0.33	-1.82
7	-27.75	5.08	8.85	35.24	0.71	2.45
8	-48.44	10.85	-6.37	51.56	(*)	(*)
9	-35.51	10.89	10.24	43.00	0.11	-0.76
10	-35.51	1.06	2.99	43.00	2.88	4.11
11	-30.10	1.87	4.76	27.46	21.98	20.59
12	-22.95	0.43	-2.77	21.59	2.60	8.07
13	-44.41	2.12	3.39	39.19	0.02	0.36
14	-19.51	1.35	-5.62	25.68	0.14	-1.43
15	-49.61	22.51	-8.73	53.13	36.38	12.81
16	-21.80	2.63	-6.93	22.95	16.04	-14.86
17	-49.61	12.64	7.72	53.13	0.59	-1.43
Sum/avg.		89.4	-0.1		131.8	0.7

(*) No comparison is possible for positive polarity at specimen no. 8 due to lack of data, Table 5.8.

As seen in Table 5.9, the sum of the squared deviations are 89.4 for negative polarity and 131.8 for positive polarity. The average deviations are -0.1% and 0.7% respectively, although the highest deviation is 10.2% for negative polarity and 20.6% for positive polarity.

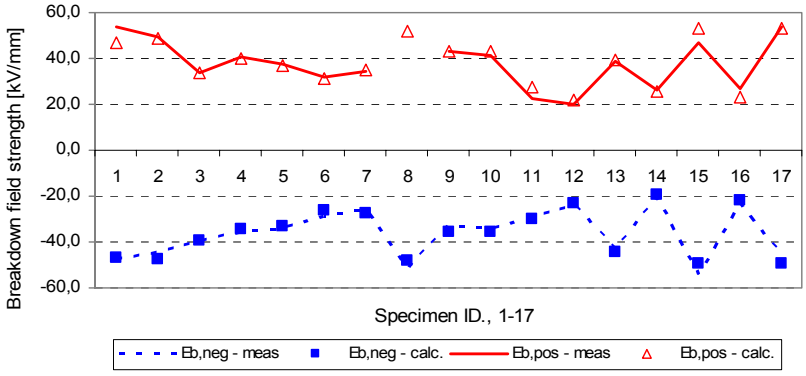

Figure 5.54 Comparison of measured breakdown field strengths and breakdown field strengths calculated based on the tracking index and the thickness of specimens for both polarities. The calculated results are obtained by using (5.1).

In Figure 5.54 the values of the actual measured breakdown field strengths (full and dotted line) and the calculated breakdown field strengths based on the tracking index and the thickness of specimens (squares and triangles) for each of the 17 specimens are plotted. The correlation for both polarities is even more evident in this figure.

Further approaches

Equation (5.1) giving the correlation shown in Figure 5.54 is derived upon the influence of thicknesses and surface characteristics experienced in both tracking and breakdown tests. Although the correlation and the accuracy are obvious and the expression is logically derived, several different attempts for a better approximation have been tried, Table 5.10.

The same procedure for optimisation has been used to find constants for the equations in Table 5.10. Values for the squared deviation and the relative deviation are given in the four right columns. The third constant c_3 introduced in (5.3) and (5.4) gives a minor improvement for both polarities. Values for these constant are given in Table 5.11.

Table 5.10 Further approaches in calculating the breakdown field strengths based on the tracking index and the thickness of specimens. The deviations are to be compared with the values in the row 'Sum/avg.' in Table 5.9.

Equation		Dev. Squared, neg	Avg dev neg [%]	Dev. Squared, pos	Avg dev pos [%]
(5.2)	$E_b = TI^{c_1} + c_2/d$	202.8	-2.0	212.9	-1.7
(5.3)	$E_b = TI \cdot c_1 + c_2/d + c_3$	88.8	0.2	131.8	0.7
(5.4)	$E_b = TI \cdot c_1 + c_2/d^{c_3}$	89.2	0.0	131.7	0.5
(5.5)	$E_b = \frac{TI \cdot c_1 + c_2}{d}$	141.5	-2.9	537.9	-5.1
(5.6)	$E_b = \frac{TI \cdot c_1}{d}$	1885.9	-16.0	1551.1	-17.2

Table 5.11 Values of c_3 in (5.3) and (5.4).

Equation	c_3 pos polarity	c_3 neg polarity
$E_b = TI \cdot c_1 + c_2/d + c_3$	-0.69	0.12
$E_b = TI \cdot c_1 + c_2/d^{c_3}$	0.99	1.02

Both equations have some similarities with (5.1) in the first approach. If c_3 in (5.3) was set to 0, the equation would be similar to (5.1). The same applies to (5.4) where a value of $c_3 = 1$ gives (5.1).

Although equations (5.3) and (5.4) show a little improvement in the accuracy compared to (5.1), this equation is selected as the most suitable due to its simplicity.

5.3.4 Discussion

A simple correlation between the tracking index and the breakdown field strength for uncoated composite materials has been found. The relationship enables a calculation of the breakdown field strength 'E_b' by only knowing the tracking index 'TI' and the thickness of the specimen 'd'. With this equation, manufacturers can perform a large number of simple tracking tests prior to the expensive high voltage testing on selected materials. The equation $E_b = TI \cdot c_1 + c_2/d$ describes this relationship where values for c_1 and c_2 are given in Table 5.12.

Table 5.12 Values of c_1 and c_2 in (5.1).

Constant	Positive polarity	Negative polarity
c_1	3.98	-1.49
c_2	58.47	-81.39

An explanation of this simple correlation could be that the homogeneity or smoothness of a materials surface is an indication of the quality of the material itself. The ability of rough surfaces to withstand tracking is restricted by scratches and air voids in the surface, as found in section 5.1. If these defects are also present inside the specimen, it explains why specimens with a low tracking index tend to have lower breakdown voltages.

Another remarkable thing is that breakdown field strengths at positive polarity is less affected by the thickness of the specimen than the breakdown field strength at negative polarity (the value of c_2 in Table 5.12). This phenomenon might indicate that negative and positive discharges for the specific breakdown test method affect a different percentage of the specimen surface. Consequently the composite volume exposed to the high electric field might be different for the two polarities, as illustrated with UV photography in section 5.2.3.4. As discussed here, a positive polarity discharge approaches the insulating surface as a filamentary branched structure possibly affecting the entire surface area equally. A negative polarity discharge on the other hand appears as short mid gab streamers with limited corona of both polarities propagating in either direction [72].

Apparently there is a major difference in positive and negative polarity discharges and the way they affect the surface of the test specimen. Some indications point in the direction that the surface area and thereby the volume of the test specimen is different for the two polarities. Other explanations could be that the negative discharges stress the surface at smaller spots with increased field enhancement as a consequence. In either case it is necessary to perform further research within this area to develop a full understanding of the differences in the constants c_1 and c_2 for negative and positive discharges.

The influence of surface coating, which is believed to play a significant role in especially the tracking characteristics, has not been incorporated in the formula.

5.4 Surface flashover tests

Previously it has been shown how streamers and leaders are initiated from all parts of the blade aiming at connecting with the lightning leader. Luckily this often happens from

conductive and exposed parts connected to ground potential, meaning that mainly external discharges will occur. Discharges from the blade that have connected successfully with the lightning leader have either originated directly from the receptors or followed a path along the surface as described in section 3.2.2. In case of direct attachment to the receptor, the particular receptor/down conductor design determines if the blade gets damaged. If the discharge channel alternatively follows the blade surface to the receptors, the thermal impact of the blade skin might be critical.

5.4.1 Purpose

This section aims at clarifying if surface properties of GFRP have any effect on the chosen discharge path from the receptor to the lightning leader. By using a test setup considering sparks from a simple receptor configuration towards a grounded sphere, it is investigated how surface contaminants as artificial pollution, artificial rain and hydrophic surfaces affects the path.

5.4.2 Test specimens and test procedure

A test specimen in this setup only experience electrical stress parallel to the plane such that the thickness in terms of its breakdown voltage is of less concern. The main feature is that the surfaces are similar with respect to coating and surface finish to what is experienced on actual blades. For this reason two specimens from each of two different manufacturers were used as well as a sample cut from an old blade which have been in service for several years, Figure 5.55.

A1, A2 Two specimens made by manufacturer no. 1 measuring 115cm by 25cm. The specimens are made according to their best practice and seem to exhibit very hydrophobic and homogeneous surfaces. Both specimens are coated

B1, B2 Two specimens made by manufacturer no. 2 measuring 115cm by 15cm. These specimens are coated with a 1.2mm gel coat layer and also repels water and moist.

C One section cut from an old blade which has been in service for several years originally made by manufacturer no. 1. The surface seems roughened and porous as a result of old manufacturing processes and the exposure to environmental conditions (moist, sun light, etc.).

Figure 5.55 Test specimen with brass electrode mounted on the surface as simulated receptor.

5.4.2.1 Test setup

The test specimens as described above were mounted horizontally with their surface facing downwards elevated above a grounded sphere with a diameter of 125mm.

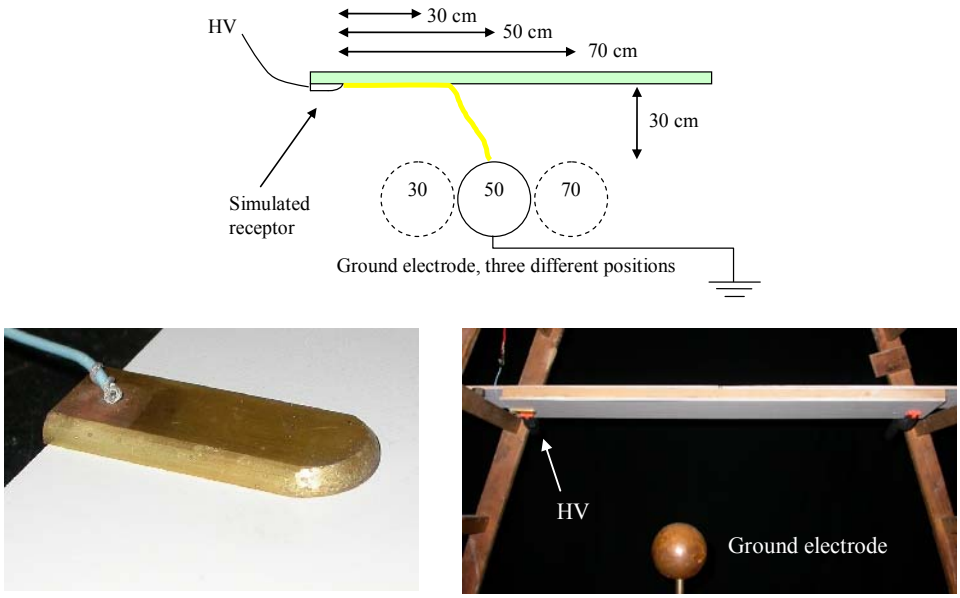

Figure 5.56 Test setup for surface flashover vs. air gap breakdown tests. Top: Schematic test setup, Lower left: Brass electrode mounted on surface as simulated receptor, Lower right: Test setup in the high voltage laboratory.

A high voltage electrode was mounted on the surface in one end of the specimen (HV), simulating the presence of a receptor, Figure 5.56. The sphere was kept at a distance of 30cm below the surface of the test specimens, and moved in three different horizontal locations 30cm, 50cm, and 70cm from the receptor, measured parallel to the surface of the specimen.

The situation with a lightning leader approaching the blade tip initiating answering leaders from the receptor was simulated by applying a voltage waveform D at the receptor. By selecting the amplitude sufficiently high to create a flashover from the receptor to the grounded sphere, the path of the flash could be investigated by means of photography.

When streamers from the high voltage electrode develop along the surface of the specimen, they deposit charge with the same polarity as the high voltage electrode itself. Many of these charges are neutralised by the spark, but since streamers might propagate further than the point where the spark attaches some of the charge might be left on the surface after the voltage has decayed, Figure 5.57.

If these charges left by the streamers after one discharge are still present when the second discharge is initiated, they might affect the discharge pattern considerably. Consequently the charges have to be removed, which was done by placing a fan at some distance from the specimen capable of blowing the charge away. After the fan was installed, no remaining charges on the surface were detected.

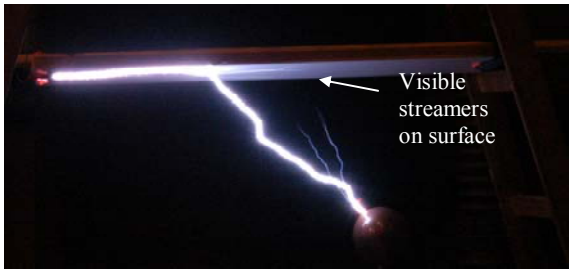

Figure 5.57 Negative polarity discharge on specimen B2 contaminated with silicone oil at a ground sphere position of '70cm'. Streamers are propagating further than the attachment point for the spark.

To investigate the influence of different surface properties, the following five cases were treated.

Clean surface.

The surface was cleaned with ethanol, and wiped carefully with a dry cloth.

Artificial rain

Artificial rain is defined in IEC 60060-1 [59] for tests of outdoor high voltage insulators subjected to naturally occurring rain. The artificial rain used in the various wet test methods is recommended for all types of test voltages and all types of apparatus, and is described by a solution with a resistivity of 100±15Ω·m measured at ambient temperature. For this application the solution is based on distilled water mixed with ammonium chloride (NH_4Cl), resulting in a measured resistivity of 93Ω·m.

Application of the artificial rain was done by mounting the dry and clean specimen in the test setup having the surface facing downwards. The artificial rain was sprayed onto the surface until an amount sufficiently to saturate the surface was reached, i.e. drops began to form on the surface and dripped off. Between each high voltage test further artificial rain was applied in order to ensure that the surface was saturated in the beginning of each test series.

Artificial pollution, dry

In IEC 60507 [65], a method for testing high voltage insulators resistance against polluted environments is described. On of the methods denoted *Salt Fog Method* uses artificial pollution consisting of salt and distilled water defined by its resistivity. The degree of pollution can be selected among a list of salinities ranging from 2.5g/L to 224g/L corresponding to volume conductivities of 0.43S/m to 20S/m. For the sake of wind turbines placed at offshore locations, a salinity of 35g/L was selected as it is referred to as a common value of seawater salinity [73]. The solution used in these tests was made by mixing Sodium chloride (NaCl) of commercial purity with distilled water giving a volume conductivity of 4.8S/m.

Since the standard concerns tests on high voltage insulators performed in climate chambers at 100% relative humidity, the method of applying the pollution is well defined. In this application the aim was to determine whether a blade subjected to a conductive contaminant as sea water and afterwards dried will act differently than a clean blade sur-

face. The application of the artificial pollution in this case was done by placing the specimen in a vertical position and spraying the solution onto the surface with a standard water atomiser. Due to the hydrophobic nature of the surfaces, the water was collected into droplets. By continuing the spraying, the drops became too heavy to stay attached on the surface and began dripping off the specimen. At this point the specimen was saturated with the saline solution and had to dry before the dry pollution test was performed.

Once the specimen has dried, salt crystals were visible almost evenly distributed across the surface.

Artificial pollution, wet

As described in the IEC 60507 [65] the conditions defined as wet artificial pollution is obtained by spraying the saline solution defined above onto the surface covered with the dry pollution. In this application it was done by mounting the specimen with the dry pollution in the test setup having the surface facing downwards. The saline solution was sprayed carefully onto the surface until the first droplets was formed just before the water began dripping off.

The high voltage tests were performed immediately after the application of the wet pollution ensuring nearly constant amount of saline solution on the surface.

Silicone oil

In order to improve the hydrophobic properties of the surface, a thin layer of silicone oil was applied onto the clean and dry specimen. After application of the oil, the surface was wiped of with a dry cloth leaving the surface very moist repelling.

5.4.2.2 Test method

For each of the five specimens, the order of the cases treated was; clean surface, artificial rain, artificial pollution dry, artificial pollution wet and silicon oil. After mounting the specimen in the test setup, the procedure was the following.

1. Adjust the Marx generator to produce positive polarity discharges at a voltage waveform D.
2. Adjust the grounded sphere to a distance of 30cm from the receptor.
3. Apply five impulses to the receptor ensuring a flashover to the grounded sphere.
4. Move the grounded sphere to a distance of 50cm from the receptor.
5. Apply five impulses to the receptor ensuring a flashover to the grounded sphere.
6. Move the grounded sphere to a distance of 70cm from the receptor.
7. Apply five impulses to the receptor ensuring a flashover to the grounded sphere.
8. Change polarity of the Marx generator to negative polarity.
9. Repeat step 2-6.

For each discharge a picture was captured enabling a measurement of the angle ‘v’ between a line from the centre of the grounded sphere to the point where the spark left the surface of the specimen and a line through the centre of the sphere perpendicular to the surface of the specimen, Figure 5.58.

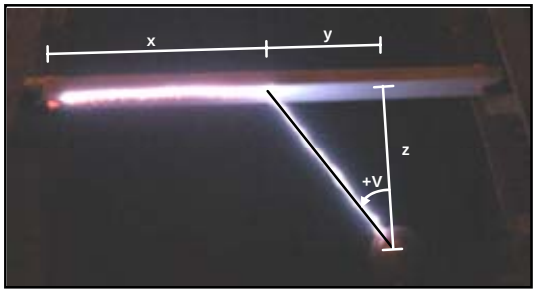

Figure 5.58 Definition of angle 'v' and other parameters used in the Surface flashover tests.

By using this test method, each specimen for any of the five different surface treatments experienced five flashovers at each position and each polarity giving a total of 150 discharges per specimen.

5.4.3 Results

Each value shown below is an average value based on five similar tests, with the given conditions (position of grounded sphere, polarity and surface property).

Table 5.13 Measured angles for various surface contaminants and electrode positions. Each value is a mean value based on five discharges.

Specimen: A1	Position, positive polarity			Position, negative polarity		
	30	50	70	30	50	70
Clean surface	41	57	64	20	19	40
Artificial rain	38	51	63	11	16	13
Artificial pollution, dry	43	58	62	21	23	35
Artificial pollution, wet	43	38	28	6	17	20
Silicone Oil	44	57	66	7	18	29
Specimen: A2	Position, positive polarity			Position, negative polarity		
	30	50	70	30	50	70
Clean surface	45	57	64	23	26	37
Artificial rain	38	51	62	10	-2	5
Artificial pollution, dry	42	56	65	15	17	34
Artificial pollution, wet	41	36	35	9	9	17
Silicone Oil	41	56	64	12	14	36
Specimen: B1	Position, positive polarity			Position, negative polarity		
	30	50	70	30	50	70
Clean surface	42	57	63	22	30	33
Artificial rain	35	57	62	-1	6	13
Artificial pollution, dry	46	55	63	13	25	38
Artificial pollution, wet	37	29	36	12	7	16
Silicone Oil	42	55	63	9	20	30

Specimen: B2	Position, positive polarity			Position, negative polarity		
	30	50	70	30	50	70
Clean surface	46	57	65	26	28	42
Artificial rain	40	50	60	7	9	12
Artificial pollution, dry	42	54	62	10	22	35
Artificial pollution, wet	23	47	38	6	10	14
Silicone Oil	45	55	62	22	27	38
Specimen: C	Position, positive polarity			Position, negative polarity		
	30	50	70	30	50	70
Clean surface	44	55	62	19	30	39
Artificial rain	39	55	57	15	34	36
Artificial pollution, dry	45	58	63	15	28	38
Artificial pollution, wet	41	35	44	22	26	34
Silicone Oil	38	52	63	9	23	34

Most of the angles in Table 5.13 are positive due to the positive angle convention on Figure 5.58. Two of the values appear to be negative, since the discharges along the surface in these cases passed the orthogonal projection of the ground sphere onto the surface, Figure 5.59.

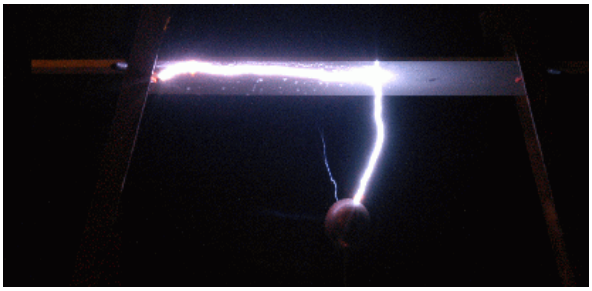

Figure 5.59 Negative discharge at specimen A2 at a ground sphere position of 50cm. Note that the discharge passes the orthogonal projection of the ground sphere on the surface, resulting in a negative angle ‘v’ using the convention on Figure 5.58.

Tests of two type A and two type B specimens were made to evaluate the consistency of the test method and to get a more reliable set of data. Considering the tests with wet surfaces (artificial rain, and particularly wet artificial pollution), the dispersion were more pronounced than tests with dry surfaces (clean, dry artificial pollution and silicone oil).

This is seen on Figure 5.60, where the graphs show the individual angles measured for specimen A1 exhibiting a surface contaminated with wet and dry artificial pollution. The triangles and diamonds represent the different measured angles at positive and negative polarity, the full line shows the average values at positive polarity and the dotted line shows the average of the values at negative polarity. The geometrical limit of angles is shown by the stabled line.

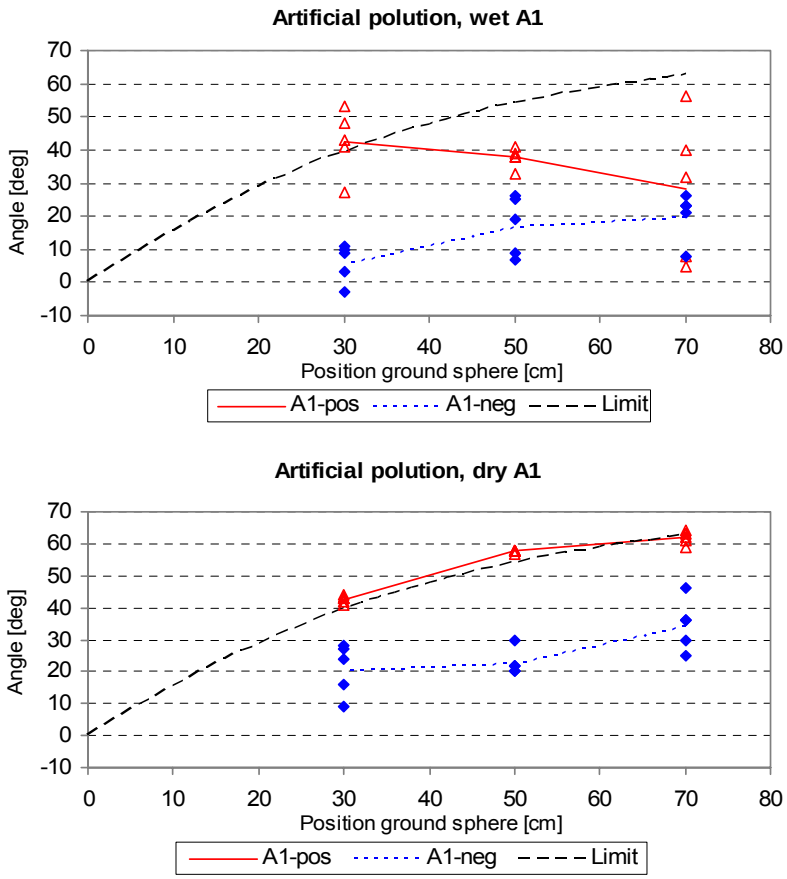

Figure 5.60 The dispersion of the data obtained with wet surfaces is larger than the case with dry surfaces. Top: Test results of specimen A1 covered with wet artificial pollution, Bottom: Test results of specimen A1 covered with dry artificial pollution.

Despite the dispersion among the individual data within the same test, the average values from tests on identical specimens (A1, A2) and (B1, B2) were quit similar. This is shown by plotting the data for both specimens of the same type in a single diagram for each surface contaminant, Appendix D. An example of such a plot is shown in Figure 5.61.

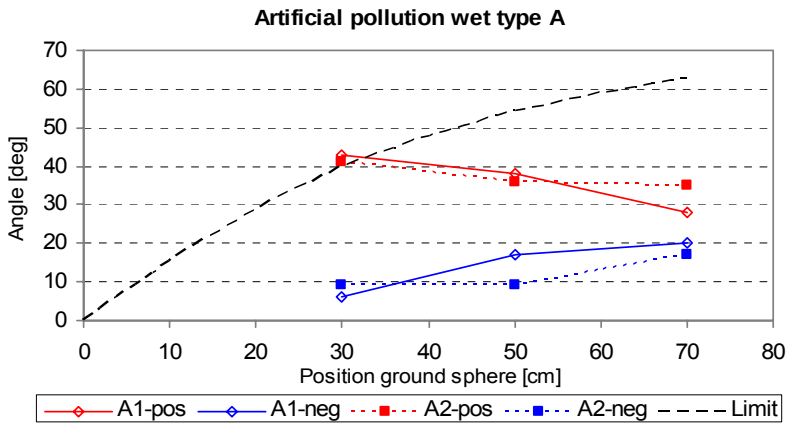

Figure 5.61 Comparison of results obtained with specimen A1 and A2 for the tests considering wet artificial pollution.

Since the results from the two identical test specimens are almost similar, the following analysis is based on average values of test results from the two sets of identical test specimens (A1, A2) and (B1, B2).

5.4.3.1 Clean surface

The plot on Figure 5.62 shows the data from tests of the three different types of test specimens.

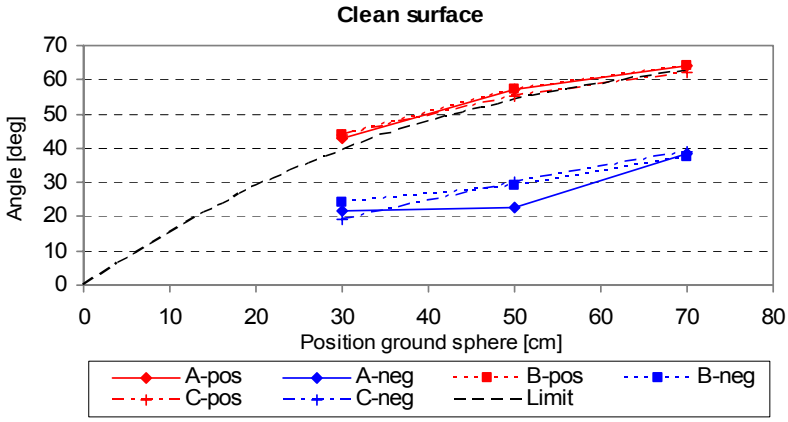

Figure 5.62 Data obtained with clean surfaces for specimens A, B and C and both polarities.

For all specimens it was evident that positive discharges jumped directly from the high voltage electrode to the grounded sphere without touching the surface. A reason for this general characteristic of polarity dependant flashover paths along insulating surfaces is

given in section 5.4.4. The negative discharges followed the surface for a certain distance whereafter they jumped to the grounded sphere. By calculating the length of the discharge path following the surface relative to the entire length along the surface x/(x+y) on Figure 5.58, a nearly constant value appears.

Table 5.14 Calculation of the relative discharge path along clean surface for negative polarity discharges.

Specimen	Distance from the orthogonal projection (x+y) [cm]	Angle [deg]	Distance along surface (x) [cm]	Relative distance (x/(x+y)) [%]	Relative to mean value [%]
A-neg	30	22	18.2	61	-7.1
	50	23	37.6	75	15.2
	70	39	46.1	66	1.0
B-neg	30	24	16.6	55	-15.0
	50	29	33.4	67	2.3
	70	38	47.0	67	2.9
C-neg	30	19	19.7	66	0.5
	50	30	32.7	65	0.2
	70	39	45.7	65	0.1

For the three different positions of the grounded sphere and for all three types of specimens the path traversed by the discharge along the surface is calculated in the third column in Table 5.14. The distance along the surface ‘x’ relative to the entire distance between the ‘receptor’ and the orthogonal projection ‘x+y’ is shown in the fourth column, and the individual values in column four relative to the mean value are shown in the fifth column. Besides two values (A-neg-50 and B-neg-30) all values lie within 10% of the average value.

Although this can not be extended directly to lightning discharges on actual blades, it is an interesting phenomena probably only valid for test setups where the orthogonal distance from the ground sphere to the surface ‘z’ is the same order of magnitude as the distance from the high voltage electrode to the orthogonal projection ‘x+y’ on Figure 5.58.

5.4.3.2 Artificial rain

The results from tests using artificial rain are shown in Figure 5.63.

Positive polarity discharges still tend to avoid the surface by attaching directly on the high voltage electrode and traversing in free air towards the ground sphere. The negative discharges follow the surface even longer than the case with clean surfaces. An exception is the naturally aged blade specimen type C where the angles for negative polarity remain nearly the same as with clean surfaces.

Looking closer at the surfaces of the new specimens A and B and comparing them to specimen C, it is obvious that the hydrophobic properties are quit different. Where A and B exhibit excellent hydrophobic properties and repels water into small discrete drops on the surface, specimen C tends to absorb the water forming a continuous layer. This effect

would probably increase the surface conductivity of specimen C compared to specimen A and B, but considering flashover during impulse voltages the permittivity and the discharge guidance of the artificial rain are probably more important.

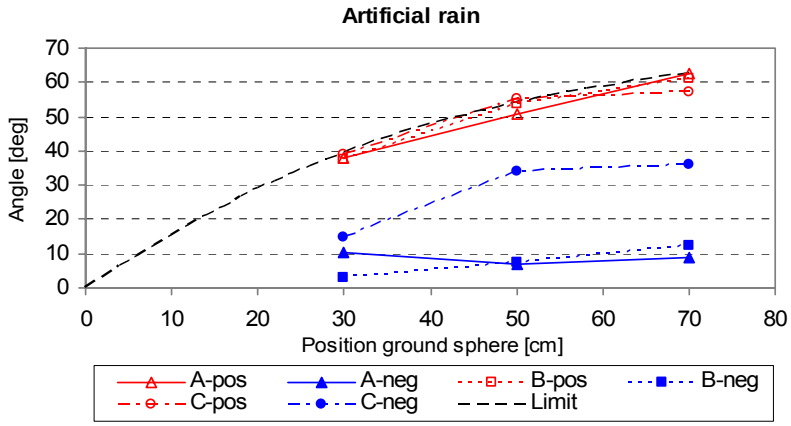

Figure 5.63 Test results using artificial rain for specimens A, B and C and both polarities.

A simple 2D model of the situation where water on the insulating surface forms into drops compared to a situation where the water is present as a continuous layer is shown on Figure 5.64. In the simulations the different materials (air, GFRP and water) are defined by their relative permittivities. A potential is applied on the left boundary, the right boundary is grounded and the upper and lower boundaries are left electrically floating without any charges present.

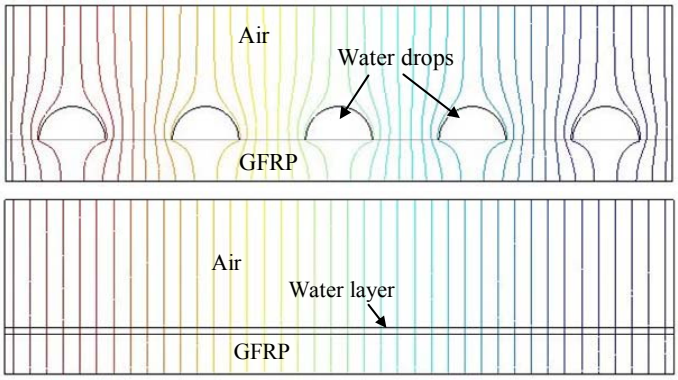

Figure 5.64 Simulation of the tangential potential distribution along the surface. Top: When water forms drops on the surface, the electric field is concentrated outside the drops as the case for specimens A and B. Bottom: The potential distribution is not affected by a continuous layer of water as seen on specimen C.

Since the permittivity of water is app. eighty times the permittivity of air, the tangential electric field would be suppressed from the water drops into the air gaps surrounding them. Similar to the functioning of diverter strips, section 2.4.1.2, the high electric field between the drops will ionise the air and create a conductive plasma guiding the discharge along specimens A and B.

By applying water on the surface of specimen C, the electric field in the tangential direction is not affected, explaining that the discharge pattern remain the same as with a clean surface. The general flashover voltage on specimens A and B is greatly reduced due to the presence of water drops allowing the discharge to propagate along the surface to the shortest possible distance to the grounded sphere, the orthogonal distance.

5.4.3.3 Dry artificial pollution

The results from the tests using dry artificial pollution are shown on Figure 5.65.

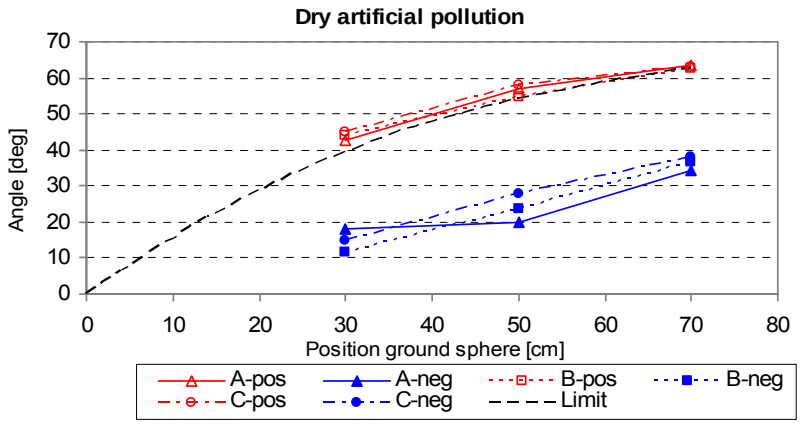

Figure 5.65 Test results using dry artificial pollution for specimens A, B and C and both polarities.

The results obtained with surfaces contaminated with dry artificial pollution exhibits the same characteristics as clean surfaces. The positive polarity discharges forms directly from the receptor towards the ground sphere not depending on the distance between the electrodes. Negative polarity discharges follows the surface for a certain distance depending on the position of the ground sphere in a manner similar to what was discussed for clean surfaces. This indicates that as long as the surface is dry, the discharge pattern is similar to what is experienced on a clean blade surface.

5.4.3.4 Wet artificial pollution

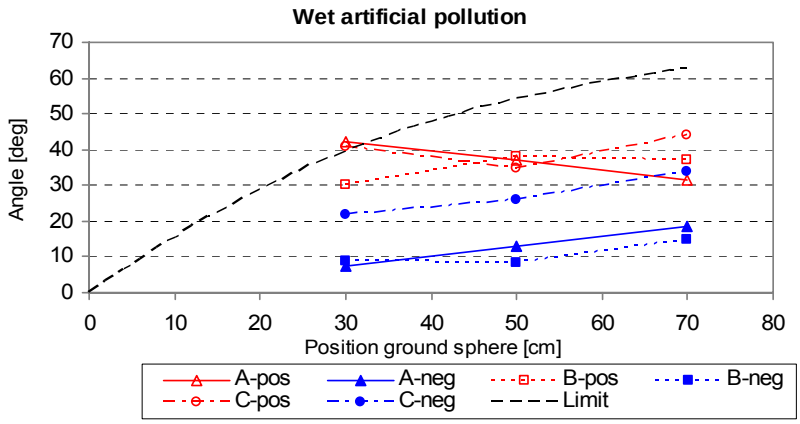

Figure 5.66 Test results for surfaces subjected to wet artificial pollution for specimens A, B and C and both polarities.

The presence of a conductive and wet layer on the surface makes the positive discharges stay attached to the surface somewhat similar to what has been experienced for negative discharges in all cases, Figure 5.66. The negative discharges follow the surface to the same extent as the case with artificial rain, where the specimen type C still is an exemption. The reason for this behavior must be the same as discussed in section 5.4.3.2

5.4.3.5 Silicone oil

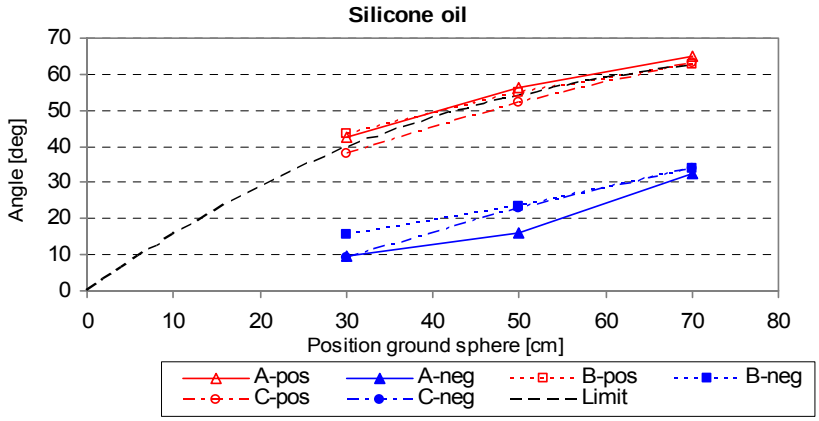

Figure 5.67 Test results considering surfaces wiped with silicone oil for specimens A, B and C and both polarities.

As for all the other cases except the wet artificial pollution, the positive discharges occurred directly from the high voltage electrode to the ground sphere considering surfaces

contaminated with silicone oil, Figure 5.67. The negative discharges behaved similarly to the case with clean surface and the dry artificial pollution, although the angles tend to be slightly smaller, Table 5.15.

Table 5.15 Comparison of angles considering negative polarity discharges for three different surface properties

Surface properties	Average angle, negative polarity discharges [deg]
Clean surface	29
Dry artificial pollution	25
Silicone oil	22

5.4.4 Discussion

A general tendency for all tests performed within this section is that negative polarity discharges followed the surface for a certain distance, whereas positive polarity discharges occurred directly from the high voltage electrode to the grounded sphere. A possible explanation of this phenomenon has been given by several physicists within discharges in long air gaps [30, 74, 75].

Considering a rod-plane gap in air with the rod energised, the space charge left by the first corona in the vicinity of the rod makes the second corona propagate from the outer regions. Since subsequent leader formation occurs from this second corona, the spark discharge never follows a straight line between the electrodes.

When an insulating rod bridges the gap between the energised rod (high voltage electrode) and the ground plane, the space charge from the first corona with same polarity as the high voltage electrode is deposited on the insulating surface. This would reject the second corona from the surface, creating a flashover away from the insulating rod, for both polarities [30]. However, partial discharges along the surface will create free electrons by photo ionisation, leaving the surface positively charged and unaffected by the polarity of the high voltage electrode [30] and [75]. This positive space charge on the surface will be enhanced as a consequence of the participation of emitted electrons in the avalanche processes. Consequently, for positive polarity, the second corona and hence the spark would be repelled from the surface whereas for negative polarity, the discharges would be attracted by the positively charged surface.

On Figure 5.68 the difference between positive and negative polarity discharges along an insulating surface is visualised. In case of a positive high voltage electrode, the electric field around the positive space charge on the surface ionises the surrounding air drawing electrons towards the anode and leaving positive space charge behind. These filamentary branches created by regions of positive space charge finally short the gap in a spark. Concerning the negative polarity discharges, the electrons from ionisation around the high voltage electrode are attracted to the positive space charge on the surface. These electrons cause ionisation of air molecules in vicinity of the surface resulting in extension of the positive space charge towards the ground electrode. Further electrons are created in vicinity of the insulating surface by means of photo ionisation which participates in the final shortening of the gap along the surface.

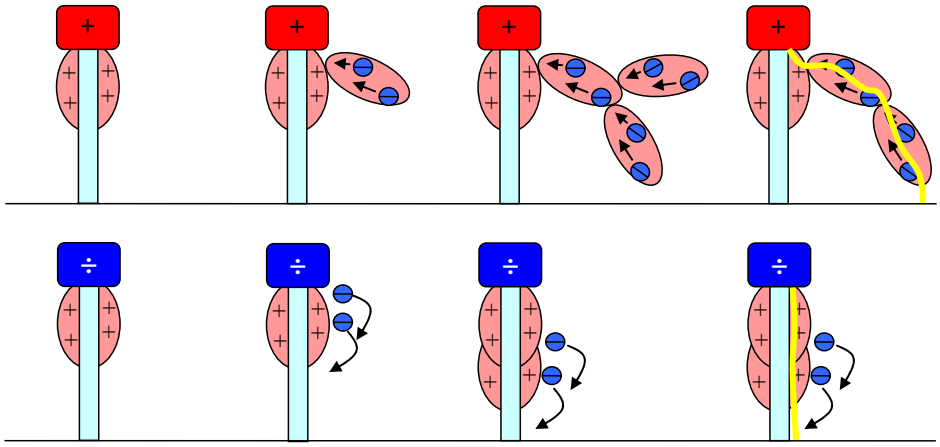

Figure 5.68 Differences in positive and negative polarity discharges along insulating surfaces. Top: Positive discharges are repelled by the positive space charge on the surface, Bottom: Negative discharges are attracted to the positive space charges, and hence follow the surface.

By comparing the results obtained with dry artificial pollution and with clean surfaces, the consequence of a dry conductive layer can be evaluated. This revealed that the presence of a conductive surface contaminant itself did not oppose an increased risk compared to a clean surface. Both negative and positive discharges behaved similar in the two cases.

Considering wet surfaces, the presence of a relatively high conductivity in the case of wet artificial pollution only affects the positive discharges giving smaller angles as defined in Figure 5.58 (not to be confused with the 'contact angle' generally defining hydrophobicity) . The negative discharges behaved similar in the two cases.

A comparison of dry and wet surfaces shows that angles measured at negative polarity on dry surfaces (clean surface and dry artificial pollution) tends to be nearly 70% larger than angles measured on wet surfaces (artificial rain and wet artificial pollution) for the same polarity. This is seen in Table 5.15, where average values of all angles measured at negative polarity for both wet and dry surfaces are calculated.

Table 5.16 The average angle experienced on dry surfaces is nearly 70% larger than on wet surfaces considering negative polarity discharges.

Surface properties	Average angle [deg]
Wet (Artificial rain and wet artificial pollution)	16
Dry (Clean surface and dry artificial pollution)	27

The presence of conductive moist formed as drops on the surface probably increases the appearing propagation speed of streamers along the surface as discussed in section 5.4.3.2. This effect means that streamers all across the wet surface leave the surface almost simultaneously, such that the answering streamers from the sphere are met at the shortest possible distance. Streamer propagation across a dry surface is much slower,

enabling the streamers emitted close to the high voltage electrode to extend further into the gap compared to streamers emitted closer to the ground sphere, Figure 5.69.

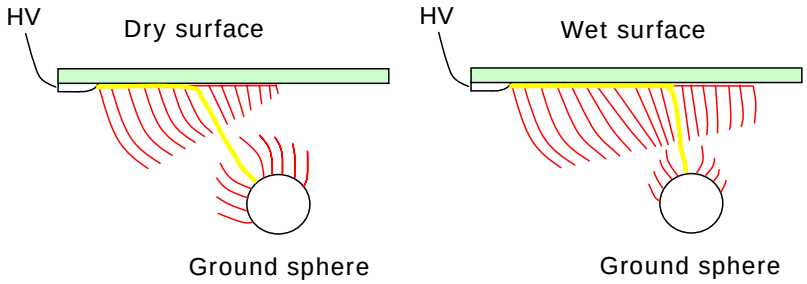

Figure 5.69 Comparison of discharge pattern for negative streamers on dry and wet surfaces. Left: The finite propagation speed of streamers along a dry surface ensures that streamers leaving the surface close to the HV electrode extend further into the air than streamers leaving further away from the HV electrode. Right: On wet surfaces the propagation speed is higher meaning that the difference in length of streamers originating different places along the surface is not that significant.

Applying these conclusions on the performance of actual blades, the recommendation must be to optimise the hydrophobic properties considering negative discharges (positive lightning strikes). Although the arguments are different, the conclusion is in good agreement with the theoretical considerations in section 4.4.2. The discharge tends to follow the surface on wet hydrophobic specimens for a longer distance, and thereby oppose a risk of thermal damage. However, since the current conduction probably occurs in conductive plasma above the surface as the case of diverter strips, the thermal impact on the surface might be minimal. A tempting diverting conclusion would be that by optimising the hydrophobic properties of the blade surfaces, the collective area of each receptor might be increased as well.

The angle measured at positive polarity is unaffected by the presence of moist, where only the conductivity of the wetting agent plays a minor role.

Silicone oil does not affect the measured angle at positive polarity either. Comparing the angles measured at negative polarity however showed a minor decrease in the angles for surfaces contaminated with silicone oil relative to clean surfaces.

5.5 Laboratory work

The test methods described in this chapter have led to some general conclusions and recommendations on designing and selecting composite materials. The various tests are easily conducted in most high voltage laboratories, and it is strongly suggested that such tests should be part of the developing of new blade materials.

Chapter 6

Full scale testing

Chapter 5 considered methods for classifying, choosing and rejecting materials for wind turbine blades. By testing different materials according to these methods some general recommendations and guidelines have been stated. These initial steps are very important in the developing of new blade designs, and should be considered each time new materials or material compositions are introduced.

When the specific materials have been selected or developed, and the entire blade design fulfils both the mechanical requirements and the specifications established by the lightning protection engineer a verification of the ability of the blade to withstand lightning discharges must take place. Such a general verification of the lightning protection system of an entire blade would enable comparison of different blade designs, and could even pass or fail new blades without any service experience. In case errors have been introduced somewhere in the process, they will be revealed in testing the final product. In the chapter 'Conclusions and recommendations for further work' in IEC 61400-24 it is also emphasised, that methods in determining the interception efficiency of lightning air termination systems must be investigated [5].

Taking the use of CFC as an example, there are many suggestions on how to protect either structural components or skins made of CFC. A general full scale test method should not distinguish between different solutions, it should rather evaluate whether the interaction of materials and protection measures will perform satisfactorily in a lightning environment.

This chapter is intended to present the ideas for a standardised full scale test method of wind turbine blades and their capability of handling the impact from natural lightning. The procedure is quit logical and adapted from methods used in the avionics industry [9]. In real life, a full lightning discharge is an impact consisting of a high electric field followed by a strong electric current. The field initiates and defines several possible paths which subsequently are heated and mechanically affected by the high amplitude current. In the laboratory such impacts requiring extremely high energy storages are not possible to reproduce. Therefore the two main components must be simulated separately in a high voltage test and a high current test.

6.1 High voltage test

6.1.1 Purpose

This section aims at defining a test method suitable to pass or fail entire blade designs with respect to their ability to withstand lightning. The test should determine which places

a lightning discharge will attach to the blade, in order to evaluate the efficiency of the installed lightning protection.

The entire blade is indeed affected by the external field prior to a lightning strike, and existing principles of designing lightning protection (rolling sphere method) also predicts a risk of getting struck inboard from the tip. However, experience from monitoring a large number of newer wind turbine blades, have shown that the majority of lightning attachments occur within the tip area, making the design of the outermost 3m or 5m most important, Figure 6.1.

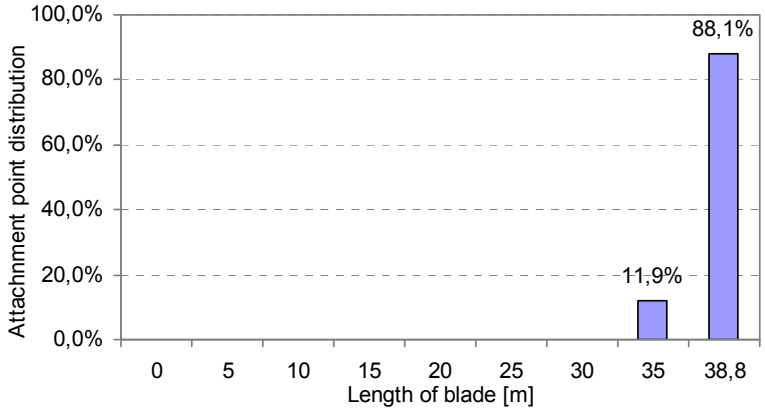

Figure 6.1 Strike data collected from 236 blades monitored during 2 years of operation. The turbines from Vestas Wind Systems were fitted with 39m blades, and the bars show the relative amount of lightning attachments to different regions of the blade. A total of 118 lightning strikes were identified.

By summing up the data in Figure 6.1 it is seen that more than 88% of all strikes occurred within the outermost 1m of the tip, and that the rest of the strikes occurred to the receptor at radius 35m.

In defining a test method, there are several aspects to consider. The test environment experienced by the blade should be somewhat similar to the conditions met in real nature. Furthermore the test method should be inexpensive and limited to such an extent that manufacturers will actually get the test done. Last but not least, a test method is not suitable if it can only be done in a very few laboratories world wide, since the only way of developing new test methods and sharing experience is by enabling the participation of a large number of laboratories.

6.1.2 SAE ARP 5416

Testing the durability of the installed lightning protection of wind turbine blades has previously been done according to the US MIL 1757 A standard [76]. The standard describes lightning verification tests for structures made of composite materials on aircrafts, but unfortunately the results are too pessimistic considering the lightning attachments on wind turbine blades [35]. Recently similar tests have been performed according to the

requirements in the SAE ARP 5416, a refinement of the US MIL 1757 A standard among others. Experiences from such tests was first published at the International Conference on Lightning and Static Electricity 2003, where LM glasfiber A/S published test results from one of their 35m blades tested at Hydro Quebec in Canada [35].

The test method used was based on the SAE ARP 5416 standard [77] and aimed at determining possible attachment points on the blade. Since the present idea of a new test method also relays on this well established standard, the situation to be investigated as well as the test principles are explained in the following.

The outer skin of large commercial aircrafts has so far mostly been made of an aluminium alloy. This is in good compliance with common lightning protection since the outer skin both shields internal wiring, and represents a very large path for the lightning current. However, radio communication and the functioning of radars will be limited by placing these antennas inside a shield of metal, meaning that they will have to penetrate the skin and only be covered by an electrical insulating material. Conductive antennas placed behind an insulating shield will on the other hand be equally attractive for the lightning discharge as the aluminium alloy next to it, making it necessary to protect these insulating structures separately [9].

On example of such a structure is the weather radar, which is fitted at the nose of the aircraft behind an electrically insulating radar dome, the radome. If such a radome located at one of the aircraft extremities is not protected, lightning attachment to the antenna through the radome might occur. The processes are similar to the ones described in Figure 3.8 where streamers originating from the antenna deposit charges on the interior. These charges increase the external electric field on the exterior surface, creating further ionisation. The charge left behind is of opposite polarity than the internal charges which finally increase the electric field across the laminate to a level where puncture occurs. This means that puncture actually occurs due to emission of streamers towards charge concentrations in the surrounding, maybe as a consequence of an approaching lightning leader, Figure 6.2. However, the structural damage happens when the lightning current has to pass the tiny puncture resulting in an increase of pressure due to heating of the arc channel within the radome [78].

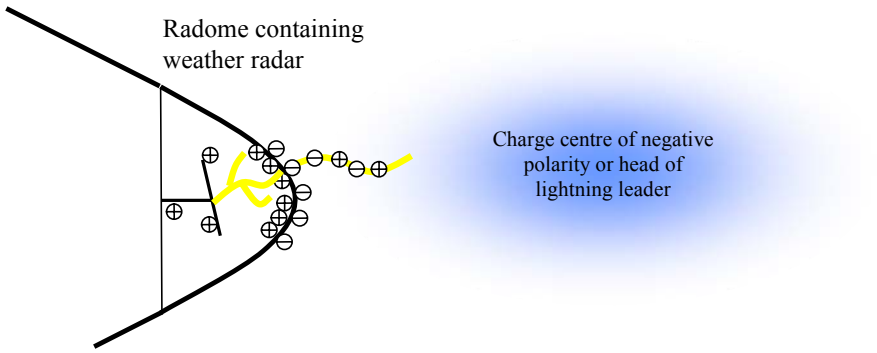

Figure 6.2 Streamer formation within the radome leads to emission of leaders from the exterior stressing the radome laminate itself.

Minor punctures are also seen on radomes as a consequence of slow charge migration on the exterior of the radome in antistatic paint and rapid field changes due to nearby lightning strikes [78].

Lightning protection of radomes is typically done by attaching diverter strips on the exterior which acts as an extension of the metal frame to which the insulating radome is attached, section 2.4.1.2. The electric field experienced by the radome during initial leader attachment has a slowly increasing nature corresponding to the voltage waveform D in section 3.1.4.2.

Based on all these considerations, the initial leader attachment test in SAE ARP 5416 §5.1 was established. Depending on the geometry of the test specimen, the specimen is either elevated and energised (Test setup A in section 5.1.1.c [77]) or placed at the floor and grounded (Test setup B in section 5.1.1.c [77]). Considering the applicability on wind turbine blades, test setup A is selected and described in the following.

1. The radome is elevated above a ground plane, and must be fitted with an internal high voltage electrode representing the antenna. Protective measures as diverter strips are applied and connected electrically to the frame of the radome and to the high voltage electrode.
2. The distance between conductive parts of the radome and the grounded plane on the floor must be kept at 1m or above, and the distance between insulating parts and the ground plane must be at least 0.5m.
3. A voltage waveform D is applied at the high voltage electrode, at an amplitude sufficient to cause a flashover to the ground plane.
4. In the standard two pulses of each polarity for several orientations of the radome are required.
5. The test is passed if all discharges of both polarities attached to the structure at places capable of handling the lightning current. If some of the discharges punctured the radome and attached to the internal high voltage electrode, the lightning protection was apparently not designed correctly.

During testing each discharge must be photographed in order to ensure that streamers origin at the test specimen and meet streamers from the ground plane closest possible to this plane. Furthermore the ground plane must be of such a size that sparks does not terminate on corners or edges of the plane.

Depending on the number of discharges and orientations chosen, such a test procedure determines whether lightning will attach to the installed protective measures or cause severe damage to the structure by puncturing. Verification of the test method has been done by testing a great amount of older radome designs which is known to be struck and comparing the results from the laboratory tests with inflight experience. This revealed a good correlation. New radomes which have passed the tests also tend to avoid being struck fatally by lightning.

6.1.3 Test method adjusted to a wind turbine blade tip

Since most of the lightning attachments are located in the tip area, the following test method focuses on this part of the blade. The steps below define the test method, which is based on SAE ARP 5416 and conditions relevant for wind turbine blades in particular.

6.1.3.1 Test specimen

The outermost 3m of the blade tip is suggested suitable for these tests. This section covers the most important area of the blade with respect to lightning, and has a size which can be handled in most high voltage laboratories. The blade tip must be either cut from an actual blade, or be made exactly similar to the conditions seen on a real blade. It should be fitted with the exact same lightning protection components as the real blade (receptor, down conductor, etc.) and the surface finish should also be completed to perfection.

6.1.3.2 Test setup

The test setup consists of the following:

1. Marx generator with internal and external resistances and capacitances configured to generate voltage waveform D pulses.
2. The measuring system capable of measuring the high voltage surges and determining the exact wave shape and time to flashover.
3. The blade tip elevated above the ground plane by means of insulating straps and oriented in different angles with horizontal and different pitch angles.
4. Digital cameras capable of photographing the discharges such that determination of the spark attachment point on the blade can be done quickly after each discharge.
5. Mirrors such that discharges from the back side of the blade can be monitored by the digital camera.

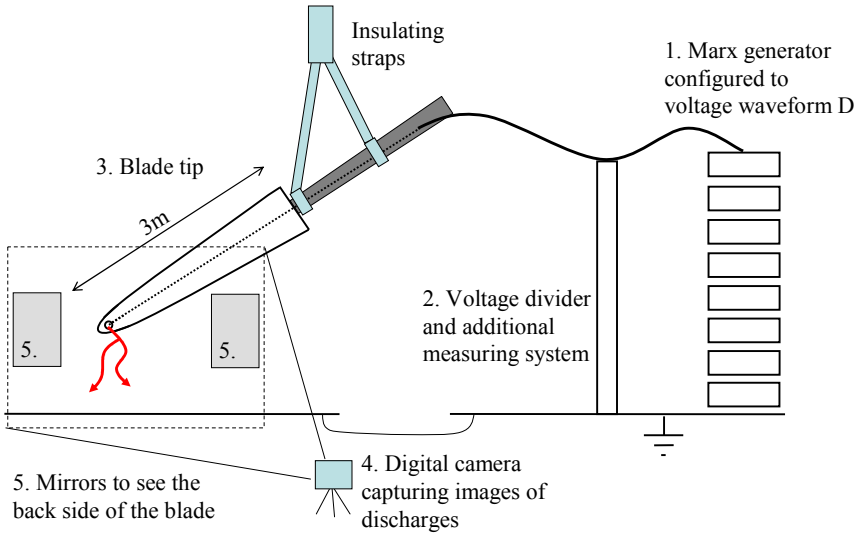

Figure 6.3 Test setup used at initial leader attachment tests.

The size of the ground plane below the blade tip on Figure 6.3 must be large enough to avoid discharges from the blade to the edges of the ground plane. In general the ground plane simulates the static field experienced by the blade prior to an upward initiated lightning strike, or the field from the head of an approaching lightning leader in case of a downward initiated strike. Since the waveform D is a relatively slow voltage surge, and

the moment of flashover appears as a fast transient the measuring system must be constructed such that the necessary wide band response is ensured.

6.1.3.3 Test procedure

The following test procedure is suggested:

1. Adjust the Marx generator to produce a double exponential voltage waveform D with positive polarity.
2. Suspend the blade tip above a ground plane such that all conductive parts connected to the down conductor system are at least 1m from the ground plane, and all other parts are at least 0.5m from the ground plane.
3. Drape the specimen with a conductive foil connected to the lightning attachment point (receptor).
4. Connect the output of a Marx generator to the down conductor at the root end of the blade tip, and apply a voltage waveform D with an amplitude sufficient to cause a flashover from the foil to the ground plane.
5. Remove the foil.
6. Apply five pulses for the present configuration of pitch angle and angle with horizontal. A picture should be taken at each discharge to ensure that streamers and leaders originate from the tip and meet streamers from the plane closest to the plane. These pictures also help in determining where the spark attached to the blade.
7. Change orientation of the blade (pitch angle etc.).
8. Repeat steps 2-7 for the decided number of different orientations.
9. Configure the generator to produce voltage surges of negative polarity.
10. Repeat steps 2-8.

Step 6 diverges from the description in SAE ARP 5416, since the standard only recommends two discharges for each orientation and each polarity. The argument is that further discharges tend to stress or electrically degrade the composite material excessively, such that the specimen might fail the test although it would have performed satisfactorily during normal operation.

Aircrafts are much different than wind turbines in the sense that they can avoid thunderstorms by postponing their flights or choosing different routes. Wind turbines are located at the same spot and must cope with all thunderstorms passing that particular area for 20 years. For this reason they will probably be hit more often than aircrafts. The initial experiences described in section 6.1.4 also showed that the discharge pattern or attachment point on the blade might change at the third or fourth discharge, meaning that further tests will reveal a more reliable image of the capability of the lightning protection system.

6.1.4 Recent tests of six blade tips

In cooperation with a Danish wind turbine manufacturer, high voltage tests on six blade tips where performed during 2005. The aim was to investigate the possibility of testing blade tips and correlating possible failures with failures experienced on blades in service. Among the blades were both older designs, newer designs and tips manufactured to test different solutions regarding the tip receptor configuration. The last test was performed on a blade tip with a retrofit receptor arrangement.

The blade tips where 3m long with the beam extending a further 3m, enabling fixation of the specimen. All tests were carried out at the high voltage laboratory at the Technical University of Denmark, with a Marx generator rated at 1200kV.

6.1.4.1 Test method

The test method followed the description in section 6.1.3, and only diverged by the number of discharges at each polarity and each orientation of the blade. Since the present standard SAE ARP 5416 only recommends two pulses, it was decided to follow this suggestion. However, experience from these tests indicates that future standards should consider increasing the number of discharges as discussed in section 6.1.3.3.

It was decided to perform the tests with the blade tip positioned in nine different orientations. For the first eight positions the blade was suspended at an angle of 45° with horizontal, whereafter the tip was pitched in steps of 45°. The ninth orientation was vertical where the blade pointed directly downwards towards the ground plane. Each position was designated a certain code according to Figure 6.4.

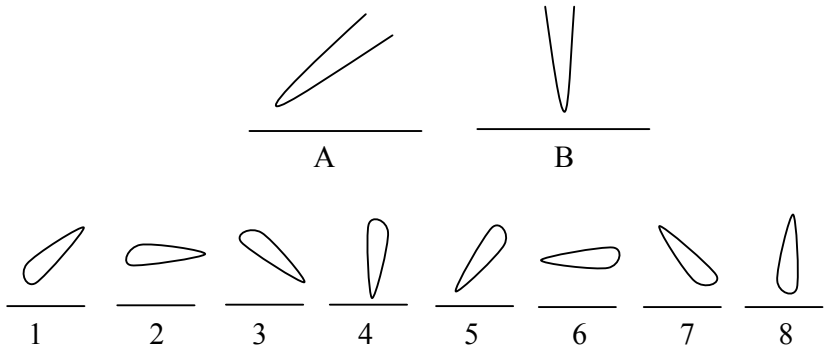

Figure 6.4 Blade positions concerning high voltage tip tests.

An orientation of the blade with an angle of less than 45° (10° or 20°) could also be possible. However, in these tests the pitch angle was regarded as being more interesting.

The voltage applied was a waveform D with a rise time of app. 100us, and a decay time of app. 6000us. For each discharge the waveform was recorded such that the peak value and the time to flashover could be determined. Images of the discharges was captured with a digital SLR camera, enabling determination of the attachment point on the blade tip and whether the connection of streamers from the specimen and the grounded plane occurred as specified, details of the camera used are given in Appendix C. A blade suspended in position A8 is shown on Figure 6.5.

For positive polarity tests, the requirement of minimum 1m between conductive parts of the blade and the ground plane was fulfilled. Considering negative polarity tests, the specific configuration of the Marx generator could not produce a voltage waveform D at an amplitude sufficient for flashover. Much of the energy was lost in the wave shaping resistor, such that the maximum output voltage of the generator dropped when generating slow pulses. For this reason the distance between the receptor and the ground plane was reduced to 80cm for negative polarity discharges.

Figure 6.5 A 3m GFRP blade tip fixed by its 3m beam elevated above the ground electrode in position A8.

6.1.4.2 Results

The following results are in terms of general considerations evaluating the test method and different critical manufacturing issues of blade tips.

Images of discharges reveal many important issues as seen on Figure 6.6. The left image shows a positive polarity discharge from the blade tip towards the ground plane. Note that the connection is located a few cm above the ground plane, where the leader originated from the blade tip meets the streamers from the ground plane. This shows that the discharge had actually started on the blade tip, just as the case with an answering leader emitted from a turbine blade by the approaching lightning leader in a thunderstorm environment.

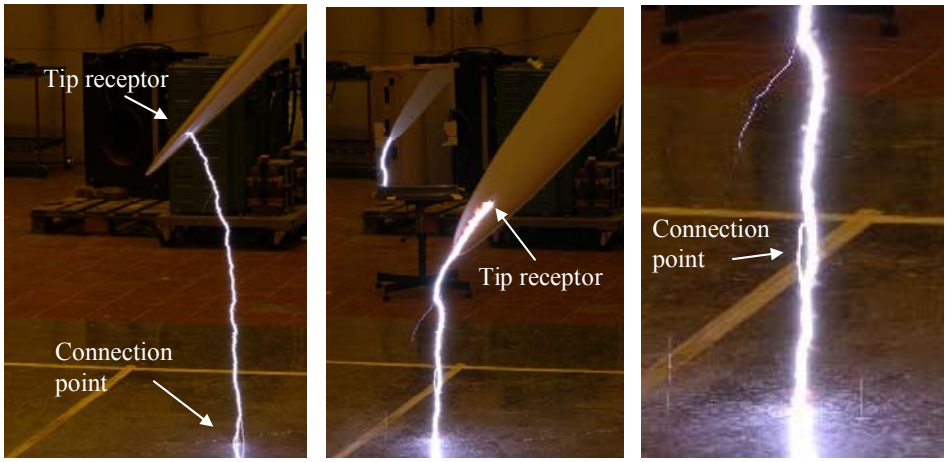

Figure 6.6 Left: Positive polarity discharge at position A2 (397kV), Middle: Negative polarity discharge at position A1 (-713kV), Right: Zoom of negative polarity discharge showing connection point of leaders and further streamers from the ground plane.

A negative polarity discharge is shown on the middle image. The connection point has, in this case, moved closer to the blade tip, possibly due to the increased voltage necessary for creating a spark at negative polarity. Due to the increased voltage and longer time

duration for creating a negative polarity flashover, the discharges from the ground plane have more time to propagate towards the blade, and hence extend further into the gap. However, since the connection points of leaders from the blade and the ground plane are still located closest to the ground plane, the results are regarded as being valid [77].

A zoom of the connection point at the negative polarity discharge is shown on the right image of Figure 6.6. Streamers coming off the ground plane are visible around the arc root of the spark. Since these streamers from the ground plane origin randomly on the aluminium plate, the geometry is large enough to avoid edge effects, and thereby fulfills the requirements by SAE ARP 5416 [77].

Six different blades with different receptor configurations and tip designs were tested during this research. Depending on the specific design, the discharge patterns behaved differently but did always reveal important issues of the construction. This enabled a scientific iterative way of improving the tip design towards a robust solution capable of handling lightning attachments.

Occasionally a discharge punctured the blade laminate, in which case the cause of failure was discussed and determined. Minor punctures are easily repaired with fast curing epoxy glue, enabling continuation of the test within 30 min. These incidents only happened at negative polarity, maybe due to the combination of increased stress (higher voltages) and the polarity dependant discharge pattern as discussed in section 6.1.4.3.

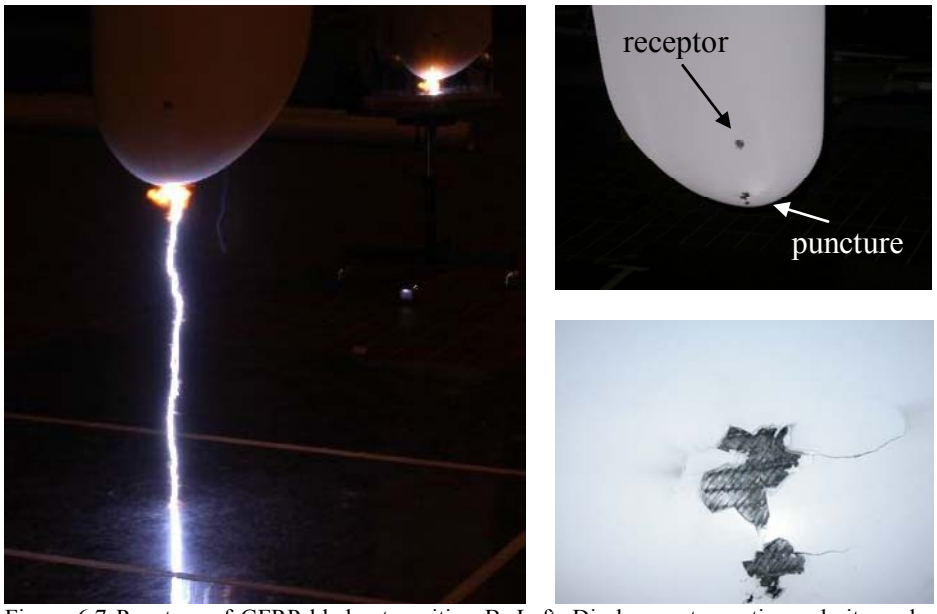

Figure 6.7 Puncture of GFRP blade at position B, Left: Discharge at negative polarity and -572kV, Right: Close up of puncture outside tip receptor.

When such failures as shown on Figure 6.7 happened, the blades were examined carefully, which always revealed uncovered parts of the internal down conductor. It was evi-

dent that internal streamers originating at these bare metal parts exposed the laminate to an extensive electrical stress leading to the breakdown. A situation in good agreement with the theory presented in Chapter 3. By changing the geometry and construction of the next tip to be tested, the risk of getting such punctures were eventually minimised. Furthermore the locations of punctures correlated very well with the experience from blades in service which have been struck by lightning.

6.1.4.3 Discussion

All tests revealed a fundamental difference between the discharges at positive and negative polarity. The positive polarity discharges jumped directly off the receptor to the ground plane at voltages around 350kV-400kV, whereas the negative discharges required nearly twice the voltage and took a path close to the surface. The reason for the different paths can be explained by the positive space charge on the surface of the blade skin for both polarities, which has been commented more thoroughly in section 5.4.4.

The difference in voltage amplitude is explained by the strongly inhomogeneous electric field and the extensive mobility of electrons compared to positive ions [27]. When the blade tip is at positive polarity, the electrons from ionisation around the tip will be drawn into the anode (the tip receptor). The remaining positive space charge will decrease the field strength around the blade tip but also increase the field in the rest of the gap. Since the electric field in the main part of the gap is relatively high due to the space charges, the onset of streamers from the blade tip leads to breakdown at relatively low voltages.

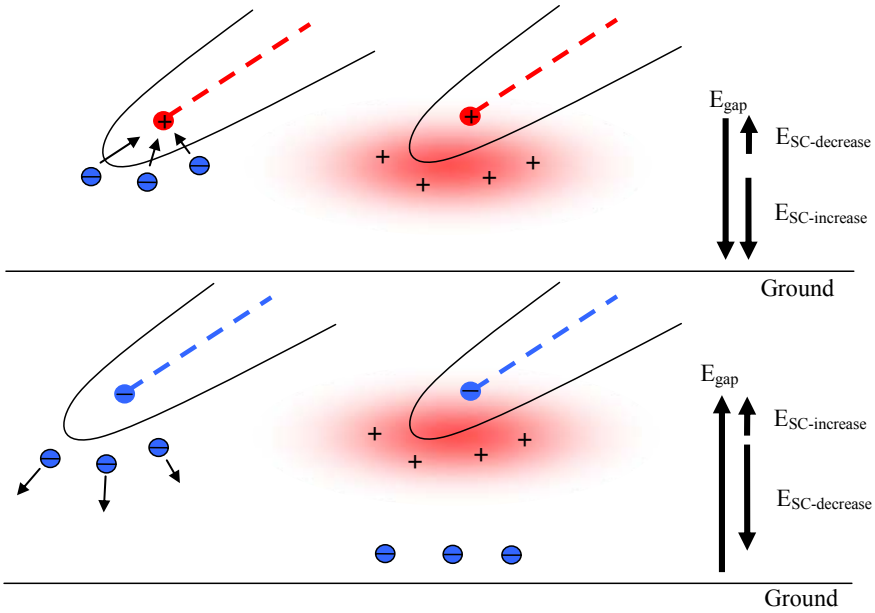

Figure 6.8 The flashover voltage for asymmetrical gaps depends on the polarity of the smallest electrode. Top: The space charge created around a blade tip at positive polarity increases the field in the main part of the gap, and hence decreases the flashover voltage. Bottom: Although the field in vicinity of the blade tip is increased at negative polarity due to positive space charge, the field in the main part of the gap tends to decrease, giving higher flashover voltages.

Considering blade tips at negative polarity, the electrons from ionisation at the tip will be repelled into the low field region and be absorbed by gas molecules or the ground electrode. The positive space charge left behind increases the field around the tip drastically and results in the onset of streamers at lower potentials than at positive polarity. However, since the electric field from the free electrons close to the ground plane and the positive space charge around the blade tip is oriented in the opposite direction of the field without space charges, the resulting field is considerably lower for negatively charged blade tips than positively charged blade tips. Hence the voltage applied for negative polarity must be higher in order to achieve a background electric field to drive the streamer discharges towards the ground electrode.

6.1.5 Streamer propagation tests

A variety of the initial leader attachment test is a test method where the voltage is quenched before the flashover occurs. This test method is not as destructive as the case where punctures might happen, and still gives some information about where streamers will origin at the blade. However, partial discharges as streamers and corona mainly emit light in the UV range meaning that conventional cameras can not be used for capturing such images, Appendix C.

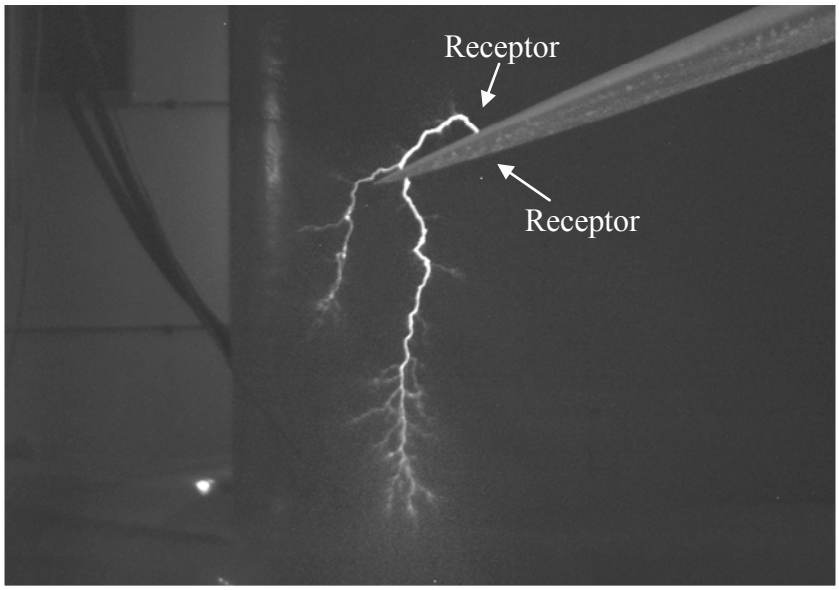

Figure 6.9 UV image of a positive streamer discharge at a blade tip energised with a voltage waveform D at app. +450 kV.

The image on Figure 6.9 was captured by applying a positive polarity voltage waveform D on the blade tip. The voltage surge was quenched at app. 450 kV in a parallel gap before the flashover developed from the blade tip. As seen on the picture, streamers and leaders origin mainly at the receptor of the blade and propagates like branches on a tree

into the low field region. Clearly the leader is connected directly to the upper receptor and traverses a path similar to what was seen for the discrete sparks on Figure 6.6

The picture of the negative streamer discharge on Figure 6.10 shows a different picture than the positive discharge. Streamers in this case are not limited to origin at the receptor, but seem to come off the surface from a wide area surrounding the receptor. It has previously been stated that insulating surfaces that participate in flashovers are positively charged for either polarity, section 5.4.4. Such a positively charged surface might attract the negative discharges from the receptor until the field is strong enough to make them leave the surface.

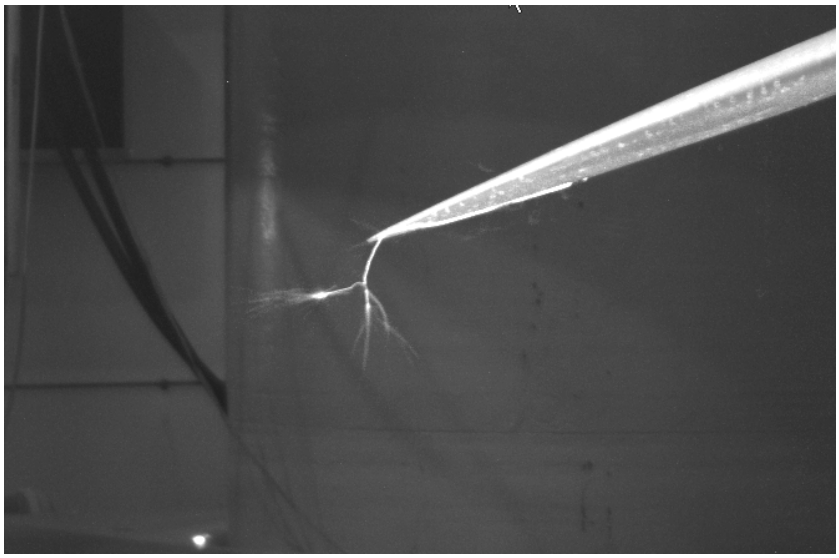

Figure 6.10 UV image of a negative streamer discharge at a blade tip energised with a voltage waveform D at app. -650kV. On the original image it is clear that streamers are emitted from the blade surface on a wider area surrounding the receptor.

Another explanation could be that, at negative polarity, the voltage and hence the field has to be nearly twice the voltage for positive polarity to create a flashover. This means that higher fields are present around the blade tip concerning negative polarity which increases the rate of ionisation, Figure 6.8. The negative polarity discharges are attracted by the positive space charge surrounding the tip resulting in streamer formation distributed across a wider area.

Comparing these tests using quenched voltages and pictures of streamer formation with the spark discharge tests in section 6.1.4, there is one major difference. The spark discharge test only shows the location of a single possible strike attachment point for each discharge, meaning that a limited number of discharges only provide data on a limited number of possible attachment points. The streamer propagation test shows competing streamers possibly coming off the blade from a wider area, which thereby indicate areas of interest others than the discrete spark attachment points in section 6.1.4. In other terms,

the streamer propagation test gives an idea of the probability distribution for streamer initiation on the blade or, considering the actual application, how exposed the receptor is compared to protrusions on the surrounding surface. These areas outside the receptors where streamer initiation occurs are important to identify since streamer formation from areas outside the intended air termination will imply a risk of failure on blades in service.

The equipment used to capture these images is rather expensive, and the results are not straight forward to derive. Considering standardised verification tests as treated in this section, it is more consistent and reproducible to refer to a finite number of discharges photographed with conventional cameras. Therefore, it is suggested that using UV photography as part of a verification test should not be a requirement, but only seen as a beneficial tool to support the design evaluation.

6.1.6 Evaluation of test method

By testing small specimens like these 3m blade tips with 3m beams extending, it is possible to perform many tests within a limited amount of time. Special tip design features and receptor configurations are easily incorporated since the size of the specimens allows easy handling to and from the factory and test facility. With a blade tip of a total length of 6m, and the orientations and number of discharges as described above, the duration of the tests when done by one person was app. 2 days. The method presented is easily extended to cover tests on other components as well, the nacelle, the anemometer, antennas etc. In these cases it might be more convenient to change the test setup such that the specimen is grounded and the plane electrode is energised, but the principle remains the same.

At negative polarity discharges (corresponding to positive lightning strikes) punctures of the blade skin occurred a couple of times. These punctures were located at the same positions as seen on real blades hit by lightning, and could always be explained by the present tip design and receptor configuration.

As commented in section 6.1.4.1, the configuration of the Marx generator used for these tests (1200kV peak) was not large enough to create a flashover of voltage waveform D at negative polarity and a distance of 1m. To precede the testing and gain experience with negative polarity tests, the distance was decreased to 80cm, still giving important results.

The general impression is that by performing regular tip tests as described during both the design phase, and as verification of the final product, valuable information which could not be achieved otherwise is gained. The present test method will hopefully be introduced in future test standards.

6.2 High current test

When a considerable number of discharges in the high voltage test have shown where the object will be struck, the initial leader attachment test is finished. If all discharges attached to the intended air terminations (receptors) the blade passed without any comments. If some of the discharges punctured the blade skin or caused other failures, the manufacturer has to explain why it occurred and make sure that changes in the design will avoid this problem in future tests.

As mentioned in Chapter 3 the physical damage is mostly related to the current. For this reason the test specimen used for the high voltage test must be subjected to a physical damage high current test showing the consequences of having the lightning current entering the structure at the locations identified by the high voltage test. In the SAE ARP 5416 test standard [77] several methods for predicting the indirect effects by induced currents are described. Considering a conventional blade tip which so far does not contain any sensitive electronics, a direct test method simulating the charge transferred and the energy released during a lightning strike is more relevant.

Such a test method could be utilised as shown on Figure 6.11.

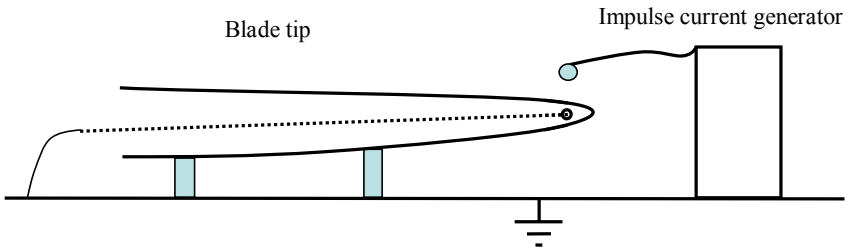

Figure 6.11 Test setup for determining the damage associated with a direct lightning strike.

The blade tip is resting on supports insulating it from the facility ground. By grounding the down conductor system and injecting current pulses at the locations found during the high voltage tests, the physical damage can be evaluated.

Current waveforms, specific energies and charge transfer must be cleared with the standards for protection of other structures from direct lightning attachment. Such information is found in IEC 62305 [32] and commented in section 3.1.4.1. As discussed previously, the blade is positioned at the most vulnerable location and should be protected according to the LPL I in the standards. Different values are associated to the different components in a lightning strike (short duration stroke, long duration stroke, continuous current) such that blades under tests should meet the worst conditions.

Table 6.1 Values for physical damage tests using high currents.

Peak current	200 kA
Average steepness	200 kA/us
Specific energy	10 MJ/ohm
Total charge transferred	300 C

Not all the parameters can be met at the same time, why specific waveforms must be used separately. The specific energy for instance is often injected by a double exponential waveform with a rise time of 10us and a decay time of 350us. The total charge on the other hand could be generated by discharging a large battery bank at a relatively lower current for a longer duration [32] and [77].

The currents must be injected in all the possible attachment points as defined by the high voltage test, and the high current test is then passed successfully if no significant damage occurs at any of the injection points. If some of the discharges result in unacceptable damage, the manufacturer must change the tip design to avoid similar damages in subsequent tests.

Typically design changes aim at improving the breakdown strengths of the laminate and minimising the field enhancement around interior sharp edges such that the high voltage tests will be passed without remarks. This in turn makes the high current test easier to pass, since it is then just a matter of designing the receptor and down conductor joints properly.

By forcing manufacturers (by means of standardisation) to perform such tests on their blades, they are deemed to focus on the importance of improving the entire design of the blade tip and the installed lightning protection. Parallel to this thesis, working groups under the IEC TC88 are being established aiming at discussing the possibility of incorporating such methods in future test standards.

Chapter 7

Discussion

The present thesis has discussed several issues concerning the lightning protection of wind turbine blades. Initially the lightning environment and the interaction with wind turbines are described, which leads to some general theoretical statements for the composite materials used. Besides these manufacturing recommendations based on experience from the high voltage industry, several test methods have been used to measure the properties of the specific materials.

In situations where standardised test methods are available, such tests are performed and related to the blade application. Since the composite materials in wind turbine blades are stressed somewhat differently than materials for common high voltage applications, several different test methods have been developed to cover these issues.

These tests combined with numerical modelling of lightning attachment points and detailed material behaviour, as well as full scale tests of the final product, form a set of useful tools in designing future blades.

The different findings are discussed from an academic point of view in this chapter, leaving the results aimed directly at improving the performance of wind turbine blades for Chapter 8.

7.1 Breakdown test method for composite materials

Several standardised test methods are used to determine the electrical breakdown strength of solid insulating materials for high voltage applications. Since the design of high voltage apparatus ensures that the materials are only subjected to a very controlled electrical stress, most test methods are constructed in a similar manner. In these cases uniform electric fields are applied across thin samples of homogeneous materials giving consistent results for these specific applications.

Considering composite insulating materials used for manufacturing the skin of wind turbine blades, at least two issues makes them different from common electrical insulation. First of all the manufacturing processes as a consequence of the size of blades results in a large amount of air filled cavities compared to what is accepted in solid high voltage insulation. Secondly the electrical stress across the laminate is applied by the presence of surface charges and streamer formations of different potentials.

For this reason a new test method for determining the electrical breakdown strength of composites was developed, ensuring the stress of a well defined volume by surface discharges, section 5.2.3. The test method was investigated by means of numerical modelling, simple experiments on various materials and UV photography, all pointing at the same evaluation that the test method is very suitable for testing inhomogeneous materials.

The developed test method was used extensively in most of the experimental work and performed consistently and reliably at all time. Due to the size and simplicity of the test specimens, the test method enabled numerous tests on both prefabricated specimens as well as samples cut from actual blades.

Only one thing remained unsolved, namely the possible polarity effect as discussed in section 5.3.4. By establishing a correlation with the tracking results, it was discovered that the breakdown field strength at positive polarity apparently was less dependant on the thickness of the specimen than the case with negative polarity. Some explanations were suggested by considering the different physical mechanisms of positive vs. negative gas discharges, but the main reason must be found by further research within this area.

Breakdown test methods of inhomogeneous composite materials might become an issue for future standardisation. At that time the specific size and geometry of the ground electrode relative to the degree of inhomogeneity should be discussed thoroughly.

7.2 Tracking tests vs. Breakdown tests

Tracking tests according to IEC Publ. 587 [1] have been performed for several composite materials. Such tests are described in section 5.1 for materials having polyester or epoxy based resins with both coated and uncoated surfaces. In section 5.3 the tracking resistance and breakdown field strength for seventeen different uncoated specimens are conducted. The tracking index is obtained according to IEC Publ. 587, whereas the breakdown strength is measured using the new test setup commented in section 5.2.3.

The aim for the investigations in section 5.3 was to correlate the tracking results with the breakdown field strengths for composite materials, so that the valuable results from an expensive test of the breakdown field strength of a certain material could be obtained by measuring the tracking index using the simple test setup in IEC Publ. 587.

Based on general results and tendencies gained from both test methods in section 5.1 and section 5.2, a very fine correlation was obtained. Equation (5.1) shown below enables a calculation of the breakdown field strength (E_b) by only knowing the thickness of the specimen (d) and the tracking index (TI).

$$E_b = TI \cdot c_1 + {c_2}/{d}$$

The values of constants c_1 and c_2 are found for the seventeen specimens by the least square method and are given in Table 7.1.

Table 7.1 Values of c_1 and c_2 in (5.1).

Constant	Positive polarity	Negative polarity
c_1	3.98	-1.49
c_2	58.47	-81.39

Specimens treated with surface coating are not considered, since coating changes the tracking resistance as found in section 5.1 but leaves the breakdown field strength more or less unaffected, section 5.2.

No definite explanation of the correlation is given. This must rely on future investigation of breakdown mechanisms of composite materials, surface properties vs. the bulk material properties and special issues considering the new test method for determining breakdown field strengths.

7.3 Full scale attachment test method

Once a blade has been designed according to all the mechanical and lightning related requirements, a test method aiming at verifying the interaction of blade design and lightning protection is suggested. As discussed in Chapter 6 such a full scale test method should not distinguish between different designs using wood, foam, GFRP or CFC, but merely evaluate whether the selected design will perform satisfactorily in a true lightning environment.

A test method aiming at predicting the consequence of having a direct lightning strike to a structure must consist of two parts. First the possible lightning attachment points are determined by a high voltage test, whereafter a simulated lightning current is driven through the attachment point towards the ground connection, in this case the termination of the down conductor in the far tip end.

Based on the initial leader attachment test described in SAE ARP 5416 [77] a test method using sections of true blade tips with an overall length of 6m has been investigated. The size is selected as a consequence of the tip being the most exposed part of the blade. Investigations of lightning attachments on a large number of newer wind turbine blades revealed that more than 88% of all strikes occurred to the outermost 1m of the tip, Figure 6.1. Furthermore the size of the test specimens and the simplicity of the test method enable the tests to be carried out in a large range of laboratories world wide.

The locations of lightning attachments found with the tip tests was compared to locations of actual lightning strikes on similar blades. A good agreement was achieved making the test method very suitable in both the design phase of new blades and as a verification of where lightning discharges will attach in the tip area.

Hopefully such a test method will be adopted by the relevant standardisation committees, forcing all blade manufacturers to consider the threat of lightning discharges equally.

7.4 Numerical modelling

Numerical modelling has been used several times during the thesis. In the early design phase of a wind turbine blade, numerical modelling can be used to predict certain material behaviour like electric field enhancement around metallic components in the blade, skin effect of various conductor geometries and the current distribution of anisotropic materials like CFC, among others.

Lightning physicists have established algorithms based on 3D static electric field calculations predicting the risk of lightning attachments to various points of a certain structure. In section 3.3 such models are implemented on both a single wind turbine as well as an entire wind farm. Although the model is at its early stage the applicability is very wide due to its flexibility, considering the simple 3D FEM calculations. Such models are constant evolving and once they are extended to cover the entire area of a structure like a

wind turbine, they will certainly be a powerful tool in designing lightning protection of the blades and the nacelle etc.

In general, numerical modelling, as used by designers of components within the power industry, is regarded a useful tool for designing lightning protection of wind turbine blades as well.

7.5 IEC pre-standardisation

Many of the test methods discussed in this thesis would be useful in a larger context. The considerations on the new test method for evaluating the breakdown strength could easily form the base for future standardisation.

The full scale test method described in Chapter 6 is considered both as a useful tool in the tip design phase, as well as a means of verifying the interaction of the blade design and the installed lightning protection. Since lightning damages have become an increasing issue, it is strongly suggested to begin incorporating such a test method in future test standards of wind turbine blades.

7.6 Future work

During the research which has led to the present thesis, several issues of great importance have turned up.

Since the vast majority of lightning discharges to wind turbine blades occur in the tip region, special focus on the tip design is required. Numerical models of electric fields and streamer formation on the exterior and the interior of the blade tip must be correlated with initial leader attachment tests for various tip designs. The documentation of such tests should be done using UV sensitive cameras, revealing discharge phenomena on areas not visible by means of conventional photography. Design of the air termination will probably be an issue closely linked to the tip design itself. This calls for a fundamental understanding of the interaction between the receptor geometry and material on one hand and the entire tip design on the other. In connection to this, the down conductor and possible junctions on the current path towards ground should be considered as well.

Propagation properties of discharges in air and along insulating surfaces should be investigated to ensure a tip design favoring the receptor as the primary source for initial corona, streamer formation and the transition into a stable leader. The intentions are not to describe or investigate so called ESE-devices (Early Streamer Emission), but to develop a tip where the lightning discharge will most certainly attach to the intended air termination. Such investigations, where velocities of different discharge phenomena interacts, can be investigated by means of high voltage tests and ultra high speed cameras, so called streak cameras.

The numerical methods for calculating possible lightning attachment points presented in section 3.3 should be investigated further. Since these models are constantly developing, as discussed in section 7.4, the implementation of the models on wind turbines will eventually give results with a reasonable accuracy. Parallel to the theoretical developing of such methods, high voltage tests on scale models should be conducted in the laboratory. By investigating the discharge attachment points on scale models of wind turbines, a correlation with the computations can be established. As long as these methods and algo-

rithms are implemented at a practical engineering level, the industry will certainly benefit from such lightning research.

As discussed above, several of the developed test methods are suitable for further work within the standardisation committees. Once experience with these test methods concerning both the electrical breakdown strength of quadratic shaped composite specimens and the full scale tip tests has been gained in other laboratories, the incorporation of such test methods in existing or future standards can be initiated.

Chapter 8

Recommendations

The following chapter is intended to sum up the findings in this thesis and recommend tools and methods useful in designing new blades. Hopefully the recommendations can be part of a checklist during the blade design to ensure that all precautions against fatal lightning damages have been taken.

8.1 General principle

The main issue in designing blades with respect to lightning protection is to accept that they are composite structures occasionally located in a very strong electric field. This implies that a wind turbine blade must be regarded as a high voltage component as well as a mechanical structure. The blade design must reflect not only the mechanical engineer's approach of optimising strength and aerodynamics, but also the lightning engineer's effort in ensuring an unambiguous lightning attachment to the protection system and a safe conduction of the lightning current towards ground.

To succeed in this quest it is very important that the lightning protection is a natural part of the blade design, so that solutions affecting the material selection and blade geometry are decided in agreement with the mechanical requirements. The lightning protection will not perform satisfactorily if it is installed as an add-on to an otherwise finished blade.

8.2 Composite material properties

Composite materials in wind turbine blades differ quite a lot from the materials used for solid high voltage insulation. The processes in blade manufacturing are optimised with respect to the mechanical application and are defined and limited by the size of blades and competition on the blade market. The result is a blade that performs very well aerodynamically but could be further optimised with respect to the interaction with the lightning environment.

At certain regions of the blade; the tip, in proximity of receptors, around junctions on the down conductor etc., it is very important to consider the electrical aspects of the composite materials as well.

8.2.1 Surface properties

Surface properties have been characterised by means of tracking tests according to IEC Publ. 587 (section 5.1), and a test considering surface flashovers (section 5.4).

Based on results from the tracking tests, it is recommended to ensure homogeneous and smooth surfaces minimising the possibility of having minor defects participating in field enhancement and following tracking erosion. The presence of dirt and other particles

can be minimised by optimising the hydrophobicity of the surface. In the case of uncoated composites it is important to avoid the possibility of discontinuities where fibre bundles of different characteristics meet. In general, mechanical discontinuities oppose a risk of creating micro cracks and other deformations in the surface where moist and dirt can attach more easily.

It was found that the fibre orientation affected the tracking resistance considerably. If the direction of the electric field is known, it is recommended to orient the uppermost layer of fibres perpendicular to the field direction. In case of the skin on wind turbine blades where the field direction is not consistent, the recommendation must be to have a fibre cloth with randomly oriented fibres closest to the surface. With respect to the recommendations of smooth surfaces, this cloth should be covered by a thin layer of resin. Finally, a comparison between epoxy and polyester based resins showed that composites using polyester failed at much lower voltages and also resulted in the most severe damages. Therefore, considering surface properties, it is recommended to use an epoxy based resin.

Based on experiences from the tests considering surface flashovers in section 5.4, the recommendation is to improve the hydrophobic properties of the surface. By maximising the hydrophobicity of the surface, water tends to appear as discrete drops and thereby guide the discharge easily across the surface similar to the functioning of diverter strips. A hydrophobic surface in connection with a lightning receptor cannot be regarded as a sufficient solution to ensure correct lightning attachment, but since it does not affect the mechanical properties and is in good agreement with the results considering tracking, it is still suggested as an advantage.

8.2.2 Volume properties

Breakdown tests have been performed in several cases during the thesis.

The initial experiments in section 5.2.2 revealed that the composite materials were governed by a volume effect. The presence of air filled cavities increased the probability of satisfying failure conditions for thicker specimens compared to thinner specimens. This was seen as a decrease in the electrical breakdown strength when the thickness of specimens was increased. Comparing different thicknesses of coating showed that the electrical breakdown strength of the overall composite was not dependant on the coating thickness, maybe due to the porosity of the coating itself. Although the air content is a difficult parameter to vary due to the manufacturing processes, it is still recommended to minimise the air content as the primary way of increasing the electrical breakdown strength of the laminate.

Considering the importance of mechanical aging, breakdown tests on specimens aged at different levels were conducted in section 5.2.4. Within the realistic range of aging as experienced by a blade in service for twenty years, there were no considerable changes in breakdown strengths. However there was a faint tendency for the area of delamination in the puncture to increase with the level of aging, but no definite conclusions could be drawn. This effect, which would clearly be a degradation of the laminate although the electric breakdown field strength remains the same, should be investigated further in a high current test.

A third test series investigating the importance of sizing and air content was performed in section 5.2.5. By testing several combinations of good and poor sizing and high and low air content, it could be concluded that the sizing does not have a considerable effect on the electrical breakdown strength, and that the volume effect was still present although to a smaller extent. Based on these results it is recommended to use the most suitable sizing from a mechanically point of view, and still minimise the air content.

8.3 Blade design

The most important recommendation concerning blade construction is to integrate the lightning protection as a natural part of the blade design. All aspects considering selection and optimisation of materials and design of lightning receptors and down conductors must be coordinated with the mechanical designers of the blade.

8.3.1 Down conductor

Before a lightning discharge has attached to the blade, the down conductor is equally visible to the electric field as the intended receptors. The only way of exposing the receptors more than the rest of the conductive components in the blade is to delay discharges from these areas compared to discharges from the receptors themselves. If successful, discharges from the receptors will extend further into the gap between the charge region in the lighting leader and the blade, resulting in a lightning attachment to the receptor. The apparent solution is to cover up all metallic components except the receptor in insulating materials, for instance by using an unshielded high voltage cable as down conductor instead of a bare stranded conductor.

Once the lightning discharge has attached to the receptor, the lightning current has to pass safely along the down conductor towards the root end of the blade. Here the inductance of the conductor becomes important, since the transient current could introduce an inductive voltage drop of several kV/m along the length of the conductor. By minimising the inductance of down conductors, the probability of side flashes and alternative current paths are minimised.

If the down conductor for a specific blade design is made as a metallic mesh on the surface, or similar, it is expected that the field enhancement along edges of such meshes will increase the risk of lightning attachments to these areas. It is therefore advised to consider the field enhancements along sharp geometries when designing the down conductor as commented in section 5.2.2.

8.3.2 Attachment point

As commented above, it is very important that the receptor appears as the most exposed attachment point for the lightning discharge. In reality, this means that the receptor has to emit stable leaders before any other part of the blade, so that leaders originating at receptors extend furthest towards the charged regions in the lightning leader.

This might be achieved by encapsulating all conductive parts in the blade and only leaving the receptors uncovered. In this sense even a thin layer of paint on the receptor might impede the streamer and leader initiation. Once a suitable design has been made, initial leader attachment tests, as described in 6.1, should be performed, using UV sensitive cameras to evaluate the discharge pattern. Numerical simulations of streamer propa-

gation around the receptors could also determine critical issues of otherwise sensible designs.

8.4 Numerical modelling

Numerical modelling based on FEM calculations is a valuable tool in many situations. In this thesis it has been used to perform simple field calculations explaining phenomena observed at the different test methods and illustrate important issues of especially anisotropic materials. Furthermore possible lightning attachment points on a single wind turbine, as well as on an entire wind farm, have been computed using theoretical algorithms of leader inception and 3D models of the various structures.

FEM modelling is used widely within the design of high voltage components and it is indeed recommended to use such tools in the selection of materials and in designing of lightning protection of wind turbine blades.

8.5 Test methods

In the selection and designing of new material compositions for wind turbine blades, laboratory testing is an important part. Many theoretical considerations can qualify or disqualify a certain material, but only in a laboratory test (or in the final application) will the issues arisen as a combination of material selection and construction geometry be revealed. The breakdown test method presented in this thesis is considered a good suggestion on how to evaluate the electrical breakdown strength of composite materials. Likewise, the tracking tests according to IEC Publ. 587 give important information on various surface properties of coatings etc.

Full scale test methods are treated in Chapter 6 and are recommended as part of the design phase of the blade tip as well as a verification of the final product. By performing these initial leader attachment tests and being capable of changing certain compositions within the tip design, the test is suitable as a design tool to consider lightning attachment. Besides blade tips, the test method is also applicable to other structures located in a zone where direct lightning attachment is possible, like the nacelle fx.

Full scale initial leader attachment tests might be incorporated as part of a test standard for wind turbine blades. Together with a high current test, as described in Chapter 6, it forms a reasonable foundation for evaluation of the efficiency of the installed lightning protection.

Conclusion

The present research has been financed by the Danish PSO-F&U funding with *Energinet.dk* as responsible administrator. During the work, numerous tests in the laboratory have supported the theoretical considerations. In association with this the delivery of test specimens and discussions regarding test methods with the Danish manufacturers have been widely appreciated.

General lightning theory has been presented, as well as the interaction with wind turbine blades. Calculation of attachment points and physics concerning attachment processes are explained and these led to some theoretical guidelines considering the materials used for blade production. To characterise the composite materials used for blade manufacture, several test methods are used. Some of them are standardised tests, where others have been developed for the purpose but are based on procedures and principles described in established test standards.

Tracking tests according to IEC Publ. 587 [1] have been performed on various GFRP specimens made by different blade manufacturers. The specimens were based on either an epoxy or a polyester resin and were either uncoated or coated with the paint and primer used in blade manufacture. The test methods showed very consistent results and led to the following recommendations to improve the tracking resistance:

- Ensure homogeneous and smooth surfaces.
- Avoid fibres parallel to the field direction or make the uppermost layer as a felt structure with randomly oriented fibres in case the field direction is unknown.
- Cover the composite with a thin layer of resin, so that fibres in the uppermost layer are avoided.
- Considering tracking resistance, it is recommended to use an epoxy based resin instead of a polyester based resin if possible.

Breakdown tests were performed in two different steps. Initially a test method using rectangular specimens with the ground electrode cast into the laminate was used whereafter a new test method with smaller quadratic test specimens and a larger test volume was investigated. The new test setup enabled tests of prefabricated specimens as well as specimens cut from blades in service and stressed the laminate with surface discharges on a well defined area. The tests were carried out on a large variety of test specimens, where parameters such as laminate thickness, coating thickness, air content, sizing quality, mechanical aging and special additives were considered. The results revealed the following:

- The composite materials exhibit a pronounced volume effect, so that the breakdown voltage of a certain specimen does not necessarily increase by increasing the thickness of the specimen. In connection to this it is important to minimise the amount of air and other impurities within the bulk material.
- The breakdown strength is not dependant on the thickness of currently used coating and primer. If the breakdown strength should be increased by applying a layer of paint or resin on the surface, new coating materials should be investigated.

- Mechanical aging did no show any change of the electrical breakdown strength within an aging level corresponding to 20 years of service.
- The breakdown strength is unaffected by the use of different sizing systems, so that the selection of sizing should depend on the most mechanically suitable solution.

By comparing results from the breakdown tests with measured tracking resistances of similar specimens, a very fine correlation was found. The formula enabled a calculation of the breakdown strength based only on the tracking index and the thickness of the specimen. These formulas enable manufacturers to perform simple tracking tests on a large range of different materials, saving the cost of the more complex breakdown tests. When a few materials have been selected based on the tracking tests and the calculated breakdown field strengths, the results can be verified by means of performing the actual and thus more reliable breakdown tests.

Full scale tests were conducted on six different blade tips to investigate the possibility of a test method to verify the overall performance of the interaction between material selection, blade design and the installed lightning protection. The initial leader attachment tests on these blade tips with an overall length of 6m (3m tips with additional 3m beams extending) showed a good correlation between the discharge pattern on blades in service and the discharges seen in the laboratory. The test method is very valuable when developing tip design and special receptor configurations, and due to the size of the test specimen the tests are easily performed in a large range of high voltage laboratories world wide. The test method is not linked to any specific type of blade, why it is useful for comparing different solutions containing CFC, GFRP or both. Hopefully such a test method will be incorporated in future test standards, so that manufacturers, owners and insurance companies have a common reference document considering lightning protection of blades.

Numerical modelling is used several in places in the thesis to characterise material properties, support theoretical considerations or explain test results, and is regarded a powerful tool in this application. Lately, models of lightning discharges describing the probability for a tall structure to launch a stable upward oriented leader have been published. The method is based on a 3D electrostatic FEM calculation and is easily performed in a FEM program on a modern desktop computer. Examples of such calculations on both a single turbine and an entire wind farm are shown.

References

[1] "IEC Publ. 587 Test methods for evaluating resistance to tracking and erosion of electrical insulating materials used under severe ambient conditions", IEC, second edition, 1984

[2] "Kapitler af vindkraftens historie i Danmark", Elmuseet, Poul La Cour Museet, Nordisk Folkecenter for Vedvarende Energi, Danmarks Vindkrafthistoriske Samling, December 2004 (Danish)

[3] "REpower 5M", description of Repower 5M wind turbine at www.repower5m.de (*)

[4] "Rekommandation 25 - Lynbeskyttelse af vindmøller", DEFU, first edition, January 1999 (Danish)

[5] "IEC TR 61400-24 Wind turbine generator systems – Part 24: Lightning Protection", IEC, first edition, June 2002

[6] Quisman, S. and M. Steen-Andersen, "Lynbeskyttelse af Vindmøller – en materiale undersøgelse af glasfiberforstærket polyester", Technical University of Denmark – Oersted-DTU, Electric Power Engineering, Master thesis 2003, (Danish)

[7] "British Wind Energy Association", list of offshore wind projects at http://www.bwea.com/offshore/worldwide.html (*)

[8] "Horns Reef", description of the Horns Reef project at http://www.hornsrev.dk/Engelsk/default_ie.htm (*)

[9] Fisher, F.A., J.A. Plumer and R.A. Perala, "Lightning protection of Aircraft", Lightning Technologies Inc., second edition, 1999

[10] Presentation by Elsam Engineering at Copenhagen Offshore Wind Conference, 26.-28. October 2005

[11] "Enercon GmbH", description of the Energon E-112 wind turbine at www.enercon.de (*)

[12] "Harakosan Europe BV", description of the Z72 wind turbine at www.harakosan.nl (*)

[13] "Vestas Wind Systems A/S", description of the V90 wind turbine at www.vestas.com (*)

[14] "Nordex N80 – technical description", description of the Nordex N80 wind turbine at www.nordex-online.com (*)

[15] "LM Glasfiber A/S", description of the LM 61.5 P at www.lmglasfiber.com (*)

[16] "Siemens Wind Power", description of the integral blade technology at www.powergeneration.siemens.com/en/windpower (*)

[17] Repower, www.repower.de

[18] WinWind Oy, www.winwind.fi

[19] Danish Wind Industry Association, www.windpower.org

[20] Madsen, S.F., "Calculated temperature rise and thermal elongation of structural components, depending on action integral of the injected lightning currents", Proceedings of the International Conference on Lightning and Static Electricity, Seattle Washington, USA, September 2005

[21] Triplett, T.E., "Lightning Strike Protection Concepts for Composite Materials", 34th International SAMPE Symposium, May 8-11 1989

[22] Drumm, F., G. Bäuml, W.J. Zischank, R. Brocke and J Schönau, "Behaviour of protected composite materials exposed to lightning impulse and continuing currents", Proceeding of the 24th International Conference on Lightning Protection, Birmingham, UK, 1998

[23] Brocke, R., J. Schönau, W.J. Zischank and G. Bäuml, "The stress caused to mesh protected composite materials at the attachment point of lightning arcs", Proceedings of the 25th International Conference on Lightning Protection, Rhodes, Greece, 2000

[24] Jomitek ApS, www.jomitek.dk (*)

[25] Uman, M.A., "The Lightning Discharge", Dover Publications Inc., second edition, 2001

[26] Chang, J.S., T.G. Beuthe, C.G. Hu, G. Stamoulis and W. Janischiewskyj, "Thundercloud Electric Field Measurement in the 553-m CN Tower During 1978-1983", Journal of Geophysical Research, Vol. 90, NO. D4, Pages 6087-6090, June 1985

[27] Kuffel, E., W.S. Zaengl and J. Kuffel, "High Voltage Engineering Fundamentals", Butterworth-Heinemann, second edition, 2000

[28] Aleksandrov, N.L., E.M. Bazelyan, "Ionization processes in spark discharge plasmas", Plasma Sources Sci. Technol. 8, 285-294, UK, 1999

[29] Allen, N.L. and P.N. Mikropoulos, "Streamer Propagation along Insulating Surfaces", IEEE Transaction on Dielectrics and Electrical Insulation Vol. 6 No. 3, 357-362, June 1999

[30] Gao, L., "Characteristics of Streamer Discharges in Air and along Insulating Surfaces", Institute of High Voltage Research, Uppsala University, Sweden, PhD thesis 2000

[31] Wagner, C.F. and A.R. Hileman, "The Lightning Stroke-II", AIEE-Transaction on Power Apparatus and Systems, vol. 80 issue 56, pp. 622-642, 1961

[32] "IEC 62305 -1 Ed. 1.0: Protection against lightning – Part 1: General principles", IEC, first edition, January 2006

[33] "IEC 1024-1-1 Protection of structures against lightning – Part 1-1: General principles– Section 1: Guide A – Selection of protection levels for lightning protection systems", IEC, first edition, August 1993

[34] "SAE ARP 5412, Eurocae ED-84, Aircraft Lightning Environment and Related Test Waveforms", Eurocae, July 1997

[35] Larsen, F.M and T. Sorensen, "New lightning qualification test procedure for large wind turbine blades", Proceedings of International Conference on Lightning and Static Electricity, Blackpool, UK, 2003

[36] Bouquegneau, C., "A Critical View on the Lightning Protection International Standard", Proceedings of the 27th International Conference on Lightning Protection, Avignon, France, 2004

[37] Salo, G. and E. Rupke, "RSPHERE, A numerical code for predicting the lightning attachments based on the Rolling Sphere Method", Proceedings of International Conference on Lightning and Static Electricity, Blackpool, UK, 2003

[38] Becerra, M. and V. Cooray, "A simplified model to represent the inception of upward leaders from grounded structures under the influence of lightning stepped leaders", Proceedings of the International Conference on Lightning and Static Electricity, Seattle Washington, USA, September 2005

[39] Becerra, M., V. Cooray and H.Z. Abidin, "Location of the vulnerable points to be struck by lightning in complex structures", Proceedings of the International Conference on Lightning and Static Electricity, Seattle Washington, USA, September 2005

[40] Becerra, M., E-mail correspondence with Mr. M. Becerra at Division for Electricity and Lightning Research, Uppsala University, Uppsala, Sweden, January 2006

[41] NetComposites, Tapton Park Innovation Centre, Brimington Road, Chesterfield S41 0TZ, UK, "Guide to composites" at www.netcomposites.com/Education.asp

[42] Bjært, N., Oral conversation with Mr. N. Bjaert at Fiberline Composites A/S, www.fiberline.com

[43] Ashby, Michael F. and David R.H. Jones, "Engineering Materials 1 – An introduction to their properties and applications", Butterworth Heinemann, second edition, 1996

[44] "IEC 1109 Composite insulators for a.c. overhead lines with a nominal voltage greater than 1000 V – Definitions, test methods and acceptance criteria", IEC, first edition, March 1992

[45] "Airbus", short description of the A380 Triple deck cargo hauler, http://www.airbus.com/en/aircraftfamilies/a380/freight.html (*)

[46] Schneider, L., Keynote address at the International Conference on Lightning and Static Electricity, Seattle Washington, USA, September 2005

[47] Cheng, D.K., "Fundamentals of Engineering Electromagnetics", Addison –Wesley, 1994

[48] Saint-Gobain Vetrotex datasheet, "E, R and D glass properties", 2002

[49] Henk, P.O., "Electrical Engineering Materials", DTU Technical University of Denmark, Department of Electric Power Engineering, third edition, 1997

[50] McAllister, I.W. and G.C. Crichton, "Electric Fields and Electrical Insulation", The Technical University of Denmark, Institut for Elteknik, 2000

[51] Balslev, N., "Elektroteknisk materialelære", Akademisk Forlag, 3. edition, 1979 (Danish)

[52] Fischer, F.A., "Mechanism of breakdown of long air gaps", Lightning Technologies Inc., September 1991

[53] Dissado, L.A. and J.C. Fothergill, "Electrical Degradation and Breakdown in Polymers", The Redwood Press, 1992

[54] Beisele, C. and B. Kultzow, "Experience with New Hydrophobic Cycloaliphatic Epoxy Outdoor Insulation Systems", IEEE Electrical Insulation Magazine, July/August 2001 – Vol. 17, No. 4.

[55] CIGRÉ, "Material properties for non-ceramic outdoor insulation, state of the art – Definition of physical parameters important for polymeric materials applied in outdoor insulation", A report from WG D1.14, August 2004

[56] Engel, R, and S. Will, "ADSS Cables with Extended Operating Lifetime", 51st seminar IWCS Coronado Springs, Florida, USA, November 2002

[57] "IEC 61302 Electrical insulating materials - Method to evaluate the resistance to tracking and erosion - Rotating wheel dip test", IEC, first edition, 1995

[58] "IEC 60112 Method for the determination of the proof and the comparative tracking indices of solid insulating materials", IEC, fourth edition, January 2003

[59] "IEC 60060-1 High-voltage test techniques, Part 1: General definitions and test requirements", IEC, second edition, November 1989

[60] "IEC 60243-1 Electrical strength of insulating materials - Test methods Part 1. Tests at power frequencies", IEC, second edition, January 1998

[61] "IEC 60243-2 Methods of test for electric strength of solid insulating materials Part 2. Additional requirements for tests using direct voltage", IEC, first edition, February 1990

[62] "IEC 60243-3 Methods of test for electric strength of solid insulating materials Part 3. Additional requirements for impulse tests", IEC, first edition, September 1993

[63] "IEC 61621, Dry, solid insulating materials - Resistance test to high-voltage, low-current arc discharges", IEC, first edition, 1997

[64] "IEC TR 62039 Polymeric materials for outdoor use under HV stress", IEC Committee draft (CD), October 2004

[65] "IEC 60507 Artificial pollution tests on high-voltage insulators to be used on a.c. systems", IEC, second edition, April 1991

[66] Lenning, F.E., "Analysis of lightning current flow in anisotropic CFRP using finite difference methods", Proceedings of International Conference on Lightning and Static Electricity, Blackpool, UK, 2003

[67] Eriksson, G. "Simulation of direct lightning thermal damage in fully 3D composite structures", Proceedings of the International Conference on Lightning and Static Electricity, Seattle Washington, USA, September 2005

[68] Comsol Multiphysics 3.2, Modelling Guide, 2005

[69] Steen-Andersen, M., S. Quisman, J. Holboell and M. Henriksen, "GFR-Materials Resistance to Lightning With Respect to Lightning Protection of Windmill Wings", Proceedings of International Conference on Lightning and Static Electricity, Blackpool, UK, 2003

[70] Akyuz, M., "Electrical discharges in air and along insulating surfaces", Institute of High Voltage Research, Uppsala University, Sweden, PhD thesis 1999

[71] Jørgensen, M.O., "Experimental Investigations Regarding the Applicability of Lichtenberg Figures to Voltage Measurements", Danmarks Naturvidenskabelige Samfund, Denmark, 1934 (Danish).

[72] Gallimberti, I., G. Bacchiega, Anne Bondiou-Clergerie and P. Lalande, "Fundamental processes in long air gap discharges", C.R. Physique 3 (2002) 1335-1359

[73] Live, D.R., "Handbook of Chemestry and Physics", CRC Press, 82nd edition 2001-2002

[74] Mikropoulos, P.N. and C.A. Stassinopoulos, "Influence of humidity of the breakdown mechanism of medium length rod-plane gaps stressed by positive impulse voltages", IEE Proc.-Sci. Meas. Technolo., Vol. 141, No. 5, September 1994.

[75] Abdel-Salam, M., P. Weiss and B. Lieske, "Discharges in Air from Point Electrodes in the Presence of Dielectric Plates – Experimental Results", IEEE Transaction on Electrical Insulation, Vol. 27, No. 2, April 1992

[76] "MIL-STD 1757A, Lightning Qualification Test Techniques for Aerospace Vehicles and Hardware", 1983

[77] "SAE ARP 5416, Eurocae ED-105, Aircraft Lightning Test Methods, Section 5", Eurocae, draft version V13, 2004

[78] Hall, A., "Thunderstorm Protection of Aircraft Radomes", Workshop presentation at the International Conference on Lightning and Static Electricity, Seattle Washington, USA, September 2005

[79] Sony datasheet, ICX413AQ Diagonal 28.40mm (Type 1.8) Frame Readout CCD Image Sensor with Square Pixel for Color Cameras, 2003

[80] Jóhannsson, H. and M.P. Rodríguez, "Discharge detector for wind turbines", Technical University of Denmark – Ørsted•DTU, Electric Power Engineering, Course 31775 – Test and measuring techniques, spring 2005

[81] Hamamatsu datasheet, "High Performance UV digital camera C8484-16C", © 2004 Hamamatsu Photonics K.K.

[82] Coastal Optical Systems Inc. datasheet, "UV CoastalOpt™ SLR lens 250nm-650nm", 2005

[83] B+W Filters, "Filter Handbook", Jos. Schneider Optische Werke GmbH, 2005

[84] Larsson, A., A. Bondiou-Clergerie and I. Gallimberti, "Numerical modelling of inhibited electrical discharges in air", J. Phys. D: Appl. Phys. 31 (1998) 1831-1840

[85] Larsson, A, "An experimental study of inhibited electrical discharges in air", J. Phys. D: Appl. Phys. 31 (1998) 1823-1830

[86] "IEC 61024-1-2 Protection of structures against lightning – Part 1-2: General principles – Guide B – Design, installation, maintenance and inspection of lightning protection systems", IEC, first edition, May 1998

[87] "IEC 62073 Guidance on the measurement of wettability of insulator surfaces", IEC, first edition, June 2003

[88] Chiba, M., A. Kumada and K. Hidaka, "Inception voltage of positive streamer and its length on PMMA in air", IEEE Transactions on Dielectrics and Electrical Insulation, Vol. 9, No. 1, February 2002

[89] Badaloni, S. and I. Gallimberti, "Basic data of air discharges", Universita' Di Padova, Instituto Di Elettrotecnica E Di Elektronica, June 1972

(*) Some of the information used in this thesis is acquired on manufacturers or related industry's homepages. For each homepage visited and used as reference, a screen dump of the actual page has been saved as a PDF-file. A copy of the specific references can be acquired by contacting Ørsted•DTU, Electric Power Engineering at The Technical University of Denmark.

Appendix A – Numerical modelling

The following appendix concerns the use of numerical methods to investigate some material properties, besides the methods for calculating lightning attachment points and electric fields at the various test methods as presented in the main thesis. It does not solve any particular task, but is more aimed at showing some examples on how 'Numerical modelling' can be used as a tool in developing blades and down conductors.

In this thesis, the numerical modelling has been performed in the commercially available Comsol Multiphysics 3.2.a environment which solves the differential equations by using the Finite Element Method. Several other programs are available for purely electrostatic applications etc., but since Comsol Multiphysics has a good interface to Matlab, and enables the calculation of coupled partial differential equations (relevant for calculation of thermal heating of a material with temperature dependant resistivity) it was chosen for this project.

This specific software supports 64bit processors, why the computations are done on a desktop computer with an AMD Athlon 64bit processor, 2GB memory and equipped with Microsoft Windows Professional 64bit edition.

Reason for modelling

In the initial design phase where different materials are in question or several blade designs are proposed, valuable information can be gained either in the laboratory by experimental tests, or by performing adequate theoretical modelling. Many issues can be solved by means of analytical mathematics as long as isotropic materials, simple geometries and homogeneous fields are considered. However, in practical engineering most problems are too complex to describe analytically, why numerical modelling like the Finite Element Method plays an important role.

When used correctly FEM calculation is a powerful tool for narrowing in the selections of suitable materials or design solutions, but since the level of detail in these calculations is finite and limited by the present computer capacity, there will always be issues not revealed by simulation. The optimum steps in engineering design are then to perform numerical simulations to a certain level whereafter laboratory testing gives the last details.

Material modelling

FEM modelling enables calculations of complex quantities when materials exhibiting special magnetic or electric properties are considered. Examples of such issues could be the current distribution in anisotropic materials in section 4.7, calculation of inductances for complex geometries (down conductors) and resistive heating in metallic components along the lightning current path.

Inductances of down conductors

When driving a transient current through a conductor, an inductive voltage drop along the conductor will develop. For lightning down conductors as discussed in section 2.4.1.1, the inductances play an important role considering the risk of side flashes during conduction of lightning currents. Different equations have been developed analytically to calculate the inductance per unit length for mainly circular geometries, but if the cross section varies beyond these simple cases numerical methods must be used.

This section presents simple methods to compare the inductance pr. unit length of various geometries using Comsol Multiphysics. Using 2D plane symmetry and the Magnetostatic application mode, the calculations are performed by solving Ampere's law for the area/volume considered [68]. The conductors are placed in a surrounding medium of air and assigned a current perpendicular to the plane. By solving the equations and integrating the magnetic energy density across the entire plane, the inductance is calculated according to the following equation:

$$W_L = \tfrac{1}{2} \cdot L \cdot I^2 \qquad \text{(eq1)}$$

Where 'W_L' is the magnetic energy density, 'L' is the inductance per unit length and 'I' is the current along the conductor. The absolute value depends on the level of detail in the simulation and the size of the considered surrounding area. Hence it is only possible to compare the inductances of different geometries than rely on the accuracy for a certain case.

Table A1 shows the inductances for several different cross sections all normalised to the inductance of a circular conductor. The conductors are all made of copper and have cross sectional areas of 50mm². The data is achieved by integrating across the volume of a cylinder with a radius of 10m surrounding the conductor, Figure A1.

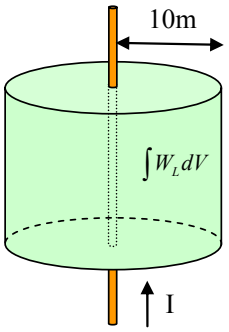

Figure A1 The inductance is calculated by integrating the magnetic energy density across the volume within a cylinder of radius 10m.

Table A1 Comparison of self inductance for various conductor geometries.

Geometry of down conductors	Inductance normalised to the inductance of a circular conductor
Circular conductor, radius 3.99mm	100%
Quadratic conductor, side length 7.07mm	100%
Rectangular conductor, 2.5mm by 20mm	94%
Pipe configuration, outer radius 20mm wall thickness 0.40mm	77%
Four circular conductors placed 20mm apart, the cross sectional area of each conductor is 12.5 mm²	90%

Since the absolute value of the inductances depends somewhat on the integration volume, only a relative comparison is possible.

Resistive heating

In the Comsol Multiphysics environment it is possible to link partial differential equations describing different physical processes. A case where this could be relevant would be the calculation of heating of a metallic conductor due to current passage. The ability of metals to conduct current is defined by their conductivity. Since the conductivity decreases with temperature, and the temperature is a result of ohmic losses by the current passing through the material, the problem constitutes of two coupled nonlinear partial differential equations.

The first equation defines how the heat is generated in a certain volume 'V' and is described by Joules Law. 'P' is the total power converted into heat (W), 'E' is the electric field (V/m) and 'J' is the current density in (A/m^2):

$$P = \int_V E \cdot J \, dv \tag{eq2}$$

By substituting the electric field with the quotient of the current density and the conductivity and integrating over time, the formula for the energy dissipated in a volume 'V' during the time 'T' becomes:

$$Q = \int_T \int_V \frac{1}{\sigma} \cdot J^2 \, dv \, dt \tag{eq3}$$

Since the energy stored as heat in a material is proportional to the mass, the specific heat capacity and the temperature difference, equation (eq3) enables a calculation of the temperature as a function of the conductivity and the current density.

The second equation defines how the conductivity depends on the temperature, where 'ρ_0' is the resistivity at the temperature 'T_0', 'α' is the temperature coefficient of resistivity and 'T' is the current temperature:

$$\sigma_T = \frac{1}{\rho_0 \cdot \left(1 + \alpha \cdot \left(T - T_0\right)\right)} \tag{eq4}$$

Equation (eq4) shows that when the temperature T increases, the conductivity decreases.

In Comsol Multiphysics these two equations can be coupled together to compute the temperature rise of a conductor. First of all the thermal and electrical properties of the material in the model have to be assigned. Secondly it is defined how the temperature depends on the conductivity and the current according to equation (eq3), and how the conductivity depends on the temperature according to equation (eq4).

An example of resistive heating of a busbar according to Figure A2 is considered

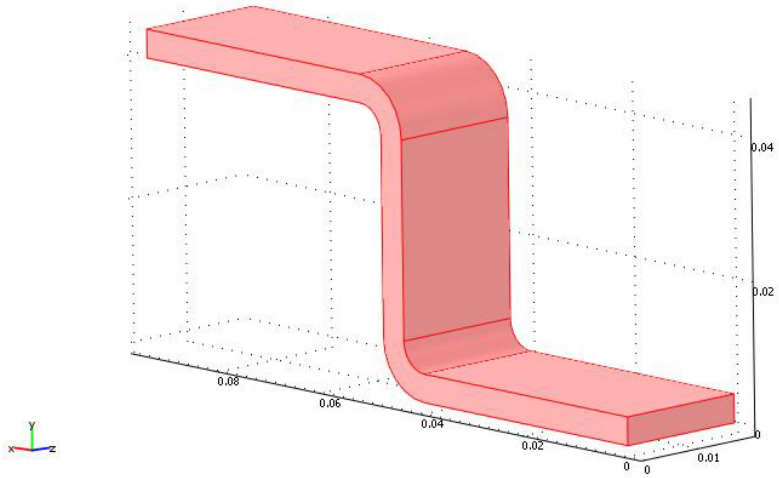

Figure A2 A copper busbar with a cross section of 4mm by 20mm for computation of resistive heating

The busbar is 4mm thick and 20mm wide, and is defined by material properties to represent copper. 30kA is injected in one end of the busbar and conducted to the ground potential at the other end. The remaining boundaries are electrically insulated, such that the only path for the current is through the conductor. The initial temperature of the conductor is 293K, and the simulation is considered adiabatic, such that no heat interaction with the surroundings takes place.

The time dependant equations are solved and the solution of the boundary temperature and the conductivity after 0.5s is plotted on Figure A3 and Figure A4.

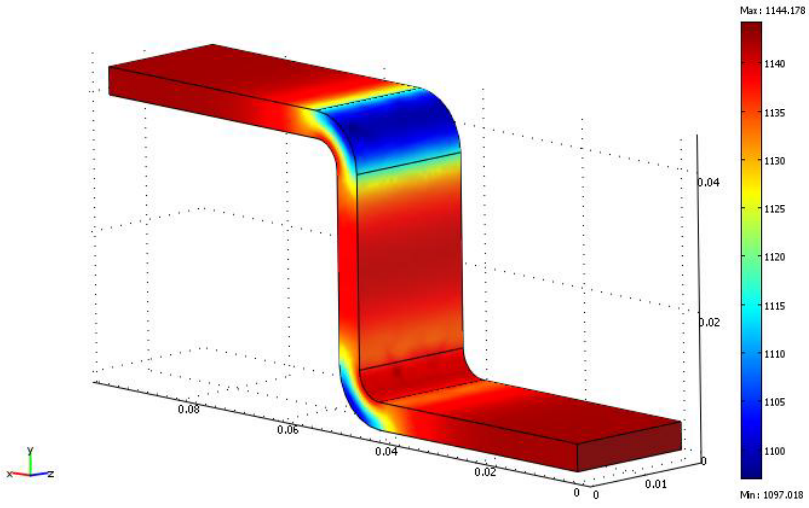

Figure A3 Boundary temperature of copper busbar after passage of 30kA in 0.5s

Since most of the current flows closest to the inner corner of the bendings on the busbar, the temperature is highest at these areas as seen on Figure A3. On Figure A4 the conductivity of the bulk material is plotted. As expected from the temperature plot, the conductivity has changed from the isotropic conductivity at T_0 to a distributed conductivity with a maximum at the outer corners of the bendings where the temperature is lowest.

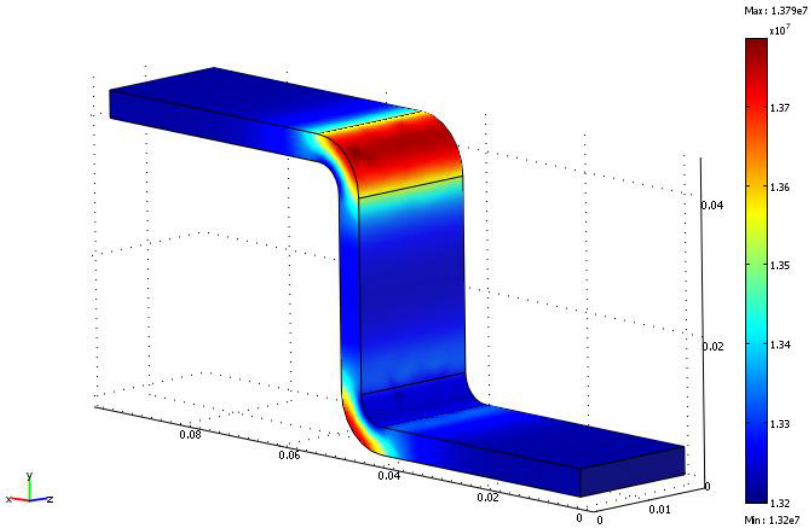

Figure A4 Conductivity of copper busbar after passage of 30kA in 0.5s

The simple case with a regular busbar shows how the different physical disciplines are linked together, and how they are fairly easy to solve using modern numerical methods. If different materials with anisotropic parameters as electrical or thermal conductivity are considered, it is just a matter of defining the subdomain and boundary correspondingly.

In general the ability of linking various physical disciplines makes it possible to perform more accurate simulations than by considering only isotropic materials with constant material parameters.

Appendix B – Issues of scaling

When full scale tests for some reason are impossible to perform, tests on smaller models are sometimes considered. In these cases the scaling of the impacts itself is often an issue of discussion. The problem arises since geometries as length, area and volume are scaled differently while material properties like conductivity or permittivity remains constant.

The following example considers the issues of scaling specific energies when determining resistive heating of a simple conductor.

The resistive heating of a circular conductor with radius 'r_1' and length 'd_1' should be determined when a current pulse with a specific energy of 'AI_1' passes through the conductor. Since the generator at disposal can not deliver such a current pulse, a scale experiment is suggested with a model of the conductor with linear geometries reduced by a factor ten. The reduction affects the geometry in the following way:

Table A2 The scaling of different quantities from full scale to a model experiment.

Parameter	Full scale	Small scale model related to full scale
Radius	r_1	$r_2 = 1/10 \cdot r_1$
Cross sectional area	$A_1 = \pi \cdot r_1^2$	$A_2 = \pi \cdot r_2^2 = \pi \cdot \left(1/10 \cdot r_1\right)^2 = 1/100 \cdot A_1$
Length	d_1	$d_2 = 1/10 \cdot d_1$
Resistance	$R_1 = \rho \cdot \frac{d_1}{A_1}$	$R_2 = \rho \cdot \frac{d_2}{A_2} = \rho \cdot \frac{1/10\, d_1}{1/100\, A_1} = 10 \cdot R_1$
Mass	$m_1 = \pi \cdot r_1^2 \cdot d_1 \cdot \delta$	$m_2 = \pi \cdot r_2^2 \cdot d_2 \cdot \delta = \pi \cdot \left(1/10 \cdot r_1\right)^2 \cdot \left(1/10 \cdot d_1\right) \cdot \delta = 1/1000 \cdot m_1$

Where 'ρ' is the electrical resistivity and δ is the density of the conductor material. If adiabatic conditions are assumed, the equation governing thermal heating of a conductor with a mass 'm', a specific heat capacity 'c_H' and a resistance 'R' as a result of the passage of a transient current with the specific energy 'AI' is written as:

$$AI \cdot R = m \cdot c_H \cdot \Delta T \qquad \text{(eq5)}$$

The full scale model should experience a current pulse with a specific energy of AI_1.

$$AI_1 \cdot R_1 = m_1 \cdot c_H \cdot \Delta T$$

$$AI_1 = \frac{R_1}{m_1} \cdot c_H \cdot \Delta T \qquad \text{(eq6)}$$

In case of the scale model, an action integral of AI_2 is required to heat the sample to the same temperature as in the full scale experiment.

$$
\begin{aligned}
AI_2 \cdot R_2 &= m_2 \cdot c_H \cdot \Delta T \\
AI_2 &= \frac{m_2}{R_2} \cdot c_H \cdot \Delta T \\
AI_2 &= \frac{\left(1/1000 \cdot m_1\right)}{\left(10 \cdot R_1\right)} \cdot c_H \cdot \Delta T \\
AI_2 &= 10^{-4} \cdot AI_1
\end{aligned}
\qquad \text{(eq7)}
$$

As seen from the calculations above the action integral should not just be reduced by the same factor of 10, or even 10^2. The Action Integral must be reduced by a factor of 10^4 in order to measure the same temperature rise as in the case with a full scale test. For this obvious reason it is very important to analyze the values to be scaled thoroughly.

Appendix C – Photographic documentation

The present Appendix aims at listing the hardware used for capturing both visible images of sparks and flashovers as well as images of streamers mainly emitting light in the Ultra Violet range (UV).

Conventional camera

For capturing ordinary images of discharges emitting light visible to the naked eye the Nikon D100 digital camera was used. The user has full control over shutter speed and aperture, and by using a remote air shutter release, the camera can be operated at places that might attain dangerous potentials. The lens used was a Nikon AF Nikkor 28-85mm 1:3.5-4.5, enabling a suitable range of zoom for both close up pictures on small test set-ups, and pictures at longer distances.

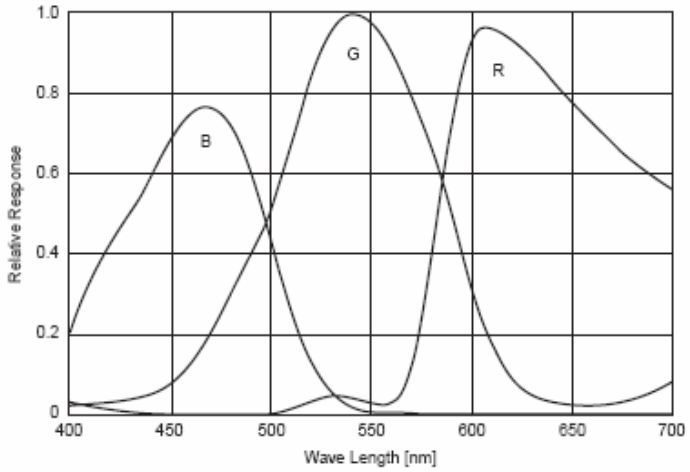

Figure A5 Spectral response of CCD chip in the Nikon D100 digital SLR camera [79].

The spectral response of the 6.1MP CCD chip in the camera shows that the sensitivity is optimised to the human eye, Figure A5. Due to the low sensitivity at wavelengths below 400nm it will not be able to capture images of sources emitting light in the UV range.

UV sensitive camera

Much of the light emitted during pre-discharge phenomena like corona and streamers occurs at wavelengths below what can be detected by the naked eye and conventional cameras. This well known fact was supported by some measurements of the light intensity at various wavelengths for a spark initiated in a small sphere gap [80]. The intensity which was measured with a monochromator and a S8745-01 photo diode is shown on Figure A6, which clearly indicates that as much as 75% of the total emitted energy occurs at wavelengths from 320nm to 380nm.

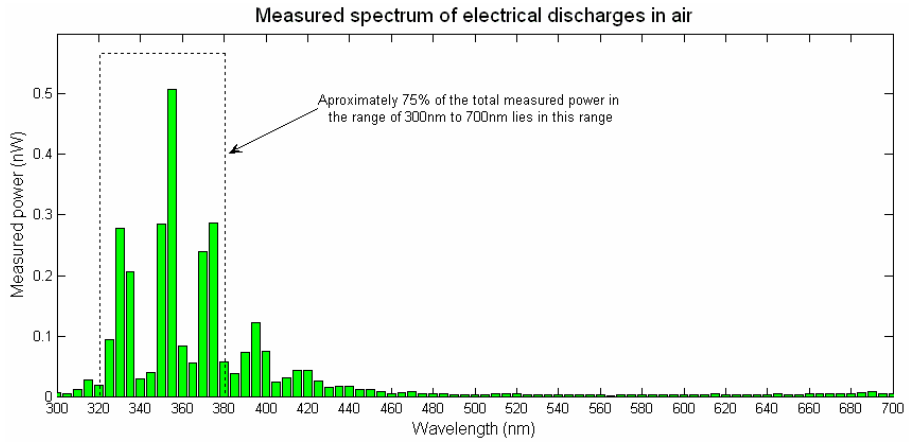

Figure A6 Spectrum of light intensity of a discrete spark in air. 75% of the total measured power emitted lies within the UV range with wavelengths between 320nm and 380nm [80]

Most often images of such incidents are captured using quartz lenses and conventional SLR cameras with UV sensitive films giving pretty good results. However in this thesis it was investigated if similar images could be obtained with digital technology. In spring 2005 the market for capturing and analysing digital UV images was investigated. The aim was to find a user friendly camera with a lens that could also be used for conventional SLR cameras. This search resulted in the following selection of camera, lens and optical filters.

Camera

A Hamamatsu C8484-16C digital camera was chosen for the task. The camera records in 16 bit monochrome with a resolution of 1344x1024 pixels, and is connected directly to a PC via an IEEE-1394 Firewire cable. Everything on the camera is controlled through the installed software and besides taking still images the camera also captures movies of UV incidents. The exposure time can be varied from 0.012ms up to 1s, and a special feature of pixel integration allows a recording where the most intense pixels from each frame within a movie are saved in a single image. This feature is very useful when filming high voltage impulses, since the recording is easily initiated a couple of seconds before the discharge and first terminated when the flashover has occurred.

The spectral response of the camera is shown on Figure A7, and indicates that light with wavelengths down to 200nm can be recorded.

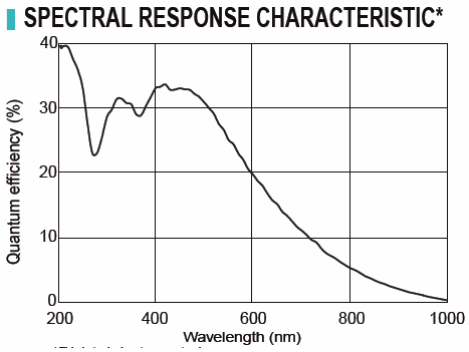

Figure A7 Spectral response of Hamamatsu C8484-16C camera [81]

The camera is equipped with a C-mount lens mount. With a special C-mount to F-mount adapter, conventional Nikon SLR Lenses are easily used with the camera.

Lens

Conventional lenses of silica glass do not allow the passage of UV light, why special lenses of quartz glass must be used. Nikon have previously made a lens for UV purposes, the UV-Nikkor 105mm f/4.5s with a bandwidth of 220nm-900nm, and with the standard Nikon F-mount compatible with all Nikon SLR cameras. Unfortunately Nikon do not produce the lens anymore, and since it has become a collectors item it seemed very difficult to obtain. After some further research it was found that an American company who was specialised in making custom designed lenses made a lens with similar characteristics as the UV-Nikkor 105mm f/4.5s lens.

The CoastalOpt™ SLR Lens from Coastal Optics is colour corrected for 250nm-650nm, has an aperture of 4.5-32 and is equipped with the Nikon F-mount. It has a 52mm filter mount for additional filters such that the spectral response can be adjusted to the specific task. The spectral response of the lens itself is shown on Figure A8

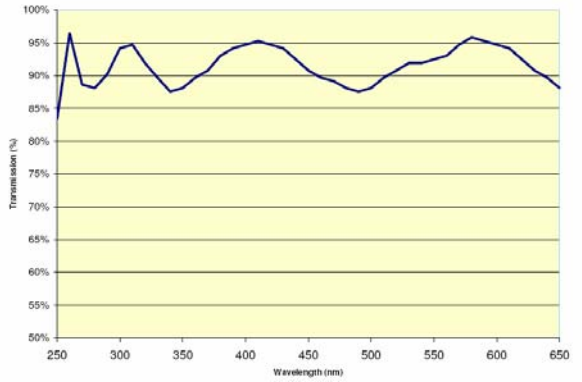

Figure A8 Spectral response of UV CoastalOpt™ SLR Lens from Coastal Optics [82]

Filters

As seen from the two spectral responses of the camera and the lens, they will enable detection of light with wavelengths from the UV region (200nm-250nm) up to near infrared (IR) (above 650nm). When images of flashovers, where both the pre-discharges as corona and streamers as well as the spark in the sense of an arc channel are to be captured, the very bright and energetic spark tends to overexpose the image. For this reason, optical filters are introduced to damp the part of the light outside a certain bandwidth for instance to damp the light within the range visible to the naked eye.

In this case the market was searched for filters that mainly allowed the passage of UV light and damped away both the visible and the infrared light. Several filters from different manufacturers were considered, *Kodak Wratten 18A, Schott UG-11, Hoya U-325C, Hoya U-340* and *Hoya U-330*. Apparently the market for such filters where also pretty limited, since they seemed very difficult to find commercially. Finally a filter from B+W, the *B+W 403 UV* was found and ordered.

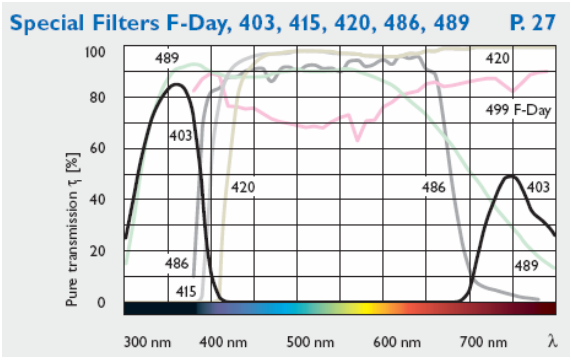

Figure A9 Spectral response of the B+W 403 UV filter shown as the black curve marked '403' [83].

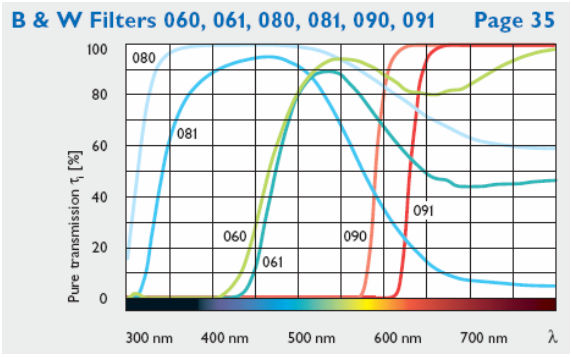

Figure A10 Spectral response of the B+W 081 blue filter shown as the blue curve marked '081' [83].

As seen on the spectral response of the filter, shown as the black curve marked 403 on Figure A9, it allows some passage of UV light between 300nm and 400nm, it blocks out the visible light from app. 400nm up to app. 700nm, and transmits some of the IR light as well. Since this specific task was to record mainly pre-discharge phenomena in the UV range, the IR light from the heating of the arc will probably disturb the images. A blue filter *B+W 081* was selected for filtering out the IR light, Figure A10. Depending on which image to capture, the filters are used separately or together in series.

In general, UV photography using this digital setup seems pretty straight forward and gives good results. The software is user friendly and contains different editing tools both during the record process and once an image is captured. However, the use of both camera settings, aperture on the lens, light settings in the laboratory and the different combinations of the filters, makes the whole task a bit complex.

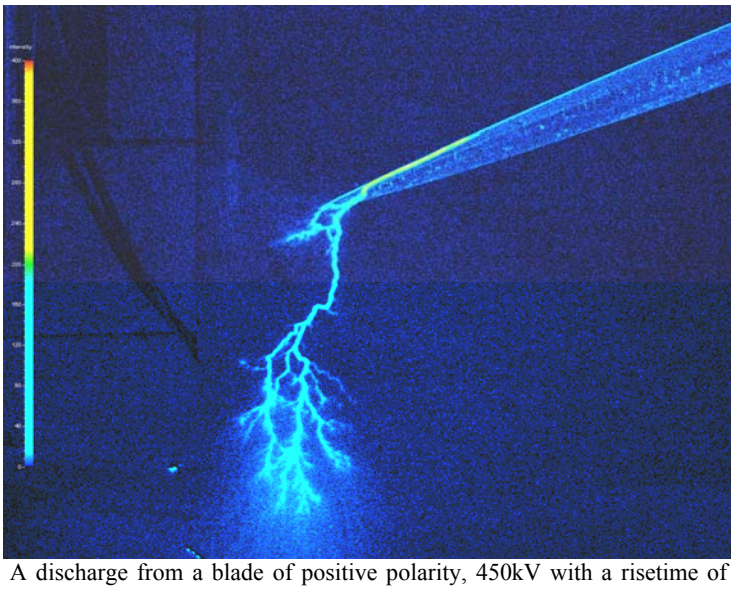

Figure A11 A discharge from a blade of positive polarity, 450kV with a risetime of 100us. The pulse was chopped prior to breakdown in another gap in parallel. Different filtering techniques in the associated software enable pseudo colouring, where individual pixels are coloured according to their intensity.

Series resistance

As mentioned previously the discrete spark in a flashover might overexpose the image such that the pre-discharge phenomena vanish. One suggestion to solve this problem was to use a large series resistance between the front capacitor and the test object.

The idea is that the pre discharge phenomena only draws a limited current such that the voltage drop across the series resistance is neglectable at this early stage. Once the leader has crossed the gap and changes into an arc, the current required for this transition introduces a voltage drop across the series resistance. If the arc exhibit a resistive nature,

and the voltage between the high voltage electrode and the ground plane is limited, then the current and thereby also the light emission from the spark is limited.

In the sense of taking pictures, this procedure works very fine. However, the development of the early discharge pattern might be affected such that the attachment points of the discrete spark might be different for a test without the series resistance. As described in literature [84], the streamer propagation *is not* inhibited, the streamer to leader transition *is* inhibited, and the final jump *is* also inhibited by the large series resistance.

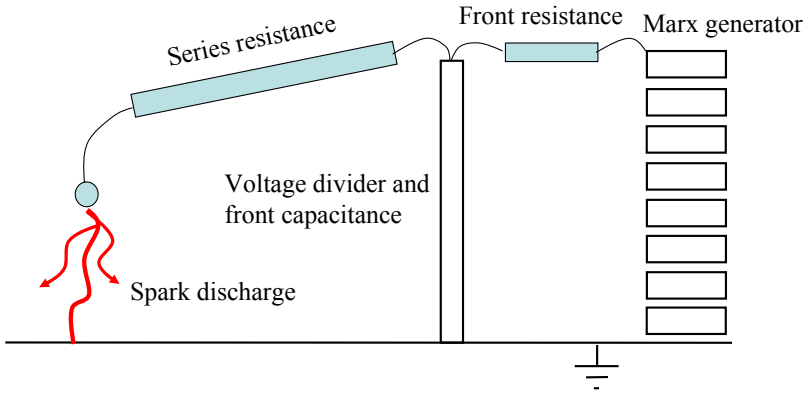

Figure A12 Test setup where a large series resistance limits the current, and hence the light emission in the flash.

Before a large series resistance is incorporated permanently in the initial leader attachment tests, the consequence of changes in the discharge pattern must be investigated thoroughly, [85].

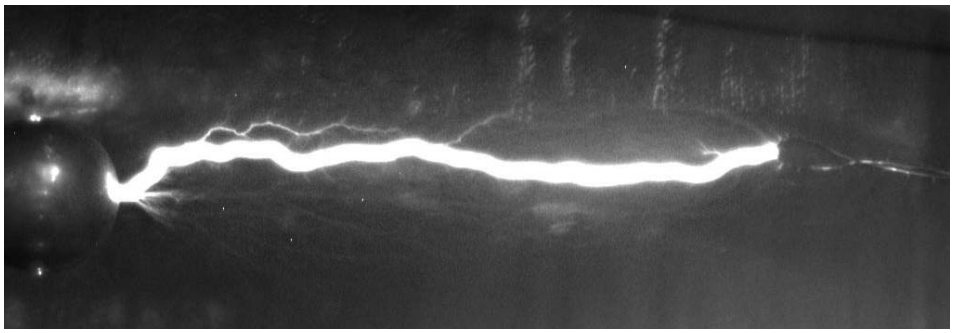

Figure A13 Flashover with a large resistance in series. The rod to the right is energised with app. 275kV, whereas the sphere to the left is grounded. Note that both the spark and streamers are visible.

Appendix D – Test results from section 5.4

The tests described in section 5.4 have been performed on two sets of similar specimens to verify the reproducibility. In each of the following plots, results from the 'surface flashover tests' are shown for the two similar specimens (A1 and A2 or B1 and B2) and for both polarities.

Despite minor deviations, the two sets of identical specimens are seen to behave similarly in all cases.

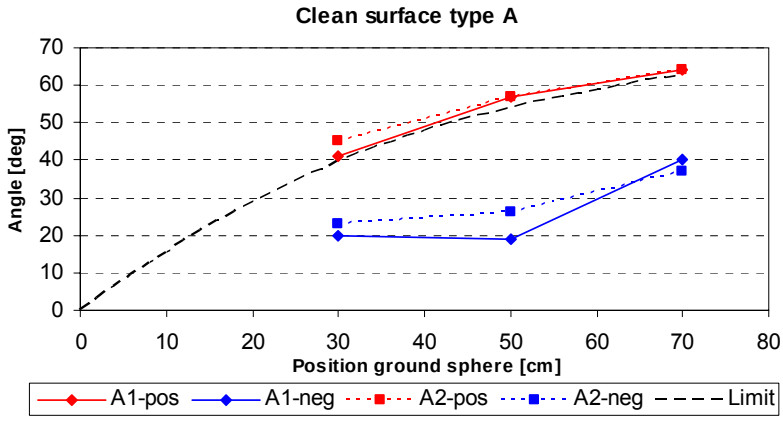

Figure A14 Comparison of data from specimen A1 and A2 considering clean surfaces.

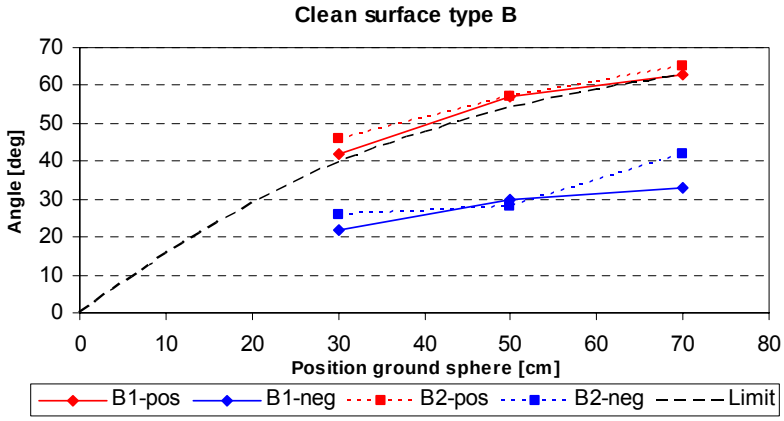

Figure A15 Comparison of data from specimen B1 and B2 considering clean surfaces.

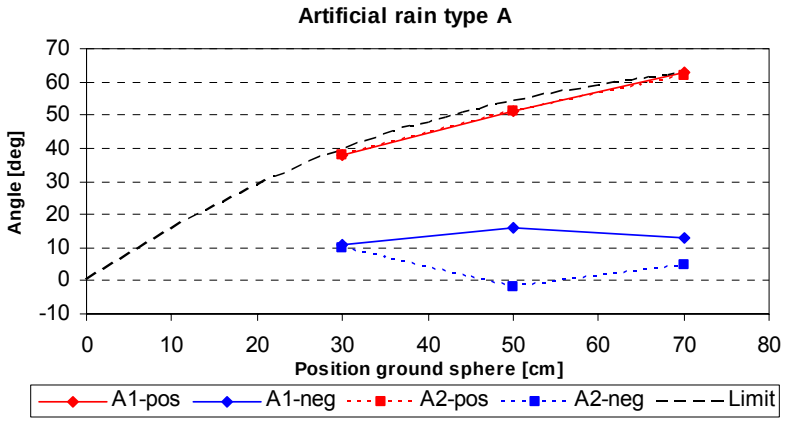

Figure A16 Comparison of data from specimen A1 and A2 considering surfaces polluted with artificial rain.

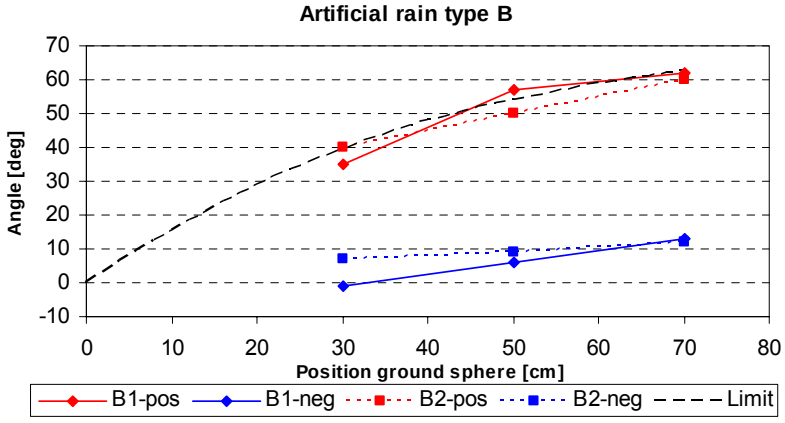

Figure A17 Comparison of data from specimen B1 and B2 considering surfaces polluted with artificial rain.

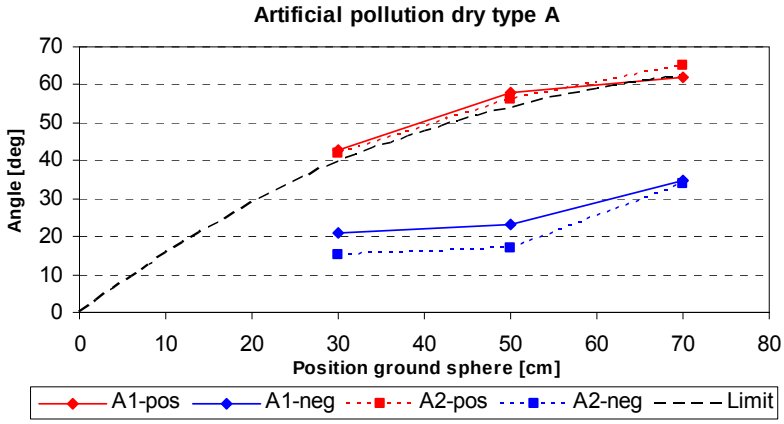

Figure A18 Comparison of data from specimen A1 and A2 considering surfaces where dry artificial pollution has been applied.

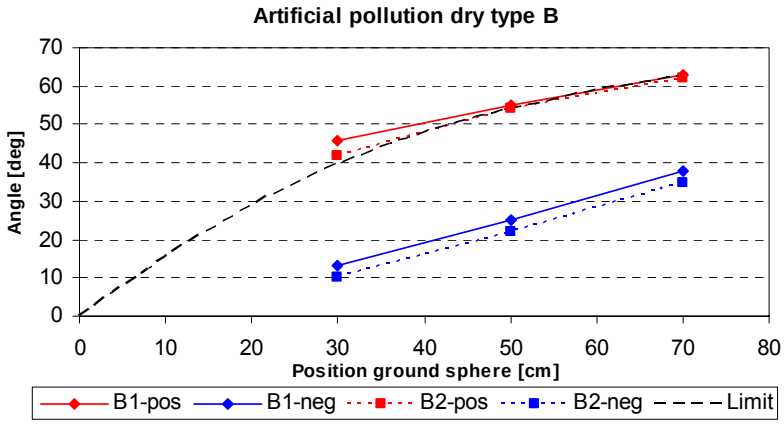

Figure A19 Comparison of data from specimen B1 and B2 considering surfaces where dry artificial pollution has been applied.

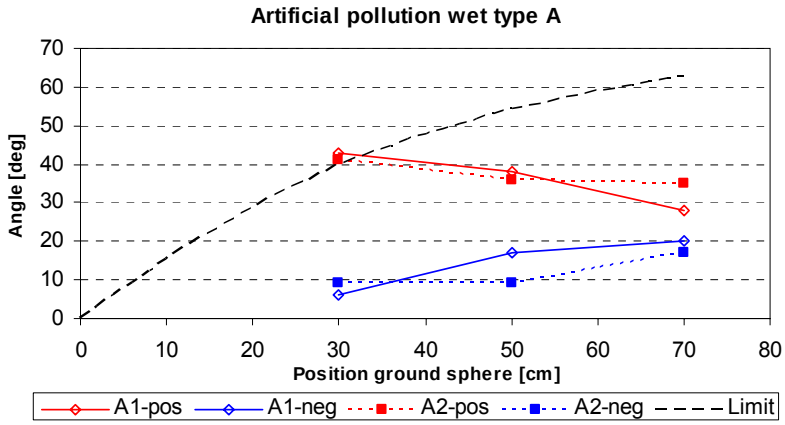

Figure A20 Comparison of data from specimen A1 and A2 considering surfaces where dry artificial pollution has been applied, followed by further wetting of the saline solution; wet artificial pollution.

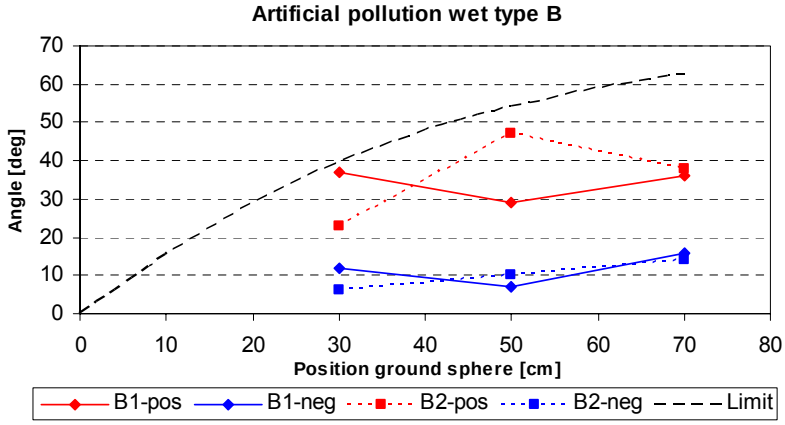

Figure A21 Comparison of data from specimen B1 and B2 considering surfaces where dry artificial pollution has been applied, followed by further wetting of the saline solution; wet artificial pollution.

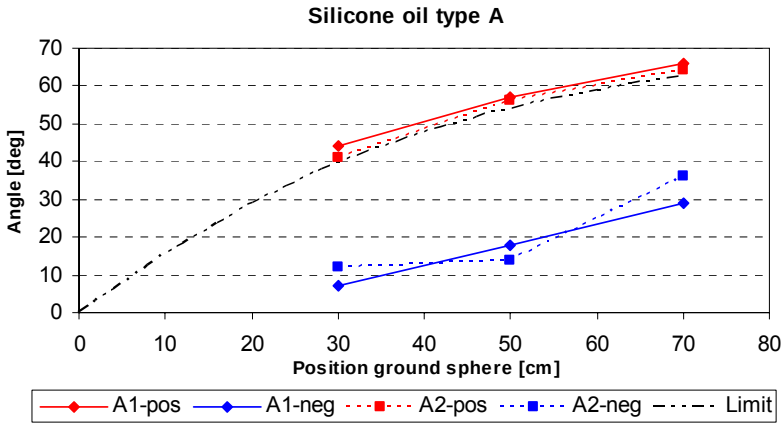

Figure A22 Comparison of data from specimen A1 and A2 considering surfaces wiped with silicone oil, giving a dry hydrophobic surface.

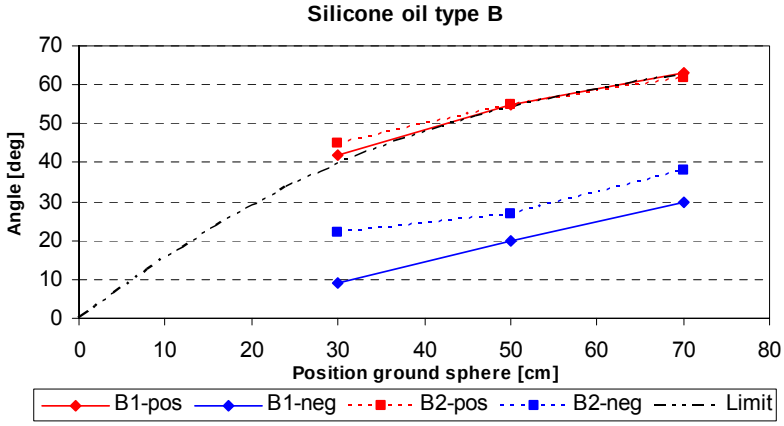

Figure A23 Comparison of data from specimen B1 and B2 considering surfaces wiped with silicone oil, giving a dry hydrophobic surface.

Appendix E – Scale model experiments

One of the standardised methods of determining lightning attachment points on aircrafts is by performing scale model experiments in the high voltage laboratory [77]. A small model of the aircraft considered is covered with conductive paint and placed in an electrode gap consisting of either a rod shaped high voltage electrode and a large ground plane in case of an approaching leader simulation, or two large plane electrodes if a triggered lightning strike is to be simulated. By applying a voltage waveform C or D [34] with an amplitude sufficient for electrical breakdown of the air gap between the electrodes, the discharge path can be monitored. Depending on the orientation of the aircraft model, the spark will typically attach to extremities as the nose radome, the wing tips, antennas on the fuselage, etc.

Considering wind turbines, similar tests could be performed. Most manufacturers already have small scale models for marketing purposes which could easily by implemented in a high voltage test. By performing a large amount of tests for various orientations of the rotor, an indication of which areas that needs the most attention would appear. The use of UV sensitive photography would also be beneficial in this case as discussed in section 6.1.5., and would probably show streamer initiation on the rear of the nacelle or from antennas and other instrumentation.

In connection with this thesis a few attachment tests on a scale model of the Vestas V90 turbine were conducted. The following pictures show two discharges to the model where the blade tip was hit each time.

Figure A24 Discharges to a scale model of a Vestas V90 wind turbine

Besides these few images no structured research or test series were implemented to cover such scale model tests. A thorough study of the attachment points determined by these small scale models and the attachment points experienced in Mother Nature must be conducted before such tests are standardised. The research should also focus on the wave shape of the transient electric field applied, in connection with the scaling itself.

Appendix F – List of papers

List of papers

The following is a list of the papers published or submitted during the project.

Published papers

Tracking tests of Glass Fibre Reinforced Polymers (GFRP) as part of Improved Lightning Protection of Wind Turbine Blades, S.F. Madsen, J. Holbøll, M. Henriksen and Niels Bjært, published at the 27th International Conference on Lightning Protection, Avignon, France, 13-16 September 2004.

Breakdown tests of Glass Fibre Reinforced Polymers (GFRP) as part of Improved Lightning Protection of Wind Turbine Blades, S.F. Madsen, J. Holbøll, M. Henriksen, F.M. Larsen, L.B. Hansen and K. Bertelsen, published on the 15th IEEE International Symposium on Electrical Insulation, Indianapolis, Indiana USA, 19-22 September 2004.

Breakdown Tests of Composite Materials, and the Importance of the Volume Effect, S.F. Madsen, J. Holbøll, M. Henriksen and S. Krog-Pedersen, Published at the 19th Nordic Insulation Symposium, Trondheim, Norway, 13-15 June 2005.

Experimental Investigation of the Relationship between Breakdown Strength and Tracking Characteristics of Composites, S.F. Madsen, J. Holbøll, M. Henriksen and J. Assentoft, Published at the 19th Nordic Insulation Symposium, Trondheim, Norway, 13-15 June 2005.

Calculated Temperature Rise and Thermal Elongation of Structural Components, depending on Action Integral of Injected Lightning Currents, S.F. Madsen, published at the International Conference on Lightning and Static Electricity, Washington Seattle, USA, 19-23 September 2005.

Direct relationship between breakdown strength and tracking index of composites, S.F. Madsen, J. Holbøll, M. Henriksen, submitted to the 16th IEEE International Symposium on Electrical Insulation, Toronto, Ontario Canada, 11-14 June 2006

New test method for evaluating the lightning protection system on wind turbine blades, S.F. Madsen, J. Holbøll, M. Henriksen, K. Bertelsen and H.V. Erichsen, submitted to the 28th International Conference on Lightning Protection, Kanazawa, Japan, 18-22 September 2006.

Lightning discharge phenomena in the tip area of wind turbine blades and their dependency on material and environmental parameters, J. Holbøll, S.F. Madsen, M. Henrisken and K. Bertelsen, submitted to the 28th International Conference on Lightning Protection, Kanazawa, Japan, 18-22 September 2006.

Submitted papers

A new principle of measuring static electric fields using two floating electrodes, S.F. Madsen, submitted to the International Conference on Lightning and Static Electricity, Paris, France, 28-31 August 2007.